DTIC FILE COPY

AGARD-LS-173

AD-A228 936

AGARD

ADVISORY GROUP FOR AEROSPACE RESEARCH & DEVELOPMENT

7 RUE ANCELLE 92200 NEUILLY SUR SEINE FRANCE

AGARD LECTURE SERIES No. 173

Missile Interceptor Guidance System Technology

La Technologie pour les Systèmes de Guidage des Missiles Intercepteurs (de Missiles ou d'Aéronefs)

DTIC
ELECTE
NOV 20 1990
S E D

DISTRIBUTION STATEMENT A
Approved for public release;
Distribution Unlimited

NORTH ATLANTIC TREATY ORGANIZATION

DISTRIBUTION AND AVAILABILITY
ON BACK COVER

90 11 19 246

AGARD-LS-173

NORTH ATLANTIC TREATY ORGANIZATION

ADVISORY GROUP FOR AEROSPACE RESEARCH AND DEVELOPMENT

(ORGANISATION DU TRAITE DE L'ATLANTIQUE NORD)

AGARD Lecture Series No.173

Missile Interceptor Guidance System Technology

La Technologie pour les Systèmes de Guidage des Missiles Intercepteurs (de Missiles ou d'Aéronefs)

Accession For	
NTIS GRA&I	X
DTIC TAB	☐
Unannounced	☐
Justification	
By	
Distribution/	
Availability Codes	
Dist	Avail and/or Special
A-1	

This material in this publication was assembled to support a Lecture Series under the sponsorship of the Guidance and Control Panel of AGARD and the Consultant and Exchange Programme of AGARD presented on 11th–12th October 1990 in Hamburg, Germany, 15th–16th October 1990 in Amsterdam, The Netherlands, and 25th–26th October 1990 in Cambridge, MA, United States.

The Mission of AGARD

According to its Charter, the mission of AGARD is to bring together the leading personalities of the NATO nations in the fields of science and technology relating to aerospace for the following purposes:

— Recommending effective ways for the member nations to use their research and development capabilities for the common benefit of the NATO community;

— Providing scientific and technical advice and assistance to the Military Committee in the field of aerospace research and development (with particular regard to its military application);

— Continuously stimulating advances in the aerospace sciences relevant to strengthening the common defence posture;

— Improving the co-operation among member nations in aerospace research and development;

— Exchange of scientific and technical information;

— Providing assistance to member nations for the purpose of increasing their scientific and technical potential;

— Rendering scientific and technical assistance, as requested, to other NATO bodies and to member nations in connection with research and development problems in the aerospace field.

The highest authority within AGARD is the National Delegates Board consisting of officially appointed senior representatives from each member nation. The mission of AGARD is carried out through the Panels which are composed of experts appointed by the National Delegates, the Consultant and Exchange Programme and the Aerospace Applications Studies Programme. The results of AGARD work are reported to the member nations and the NATO Authorities through the AGARD series of publications of which this is one.

Participation in AGARD activities is by invitation only and is normally limited to citizens of the NATO nations.

The content of this publication has been reproduced directly from material supplied by AGARD or the authors.

Published September 1990

Copyright © AGARD 1990
All Rights Reserved

ISBN 92-835-0587-5

Printed by Specialised Printing Services Limited
40 Chigwell Lane, Loughton, Essex IG10 3TZ

Abstract

Most operational interceptor tactical guidance systems are employing technologies which were developed more than two decades ago. Newer technologies have been slow to replace these mature technologies that meet the requirements; however, future interceptor guidance systems will have more demanding requirements and technological advances have great payoff potential. The Lecture Series will bring together a group of speakers with both outstanding practical and theoretical experience in interceptor guidance system technology. These speakers will provide the audience with the guidance system technology fundamentals which will serve as background so that theoretical advances in future and proposed systems can be both understood and appreciated.

This Lecture Series, sponsored by the Guidance and Control Panel of AGARD, has been implemented by the Consultant and Exchange Programme.

Abrégé

La plupart des systèmes opérationnels de guidage tactique de missiles intercepteurs font appel à des technologies qui datent de plus de vingt ans. Les nouvelles technologies tardent à remplacer ces technologies classiques qui continuent cependant à répondre aux besoins actuels. Les spécifications des futurs systèmes de guidage des intercepteurs seront plus exigeantes et elles offriront ainsi de nombreuses possibilités aux technologies nouvelles.

Ce cycle de conférences rassemble un groupe de conférenciers ayant une vaste expérience pratique et théorique des technologies des systèmes de guidage des missiles intercepteurs. Ils fourniront aux participants une synthèse des éléments de base des systèmes de guidage qui permettra de mieux comprendre et d'apprécier les avancées théoriques des sytèmes futurs et proposés.

Ce cycle de conférences est présenté le cadre du programme de consultants et des échanges, sous l'égide du Panel AGARD du Guidage et du Pilotage.

List of Authors/Speakers

Lecture Series Director: Mr P.Zarchan
C.S. Draper Laboratory, Inc.
555 Technology Square
Cambridge, Mass 02139
United States

AUTHORS/SPEAKERS

Mr F.Burel
Aérospatiale
Centre des Gâtines
Dept. ECS
91370 Verrières-le-Buisson
France

Dr O.Deutsch
C.S. Draper Laboratory Inc.
555 Technology Square
Cambridge, Mass 02139
United States

Dr U.Hartmann
Bodenseewerk
Gerätetechnik GmbH
Postfach 10 11 55
D-7770 Überlingen
Germany

Mr W.Kaufmann
Building 262, Mail Stop B68
Hughes Aircraft Company
8433 Fallbrook Avenue
Canoga Park, CA 91304
United States

Dr R.V.Lawrence
Royal Aerospace Establishment
Farnborough, Hampshire
GU14 6TD
United Kingdom

Dr R.L.Reichert
The Johns Hopkins University
Applied Physics Laboratory
Johns Hopkins Road
Building 1 East 134
Laurel, Maryland 20723-6099
United States

Dr D.Yost
The Johns Hopkins University
Applied Physics Laboratory
Johns Hopkins Road
Building 1 East 134
Laurel, Maryland 20723-6099
United States

Contents

	Page
Abstract/Abrégé	iii
List of Authors/Speakers	iv
Partial contents:	Reference
Introduction and Overview by P.Zarchan	1
Modern Robust Control for Missile Autopilot Design by R.T Reichert and D.J.Yost	1
Midcourse Guidance Techniques for Advanced Tactical Missile Systems by U.Hartmann	2
Flight Control Design Issues in Bank-to-Turn Missiles by W.A.Kaufmann	3
Guidance Simulation Model of Anti Sea-Skimmer Missile by F.Burel	4
Advanced Missile Guidance by R.V Lawrence	5
Micro Based Technology – A New Tool for Missile Guidance System Design and Visualization by P.Zarchan	6
Interactions between Battle Management and Guidance Law Design for a Strategic Interceptor by O L.Deutsch	7
Guidance Methods for Tactical and Strategic Missiles by P.Zarchan	8

Keywords: Turning flight; Antimissile defense systems; Intercept trajectories. (EDC)

Introduction and Overview
Missile Interceptor Guidance System Technology
(Guidance System Technologies Used In Interceptor Missiles Against Other Missiles Or Airplanes)

Paul Zarchan
The Charles Stark Draper Laboratory, Inc.
Cambridge, MA, USA 02139

Theme

Most operational interceptor tactical guidance systems are employing technologies which were developed more than two decades ago. Newer technologies have been slow to replace these mature technologies that meet the requirements; however, future interceptor guidance systems will have more demanding requirements and technological advances have great payoff potential. The Lecture Series will bring together a group of speakers with both outstanding practical and theoretical experience in interceptor guidance system technology. These speakers will provide the audience with the guidance system technology fundamentals which will serve as background so that theoretical advances in future and proposed systems can be both understood and appreciated.

Overview of the Lectures

Lecture 1:

The first lecture is by Dr. Robert T. Reichert of the U.S. and is entitled " Modern Robust Control For Missile Autopilot Design." This lecture examines the applicability of H_∞ control to the design of automatic flight control systems for highly maneuverable, tail-controlled missiles. The fundamentals of modern control system analysis and synthesis are reviewed and emphasis is placed on formulating frequency domain weighting functions for design specification. A numerical example is included to clarify all concepts.

Lecture 2:

The second lecture is by Dr. U. Hartmann of Germany and is entitled "Midcourse Guidance Techniques For Advanced Tactical Missile Systems." The lecture gives an introduction into the operational requirements and operational aspects of inertial midcourse guidance systems. Different midcourse guidance principles such as pure inertial guidance, updated inertial and aided inertial are discussed with their benefits and drawbacks. The paper also describes various prelaunch alignment methods and discusses their relative merits from an overall system point of view.

Lecture 3:

The third lecture is by Mr. Walter Kaufmann of the U.S. and is entitled "Flight Control Design Issues In Bank To Turn Missiles." This paper discusses various design issues encountered in the synthesis of bank-to-turn autopilots for several proposed air-launched guided missile configurations. Included in the paper is a discussion of the various tradeoffs between bank-to-turn and skid-to-turn configurations. The relative merits of several bank-to turn control laws are presented with respect to the type of airframe, propulsion and guidance required for the mission under consideration. The coupling phenomenon is discussed and methods for decoupling are presented.

Lecture 4:

The fourth lecture is by Mr. F. Burel , of France and is entitled "Guidance Simulation Model of Anti Sea-Skimmer Missile." The paper presents a simulation methodology for estimating the survivability of ships and their protective frigate, facing a salvo of maneuvering sea-skimmers. The simulation model includes such realistic effects as defense system errors and midcourse radar noise. A detailed model of the threat, including the three phase of flight, are incorporated in the simulation model.

Lecture 5:

The fifth lecture is by Dr. R. V. Lawrence of England and is entitled "Advanced Missile Guidance." The paper relates guidance issues through the zero-control or zero effort miss. Algebraic expressions for the zero effort miss, as a function of the missile-target range, are derived and presented for four sample systems. The relationship between proportional navigation, optimal guidance, and zero effort miss are derived and discussed. Finally, the impact of optimal evasive target maneuvers on system performance are presented.

Lecture 6:

The sixth lecture is given by Mr. Paul Zarchan of the U.S. and is entitled "Micro Based Technology - A New Tool For Missile Guidance System Design and Visualization." Several interceptor guidance system related examples are presented. The paper first demonstrates that these examples can be made to work on microcomputers with CPU running times which are very attractive and turn around times (i.e. time for engineer to get the answer in a useful form) that are far superior to that offered by a time-shared mainframes. It is then shown how numerical output can be enhanced, in real time, with the graphics visualization technology which is currently available with microcomputers. Each of the examples demonstrates how the enhanced answers offer the designer a visualization which not only gives a deeper insight into the problem being solved, but in addition allows an engineer to rapidly iterate cases to get an acceptable design.

Lecture 7:

The seventh lecture is given by Dr. Owen Deutsch of the U.S. and is entitled "Interactions Between Battle Management and Guidance Law Design For A Strategic Interceptor ." This paper switches the focus of the Lecture Series from one-on-one tactical missile considerations to proliferated strategic interceptor technology. The paper demonstrates that acceptable solutions require consideration of all systems issues and that battle management functions should not be decoupled from guidance law design. A system level simulation which incorporates all significant error sources to the battle manager is described. Knowledge gained, in terms of execution speed, user interaction and insights generated are presented through several unifying examples.

Lecture 8:

The eighth and final lecture is given by Mr. Paul Zarchan of the U.S. and is entitled "Guidance Methods For Tactical and Strategic Missiles." The paper reviews methods of guidance which are applicable to both tactical and strategic missiles. Guidance concepts, which were originally developed for the tactical world, are extended for application to the strategic world not only to gain insight but also to predict strategic interceptor fuel consumption and performance. Nonlinear engagement simulation results indicate that the divert requirement formulas (derived in the paper) for prediction error, apparent target acceleration and guidance law are not only useful but are in fact accurate indicators of strategic interceptor requirements. Numerous examples are presented to clarify and illustrate concepts.

Concluding Remarks

The lecturers participating in this Lecture Series will present the results of many years of practical experience with interceptor guidance system technology. The intended result of this Lecture Series is the transfer of knowledge that can lead to newer and better interceptor guidance systems throughout the NATO community.[1]

References

1. Schmidt, G. T. (editor), Kalman Filter Integration of Modern Guidance and Navigation Systems, AGARD Lecture Series No. 166, June 1989.

MODERN ROBUST CONTROL FOR MISSILE AUTOPILOT DESIGN

by

Robert T.Reichert
and
David J.Yost
The Johns Hopkins University
Applied Physics Laboratory
Johns Hopkins Road
Building 1 East 134
Laurel, Maryland
United States

ABSTRACT

This paper examines the applicability of H_∞ control to the design of automatic flight control systems for highly maneuverable, tail-controlled missiles. The fundamentals of modern-robust-control analysis and synthesis are reviewed. Problem formulation with emphasis on selection of frequency domain weighting functions for design specifications and the role of modelling uncertainty are considered. An example problem is included as a tutorial overview of these methods.

1.0 INTRODUCTION

Future homing missiles will need to cope with demands for greater range and higher maneuverability resulting in more stringent autopilot performance requirements. Design techniques, used in current practice, are limited and often result in less capable system performance. However, recent advances in robust-control theory (Ref. [1-4]) offer good prospects for meeting the design needs of next generation missiles. Several anticipated benefits of the robust-control design approach are: greater flexibility in the choice of airframe geometry, full use of available airframe maneuver capability and greater tolerance to uncertainty in design models.

Robust-control design methods optimize performance and stability based on engineering models which include performance specifications and descriptions of how uncertainty modifies the nominal plant model. H_∞ optimal control provides the basis for controller synthesis while μ-analysis characterizes performance and stability in the presence of a defined structure for uncertainties. The combination of these two powerful concepts leads to a synthesis procedure that explicitly accounts for a specified level and structure of uncertainty in the nominal plant model. This paper focuses on showing the fundamentals of applying H_∞ optimal control and μ-analysis to a hypothetical missile-autopilot example.

This paper is organized as follows. We will begin with a review of several key concepts in modern-robust control analysis and synthesis. This material is drawn from references (Ref. [1,2,10,11]). A description of the tail-controlled missile problem and a hypothetical model will be described next. This material is followed by a definition of the uncertainty model and H_∞ optimal-control interconnection structure. Lastly, a comparison of three designs is made to illustrate various performance characteristics of H_∞ controllers.

2.0 ANALYSIS REVIEW

Definition: Linear Fractional Transformation (LFT). Consider the complex matrix partitioned as

$$M = \begin{bmatrix} M_{11} & M_{12} \\ M_{21} & M_{22} \end{bmatrix}$$

derived from the following linear equations

$$\begin{bmatrix} z \\ e \end{bmatrix} = M \begin{bmatrix} w \\ v \end{bmatrix}$$

$$w = \Delta z$$

where the size of Δ is such that $M_{11}\Delta$ is square. This set of equations is well posed if the inverse of $I-M_{11}\Delta$ exists, in which case the vectors e and v will satisfy $e = F_u(M,\Delta)v$ where

$$F_u(M,\Delta) = M_{22} + M_{21}\Delta(I-M_{11}\Delta)^{-1}M_{12}.$$

If viewed in a feedback block-diagram sense, the notation used here denotes the LFT formed by closing the upper loop (hence, subscript u) of M with Δ. M_{22} may be viewed as a nominal element and Δ as a linear-fractional uncertainty. The matrices M_{11}, M_{12}, M_{21} and $F_u(M,\Delta)$ describe how Δ affects the nominal element.

The framework for analysis and synthesis, used here, is based on LFT's as shown in Figure (1). Any linear interconnection of inputs (v,u), outputs (e,y) and uncertainties (Δ) may be rearranged as shown in Figure (1a). P represents the system interconnection structure, K the controller and Δ the uncertainty. v is a vector of exogenous inputs such as reference commands, disturbances and noise. e is a vector of error signals to be kept small. y is a vector of sensor measurements and u is a vector of control signals. The convention adopted here is to normalize exogenous inputs (v), errors (e) and uncertainty (Δ) to 1. This requires that all scalings be absorbed into P. Within this framework we will be concerned with 2 LFT structures; one for analysis (Figure (1b)):

$$F_u(G,\Delta) = G_{22} + G_{21}\Delta(I-G_{11}\Delta)^{-1}G_{12},$$

where G is obtained by absorbing the controller K into P, and one for synthesis (Figure (1c)):

$$F_l(P,K) = P_{11} + P_{12}\Delta(I-P_{22}\Delta)^{-1}P_{21}.$$

In the absence of uncertainty the nominal performance measure is given by

$$\|G_{22}\|_\infty = \sup_\omega \bar{\sigma}(G_{22}(j\omega)),$$

and relates the worst-case response, over frequency, to the exogenous input. Nominal stability, a weak requirement, is attained by K stabilizing only the nominal plant.

When uncertainty is considered, the analysis problem involves: determining the robust stability of G in the presence of an uncertain but bounded set of Δ's, and for robust performance, determining if e remains in a desired set of responses for all permissible sets of Δ and exogenous inputs v. Stability for unstructured uncertainty (only $\bar{\sigma}(\Delta)\le 1$ is known) depends only on $\|G_{11}\|_\infty \le 1$, and performance depends only on $\|G\|_\infty$. However, norm bounds of this type are inadequate for determining robust performance or stability with realistic models of structured uncertainty in the plant. The structured singular value (μ) was introduced to deal with these more complicated situations (Ref. [5]).

In defining μ, we begin by specifying that Δ belongs to the set of block-diagonal, complex-valued, bounded uncertainties:

$$\underline{\Delta} = \{\mathrm{diag}(\Delta_1,\Delta_2,\ldots,\Delta_n) \mid \bar{\sigma}(\Delta_i)\le 1\}.$$

For $M \in C^{n\times n}$, $\mu(M)$ is defined:

$$\mu(M) = \frac{1}{\min\{\bar{\sigma}(\Delta) \mid \Delta\in\underline{\Delta},\ \det(I-M\Delta)=0\}}$$

unless no $\Delta \epsilon \underline{\Delta}$ makes $I-M\Delta$ singular, in which case $\mu(M)=0$. The function μ is dependent upon the structure of Δ and has the property $\mu(\alpha M)=|\alpha|\mu(M)$.

The following bounds, which are relatively easier to compute, are defined for μ:

$$\sup_{U \epsilon \underline{U}} \rho(MU) \le \mu(M) \le \inf_{D \epsilon \underline{D}} \bar{\sigma}(DMD^{-1})$$

where

ρ denotes spectral radius
σ denotes maximum singular value

$$\underline{U} = \{ \mathrm{diag}(U_1, U_2, \ldots, U_n) | U_i^* U_i = I \}$$

$$\underline{D} = \{ \mathrm{diag}(d_1 I, d_2 I, \ldots, d_n I) | d_i \epsilon R_+ \}$$

where the structures of $\underline{U}$ and $\underline{D}$ match Δ. Note that U and D leave Δ invariant:

$$\bar{\sigma}(\Delta U) = \bar{\sigma}(U\Delta) \text{ and } D^{-1}\Delta D = \Delta.$$

The following two theorems (Ref. [6]) establish the relevance of μ for studying robustness of feedback systems with structured uncertainty.

Theorem: Robust Stability

$$F_u(G,\Delta) \text{ stable } \forall\ \Delta \epsilon \underline{\Delta} \text{ iff } \sup_{\omega} \mu(G_{11}(j\omega)) \le 1.$$

Theorem: Robust Performance

$$F_u(G,\Delta) \text{ stable and } \|F_u(G,\Delta)\|_\infty \le 1$$
$$\forall\ \Delta \epsilon \{\mathrm{diag}(\Delta, \Delta_{n+1})\} \text{ iff } \sup_{\omega} \mu(G(j\omega)) \le 1.$$

3.0 SYNTHESIS REVIEW

For synthesis it is assumed that performance weightings and scaling factors are absorbed as part of the interconnection structure (P in Figure (1.c)) so that v' and e' are properly normalized to 1. For the H_∞ **optimal-performance problem** the synthesis goal is to find a stabilizing controller K which minimizes $\|F_l(P,K)\|_\infty$ where

$$e' = F_l(P,K)\ v'$$
$$F_l(P,K) = P_{11} + P_{12}\Delta(I-P_{22}\Delta)^{-1}P_{21}.$$

To illustrate the two-Riccati equation state-space solution (Ref. [1,2]) to this problem, consider the following representation and matrix partition for the interconnection structure P(s):

$$\dot{x} = Ax + B_1 v' + B_2 u$$
$$e' = C_1 x + D_{12} u$$
$$y = C_2 x + D_{21} v'$$

where x is the state vector, v' is the exogenous input vector, e' is the error vector, u is the control vector, and y is the measurement vector; we then denote the matrix partition

$$P(s) = \left[\begin{array}{c|cc} A & B_1 & B_2 \\ \hline C_1 & 0 & D_{12} \\ C_2 & D_{21} & 0 \end{array}\right]$$

We have assumed that $D_{11}=0$ and $D_{22}=0$ in order to simplify the equations shown here. The more general case is treated in [2]. In addition to the above assumptions, it is required that (A,B_2,C_2) be stabilizable and detectable; rank D_{12}= number of control inputs; rank D_{21}= number of measurements; $D_{12}=[0\ I]'$ and $D_{21}=[0\ I]$. The last two requirements may be achieved by appropriate scaling of u and y and a unitary transformation of v' and e'.

In the solution technique we will make use of the following notation for the Hamiltonian matrix and algebraic Riccati (ARE) equation:

$$H = \begin{bmatrix} A & R \\ Q & -A^* \end{bmatrix}$$

where X will be the solution to the ARE:

$$A^*X + XA + XRX - Q = 0$$

and will be denoted as $X = \mathrm{Ric}(H)$.

To proceed, consider the problem of finding a controller K(s) to satisfy the performance goal of $||F_1(P,K)||_\infty < \gamma$. We define two Hamiltonian matrices :

$$H_1 = \begin{bmatrix} (A-B_2D_{12}^*C_1) & \gamma^{-2}B_1B_1^* - B_2B_2^* \\ C_1^*(-I+D_{12}D_{12}^*)C_1 & -(A-B_2D_{12}^*C_1)^* \end{bmatrix}$$

$$H_2 = \begin{bmatrix} (A+B_1D_{21}^*C_2)^* & \gamma^{-2}C_1^*C_1 - C_2^*C_2 \\ B_1(-I+D_{21}^*D_{21})B_1^* & -(A+B_1D_{21}^*C_2) \end{bmatrix}$$

with ARE solutions denoted $X_\infty=\mathrm{Ric}(H_1)$ and $Y_\infty=\mathrm{Ric}(H_2)$. The state-space equations for the controller $K(s)=[u(s)/y(s)]$ are given:

$$\dot{\bar{x}} = A\bar{x} + (\gamma^{-2}Y_\infty C_1^*)\bar{e}' + F(y-\bar{y})$$
$$\bar{e}' = C_1\bar{x} + D_{12}u$$
$$u = G\bar{x}$$
$$F = B_1D_{21}^* + Y_\infty C_2^*$$
$$G = -(D_{12}^*C_1 + B_2^*X_\infty)Z_\infty$$
$$Z_\infty = (I - \gamma^{-2}Y_\infty X_\infty)^{-1}$$

where $\bar{x}$ denotes the state estimate, $\bar{e}'$ denotes the estimate of the worst-case error and $\bar{y}$ denotes the measurement estimate. This controller has the observer/full-state feedback structure familiar to LQG optimal control. However, the addition of the worst-case error to the state dynamics represents a departure from this familiar structure.

The optimal H_∞ controller is found by performing a minimizing search in γ. The smallest value of γ is chosen consistent with the following requirements: $X_\infty \geq 0$, $Y_\infty \geq 0$ and $\rho(X_\infty Y_\infty) < \gamma^2$.

Thus far, the H_∞ synthesis framework described here is only useful for optimization in an input/output setting. No mention of uncertainty (internal to the nominal plant model) enters the formulation of the **optimal-performance problem**. In order to address uncertainties, the H_∞ **optimal-performance problem** posed here may be viewed as an H_∞ **robust-stabilization problem** with respect to the uncertainty structure shown in Figure (2). This transformation of the problem in effect combines input/output performance objectives with stability to plant uncertainty objectives. Here Δ is considered to be a full-block of unstructured uncertainty (only $\bar{\sigma}(\Delta)\leq 1$ is known). That is, find K to stabilize the system and to minimize:

$$\|F_u(F_l(P,K),\Delta)\|_\infty \ \forall\ \Delta \mid \bar{\sigma}(\Delta)\leq 1.$$

Clearly, this represents a more conservative synthesis problem than may be intended, because the true structure of Δ may be ignored. In reality, Δ in Figure (2), has a structure dictated by the true uncertainty (which we denote $\Delta_u | \Delta_u \epsilon \underline{\Delta}$) and a full-block structure for the e/v transfer function (which we denote Δ_p). This yields an actual structure for Δ, in Figure (2), of :

$$\Delta = \begin{bmatrix} \Delta_u & 0 \\ 0 & \Delta_p \end{bmatrix}$$

It should be noted that an H_∞ controller could be obtained without regard to the presence of internal modeling uncertainties (i.e., by removing the exogenous inputs and errors associated with the uncertain elements). This is equivalent to solving the **optimal-performance problem** posed above. However, this approach removes all conservatism by assuming that the design model is a perfect representation of the plant response. The resulting design will likely exhibit very poor robust performance and stability in the presence of the real plant.

In order to reduce conservatism, without removing it altogether, we will need to merge the two powerful techniques of H_∞ optimization and μ-analysis. Recall that an upper bound for μ may be obtained by a scaling operation and application of the $\|\cdot\|_\infty$. Incorporating this μ related concept with H_∞ synthesis, the problem becomes one of finding a controller K and a frequency dependent scaling matrix D(s) such that $\|D(s)\ F_l(P,K)\ D(s)^{-1}\|_\infty$ is minimized. The approach taken here is to alternate between finding K, to minimize the above expression for a fixed D(s), and then to find a minimizing D(s) for a fixed K. This latter step is conducted point-by-point in frequency with a different constant D matrix result for each frequency point. The data for the elements of D may be fit with real-rational, minimum-phase, stable and invertible SISO transfer functions. The frequency dependent matrix D(s) is comprised of the SISO transfer function fits. This μ-synthesis technique (D-K iteration) has been used extensively elsewhere to obtain robust control laws.

We will examine the performance characteristics of the three design approaches discussed here: H_∞ **optimal-performance**, H_∞ **robust-stabilization** and μ-synthesis.

4.0 PROBLEM DESCRIPTION

Consider the missile-airframe control problem illustrated in Figure (3). When the vehicle is flying with an angle of attack (α), lift is developed. This lift may be represented as acting at a central location (center of pressure). The vehicle will be statically stable or unstable (without corrective tail deflections) depending on the location of the center of pressure

relative to the center of mass. The control problem requires that the autopilot generate the required tail-deflection (δ) to produce an angle of attack, corresponding to a maneuver called for by the guidance law, while stabilizing the airframe rotational motion. Sensor measurements for feedback typically include missile rotational rates (from rate gyros) and normal acceleration (from accelerometers). Reasonably accurate mathematical models of the rigid-body transfer functions from tail-deflection to the sensor outputs are generally available for design.

Typical uncertainties to be considered in this control problem include: aerodynamic characteristics, mass and balance, wind, flexible mode dynamics, actuator nonlinearities and sensor nonlinearities and noise. The first three uncertainties generally are handled by using sufficiently wide bandwidth feedback loops, while the last three uncertainties in the list act to restrict the amount of bandwidth that may be used practically.

For the problem considered here, it is desired to design one controller to track commanded acceleration maneuvers with a steady state accuracy of 0.5% and a time constant of less than 0.2 seconds. The controller must provide robust performance over a wide range of angles of attack and must avoid saturating tail-deflection actuator rate capabilities as well as avoid high-frequency instabilities caused by unmodelled flexible-body modes.

5.0 MISSILE MODEL

The nonlinear state equations for this control problem are given as:

$$\dot{\alpha} = (\cos^2(\alpha)/mu)[F_z] + q$$
$$\dot{q} = M_y / I_y$$

where

F_z = $C_n(\alpha,\delta)$ QS (lbs)
M_y = $C_m(\alpha,\delta)$ QSd (ft-lbs)
Q = dynamic pressure (lbs/ft^2)
S = reference area (.44 ft^2)
d = diameter (.75 ft)
m = mass (13.98 slugs)
I_y = pitch moment of inertia (182.5 slug-ft^2)
u = velocity component along missile center line (3109.3 cosα ft/sec).

The aerodynamic coefficients C_n and C_m are given by the following polynomial expressions:

$$C_n = a\alpha^3 + b\alpha^2 + c\alpha + d\delta$$
a = .000103
b = -.00945
c = -.170
d = -.034

$$C_m = a\alpha^3 + b\alpha^2 + c\alpha + d\delta$$
a = .000215
b = -.0195
c = .051
d = -.206

These values given here are purely hypothetical and are intended for tutorial uses only. The angle of attack is assumed to range over 0 to 20 degrees.

The nonlinear state equations are linearized about trim operating points (M_y = 0) to form linear state-space equations of the form:

$$\dot{x} = Ax + Bu$$
$$y = Cx + Du$$

where $x=[\alpha\ q]$, $u=[\delta]$, and $y=[q\ \eta_z]$. Here, η_z represents the accelerometer measurement (assumed to be at the center of mass). For an angle of attack of 0 degrees, the state-space matrices are:

$$A = \begin{bmatrix} -0.6 & 1. \\ 32.4 & 0. \end{bmatrix}, \quad B = \begin{bmatrix} -.12 \\ -130.8 \end{bmatrix}$$

$$C = \begin{bmatrix} 0 & 1. \\ -1.02 & 0. \end{bmatrix}, \quad D = \begin{bmatrix} 0 \\ -.203 \end{bmatrix}$$

For an angle of attack of 20 degrees, the state-space matrices are:

$$A = \begin{bmatrix} -1.18 & 1. \\ -300.2 & 0. \end{bmatrix}, \quad B = \begin{bmatrix} -.11 \\ -130.8 \end{bmatrix}$$

$$C = \begin{bmatrix} 0 & 1. \\ -2.54 & 0. \end{bmatrix}, \quad D = \begin{bmatrix} 0 \\ -.203 \end{bmatrix}$$

As a representative average model to use in the design process we will select the following state-space matrices. These do not actually correspond to a given linearization about an operating angle of attack, rather they represent an average value for each element of the matrices when examined over the entire angle of attack range.

$$A = \begin{bmatrix} -0.9 & 1. \\ -134.0 & 0. \end{bmatrix}, \quad B = \begin{bmatrix} -.117 \\ -130.8 \end{bmatrix}$$

$$C = \begin{bmatrix} 0 & 1. \\ -1.78 & 0. \end{bmatrix}, \quad D = \begin{bmatrix} 0 \\ -.203 \end{bmatrix}$$

In addition to these dynamics, it is assumed that the missile tail-deflection actuator may be represented with a second order linear transfer function:

$$\frac{\delta}{\delta_c}(s) = \frac{1}{(s/\omega_a)^2 + (1.4s/\omega_a) + 1}$$

$\omega_a = 150$ rad/sec.

6.0 UNCERTAINTY DESCRIPTION

Three uncertainty descriptions will be used for this design example. The first captures the dominant effect of aerodynamic deviations from the assumed design model. The second represents uncertainty in the actuator gain and phase characteristics. And the last represents unmodelled dynamics. Figure (4) illustrates the location of the uncertain elements (Δ_i) in the design model. The controller must handle the aerodynamic variations that result from operating over the angle of attack range from 0 to 20 degrees. Examining the state-space matrices over this range we see that the A(2,1) element varies by as much as 140%. As expected, this term varies the most because it relates directly to the rotational stability of the rigid-body airframe. We will need to incorporate a parametric uncertain model to capture the uncertainty in this term.

Variations in the other terms are known to be far less significant, from physical considerations, and will be ignored. The normalizing scale factor for Δ_1 (k in Figure (4)) for this example is 1.25. The effect of this uncertainty will be to make maximum use of the rate-gyro sensor for an inner-loop feedback path to desensitize the system from variations in the rotational aerodynamics.

The second uncertainty (Δ_2 in Figure (4)) captures uncertainty in the actuator gain and phase characteristics. With a normalizing scale factor of c=.6, this uncertainty structure represents as much as 35 degrees phase uncertainty and gain variation from approximately .6 to 2.5). This uncertainty will have the effect of preserving gain and phase margin in the inner loop.

The third uncertainty (Δ_3 in Figure (4)) is used to represent unmodelled flexible-mode dynamics. Figure (5) illustrates the frequency dependent weighting function $W_u(s)$ and a representative flexible mode transfer function from tail-deflection to rate-sensor measurement. The weighting functions represents a frequency dependent magnitude bound on the unmodelled transfer function. For conservativeness we elect to over-bound the high frequency characteristics substantially. The effect of this uncertainty will be to limit the bandwidth available to the controller to handle aerodynamic variations.

7.0 INTERCONNECTION STRUCTURE

Thus far, we have defined the nominal model of the plant and the uncertainty structure for this problem. The remaining portion of the interconnection structure to be defined is associated with the performance goals (i.e, exogenous inputs and errors associated with the tracking performance specifications). Figure (6) illustrates the input/output diagram for the interconnection structure chosen here.

As stated earlier, the performance objective is to track step commands (η_c) with a 0.5% tracking accuracy and a maximum time constant of 0.2 seconds. To accomplish this we will define a frequency dependent weighting function that will be applied to the tracking error signal ($\eta_c - \eta$) (i.e., a sensitivity weighting function):

$$W_S(s) = \frac{(14.9451\ s + 200)}{(42.7003\ s + 1)}$$

This weighting function has a low frequency gain of 200 (for 0.5% tracking accuracy) a gain crossover frequency of 5 r/s (for 0.2 sec time constant or better) and a high frequency gain of 0.35 to limit overshoot.

One additional exogenous input to be defined is the rate-gyro sensor noise. Recall that this input is required in order to satisfy the rank of D_{21} requirement. For this problem it is assumed that the gyro is a nearly perfect device. A scale factor of .001 is applied to this input. In practice, if realistic gyro characteristics were available, a frequency dependent weighting would be appropriate to characterize the anticipated noise spectrum.

Lastly, we define an additional performance output that will not significantly alter the characteristics of the solution. However, it is included to satisfy the rank of D_{12} requirement for the H_∞ optimal-performance synthesis case. This output is formed by placing a small constant weighting (.001) on the commanded tail-fin deflection.

8.0 COMPARISON OF H_∞ and μ-SYNTHESIS DESIGNS

We will examine three controller designs. The first design will be obtained by solving the H_∞ optimal-performance problem. The second and third controllers will be obtained by solving first for the H_∞ robust-stabilization controller and then the μ-synthesis controller. The software provided in (Ref. [8]) was used to perform the design steps.

Consider first the controller obtained by solving the H_∞ optimal-performance problem. Recall that this approach ignores the uncertainty description by assuming that the given plant model is a perfect representation of the real plant to be controlled. For this case the interconnection structure is obtained by removing the top three exogenous inputs and error outputs shown in Figure (6). Figure (7) shows three step responses obtained using this controller. The three responses correspond to the design model response and for models obtained by linearizing the airframe at 0 and 20 degrees angle of attack. The response for the design model shows a very good response. However, when the plant deviates from the design model (here the deviation is due to a change in angle of attack) very poor performance is seen for α=20 degrees, and an unstable response is obtained for α=0 degrees. Upon close inspection of the controller dynamics, it is seen that the controller is actually cancelling the plant dynamics and substituting dynamics that satisfy the performance goals. This cancellation of model dynamics is the source of the poor performance observed here.

The lack of robustness observed with the H_∞ optimal-performance controller clearly motivates the need to include modelling uncertainty in the problem formulation. We will proceed along this direction by using the full interconnection structure show in Figure (6). The last two controllers to be examined here are obtained by solving the H_∞ robust-stabilization problem and by performing the D-K iteration to obtain the μ-synthesis controller.

For the first step of the D-K iteration, the frequency dependent D-scale matrices were initialized to identities of the appropriate sizes. The resulting controller from this first pass is the H_∞ robust-stabilization controller (i.e., the controller designed with respect to the conservative model of Δ in Figure (2)). For the first pass the performance level of $\|F_1(P,K)\|_\infty = 2.0$ was attained. For the final D-K iteration the robust-performance level $\|D(s)\ F_1(P,K)\ D(s)^{-1}\|_\infty = 1.07$ was achieved. For evaluation purposes the H_∞ controller was reduced from 8th order to 7th and the μ controller was reduced from 20th order to 8th, using a balanced truncation model reduction procedure (Ref. [9]).

Figure (8) illustrates the step response performance characteristics of the H_∞ robust-stabilization controller for the design model, and for the model linearized at two angles of attack (0 and 20 degrees). Figure (9) illustrates the μ-synthesis performance for the same three plant models. Clearly, the μ-synthesis controller exhibits superior tracking performance. Not shown here is that both designs satisfy the goal of gain stabilizing the unmodelled flexible-mode dynamics and that single-loop stability margins are very good (better than 6db and 35 degrees at the actuator input and at the sensor outputs).

Comparing the worst case perturbation matrices for the H_∞ and μ designs:

$$H_\infty = \begin{bmatrix} 0.0990 & -0.3416 & -0.2049 & -0.1384 \\ 0 & 0 & 0 & 0 \\ 0.0057 & -0.0195 & -0.0117 & -0.0079 \\ -0.0568 & 0.1959 & 0.1176 & 0.0794 \\ 0 & 0 & 0 & 0 \end{bmatrix}$$

$$\mu = \begin{bmatrix} 0.9346 & 0 & 0 & 0 \\ 0 & 0.9346 & 0 & 0 \\ 0 & 0 & -.9346 & 0 \\ 0 & 0 & 0 & 0.9346 \\ 0 & 0 & 0 & .001 \end{bmatrix}$$

shows how the full-block uncertainty structure assumed in the H_∞ synthesis allows interaction between the various uncertainty structures and the performance inputs and outputs. Allowing this interaction presents a much more conservative design challenge and consequently the H_∞ design was unable to attain acceptable performance. It should be noted that only the real part of the worst-case uncertainties are shown above, however, in this case the imaginary parts were negligible.

As a final check on performance of the μ controller, a nonlinear simulation response of the system is shown in Figure (10). The autopilot was commanded to develop a 25g acceleration response, and as expected the controller performs very well.

9.0 SUMMARY

Design for robust performance and stability requires, at a minimum, that the designer:

1. define a nominal model of the plant to be controlled,
2. define an uncertainty structure to characterize a family of plants in which it is anticipated that the real plant resides, and
3. express performance goals with normalized exogenous inputs and frequency weighted errors.

Use of a synthesis procedure, such as μ-synthesis, which preserves the structural relationship between uncertainties and performance elements, in the interconnection structure, is essential. Failure to account for this structured relationship may lead to overly conservative specifications and poor designs.

REFERENCES

1. J.C. Doyle, K. Glover, P. Khargonekar and B.A. Frances, "State-space Solutions to Standard H_2 and H_∞ Control Problems," ACC, Atlanta, GA, June 1988.
2. K. Glover, and J.C. Doyle, "State Space Formula for all Stabilizing Controllers that Satisfy an H-infinity Norm Bound and Relations to Risk Sensitivity", Systems and Control Letters, Vol 11, 1988.
3. G. Stein, "Beyond Singular Values and Loop Shapes," to appear AIAA Journal of Guidance and Control.
4. M. Safonov, and D. Limebeer, "Simplifying the H-infinity Theory via Loop Shifting," IEEE CDC Proceedings, 1988.
5. J.C. Doyle, "Performance and Robustness Analysis for Structured Uncertainty," IEEE CDC Proceedings, 1982.
6. J.C. Doyle, "Structured Uncertainty in Control System Design," IEEE CDC Proceedings, 1985.
7. B.A. Francis, "A course in H_∞ Control Theory," Springer-Verlag, Berlin, 1987.
8. "MUSYN Robust Control Short Course Notes and Software," September 1989, Arcadia CA.
9. R.Y. Chiang, and M.G. Safonov, "Robust-Control Toolbox for use with MATLAB and the Control System Toolbox", The Mathworks Inc.
10. A. Packard and J.C. Doyle, "Robust Control of Multivariable and Large Scale Systems", Honeywell SRC Final Technical Report, prepared for AFOSR, March 1988.
11. G.J. Balas and J.C. Doyle, "Robustness and Performance Tradeoffs in Control Design for Flexible Structures", submitted to IEEE CDC 1990.

Figure 1a. General Structure

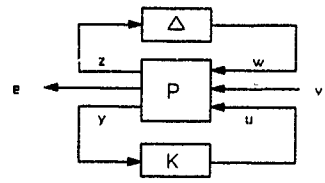

Figure 1b. Analysis

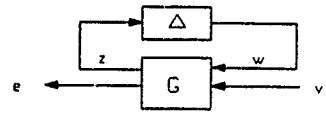

Figure 1c. Synthesis

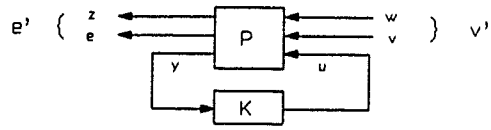

Figure 2. H_∞ Robust Stabilization

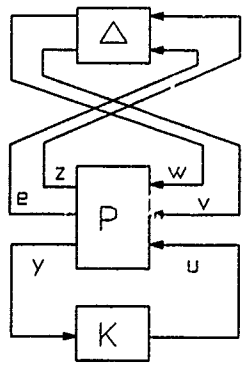

Figure 3. Tail-Controlled Missile Problem

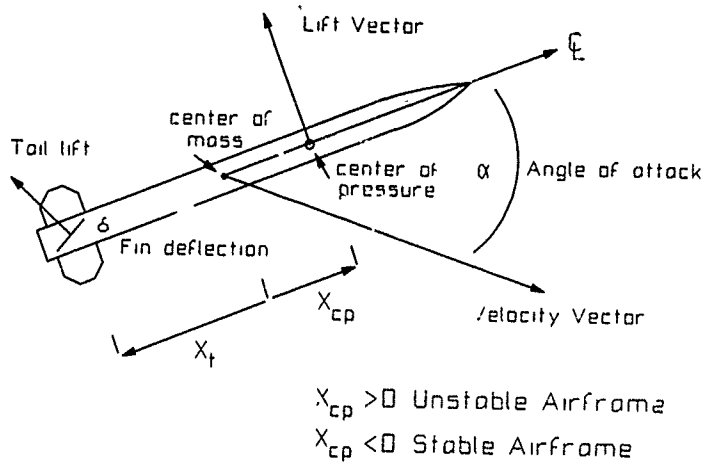

Figure 4. Structured Uncertainty Model

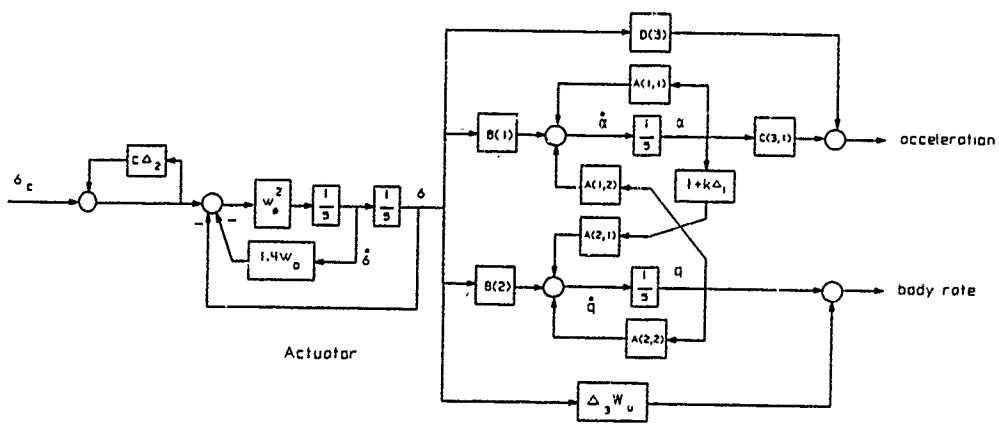

Figure 5. Unmodelled Flexible Mode Dynamics and Weighting Function

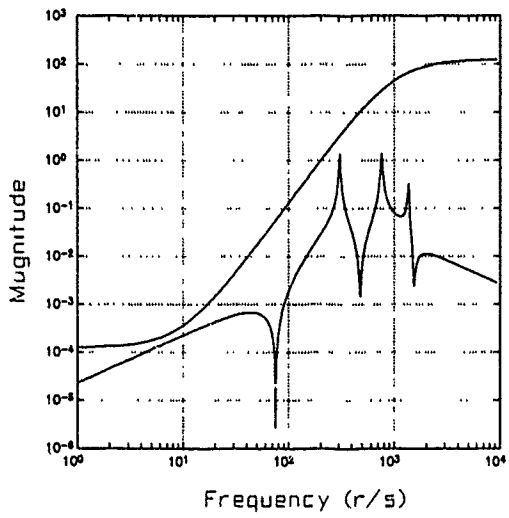

Figure 6. Interconnection Structure Input/Output Diagram

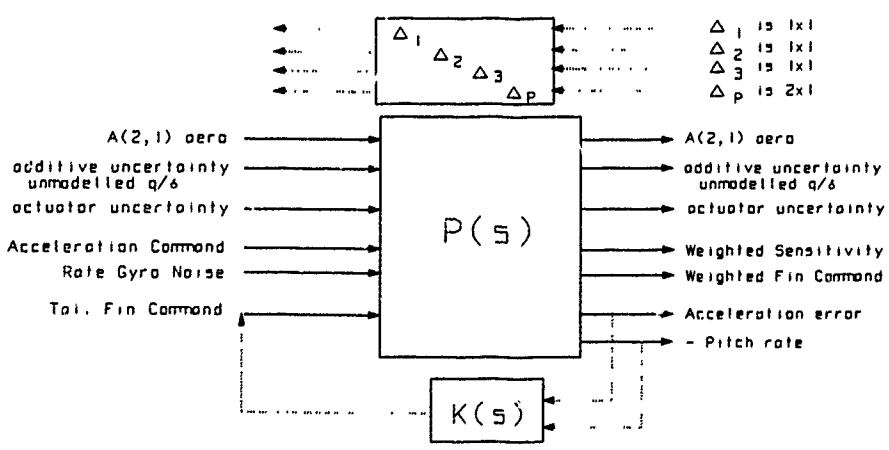

Figure 7. H_∞ Optimal-Performance Design

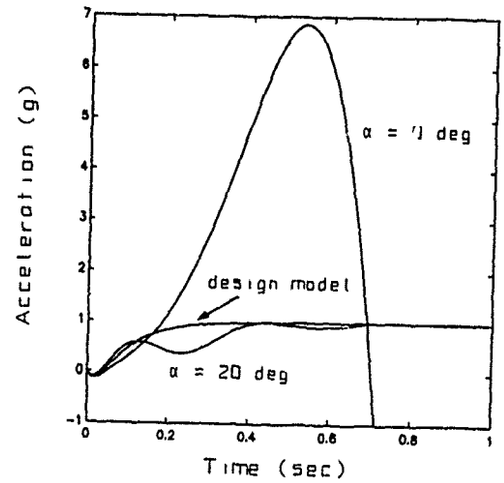

Figure 8. H_∞ Robust-Stabilization Design

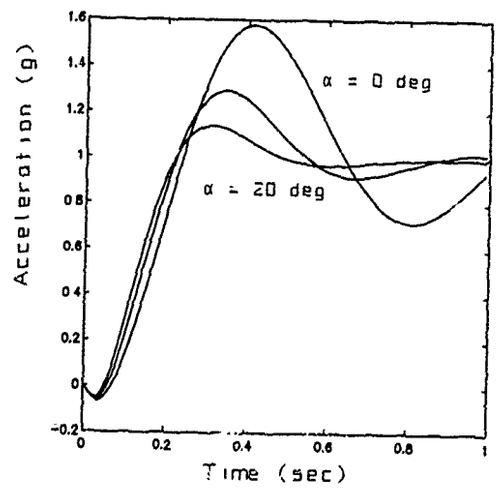

Figure 9. μ-Synthesis Design

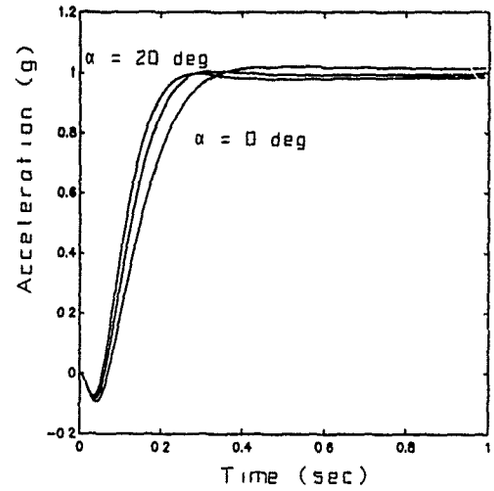

Figure 10. Nonlinear Simulation Response
μ-Synthesis Design

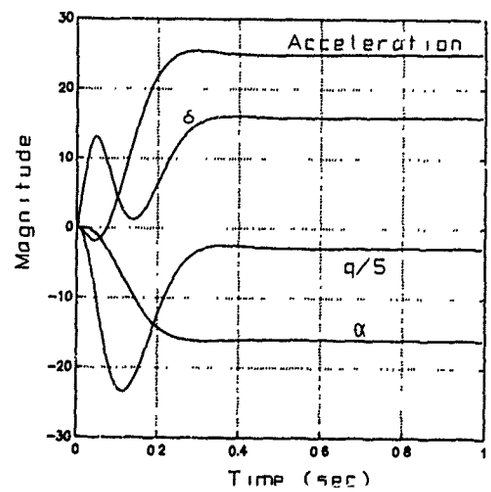

MIDCOURSE GUIDANCE TECHNIQUES FOR ADVANCED TACTICAL MISSILE SYSTEMS

by

Ulrich Hartmann
Bodenseewerk Geratetechnik GmbH
Intelligent Systems Division
Postfach 10 11 55
D-7770 Uberlingen
Germany

Summary

Midcourse Guidance Techniques can significantly improve operational aspects as well as overall performance of tactical missile systems. Operational requirements such as conformal carriage in case of air-to-air-missiles or canister launch in case of ship-based systems can only be met by a lock-after-launch capability of the guidance system. On the other hand, seeker acquisition ranges may not be able to match the kinematic capabilities of the missile for a variety of reasons which may include adverse weather conditions and counter-measures.

The paper addresses a number of operational aspects relevant to the design of midcourse guidance systems and the essential prerequisites for their application. Basic options of midcourse guidance, such as pure inertial, updated inertial and aided inertial as well as the fundamental elements including inertial navigation and target prediction are discussed. Proper initialization and alignment of the guidance and navigation system are presented as further key issues. The alignment problem is defined and a number of methods to achieve adequate alignment are described.

The paper concludes with a review of different techniques for the performance assessment and the most important performance criteria for handover from midcourse to terminal guidance.

1. INTRODUCTION

1.1 Background

Most of the missile systems which are currently in service and which became operational in the 70's and early 80's rely on lock-before launch or require target radar illumination during the full flight time or at least a significant part of it. Among the few exceptions are long-range missiles such as sea-skimmers which make use of inertial midcourse guidance techniques during most of the flight before active radar homing takes place in the terminal flight phase.

The operational requirements for advanced missile systems which are now in various development phases ranging between feasibility and full scale development ask however for features such as

- fire and forget or launch and leave in connection with long firing ranges
- the simultaneous engagement of several targets
- the capability to cope with natural or man made obstacles temporarily obstructing the line of sight
- the capability to acquire and track targets with very small Radar or IR-signatures in connection with various countermeasures.

Inertial guidance techniques are very useful to support technical solutions to meet these requirements. The basic technologies of inertial guidance are known since World War II and have been reviewed in several papers and publications (/1/ to /4/). However, for many years the hardware realization of inertial guidance was expensive and required significant mass and volume, which was prohibitive for relatively small tactical missiles. An overview of the technology available in the early 60's is presented in /5/.

This situation has changed drastically since strapdown inertial systems are available (/6/, /7/). Advanced sensor technologies in connection with highly integrated digital electronics allow the construction of cost-effective Inertial Navigation Units (INU) within the mass and volume constraints of even small tactical missiles. The performance of these INU's is however only partly determined by the accuracy of the inertial sensors and the associated signal processing. Other important design parameters are the methods used to align and to aid the INU. There is a variety of possibilities to aid the INU which may include the usage of the radar of the launch vehicle, the determination of position fixes using image processing or satellite navigation techniques (GPS). Finally, the design of the INU is a trade-off between the accuracy of the sensors and the signal processing, the alignment and the aiding techniques used. Fig. 1.1 shows the basic INU definition chosen for this paper.

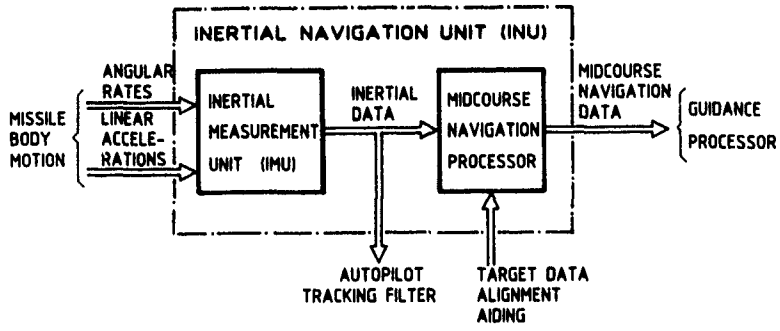

Fig. 1.1 Definition of a Missile INU

1.2 Operational Aspects

Whilst the actual implementation of a midcourse guidance system is very much dependent on the special application, there are a number of common fundamental operational aspects which must be considered in the early design stage of every project.

- Successful use of midcourse guidance depends on the capability of target detection and identification typically over a range which is significantly longer than the acquisition range of the missile seeker. The detection range itself, the angular accuracy of the line-of-sight (LOS) measurements and the data which can be provided by the target acquisition system are of crucial importance for the design.

  In cases where active Radars are used for target detection (valid for most applications) the data in general include range and bearing (azimuth and elevation) measurements. Additionally the radar signal processing may provide estimates of the LOS-rate, the target velocity vector or even estimates of target acceleration.

  However, midcourse guidance techniques may also be of interest in cases where the target can only be detected by passive means, e.g. Radar Warning Receivers (RWR) or Forward Looking Infra-Red (FLIR)-Systems. Measured range data cannot be provided by these sensors, however it may be possible to generate range estimates for certain engagement conditions, if the sensor offers sufficient pointing accuracy and resolution.

- Midcourse guidance is always based on an INU on board the missile. This leads to the requirement to transfer target designation data from the launch vehicle to the missile and to initialize the missile INU properly. Therefore the angular orientation of the Inertial Measurement Unit (IMU) of the missile with respect to the reference system of the launch vehicle must be known or determined by a process called alignment.

  In case of ground based systems, where the missiles are stored in fixed containers, it is possible to complete this alignment process at any time after missile installation and to store the transformation matrices within the INU. The alignment process may be more complicated in cases where the missile is launched from a moving vehicle like an aircraft or ship. Vehicles are normally subjected to structural deformations caused by maneuver loads and environmental effects and therefore it may be necessary to execute a fast "dynamic" alignment immediately before missile launch.

  The accuracy which can be obtained as a result of the alignment process for a given time depends heavily on the motion of the vehicle - which influences the observability of the misalignment angles - ,the vibration levels and the quality of the inertial sensors. The alignment method is therefore closely related to the overall performance requirements (e.g. missile reaction time) and to the total error budget of the INU.

- The necessity of data links between the target detection and tracking device and the missile depends on the duration of midcourse guidance and the agility of the target. For short guidance times or stationary targets it is possible to rely on pure inertial guidance which is fully compatible with the operational requirement for "fire and forget". In case of stationary targets <u>and</u> longer midcourse guidance phases (in the order of a minute) it can be advantageous and cost-effective to update the INU by position data obtained by independent sensors. This may be a GPS (Global Positioning System) receiver which allows frequent and accurate position fixes or an imaging sensor, which determines the deviation of landmarks from their INU computed location by passive (preferably) or active means.

For agile targets and longer midcourse guidance phases it is inevitable to update the target position in order to guide the missile into a reasonable acquisition basket for terminal homing. This requires a data link between the missile and the target tracker. The moderate update rate requirements (in the order of 1 Hz or less) allow still the engagement of multiple targets. If a data link exists, it can also be used to aid the missile INU and to remove residual alignment errors. However, it should be observed that in this case the guidance system is no longer completely autonomous.

The typical flight phases of the missile are shown in Fig. 1.2. The missile can be launched after proper alignment and initialisation. The launch phase is finished when a safe separation from the launch vehicle is achieved and the guidance commands can be applied. The major optimization criteria for the midcourse guidance laws aim at favourable conditions for seeker lock-on (handover) and terminal guidance (zero effort miss). Finally small missdistance and high lethality are the performance criteria to be met by the terminal guidance system.

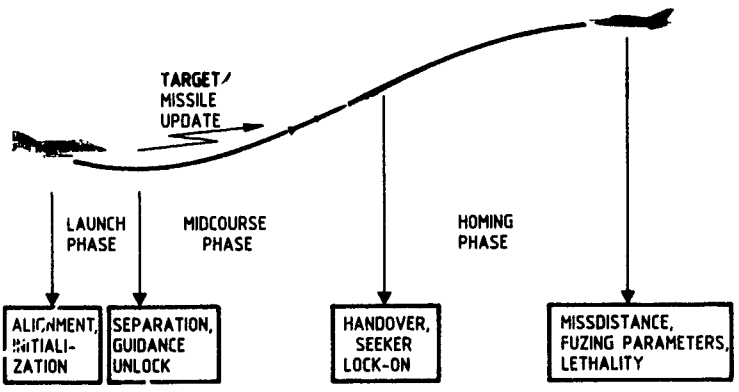

Fig. 1.2 Typical Missile Flight Phases and Optimization Criteria

2. MIDCOURSE GUIDANCE TECHNIQUES

2.1 General Requirements

As indicated in Fig. 1.2 the general objective for the midcourse guidance phase is to optimize the hand-over conditions for the seeker guided terminal phase. These are strongly influenced by the operational scenario and the seeker design, i.e. as an example they will be much different for an anti-radiation missile, for a radar-guided anti-sea-skimmer missile ore an IR-guided short-range air-to-air-missile. However, in practice the desired handover conditions are degraded by two error groups which can be summarized as follows:

Navigation dependent errors.

In general, the navigation errors are under the responsibility and the control of the missile guidance system design authority. They include attitude, velocity and position errors. Attitude and position errors have an impact on the seeker field-of-view (FOV) requirements during acquisition. In case of radar seekers velocity errors contribute to errors of the expected Doppler frequency and may increase acquisition time as the consequence. These errors should not contribute in a significant way to the line-of-sight error due to the target uncertainty in position and velocity.

Scenario dependent errors.

These errors are usually specified parameters for the missile designer. They include errors of the fire control or target designation system and the target maneuver uncertainty They depend also on the availability of a data link from the launch vehicle to the missile.

The effects of these errors can be judged by two criteria which are of major importance for the design of the guidance system.

The seeker error angle as shown in a simple sketch in Fig. 2.1 is a measure of the required seeker FOV at lock-on. It depends obviously not only on the missile attitude error $\Delta\Psi$ but additionally on the cross-range position error and the seeker acquisition range R_A which is strongly influenced by the scenario.

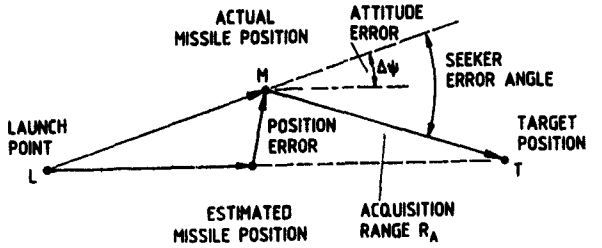

Fig. 2.1 Definition of Seeker Error Angle

<u>Zero-effort-miss</u> is an indicator of the overall performance of the midcourse guidance system and a measure for the terminal maneuver requirements, necessary to reduce miss-distance down to acceptable levels for the endgame. Zero-effort-miss is defined as the miss-distance which must be expected when target and missile continue their flight path after lock-on without any maneuver. Following the definitions of Fig. 2.2 zero-effort-miss is defined by

$$|\underline{R}_{ZEM}| = \frac{|\underline{R}_{MT}|^2}{|\underline{V}_r|} \, |\dot{\underline{\sigma}}| \tag{2.1}$$

where the relative velocity is given by

$$\underline{V}_r = \underline{V}_T - \underline{V}_M \tag{2.2}$$

and the LOS-rate by

$$\dot{\underline{\sigma}} = \frac{\underline{R}_{MT} \times \underline{V}_r}{|\underline{R}_{MT}|^2} \tag{2.3}$$

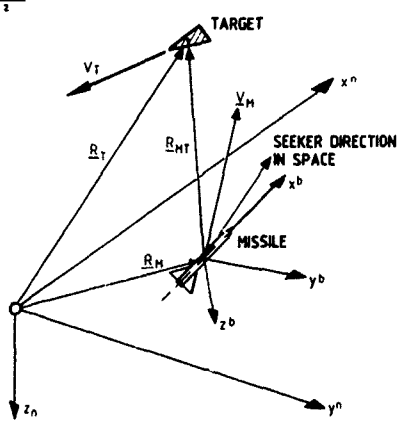

Fig. 2.2 Missile-Target Relative Geometry

2.2 Guidance Options and Principles

2.2.1 Basic Options

A number of guidance options are available dependent on the information supplied prelaunch or after launch. These options may be categorized in the following groupings:

- Pure inertial guidance.

  The target information is only supplied up to the instant of missile launch and no data link exists during the remainder of the flight. This approach meets the "fire and forget" requirement. However, it is only applicable for stationary targets or short flight times in case of maneuvering targets.
  The latter case puts also challenging requirements on the seeker design as the target uncertainty can only be overcome by large fields-of-view (FOV), long acquisition ranges and short acquisition times. On the other hand, if the target uncertainty becomes the dominant error it may be possible to get away with fairly simple in-flight alignment procedures (see Section 3) and possibly low grade inertial sensors.

- Updated inertial guidance.

  The midcourse guidance system is updated in regular intervals with respect to the target state, i.e. target position, velocity or even acceleration. Therefore the target uncertainty is limited to much lower values which obviously depend on the update rate and the measurement accuracy of the target tracking system. On the other hand this is no longer a "fire and forget" approach as an ongoing tracking of (multiple) targets and a data link is necessary. A medium to high grade inertial sensor package and proper in-flight alignment is required in order to match the reduced level of target uncertainty.

- Aided inertial guidance.

  In addition to the target state the data link provides information on the actual missile position, i.e. the radar has to track the target and the own missile simultaneously which leads to a further increase of the tracking system load. However, this method offers a number of advantages which may be quite attractive from an overall systems point of view.

  Firstly, the need for an accurate preflight alignment of the missile INU can be abandoned. As the target and the missile are tracked by the same system, it is possible to estimate and to remove the initial alignment error successfully as will be shown later (Section 2.2.5). This can lead to significant reductions in reaction time.

  Secondly, a continuous update of target position allows the use of medium grade inertial sensors as the guidance system relies on inertial guidance only during the relatively short update intervals on inertial guidance.

  Thirdly, as the target and the own missile position are well known, it may be possible to reduce the seeker requirements with respect to FOV and acquisition range. This can be crucial for an employment of the system in adverse conditions.

2.2.2 Elements of Midcourse Guidance

A general block diagram of an overall missile guidance system including midcourse guidance functions is shown in Fig. 2.3. The lower part of the block diagram shows the basic functions of seeker guided missiles. There is a large variety of practical realizations ranging from infra-red missiles to radar missiles with passive and active seekers which shall not be addressed in this paper. As a common aspect of all these designs, the midcourse guidance system leads to a significant extension of the operational capabilities of the missile in situations where the seeker is not able to acquire or to track a target. It is therefore quite evident, that the INU has to fit into the overall guidance concept and to provide predicted guidance information when no seeker track is available. In this function the INU provides the necessary inputs to guide the missile as well as the seeker control demands.

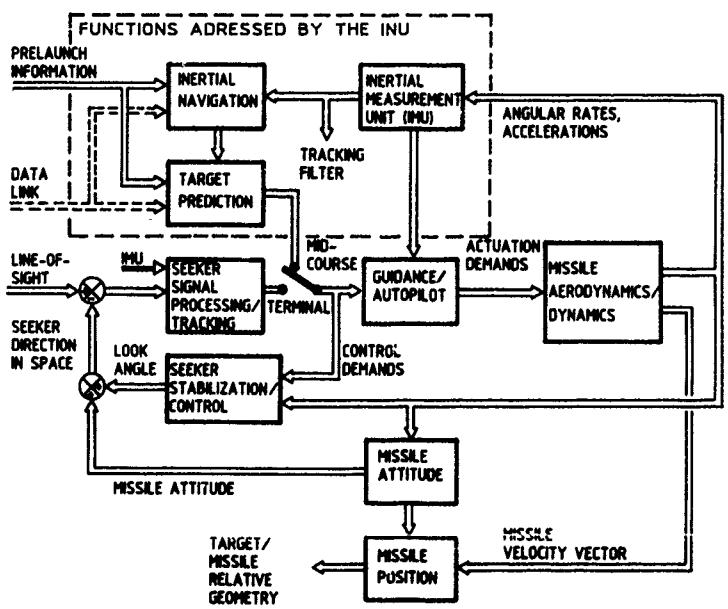

Fig. 2.3 General Guidance System Block Diagram

There are three major functional blocks within the missile INU (Fig. 2.3) which can be characterized as the Target Prediction Block, the Inertial Navigation Block and the Inertial Measurement Unit (IMU).

The guidance laws used during the midcourse phase are specially designed for each application. For example in one case it may be required to apply an altitude hold mode in the vertical plane and pursuit guidance in the horizontal plane. In others it may be desirable to carry out a pop-up maneuver in the vertical plane or to use an optimal guidance law in both steering axes.

In the following sections the basic elements which provide the necessary information for midcourse guidance will be discussed and no attempt will be made to review the broad variety of possible guidance laws (e.g. /8/). These basic elements considered to be essential for midcourse guidance are the information about

- the own attitude, acceleration, velocity and position
- the predicted target acceleration, velocity and position.

Based on that information it is straightforward to derive range, range-rate (closing velocity), sightline spin and LOS-direction with respect to the missile (i.e. the seeker look angle demands).

In general it shall be assumed that the target tracking system is able to provide at least up to the instant of launch the following information with respect to a reference frame:

- LOS direction in space
- LOS rate
- Range and range rate
- Target acceleration.

In most airborne, shipborne or ground-based tactical air-defense systems the target is detected and allocated with respect to a tangent frame, which is defined as an earth-fixed frame, aligned with a geographic frame at a fixed location on the earth, usually the missile launch point (/9/). The geographic frame is aligned with the north, east and down directions.

The problems of target tracking which are closely related to target prediction and state estimation have been discussed extensively in the literature (e.g. /10/ to /13/). It should be noted that it is not always possible to generate the complete set of information; e.g. if the target tracking system does not provide range data, there is no way to predict target range during midcourse. In cases where the information provided by the tracking system is incomplete, it is necessary to replace the missing data by reasonable assumptions. This, however, can lead to a significant degradation of the target prediction accuracy after launch. The target tracking system is therefore an important and limiting factor of midcourse guidance.

2.2.3 Target Prediction

In general target track data are provided in spherical coordinates (see Fig. 2.4), i.e. the LOS-frame (l). These data can be processed for target prediction in two different ways

- The range data and derivatives (R, $\dot{R}$, $\ddot{R}$) and the sightline spin data and derivatives ($q_{\parallel}$, $\dot{q}_{\parallel}$, $r_{\parallel}$, $\dot{r}_{\parallel}$) can be converted to equivalent data in the rectangular tangent frame. The flight path is then predicted in the tangent frame. This may offer the opportunity to make better use of some known a-priori information on the target characteristics.

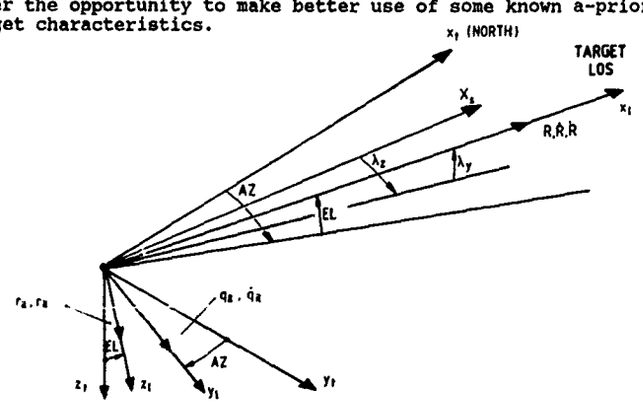

Fig. 2.4 Definition of Tracking Parameters

- Target prediction is continued in the LOS-system, where the motion of the missile after launch is taken into account.

The target prediction algorithm is highly nonlinear in both cases and must be initialized before missile launch. It may be updated via the data link. The algorithm itself depends on the type of target (e.g. aircraft, missile, ship, tank) and has to be adapted in accordance with the data available from the fire control system.

The problem is illustrated in Fig. 2.5 where an estimated target position at time $t = t_o$ (launch) has to be predicted for $t = t_k$. This can be achieved by extrapolating a kinematic model of the target. For example, the kinematic equations can be formulated with respect to a path-fixed frame (superscript k)

$$\dot{\underline{v}}_T^k + \underline{\omega}_{ik}^k \times \underline{v}_T^k = \underline{a}_T^k \tag{2.4}$$

where the target acceleration is modeled as a first order stochastic process with known variance

$$\frac{d\underline{a}_T^k}{dt} = \underline{A}_T\, \underline{a}_T^k + \underline{w}_T \tag{2.5}$$

The target velocity vector is then transformed to a reference frame t

$$\underline{v}_T^t = \underline{c}_k^t\, \underline{v}_T^k \tag{2.6}$$

and position is determined by integration

$$\underline{R}_T^t = \int_{t_o}^{t_k} \underline{v}_T^t\, dt + \underline{R}_T\,(t_o) \tag{2.7}$$

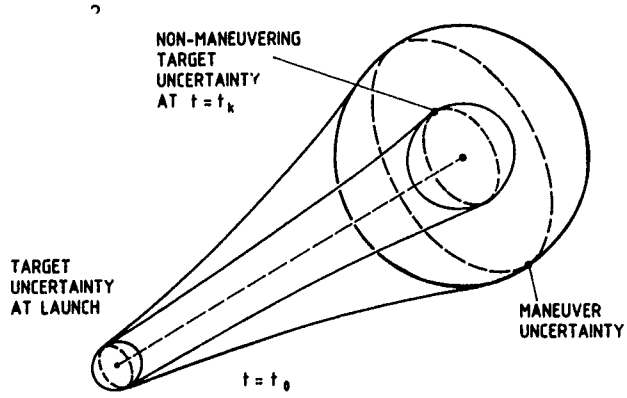

Fig. 2.5 Uncertainties of Target Prediction

The following definitions are used in Eqs. (2.4 to 2.6)

$$\underline{v}_T^k = (V_T,\ 0,\ 0) \tag{2.8}$$

$$\underline{\omega}_{ik}^k = (-s_\gamma \dot{\chi},\ \dot{\gamma},\ c_\gamma \dot{\chi}) \tag{2.9}$$

$$\underline{c}_k^t = \begin{bmatrix} c_\gamma c_\chi & -s_\chi & s_\gamma c_\chi \\ c_\gamma s_\chi & c_\chi & s_\gamma s_\chi \\ -s_\gamma & 0 & c_\gamma \end{bmatrix} \tag{2.10}$$

with $s_\gamma = \sin\gamma$, $c_\gamma = \cos\gamma$ etc.

Eqs. (2.4) to (2.7) can be combined to a nonlinear, time-variant 9th-order state equation, which can be used to predict target position. As the missile position $\underline{R}_M$ and velocity $\underline{V}_M$ is known from the navigation calculations, it is possible to determine the relative geometry and the necessary guidance and seeker pointing demands.

The LOS rate is given in the tangent frame by

$$\underline{\omega}^t_{LS} = (\underline{R}^t_{MT} \times \underline{v}^t_{MT})/|\underline{R}^t_{MT}|, \tag{2.11}$$

where the LOS and relative velocity are defined by

$$\underline{R}^t_{MT} = \underline{R}^t_T - \underline{R}^t_M \tag{2.12}$$

and

$$\underline{v}^t_{MT} = \underline{v}^t_T - \underline{v}^t_M \quad . \tag{2.13}$$

The direction cosine-matrix (DCM) $\underline{C}^s_t$, computed by the navigation algorithms (Section 2.2.4) is then used to transform the LOS-unity vector $\hat{R}_{MT}$ and the LOS-rate to missile body axes (superscript s)

$$\underline{\omega}^s_{LS} = \underline{C}^s_t \, \underline{\omega}^t_{LS} \tag{2.14}$$

$$\hat{\underline{R}}^s_{MT} = \underline{C}^s_t \, \hat{\underline{R}}^t_{MT} \tag{2.15}$$

where they are required to determine the guidance demands. The look angle demands of the seeker can be calculated from the LOS unity vector

$$\hat{\underline{R}}^s_{MT} = \underline{C}^s_1 \begin{bmatrix} 1 \\ 0 \\ 0 \end{bmatrix} , \tag{2.16}$$

where $\underline{C}^s_1$ is defined as the LOS to missile body DCM (see Eq. 2.27).
The cartesian look angles are obtained from

$$\lambda_y = \sin^{-1} (\hat{R}^s_{MT,z}) \tag{2.17}$$

$$\lambda_z = \tan^{-1} (\hat{R}^s_{MT,y}/\hat{R}^s_{MT,x}) \tag{2.18}$$

Alternatively it may be appropriate to predict the relative geometry directly, due to the fact that target measurements are usually provided in relative LOS-coordinates. To predict the line-of-sight (see Fig. 2.2) we use the 2nd derivative of the LOS-vector

$$\frac{d^2}{dt^2} \underline{R}_{MT|i} = \underline{a}_T - \underline{a}_M = \frac{d^2}{dt^2} \underline{R}_{MT|1} + \dot{\underline{\omega}}_{i1} \times \underline{R}_{MT} + 2(\underline{\omega}_{i1} \times \frac{d}{dt} \underline{R}_{MT|1}) + \underline{\omega}_{i1} \times (\underline{\omega}_{i1} \times \underline{R}_{MT}) \tag{2.19}$$

where $|i$ denotes the derivative with respect to the inertial frame and $|1$ with respect to the LOS-frame, $\underline{a}_M$ the missile acceleration, and $\underline{\omega}_{i1} = (p_{i1}, q_{i1}, r_{i1})$ defines the angular rate vector of the LOS with respect to the LOS-frame.

If Eq. (2.19) is resolved into its components with respect to the pointing system, we obtain with $R^1_{MT} = (R_{MT}, 0, 0)$

$$\begin{aligned} \ddot{R}_{MT} &= a^1_{Tx} - a^1_{Mx} + R_{MT} (q^2_{i1} + r^2_{i1}) \\ \dot{q}_{i1} &= -\frac{1}{R_{MT}} (a^1_{Tz} - a^1_{Mz} + 2q_{i1} \dot{R}_{MT}) + p_{i1} r_{i1} \\ \dot{r}_{i1} &= \frac{1}{R_{MT}} (a^1_{Ty} - a^1_{My} - 2r_{i1} \dot{R}_{MT}) - p_{i1} q_{i1} \end{aligned} \tag{2.20}$$

Eq. (2.20) and the target model (2.5) can be combined to form a nonlinear, time-variant state equation

$$\frac{d}{dt} \begin{bmatrix} a^1_{Tx} \\ a^1_{Ty} \\ a^1_{Tz} \\ R_{MT} \\ \dot{R}_{MT} \\ q_{i1} \\ r_{i1} \end{bmatrix} = \left[\begin{array}{ccc:cccc} & A_T & & & \underline{0} & & \\ \hline 0 & 0 & 0 & 0 & 1 & 0 & 0 \\ 1 & 0 & 0 & (q^2_{i1}+r^2_{i1}) & 0 & 0 & 0 \\ 0 & 0 & -1/R_{MT} & 0 & 0 & -2/t_{go} & p_{i1} \\ 0 & 1/R_{MT} & 0 & 0 & 0 & -p_{i1} & -2/t_{go} \end{array}\right] \underline{x} + \left[\begin{array}{c} \underline{0} \\ \hline 0 \\ -a^1_{Mx} \\ a^1_{Mz}/R_{MT} \\ -a^1_{My}/R_{MT} \end{array}\right] \tag{2.21}$$

In the state equation (2.21) the following definition is used for the time-to-go

$$t_{go} = \frac{R_{MT}}{\dot{R}_{MT|1}} \tag{2.22}$$

and the LOS-roll rate p_{i1} is obtained from

$$\underline{\omega}^{1}_{i1} = \underline{C}^{1}_{s}\,\underline{\omega}^{s}_{is} + \underline{\omega}^{1}_{s1} \tag{2.23}$$

where

$$\underline{\omega}^{s}_{is} = (p_{is},\ q_{is},\ r_{is}) \tag{2.24}$$

is the measured angular rate of the missile and $\underline{\omega}_{s1}$ is the relative rotation rate of the LOS with respect to the missile, given by

$$\underline{\omega}^{1}_{s1} = (-s_{1y}\,\dot{\lambda}_z,\ \dot{\lambda}_y,\ c_{1y}\,\dot{\lambda}_z) \tag{2.25}$$

From Eqs. (2.23) through (2.25) we obtain

$$p_{i1} = \frac{1}{c_{1y}}\,(p_{is}\,c_{1z} + q_{is}\,s_{1z} - r_{i1}\,s_{1y}) \tag{2.26}$$

with $s_{1y} = \sin(\lambda_y)$, $c_{1y} = \cos(\lambda_y)$ etc.

The transformation matrix

$$\underline{C}^{1}_{s} = \begin{bmatrix} c_{1z}\ c_{1y} & \vdots & c_{1y}\ s_{1z} & \vdots & -s_{1y} \\ -s_{1z} & \vdots & c_{1z} & \vdots & 0 \\ s_{1y}\ c_{1z} & \vdots & s_{1y}\ s_{1z} & \vdots & c_{1y} \end{bmatrix} \tag{2.27}$$

which is also required to transform the measured missile acceleration

$$\underline{a}^{1}_{s} = \underline{C}^{1}_{s}\,\underline{a}^{s}_{s} \tag{2.28}$$

must be initialized properly at missile launch. $\underline{C}^{1}_{s}$ can be updated by directly integrating the look angle rates

$$\begin{aligned} \lambda_y(t) &= \int (q_{i1} + p_{is}\,s_{1z} - q_{is}\,c_{1z})\,dt + \lambda_y\,(t=0) \\ \lambda_z(t) &= \int \frac{(r_{i1} - p_{is}\,c_{1z}\,s_{1y} - q s_{1z}\,s_{1y} - r c_{1y})}{c_{1y}}\,dt + \lambda_z\,(t=0) \end{aligned} \tag{2.29}$$

which can also be considered as an augmentation of the state vector of Eq. (2.21). Eqs. (2.21), (2.26), (2.28), and (2.29) form a highly nonlinear set of 9 state equations

$$\underline{x}(t) = \underline{A}(\underline{x}(t), t)$$

which can be used to predict all relevant guidance parameters.

2.2.4 Inertial Navigation

The missile navigates with respect to a tangent frame which is an earth-fixed frame with its origin typically at the missile launch point. By definition it rotates with an angular rate identical to the earth rate with respect to inertial axes. In contrast to the local geographic frame used in many applications of terrestrial navigation, the angular rate resulting from vehicle motion is not involved in the navigation algorithms. The x-axis of the tangent frame may be north oriented, but other orientations given by the target system (e.g. towards the LOS) may be possible as well.

A block diagram of the navigation system is shown in Fig. 2.6. The specific force vector in coordinates of the tangent frame (/9/) is given by

$$\underline{f}^{t} = \underline{C}^{t}_{i}\,\underline{r}^{i} - \underline{g}^{t} \tag{2.30}$$

where $\underline{G}$ is the gravity acceleration at the missile position, resolved in tangent frame axes and $\underline{r}^i$ is the missile position vector with respect to an earth-centered, inertial frame. The velocity with respect to the tangent frame can be defined as

$$\underline{v}^t \doteq \underline{C}_e^t \cdot \dot{\underline{r}}^e \tag{2.31}$$

The specific force vector can then be expressed as

$$\underline{f}^t = \underline{v}^t + 2\underline{\Omega}_{ie}^t \, \underline{v}^t - \underline{g}^t \quad , \tag{2.32}$$

where $\underline{\Omega}_{ie}^t$ is the skew-symmetric rotation matrix (L_o = geographic latitude at origin of tangent plane, ω_{ie} = angular rate of the earth)

$$\underline{\Omega}_{ie}^t = \begin{bmatrix} 0 & : \omega_{ie} \sin L_o & : 0 \\ -\omega_{ie} \sin L_o & : 0 & : -\omega_{ie} \cos L_o \\ 0 & : \omega_{ie} \cos L_o & : 0 \end{bmatrix} \tag{2.33}$$

and

$$\underline{g}^t = \underline{G}^t - \underline{C}_i^t \; \underline{\Omega}_{ie}^i \, \underline{\Omega}_{ie}^i \, \underline{r}^i \tag{2.34}$$

which combines the effects of gravity and centrifugal acceleration. (Eq. 2.34) depends only on the actual location of the missile and can be simplified for a homogenous, spherical earth and a north-oriented tangent frame to

$$\underline{g}^t = \frac{g_o \, r_E^2}{(r_E + h)^2} \begin{bmatrix} -\Delta L \\ -\Delta l \cos L_o \\ 1 \end{bmatrix} \tag{2.35}$$

It should be noted that the direction of the gravity vector changes in t-coordinates during flight and ΔL, Δl are the (small) changes in terrestrial latitude and longitude respectively.

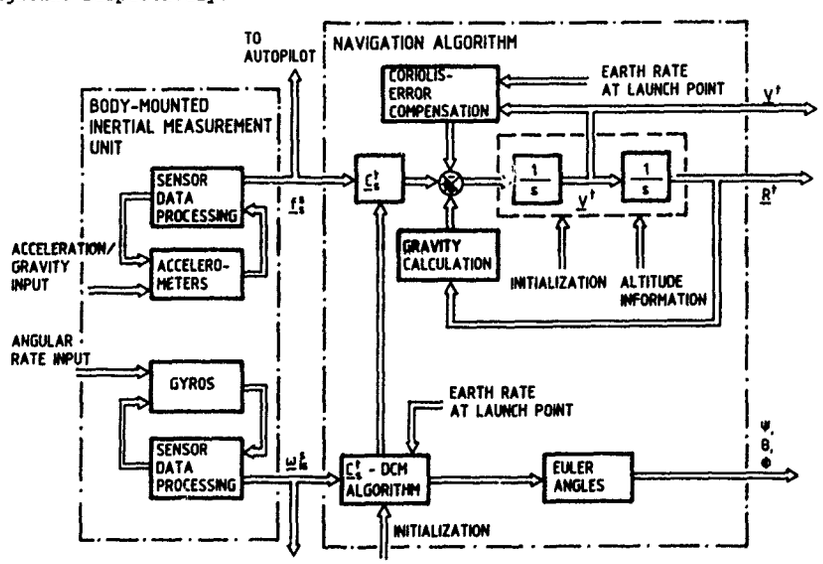

Fig. 2.6 Strapdown Navigation in Tangent-Frame Coordinates

The most important issue in strapdown navigation is the determination of the transformation matrix $\underline{C}_s^t$, which converts the acceleration measurements from sensor axes (s) to the tangent frame. Different methods have been investigated with respect to numerical efficiency and accuracy when strapdown navigation became a feasible technology (e.g. /14/, /15/, /16/, /17/). As a standard method the quaternion updating algorithm shall be summarized briefly.

A quaternion is defined as a scalar q_o and a vector with orthogonal components

$$Q = q_o + q_1 \underline{i} + q_2 \underline{j} + q_3 \underline{k} \tag{2.36}$$

The elements of the quaternion are initialized with the Euler angles Ψ_L, θ_L, ϕ_L at launch

$$
\begin{aligned}
q_o &= \cos\frac{\Psi_L}{2}\cos\frac{\theta_L}{2}\cos\frac{\phi_L}{2} + \sin\frac{\Psi_L}{2}\sin\frac{\theta_L}{2}\sin\frac{\phi_L}{2} \\
q_1 &= \cos\frac{\Psi_L}{2}\cos\frac{\theta_L}{2}\sin\frac{\phi_L}{2} - \sin\frac{\Psi_L}{2}\sin\frac{\theta_L}{2}\cos\frac{\phi_L}{2} \\
q_2 &= \cos\frac{\Psi_L}{2}\sin\frac{\theta_L}{2}\cos\frac{\phi_L}{2} + \sin\frac{\Psi_L}{2}\cos\frac{\theta_L}{2}\sin\frac{\phi_L}{2} \\
q_3 &= \sin\frac{\Psi_L}{2}\cos\frac{\theta_L}{2}\cos\frac{\phi_L}{2} - \cos\frac{\Psi_L}{2}\sin\frac{\theta_L}{2}\sin\frac{\phi_L}{2}
\end{aligned}
\tag{2.37}
$$

and updated during flight based on the quaternion differential equation

$$
\dot{\underline{q}} = \begin{bmatrix} q_o \\ q_1 \\ q_2 \\ q_3 \end{bmatrix} = \frac{1}{2}\begin{bmatrix} -q_1 & -q_2 & -q_3 \\ q_o & -q_3 & q_2 \\ q_3 & q_o & -q_1 \\ -q_2 & q_1 & q_o \end{bmatrix} \underline{\omega}^{s}_{ts} \tag{2.38}
$$

where $\underline{\omega}^{s}_{ts} = (p_{ts}, q_{ts}, r_{ts})$ is the body rate vector in sensor axes with respect to the tangent frame.

In cases where the rotation rate of the tangent frame must be taken into account

$$\underline{\omega}_{ts} = \underline{\omega}_{is} - \underline{\omega}_{it} \quad ,$$

Eq. (2.38) can be modified to

$$
\dot{\underline{q}} = \frac{1}{2}\begin{bmatrix} -q_1 & -q_2 & -q_3 \\ q_o & -q_3 & q_2 \\ q_3 & q_o & -q_1 \\ -q_2 & q_1 & q_o \end{bmatrix} \underline{\omega}^{s}_{is} - \frac{1}{2}\begin{bmatrix} q_1 & q_2 & q_3 \\ q_o & q_3 & q_2 \\ -q_3 & q_o & q_1 \\ q_2 & -q_1 & q_o \end{bmatrix} \underline{\omega}^{t}_{it} \tag{2.39}
$$

where $\underline{\omega}^{t}_{it}$ is a <u>constant</u> vector for a given launch latitude L_o

$$\underline{\omega}^{t}_{it} = (\omega_{ie}\cos L_o,\ 0,\ -\omega_{ie}\sin L_o) \tag{2.40}$$

As strapdown inertial systems are implemented in discrete time, it is necessary to develop discrete time versions of Eq. (2.39). For this purpose, it is a common approach to expand the quaternions and the measured angular increments into power series (Taylor's series)

$$\underline{q}_{k+1} = \underline{q}_k + T\,\dot{\underline{q}}_k + \frac{T^3}{2}\ddot{\underline{q}}_k + \frac{T^3}{6}\dddot{\underline{q}}_k + \ldots \tag{2.41}$$

$$\phi_{x,k+1} = T\,p_k + \frac{T^2}{2}\dot{p}_k + \frac{T^3}{6}\ddot{p}_k + \ldots \tag{2.42}$$

where T denotes the integration step size between the sampling intervals k and k+1, and $\phi_{x,k+1}$ the angular increment in roll. Similar equations as Eq. (2.42) hold for the angular increments in pitch $\phi_{y,k+1}$ and yaw $\phi_{z,k+1}$. A third order discrete time algorithm for the quaternions can be derived from Eqs. (2.41) and (2.42) which is only based on the angular increments. The first element of the quaternion can then be expressed as (e.g. /18/)

$$q_{o,k+1} = q_{o,k}\left(1 - \frac{1}{8}\phi^2_{s,k+1}\right)$$

$$-q_{1,k}\left(\frac{\phi_{x,k+1}}{2} - \frac{\phi^2_{s,k+1}\,\phi_{x,k+1}}{48} - \frac{\phi_{y,k+1}\,\phi_{z,k} - \phi_{z,k+1}\,\phi_{y,k}}{24}\right)$$

$$-q_{2,k}\left(\frac{\phi_{y,k+1}}{2} - \frac{\phi^2_{s,k+1}\,\phi_{y,k+1}}{48} - \frac{\phi_{z,k+1}\,\phi_{x,k} - \phi_{x,k+1}\,\phi_{z,k}}{24}\right)$$

$$-q_{3,k}\left(\frac{\phi_{z,k+1}}{2} - \frac{\phi^2_{s,k+1}\,\phi_{z,k+1}}{48} - \frac{\phi_{x,k+1}\,\phi_{y,k} - \phi_{y,k+1}\,\phi_{x,k}}{24}\right) \qquad (2.43)$$

with the sum of the squared angular increments

$$\phi^2_{s,k+1} = \phi^2_{x,k+1} + \phi^2_{y,k+1} + \phi^2_{z,k+1} .$$

Similar expressions as Eq. (2.43) are obtained for q_1, q_2 and q_3. It should be noted that the application of Eq. (2.43) (which is based on Eq. 2.42) as well as the direct transformation of the measured acceleration to the navigation frame is limited in a strict sense to situations, where both the acceleration vector and the rotation vector retain their direction in space during an integration interval. Especially in the case of non-rigid, vibrating vehicles this will not be really true. On the other hand, the navigation accuracy requirements of tactical missiles are much less demanding than those of high precision navigation systems and, in addition, today's advanced signal processor systems allow high iteration rates. Nevertheless, the algorithm drift induced by computational simplifications must be checked carefully and assessed properly within the overall error budget. This may require certain algorithm refinements.

The relationship between the quaternion elements and the direction cosine matrix is given by

$$\underline{C}^t_s = \begin{bmatrix} q_o^2 + q_1^2 - q_2^2 - q_3^2 & 2\,(q_1 q_2 - q_o q_3) & 2\,(q_3 q_1 - q_o q_2) \\ 2\,(q_1 q_2 + q_o q_3) & q_o^2 - q_1^2 + q_2^2 - q_3^2 & 2\,(q_2 q_3 - q_o q_1) \\ 2\,(q_3 q_1 - q_o q_2) & 2\,(q_2 q_3 + q_o q_1) & q_o^2 - q_1^2 - q_2^2 + q_3^2 \end{bmatrix} \qquad (2.44)$$

The actual Euler angles can then be extracted form the $\underline{C}^t_s$-DCM as

$$\Psi = \tan^{-1}\frac{C^t_{s,21}}{C^t_{s,11}} = \frac{2(q_1 q_2 + q_o q_3)}{q_o^2 + q_1^2 - q_2^2 - q_3^2}$$

$$\theta = -\sin^{-1} C^t_{s,31} = 2\,(q_o q_2 - q_3 q_1) \qquad (2.45)$$

$$\phi = \tan^{-1}\frac{C^t_{s,32}}{C^t_{s,33}} = \frac{2(q_2 q_3 + q_o q_1)}{q_o^2 - q_1^2 - q_2^2 + q_3^2}$$

In the practical application of the quaternion update algorithm, orthogonality and normalization errors appear in the $\underline{C}^t_s$-DCM and the quaternions. They are usually corrected in regular intervals using the equations

$$\underline{C}_C = \underline{C} + \frac{1}{2}\,\underline{C}\,(\underline{I} - \underline{C}^T\,\underline{C}) \qquad (2.46)$$

which removes the orthonormalization errors from the DCM, and

$$Q_C = Q + \frac{1}{2}\,Q\,(1 - QQ^*) \qquad (2.47)$$

which removes the quaternion normalization error $|\Delta Q|$ using

$$Q^* = q_o - q_1\underline{i} - q_2\underline{j} - q_3\underline{k}$$

and

$$QQ^* = q_o^2 + q_1^2 + q_2^2 + q_3^2 \approx 1 + 2\,|\Delta Q| .$$

Referring to Fig. 2.6 it can be summarized that the navigation calculations can be performed through the following steps:

1. The direction cosine matrix from the sensor (s)-frame to the tangent frame is computed using the body fixed angular rate measurements provided in the (s)-frame. If required, these may be compensated by the earth-rate components (in some practical applications these are not important).

2. The specific force measurements, carried out in the sensor-frame, are transformed to the tangent frame via the $\underline{C}_s^t$-DCM

3. The gravity contributions (Eq. (2.34)) to the specific force measurements (Eq. 2.32) are removed.

4. The Coriolis accelerations (see Eq. 2.32)) due to the rotating t-frame are compensated, if necessary. The typical contribution is about 10 mg.

5. Velocity and position are obtained by integration. For this purpose a standard trapezoidal integration technique can be used. The "altitude"-channel may be supported by some independent, external altitude information.

6. The Euler angles are extracted from the $\underline{C}_s^t$-DCM, if they are required for guidance purposes.

2.2.5 Aided Inertial Navigation

This is a technique widely used in long-range navigation. The inherent disadvantage of inertial navigation, the continuously and accelerated growth of the navigation error, is removed by independent position measurements. This requires of course additional hardware (e.g. radar altimeters, GPS receivers) and may lead to a system which is no longer fully passive or autonomous.

For tactical missiles aided inertial navigation may be of interest for mainly two reasons:

- To compensate initialization errors
- To improve the accuracy of the terminal flight phase

As the additional hardware expenses should be minimized, there are only a limited number of possibilities to obtain independent position information. These include the use of

- the tracking radar of the launch vehicle, which may be able to track the target and the own missile simultaneously
- the missile seeker, which may be able to detect and to localize certain terrain features or man made objects
- GPS receivers, which can provide accurate position and altitude information (typically 1-σ values of 5 to 7.5 m for P-Code and 10 to 17 m for C/A-Code).

A block diagram of the basic principle is shown in Fig. 2.7. The position determined by the navigation algorithm is compared with the measured position. The position error is then used to estimate the significant error sources and to correct them in the navigation algorithm.

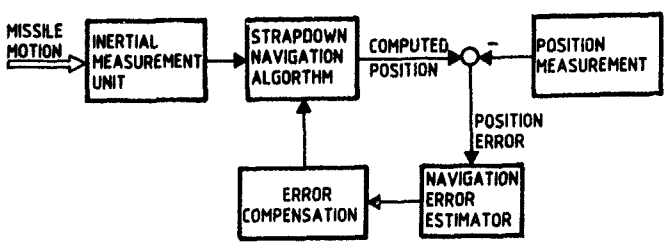

Fig. 2.7 Block Diagram of Aided Inertial Navigation

As an example, the initial misalignment of the navigation frame shall be estimated (see also Section 3). The constant misalignment angles lead to equivalent acceleration errors in the navigation frame. If we define the erroneous $\tilde{\underline{C}}_s^t$-DCM as

$$\tilde{\underline{C}}_s^t = [\underline{I} + \Delta\underline{C}^t]\ \underline{C}_s^t \qquad (2.48)$$

with

$$\Delta \underline{C}^t = \begin{bmatrix} 0 & -\varepsilon_z & \varepsilon_y \\ \varepsilon_z & 0 & -\varepsilon_x \\ -\varepsilon_y & \varepsilon_x & 0 \end{bmatrix}$$

then we obtain the following acceleration error in the t-frame

$$\Delta \dot{\underline{v}}^t = \Delta \underline{C}^t \, \underline{C}_s^t \, \underline{a}^s = \Delta \underline{C}^t \, \underline{a}^t = \underline{\Lambda}^t \, \underline{\varepsilon} \tag{2.49}$$

where

$$\underline{\Lambda}^t = \begin{bmatrix} 0 & a_z^t & -a_y^t \\ -a_z^t & 0 & a_x^t \\ a_y^t & -a_x^t & 0 \end{bmatrix} , \quad \underline{\varepsilon} = \begin{bmatrix} \varepsilon_x \\ \varepsilon_y \\ \varepsilon_z \end{bmatrix}$$

The position error is given by

$$\Delta \dot{\underline{R}}^t = \Delta \underline{v}^t \tag{2.50}$$

and for constant misalignment angles we can write

$$\dot{\underline{\varepsilon}} = \underline{0} \tag{2.51}$$

Eqs. (2.49) to (2.51) can be rearranged and combined to the navigation error state equation

$$\dot{\underline{x}} = \begin{bmatrix} \underline{0} & \underline{I} & \underline{0} \\ \underline{0} & \underline{0} & \underline{\Lambda}^t \\ \underline{0} & \underline{0} & \underline{0} \end{bmatrix} \underline{x} = \underline{A} \, \underline{x} \tag{2.52}$$

with $\underline{x} = \begin{bmatrix} \Delta \underline{R}^t \\ \Delta \underline{v}^t \\ \underline{\varepsilon} \end{bmatrix}$

The measurement equation in case of position measurements is defined by

$$\underline{z}_k = [\underline{I} \;\; \underline{0} \;\; \underline{0}] \, \underline{x} + \underline{v}_k \tag{2.53}$$

Eqs. (2.52) and (2.53) can then be converted to a discrete time formulation and processed by Kalman filtering techniques (see also Section 3.3). The state vector of the navigation error can also be augmented to include other error sources such as accelerometer scale factor and bias errors.

Fig. 2.8. shows as an example a result which has been obtained for three identical alignment errors of $\varepsilon_x = \varepsilon_y = \varepsilon_z = 20$ mrad and a situation where the missile was tracked by the own radar of the launch vehicle with an update rate of 2 Hz. The accuracy of the tracking radar was assumed to be 1 mrad (1 σ) in azimuth and elevation and 10 m in range (1 σ).

The upper curve shows the rapid growth of the navigation error without aiding. The error reaches a magnitude of about 300 m after a flight time of 12 sec. With aiding (lower curve) the position error is drastically reduced and never exceeds a value of about 35 m.

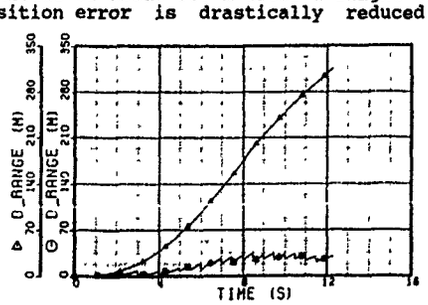

Fig. 2.8 Position Aiding Used to Estimate Initial Alignment Errors

2.2.6 Inertial Sensors

The requirements imposed on inertial measurement units of tactical missiles are characterized by very strong demands on mass, volume and cost and, in general, by moderate demands with respect to accuracy.

Table 2.1 and Table 2.2 give an overview on what may be considered as typical accuracy classes of angular rate sensors and accelerometers for tactical missile applications.

	Accuracy Classes		
Error Source (1 σ)	Low	Medium	High
Fixed Bias (°/h)	100	20	2
g-dependent Drift (°/h/g)	60	15	-
g^2-dependent Drift (°/h/g^2)	2	0.2	-
Scale factor (%)	1	0.2	0.01
Input Axis Misalignment (mrad)	5	2	0.5

Table 2.1 Accuracy Classes of Angular Rate Sensors

	Accuracy Classes		
Error Source (1 σ)	Low	Medium	High
Bias (mg)	50	10	2
Scale factor (%)	1	0.3	0.1
Input Axis Misalignment (mrad)	5	2	0.5

Table 2.2 Accuracy Classes of Accelerometers

These accuracy classes are generally not related to specific sensor technologies with the exception of the "high accuracy" angular rate sensors. This sensor class does not show any g-dependent drift terms and is therefore related to the laser gyro technology.

Despite of the general technical move towards solid-state, optical rate sensors (Ring Laser Gyros, Fiber Optic Gyros, Integrated Optics Gyros) there is still a large variety of "mechanical", competitive sensors on the market, which also took significant advantage of the progress in digital microelectronics.

As a result, today's sensor technologies offer highly integrated measurement units within the mass and volume constraints of typically 1 kg and 1 ltr including electronics. The performance data of these sensor packages are only partly determined by the requirements of midcourse guidance. Other important requirements may result from autopilot design, seeker stabilisation ("strapdown"-seeker) and seeker signal processing.

3. ALIGNMENT TECHNIQUES

3.1 Definition of the Alignment Problem

The target designation data i.e. LOS, range etc. are measured with respect to a master reference system (index: m), which is located within the launch vehicle. Similarly the data required to initialize the INU of the missile are available with respect to the same reference system. It is therefore necessary to transfer these data from the launch vehicle to the missile INU via a transformation matrix $\underline{C}^s_m$, where s designates the sensor frame of the missile. The transformation matrix $\underline{C}^s_m$ can be split up into a nominal, predetermined (fixed) part $\underline{C}^r_m$ and an unknown (time-varying) part $\underline{C}^s_r$, which leads to

$$\underline{C}^s_m = \underline{C}^s_r \cdot \underline{C}^r_m \qquad (3.1)$$

The transformation matrix $\underline{C}^s_r$ is determined by the misalignment angles ε_x, ε_y, ε_z which are usually small (see Table 3.1). Based on this assumption, the transformation matrix can be defined as

$$\underline{C}_r^s = \begin{bmatrix} 1 & \varepsilon_z(t) & -\varepsilon_y(t) \\ -\varepsilon_z(t) & 1 & \varepsilon_x(t) \\ \varepsilon_y(t) & -\varepsilon_x(t) & 1 \end{bmatrix} \tag{3.2}$$

where $\varepsilon_i(t) = \varepsilon_{io} + \varepsilon_{iv}(t)$, $i = x, y, z$ (3.3)

The static or quasi-static misalignment angles ε_{io} are typically caused by structural and mounting tolerances. However long-term- and environmental effects such as structural aging and temperature differences, especially for large structures, e.g. ships, may result in additional errors.

On top of the static misalignment angles we find structural distortions and oscillations caused by maneuver loads and loads created by gusts or waves. A summary of typical values for the misalignmet angles of missile stations (including g-loads) is shown in Table 3.1.

Vehicle	MSL Station	Azimuth	Elevation	Roll
Aircraft	Fuselage	5 mrad	5 mrad	3 mrad
	Wing	10 mrad	20 mrad	50 mrad
Ship	--	10 mrad	10 mrad	5 mrad

Table 3.1 Typical Values (1 σ) for the Misalignment Angles at Different Missile Stations

The structural oscillations $\varepsilon_{iv}(t)$ are ranging from fairly low frequencies of 0.1 ... 0.3 Hz and amplitudes of 10 mrad for ships up to 8 ... 10 Hz and amplitudes of 5/10 mrad (azimuth/elevation) for the wing stations of aircraft. These structural oscillations show usually small damping ratios of about 0.03 ... 0.08. The mean values of $\varepsilon_{iv}(t)$ are assumed to be zero. If the fundamental flexure modes of the vehicle are known, they can be modelled as a periodic random variable (/19/).

The misalignment angles can have significant effect on the performance and the design of the midcourse guidance system. The guidance system of the missile may be able to tolerate the misalignment angles in some cases, however, in other cases it may be necessary to spend considerable effort to obtain best estimates of the error angles by dynamic alignment techniques.

It should be noted that on top of the misalignment angles quoted for each missile station there are additional misalignment angles of each instrument (gyro or accelerometer) with respect to the nominal sensor frame. However, these misalignment angles are normally compensated as a part of the IMU calibration process down to values which are significantly smaller than the error angles of missile stations. They are therefore ignored in the remainder of this paper.

3.2 "One Shot"-Alignment

This is the simplest method which can only be used, if the missile guidance system is fairly tolerant with respect to alignment errors or if aiding techniques similar to those described in Section 2.2.5 are used. In this case the misalignment angles are usually determined by ground measurements and flight tests on a test aircraft. The flight tests give the opportunity to measure the misalignment angles as a function of the flight conditions, such as the instantaneous aircraft maneuver factor or the actual loading situation.

The transformation matrix $\underline{C}_r^s$ is then stored in the fire control system for each missile station as a function of the flight condition and is used at launch without any further correction. It is therefore obvious that this method is only able to compensate the most significant and stable errors. Alternative methods use inertial measurement matching between the airborne or shipborne master reference and the missile INU and are far more accurate than the "one shot" method. They will briefly be discussed in the following sections.

3.3 Dynamic Alignment on a Moving Base

The alignment between the master INU onboard the launch vehicle and the missile INU can be achieved by comparing directly the measurements of the inertial sensors (i.e. angular rates and/or linear accelerations) or by comparing the computed estimates of attitude, velocity and position. The comparison of the data derived at each location leads to the possibility to deduce the relative orientation of the two reference frames (/20/, /21/).

This method of alignment is generally able to provide accurate results, however, a couple of important points must be observed:

- Dynamic alignment depends on the existence and the type of motion of the launch vehicle. In special cases the misalignment angles may be not or only poorly observable. A low level of motion generally increases the time required to estimate the misalignment angles with reasonable accuracy. To enhance the observability it may be useful to carry out special maneuvers (/22/).

- The comparison of noisy measurements needs time to allow for some kind of filtering. It is therefore obvious that the alignment process cannot be initiated when the fire command is applied. This would lead to unacceptable launch delays.

- The separation of the master and the missile IMU requires kinematic corrections, the so-called "lever-arm-corrections". It is therefore necessary to know the relative positions of the IMU's exactly. The general equation of the lever arm correction is

$$\underline{a}_{ms} = \underline{a}_m + \dot{\underline{\omega}}_{im} \times \underline{r}_{ms} + \underline{\omega}_{im} \times (\underline{\omega}_{im} \times \underline{r}_{ms}) \qquad (3.4)$$

  where $\underline{a}_{ms}$ is the computed acceleration at the location of the slave system based on the measured acceleration $\underline{a}_m$ of the master IMU, $\underline{r}_{ms}$ is the position vector of the missile IMU with respect to the master IMU and ω_{im} is the measured angular rate of the master IMU (see Fig. 3.1).

- The accuracy of the alignment process will not only be limited by the noise and vibration levels but additionally by instrument errors. Especially bias, scale factor and cross-coupling errors can play an important role. If the instrument errors of the missile IMU are significantly larger than those of the reference system, which is usually the case, it is possible to include the error models of the instruments in the estimation process. In this case the filter formulation not only provides estimates of the misalignment angles, but additionally estimates of the errors of the missile IMU. These can then be used for a re-calibration of these instruments (/20/).

- Timing differences between the data delivered by the master and the missile IMU can lead to significant errors (/23/). To allow a proper comparison of the measurements generatd by the two IMU's they must be taken at the same instant. This is not trivial as both IMU's are normally not designed to operate together and work with independent clocks. In order to get a proper synchronization of the measurements it may be necessary to apply interpolation schemes.

In practice dynamic alignment may use quite different algorithms with respect to type and complexity. The basic methods which can be found in many applications are Least-Squares (LS)-Estimation and Kalman-Filter (KF)-Estimation techniques. The following sections are intended to give a quick overview.

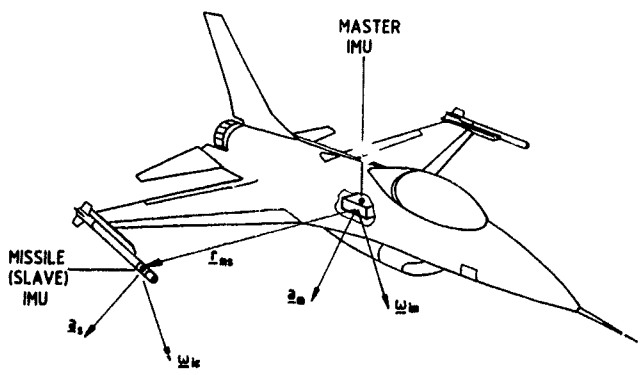

3.3.1 State Vector Representations of the Alignment Process

The data basically available for the alignment process are angular rate and acceleration measured with respect to the master and the slave or missile sensor axis system. The differences between both measurements are compared in the common reference system.

Fixed misalignment angles

The requirement for angular rate matching is given by

$$\underline{C}_m^r \underline{\omega}_{im}^m - \underline{C}_s^r \underline{\omega}_{is}^s = \underline{\omega}_{im}^r - \underline{C}_s^r \underline{\omega}_{is}^s = \underline{0} \tag{3.5}$$

Eq. (3.2) can be written as

$$\underline{C}_s^r = \underline{I} + \Delta \underline{C}_s^r = \underline{I} + \begin{bmatrix} 0 & -\varepsilon_z & \varepsilon_y \\ \varepsilon_z & 0 & -\varepsilon_x \\ -\varepsilon_y & \varepsilon_x & 0 \end{bmatrix} \tag{3.6}$$

After combining Eqs. (3.5), (3.6) and re-arranging terms we obtain

$$\Delta \underline{\omega}_{sm} = \underline{\omega}_{is}^s - \underline{\omega}_{im}^r = \underline{\Omega}_{is}^s \underline{\varepsilon} \tag{3.7}$$

with $\underline{\varepsilon} = (\varepsilon_x, \varepsilon_y, \varepsilon_z)$ and (see also Eq. 2.24)

$$\underline{\Omega}_{is}^s = \begin{bmatrix} 0 & -r_{is} & q_{is} \\ r_{is} & 0 & -p_{is} \\ -q_{is} & p_{is} & 0 \end{bmatrix} \tag{3.8}$$

Similarly we obtain for acceleration matching

$$\underline{C}_m^r \underline{a}_{ms}^m - \underline{C}_s^r \underline{a}_s^s = \underline{0} \tag{3.9}$$

where $\underline{a}_{ms}$ is given by Eq. (3.4). Using Eq. (3.6) we can write

$$\Delta \underline{a}_{sm} = \underline{a}_s^s - \underline{a}_{ms}^r = \underline{\Lambda}_s^s \underline{\varepsilon} \tag{3.10}$$

with $\underline{a}_s^s = (a_{sx}, a_{sy}, a_{sz})$ and

$$\underline{\Lambda}_s^s = \begin{bmatrix} 0 & -a_{sz} & a_{sy} \\ a_{sz} & 0 & -a_{sx} \\ -a_{sy} & a_{sx} & 0 \end{bmatrix} \tag{3.11}$$

Eqs. (3.7) and (3.11) can be combined for simultaneous angular rate and acceleration matching

$$\begin{bmatrix} \Delta \omega_{sm} \\ \hline \Delta \underline{a}_{sm} \end{bmatrix} = \begin{bmatrix} \underline{\Omega}_{is}^s \\ \hline \underline{\Lambda}_s^s \end{bmatrix} \underline{\varepsilon} \tag{3.12}$$

Time-varying misalignment angles

To derive the state vector equation of the time-varying alignment error $\underline{\varepsilon}$ we take the DCM

$$\underline{C}_s^i = \underline{C}_m^i \underline{C}_s^m \tag{3.13}$$

as a starting point. After differentiating $\underline{C}_s^i$ and using the basic relationship

$$\dot{\underline{C}}_s^i = \underline{C}_s^i \underline{\Omega}_{is}^s \tag{3.14}$$

we obtain for the relative angular rate matrix

$$\underline{\Omega}_{ms}^s = \underline{\Omega}_{is}^s - \underline{C}_r^s \underline{\Omega}_{im}^r \underline{C}_s^r \tag{3.15}$$

It can be shown after differentiation of Eq. (3.1) that

$$\underline{\Omega}_{rs}^s = \underline{\Omega}_{ms}^s$$

Expansion of Eq. (3.15) in connection with Eq. (3.6) yields

$$\Omega^s_{rs} = \Omega^s_{is} - \Omega^r_{im} - \Omega^r_{im}\,\Delta\underline{C}^r_s - \Delta\underline{C}^s_r\,\Omega^r_{im} - \underbrace{\Delta\underline{C}^s_r\,\Omega^r_{im}\,\Delta\underline{C}^r_s}_{\text{higher order term is neglected}} \tag{3.16}$$

Eq. (3.16) can be resolved with respect to the individual matrix elements, and after a re-arrangement with respect to the alignment error we obtain

$$\dot{\underline{\varepsilon}} = -\Omega^r_{im}\,\underline{\varepsilon} + \Delta\underline{\omega}_{sm} \tag{3.17}$$

The alignment error $\underline{\varepsilon}$ can be observed via the acceleration error (Eq. 3.10).

Time-varying misalignment angles in connection with scale factor errors and bias (/20/)

In general the quality of the master IMU will be significantly superior to the missile IMU. Therefore the accuracy of the alignment may be degraded due to bias and scale factor of the missile IMU errors. The alignment process can be improved by taking these errors into account. On the other hand the scale factor and bias error estimates can be used to calibrate the missile IMU immediately before launch, which in turn leads to improved navigation accuracy during midcourse guidance.

The "true" angular roll rate of the missile IMU may be defined as

$$p_{is} = \bar{p}_{is} - \Delta S_p\,\bar{p}_{is} - B_p \tag{3.18}$$

where $\bar{p}_{is}$ is the measured roll rate and ΔS_p, B_p are the relevant scale factor and bias errors. The errors are assumed to be constant, i.e. $\Delta\dot{S}_p = 0$ and $\dot{B}_p = 0$. Similar equations can be defined for the pitch and yaw rates. These equations can be used to augment the state vector which leads to the following matrix differential

$$\begin{bmatrix} \underline{\varepsilon} \\ \Delta\underline{S} \\ \underline{B} \end{bmatrix} = \left[\begin{array}{c:ccc:ccc} & -p_{is} & 0 & 0 & -1 & 0 & 0 \\ \Omega^r_{im} & 0 & -q_{is} & 0 & 0 & -1 & 0 \\ & 0 & 0 & -r_{is} & 0 & 0 & -1 \\ \hdashline \underline{0} & & \underline{0} & & & \underline{0} & \\ \hdashline \underline{0} & & \underline{0} & & & \underline{0} & \end{array}\right] \begin{bmatrix} \underline{\varepsilon} \\ \Delta\underline{S} \\ \underline{B} \end{bmatrix} + \underline{B}\,\Delta\bar{\underline{\omega}}_{sm} \tag{3.19}$$

with

$$\underline{B} = \begin{bmatrix} I \\ \hdashline 0 \\ \hdashline 0 \end{bmatrix} \qquad \text{and} \qquad \Delta\bar{\underline{\omega}}_{sm} = \bar{\underline{\omega}}^s_{is} - \underline{\omega}^r_{im}$$

The method can also be extended to deal with acceleration dependent drift parameters as a separate error source.

Velocity/Position Matching

Instead of using the data provided directly by the master and the missile IMU, namely the angular rates and linear accelerations, it is possible to compare the velocity or the position estimates of both systems. The velocity or position errors will also propagate as a function of the misalignment angles. It is therefore necessary to augment the state/vectors of Eq. (3.17) or Eq. (3.19) further by the velocity and the position error (see also Section 2.2.5).

This approach has the potential for increased accuracy because it relies on the "long term" effects of misalignment. It has also definite advantages under calm environmental conditions. However, it also increases the computational burden of the alignment processor and it takes more time based on the fact that the velocity and position errors need naturally some time to propagate.

3.3.2 Alignment Processing Algorithms

The algorithms used for the alignment process can be - broadly speaking - separated into

- Least Squares Estimation (LS)

and

- Kalman Filtering (KF).

In case of static or quasi-static misalignment angles as described by Eq. (3.12) the estimation process is based on linear measurements which are corrupted by zero-mean noise. No further assumptions are made with respect to the statistical properties of the estimation problem.

To solve this estimation problem we can use a sequential least-squares estimation algorithm (e.g. /24/), which is summarized briefly. We assume a time sequence of linear measurements (e.g. corresponding to Eq. (3.12))

$$\underline{z}_i = \underline{H}_i \underline{x} + \underline{v}_i \qquad , \; i = 1,\ldots k \tag{3.20}$$

corrupted by zero-mean noise. These measurements are then processed in such a way that the quadratic measure of the estimated parameter vector $\underline{x}_k$

$$J(\hat{\underline{x}}_k) = \frac{1}{2} (\underline{z}_k - \underline{H}_k \hat{\underline{x}}_k)^T \underline{R}_k^{-1} (\underline{z}_k - \underline{H}_k \hat{\underline{x}}_k) \tag{3.21}$$

is minimized, where the matrices $\underline{z}_k$, $\underline{H}_k$ are defined by the composite matrix of all observations

$$\underline{z}_k = \begin{bmatrix} \underline{z}(1) \\ \underline{z}(2) \\ \vdots \\ \underline{z}(k) \end{bmatrix} \qquad \text{and} \quad \underline{H}_k = \begin{bmatrix} \underline{H}(1) \\ \underline{H}(2) \\ \vdots \\ \underline{H}(k) \end{bmatrix}$$

and $\underline{R}_k^{-1}$ is an appropriate, symmetric and positive definite weighting matrix. This leads to the well known "batch" version of least-squares estimation

$$\hat{\underline{x}}_{k_{LS}} = (\underline{H}_k^T \underline{R}_k^{-1} \underline{H}_k)^{-1} \; \underline{H}_k^T \underline{R}_k^{-1} \underline{z}_k \tag{3.22}$$

In practice it is very desirable to work with a sequential form of Eq. (3.22), which is given by the following equations

$$\hat{\underline{x}}_{LS}(k) = \hat{\underline{x}}_{LS}(k-1) + \underline{K}(k)[\underline{z}(k) - \underline{H}(k)\, \hat{\underline{x}}_{LS}(k)] \tag{3.23 a}$$

$$\underline{K}(k) = \underline{P}(k)\, \underline{H}^T(k)\, \underline{R}^{-1}(k) \tag{3.23 b}$$

$$\underline{P}(k) = (\underline{I} - \underline{P}(k-1)\, \underline{H}^T(k)\, [\underline{R}(k) + \underline{H}(k)\, \underline{P}(k-1)\, \underline{H}^T(k)]^{-1}\, \underline{H}(k))\, \underline{P}(k-1) \tag{3.23 c}$$

Eq. (3.23 b) can be interpreted as a time-varying gain matrix, where

$$\underline{P}(1) = [\underline{H}^T(1)\, \underline{R}^{-1}(1)\, \underline{H}(1)]^{-1} \tag{3.24}$$

is used as a starting matrix. The sequential least-squares estimator can be modified to cope with slowly varying estimation parameters by a "fading memory"-technique (/25/, /26/).

This method ensures by (exponential) weighting factors that recent measurement data have a stronger influence on the parameter estimates than old data.

Kalman filtering techniques are used to estimate dynamic error parameters. Theory and application of Kalman filtering have been discussed extensively in the literature (e.g. /19/, /27/ to /29/), however, the basic equations of the well known discrete Kalman filter are repeated here for the sake of completeness.

The state estimate update <u>across</u> each measurement is given by

$$\hat{\underline{x}}_{KF}(k|k) = \hat{\underline{x}}_{KF}(k|k-1) + \underline{K}(k)\, [\underline{z}(k) - \underline{H}(k)\, \hat{\underline{x}}_{KF}(k|k-1)] \tag{3.25 a}$$

where $k|k$ and $k|k-1$ denote quantities at time t_k, however, based on measurements taken up to time t_k or t_{k-1} respectively.

The Kalman gain matrix is given by

$$\underline{K}(k) = \underline{P}\ (k|k)\ \underline{H}(k)^T\ \underline{R}^{-1}\ (k) \qquad (3.25\ b)$$

with $\underline{R}(k)$ denoting the measurement noise covariance matrix. The error covariance update is defined by

$$\underline{P}(k|k) = [\underline{I} - \underline{K}(k)\ \underline{H}(k)]\ \underline{P}(k|k-1) \qquad (3.25\ c)$$

The state vector estimate $\hat{\underline{x}}_{KF}(k)$ and the error covariance matrix $\underline{P}(k)$ are extrapolated between measurements by

$$\hat{\underline{x}}_{KF}(k|k-1) = \underline{F}(k,k-1)\ \hat{\underline{x}}_{KF}\ (k-1|k-1) + \underline{G}(k,k-1)\ \underline{u}\ (k-1) \qquad (3.26)$$

$$\underline{P}(k|k-1) = \underline{F}(k,k-1)\ \underline{P}(k-1|k-1)\ \underline{F}^T(k,k-1) + \underline{Q}(k-1) \qquad (3.27)$$

where $\underline{F}$ and $\underline{G}$ are the state transition matrix and the input matrix from time t_{k-1} to t_k. The input vector $\underline{u}(k)$ is given by the angular rate error (Eq. 3.17) and $\underline{Q}(k)$ denotes the process noise covariance matrix.

The comparison of Eqs. (3.23) and Eqs. (3.25) shows some similarities. However, it should be noted firstly that the least-squares estimator treats the estimation problem solely as a deterministic optimization problem, whereas the Kalman filter is a minimum variance estimator. Secondly, the Kalman filter is able to take the dynamics of the estimation problem into account.

A typical simulation result for the least-squares alignment is shown in Fig. 3.2 for a level flight condition followed by a steady turn with a roll angle of 80 deg. Simultaneous acceleration and angular rate matching is used with a measurement noise of 50 mg and 500°/h respectively. It can be seen that the azimuth alignment error is not observable until the turn is initiated. After that all alignment angles are reduced down to a fraction of 10 % within about 2.5 sec.

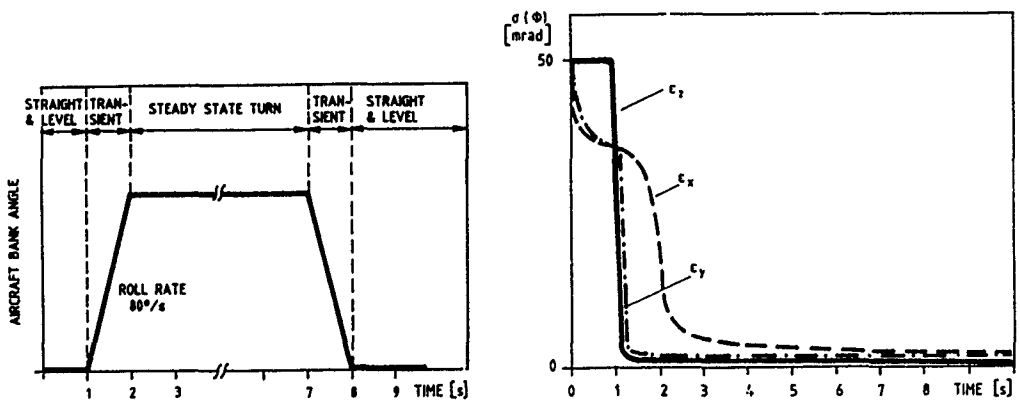

Fig. 3.2 Least-Squares Alignment Applied in Acceleration/Angular-Rate Matching

4. PERFORMANCE ASSESSMENT

4.1 Compilation of Error Sources

The midcourse guidance criteria have been reviewed in Section 2.1. The actual system design requires a detailed summary of all individual error sources and an assessment of their effects on the performance data of interest.

An example is shown in Fig. 4.1, where the influence of various error sources on the expected seeker LOS error during missile flight is illustrated. The seeker LOS error is an important seeker and missile design parameter in many applications. It may be a design driver for the seeker acquisition range and field-of-view and an important factor for the missile maneuverability requirement. As far as the navigation system is concerned, the seeker LOS error is caused by two different effects, the attitude error and the position error. The attitude or direction error is basically influenced by misalignment errors and gyro errors. The position error or LOS displacement is dominated by accelerometer and initialization errors. In addition both errors are influenced by the algorithm design and computational/quantization effects.

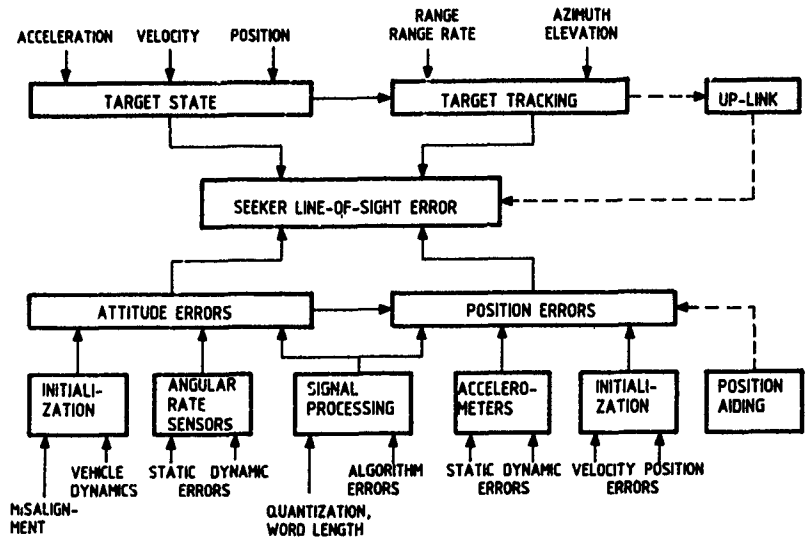

Fig. 4.1 Summary of Error Effects on Seeker LOS

The navigation errors may possibly be reduced by aiding techniques as discussed in Section 2.2.5. The other - in many cases dominant - error source is target uncertainty. The target state is provided by the target tracking system at least up to the instant of missile launch. Thereafter the target uncertainty may grow rapidly due to unknown target maneuvers if no further updates can be provided by the target tracker and an appropriate up-link.

An indication of typical errors and factors influencing the seeker LOS error is given in Table 4.1 for the navigation effects and in Table 4.2 for the target uncertainty. A similar compilation, which includes the relevant numerical values, has to be established for every special application.

Angular Rate Sensors	Accelerometers	Initialization
Day-to-Day Bias Stability In-Run Bias Stability g-dependent Drift g^2-dependent Drift Scale Factor Error Non-Linearity Sensor Misalignment Dynamic Cross Coupling Temperature Sensitivities	Day-to-Day Bias Stability In-Run Bias Stability Scale Factor Error Non-Linearity Sensor Misalignment Cross Coupling Temperature Sensitivities	Misalignment Angles Vehicle Dynamics Velocity Error Position Error

Table 4.1 Summary of Sensor and Initialization Errors

Target State	Target Tracking	Target Update
Jerk Acceleration Velocity Position	Range/Range Rate Azimuth/Elevation Sightline rate Sightline acceleration Data Staleness	Data rate Launch vehicle position Launch vehicle attitude

Table 4.2 Parameters Affecting Target Uncertainty

4.2 Assessment of Error Budgets

Performance assessment is the step to follow after the compilation of the system error sources has been completed. The aim of this step is not only to prove that the performance requirements can be met, which is no doubt the primary purpose. Another very important aspect of this assessment is the establishment of a source-by-source break-down

of the individual error contributions to the resulting performance figures, which is often understood as an error budget. The error budget gives an opportunity to come up with a well balanced system design, which reveals on the one hand the specifications of the critical, most dominant components and avoids on the other hand the over-specification of devices with only minor contributions to the overall error. For example, if the target LOS uncertainty is in the order of some degrees, it makes little sense to design an inertial guidance system with an accuracy of 0.1 degree equivalent LOS error.

The methods used to assess the error budget are chosen in accordance with the actual design progress. In the early design stage it may be sufficient to use simple order-of-magnitude or covariance analysis methods. In the final stages it will be necessary to use detailed mathematical models of the overall system to prove and to verify the design by simulation techniques.

An example for a simplified order-of-magnitude assessment is shown in Table 4.3 as a function of the flight time t. The definitions are chosen in accordance with Fig. 4.1. Due to the simplifications the method is limited to first-order effects. Some of the error sources shown in Table 4.3 can be interpreted as "root-sum-square"-values (e.g. drift D), i. e. they can include different effects like g-dependent and g^2-dependent drift. It should be noted that the simplified analysis is based on average values of the flight parameters of interest (e.g. average acceleration, velocity etc.). After evaluating Table 4.3 the resultant seeker LOS error is given by the root-sum-square error

$$\Delta\Psi = \sqrt{\Delta\Psi_A^2 + \Delta\Psi_T^2 + \Delta\Psi_M^2} \quad .$$

ATTITUDE ERRORS	CONTRIBUTION	POSITION ERRORS	CONTRIBUTION	TARGET UNCERTAINTY	CONTRIBUTION
MISALIGNMENT	$\Delta\Psi_1 = \varepsilon_0$	MISALIGNMENT	$\Delta R_{M1} = \frac{1}{2} g\, \varepsilon_0\, t^2$	CROSS RANGE	$\Delta R_{T1} = \Delta R$
DRIFT	$\Delta\Psi_2 = D \cdot t$	INITIAL HEADING	$\Delta R_{M2} = \Delta\chi_0 \cdot R_M$	LOS-RATE	$\Delta R_{T2} = R_{T0} \Delta\dot{\sigma} \cdot t$
SCALE FACTOR (= average angular rate)	$\Delta\Psi_3 = \Delta S \cdot \bar{\omega} t$	ACCELEROMETER BIAS	$\Delta R_{M3} = \frac{1}{2} B \cdot t^2$	LOS-ACCELERATION	$\Delta R_{T3} = \frac{1}{2} R_{T0} \Delta\ddot{\sigma} t^2$
		DRIFT INDUCED ACCELERATION	$\Delta R_{M4} = \frac{1}{6} g\, D \cdot t^3$		
		GYRO DRIFT	$\Delta R_{M5} = \frac{1}{2} D\, R_M\, t$		
		INITIAL VELOCITY	$\Delta R_{M6} = \Delta V \cdot t$		
RESULTANT ERROR	$\Delta\Psi_A = \sqrt{\Sigma \Delta\Psi_i^2}$		$\Delta\Psi_M = \sqrt{\Sigma \Delta R_{Mi}^2}$		$\Delta\Psi_T = \sqrt{\Sigma \Delta R_{Ti}^2}$

Table 4.3 Simplified Midcourse Guidance Error Budget

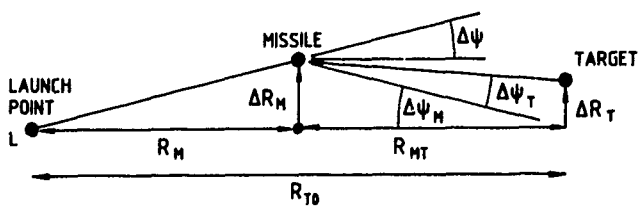

Fig. 4.1 Definitions for Simplified Error Analysis

The time-varying, linear covariance analysis represents a more sophisticated tool. The method (e.g. /20/) is based on a discrete time formulation of the error equation

$$\underline{x}_k = \underline{F}_{k-1}\, \underline{x}_{k-1} + \underline{G}_{k-1}\, \underline{w}_{k-1} \tag{4.1}$$

(See Eq. 2.52 as an example.) It can be shown that the covariance matrix of the error vector

$$\underline{P}_k = E\,[\underline{x}_k\, \underline{x}_k^T]$$

propagates according to

$$\underline{P}_k = \underline{F}_{k-1}\, \underline{P}_{k-1}\, \underline{F}_{k-1}^T + \underline{Q}_{k-1} \tag{4.2}$$

where

$$Q_k = E\,[(G_k\,W_k)\,(G_k\,W_k)^T]$$

defines the input noise covariance matrix (e.g. acceleration "noise", angular rate "noise"). After having established the basic error state equations, the covariance matrix is obtained by simple matrix algebra.

The covariance analysis tool can also be extended to include measurements (i.e. target and missile updates). In this case the method follows closely the standard Kalman filter equations as shown in Section 3.3.2. As the method is based on a linear (small perturbation) error model, the error propagation can be computed reasonably fast and the effects of the different error groups can be investigated.

In the final design stage, the error budget is determined and proven by a detailed simulation model which describes all non-linear and time-varying features of the system. As this step is the most expensive one, it is highly desirable to optimize the system as far as possible by simpler methods.

The basic scheme of such a simulation model is shown in Fig. 4.2. It includes a full representation of the missile and the missile/target kinematics. The modelling of "high frequency" effects such as body-bending and vibration typically requires integration step sizes in the order 1 msec or less. The most important submodules with respect to midcourse guidance are related to the inertial sensors and the strapdown-navigation algorithm. The inertial sensor models may represent the full sensor dynamics, such as the caging loop dynamics in case of dynamically tuned gyros or the dither motion in case of ring laser gyros, noise and additionally the error sources listed in Table 4.1. The strapdown algorithms illustrated in Fig. 2.6 should also represent computational errors caused by quantization and finite word length if applicable. The computed missile attitude and position is then compared against the true values and further assessment criteria such as the seeker error angle at handover and zero effort miss.

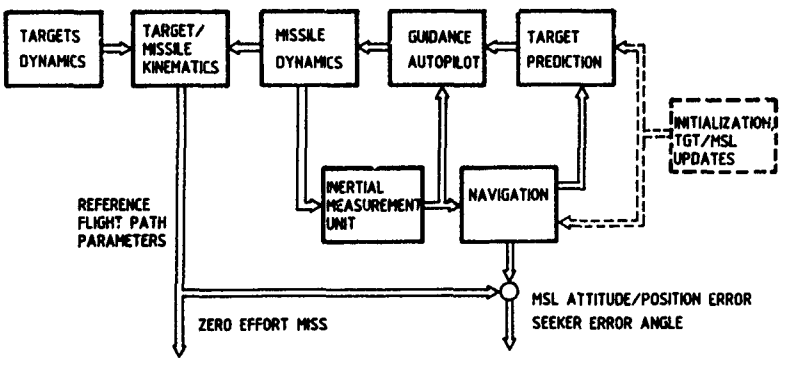

Fig. 4.2 Midcourse Guidance Performance Evaluation Scheme

The "Monte-Carlo"-technique is an approach frequently used for this type of investigations. The method requires a definition of the random parameters of the system and an appropriate description of the random process (e.g. uniform or gaussian distribution). The simulation is then repeated several times where the random parameters (e.g. gyro drift, accelerometer bias etc.) are automatically selected by appropriate random number generators at the beginning of each run. The results of a suffiently large number of simulation runs are then statistically evaluated and can be visualized by histograms or bar charts. This is shown in Fig. 4.3. as an example for zero-effort-miss (ZEM) and the seeker error angle at handover. The mean value

$$\bar{x} = \frac{1}{m} \sum_{i=1}^{m} x_i$$

and the standard or root-mean-square (RMS) deviation

$$\sigma = \sqrt{\frac{\Sigma(x_i-\bar{x})^2}{m}}$$

are calculated from the simulation results. If missdistance $d = \sqrt{\Delta y^2+\Delta z^2}$ can be interpreted as a Rayleigh process, it is possible to derive analytic density and distribution functions

$$f(d) = \frac{d}{\bar{\sigma}^2} e^{-d^2/2\bar{\sigma}^2}$$

$$F(d) = 1 - e^{-d^2/2\bar{\sigma}^2}$$

as indicated in Fig. 4.3 a, where the variance $\bar{\sigma}^2$ must be fitted to the simulation results

$$\bar{\sigma}^2 = \bar{x} \Big/ \sqrt{\frac{\pi}{2}}$$

and

$$\bar{\sigma}^2 = \sigma^2 \; / \left(2 - \frac{\pi}{2}\right) .$$

The error budget of a specified performance variable can be derived, if the complete process is repeated several times by successively increasing the number of error groups (the consideration of individual errors may be very costly). Such error budgets can be represented as bar charts, illustrating the impact of individual error groups, as shown in Fig. 4.3 b.

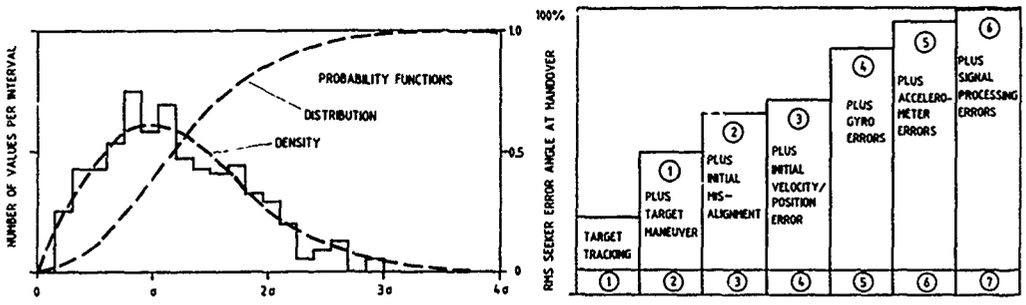

a. Missdistance Histogram

b. Error Budget Bar Chart

Fig. 4.3 Statistical Evaluation of Monte-Carlo-Simulation Runs

5. CONCLUDING REMARKS

Midcourse guidance techniques are very useful to extend the operational capabilities of tactical missiles and to meet a number of top-priority requirements. The impact on missile cost and weight are moderate as the IMU as the "heart" of the midcourse guidance system takes advantage of modern sensor technologies and digital microelectronics. Moreover, the IMU is also an integral part of the overall guidance system and provides the inertial data for the autopilot and the seeker stabilization and tracking algorithms.

The actual design of the midcourse guidance system depends strongly on the means to initialize the guidance system before launch, the availability and update rate of a data link and the acquisition performance of the seeker in a given target/background situation. Proper prelaunch initialization requires accurate target information and small misalignment errors. Any degradation of target information, especially if no data link exists, leads to an increase of the target error at handover and consequently to more difficult requirements with respect to seeker acquisition range, field-of-view and missile maneuverability. It is therefore a major design aim of the midcourse guidance system to keep the handover errors at levels which do not significantly degrade the unavoidable target uncertainty.

6. REFERENCES

[1] E. Fischel — Inertiale Navigationssysteme
Interavia, 1960, p. 1422-1426

[2] R. C. Duncan, A. S. Gunnarson — Inertial Guidance, Navigation and Control Systems
Journal of Spacecraft and Rockets, 1964, p. 577-587

[3] C. S. Draper — Origins of Inertial Navigation
Journal of Guidance and Control, 1981, p. 449-463

[4] F. K. Müller — A History of Inertial Guidance
Journal of the British Interplanetary Society, 1985, p. 180-192

[5] C. S. Draper et al — Space Navigation, Guidance and Control
AGARD Lecture Series, 1965

[6] --- — Strapdown Inertial Systems
AGARD Lecture Series No. 95, 1978

[7] --- — Advances in Strapdown Inertial Systems
AGARD Lecture Series No. 133, 1984

[8] V. H. L. Cheng, N. K. Gupta — Advanced Midcourse Guidance for Air-to-Air Missiles,
J. Guidance, Vol. 9, No. 2, pp. 135-142

[9] J. K. R. Britting — Inertial Navigation Systems Analysis
John Wiley & Sons, New York 1971

[10] Y. Bar-Shalom, T. B. Fortmann — Tracking and Data Association
Academic Press, Orlando, 1988

[11] C.-B. Chang, J. A. Tabaczynski — Application of State Estimation to Target Tracking
IEEE Transaction on AC, Vol. AC-29, No. 2, pp. 98-109, Feb. 1984

[12] R. A. Singer — Estimating Optimal Tracking Filter Performance for Manned Maneuvring Targets
IEEE Trans. Aerospace and Electronic Systems, Vol. AES-6, No. 4, pp. 473-483, July 1970

[13] J. B. Pearson, E. B. Stear — Kalman Filter Applications in Airborne Radar Tracking
IEEE Trans. Aerospace and Electronic Systems, Vol. AES-10, No. 3, pp. 319-329, May 1974

[14] NASA/United Aircraft Corp. — A Study of the Critical Computational Problems Associated with Strapdown Inertial Navigation Systems
NASA CR 968, Washington D. C., April 1986

[15] A. Van Bronkhorst — Strapdown System Algorithms, AGARD Lecture Series No. 95, Strapdown Inertial Systems - Theory and Application, June 1978

[16] P. G. Savage — Strapdown System Algorithms
AGARD Lecture Series No. 133, "Advances in Strapdown Inertial Systems", May 1984

[17] D. Wick, M. Kopf — Analysis, Development and Testing of Strapdown Signal Processing for High Vibration and Dynamic Environment
AGARD Conference Proceedings CP 431

[18] R. McKern, H. Musoff — Strapdown Attitude Algorithms from a Geometric Viewpoint
J. Guidance and Control, Vol. 4, No. 6, pp. 657-661, Nov. 1981

[19] A. Gelb — Applied Optimal Estimation
MIT-Press, Cambridge, Mass, 1974

[20] W. Boch, U. Krogmann — Fast Transfer Alignment for Air-Launched Missile INS
AGARD Conference Proceedings CP 411, 1986

[21] D. H. Titterton, J. L. Weston — Dynamic Shipboard Alignment Techniques
Symposium Gyro Technology 1987, Stuttgart, Germany, Conference Proceedings;
Editor: H. Sorg, Universitat Stuttgart, Institut für Mechanik

[22] I. Y. Bar-Itzhack, B. Porat — Azimuth Observability Enhancement During Inertial Navigation System In-Flight Alignment
J. Guidance and Control, Vol. 3, No. 4, pp. 337-344, 1980

[23] I. Y. Bar-Itzhack, Y. Vitek — The Enigma of False Bias Detection in a Strapdown System During Transfer Alignment
J. Guidance, Vol. 8, No. 2, pp. 175-180, 1985

[24] A. P. Sage, J. L. Melsa — Estimation Theory with Applications to Communications and Control
McGraw-Hill Book Company, New York, 1971

[25] P. Eykhoff — System Identification
John Wiley, New York, 1974

[26] U. Hartmann, V. Krebs — Command and Stability Systems for Aircraft: A New Digital Adaptive Approach in "Adaptive Methods for Control System Design" (Editor: M. M. Gupta)
IEEE Press, New York, 1986

[27] H. W. Sorenson (Editor) — Kalman Filtering: Theory and Application
IEEE Press, New York, 1985

[28] --- — Theory and Application of Kalman Filtering,
AGARDOGRAPH AG 139, 1970

[29] --- — Advances in the Techniques and Technology of the Application of Nonlinear Filters and Kalman Filters
AGARDOGRAPH AG 256, 1982.

FLIGHT CONTROL DESIGN ISSUES IN BANK-TO-TURN MISSILES

BY
W. A. KAUFMANN
SENIOR SCIENTIST
HUGHES AIRCRAFT COMPANY
8433 Fallbrook Ave.
Canoga Park, CA 91304-0445

SUMMARY

This paper discusses design issues encountered in the systhesis of bank-to-turn autopilots for several proposed air-launched tactical guided missile configurations. Some approaches to dealing with these issues are also discussed. Much of the material was developed from experience gained in the design of an autopilot for a medium range air-to-air missile configuration incorporating an integral rocket-ramjet propulsion system. Therefore, emphasis is placed on that type of system. None of the bank-to-turn autopilots have been flight tested, so only simulation results can be presented.

The first issued discussed is why a designer would consider bank-to-turn control instead of the conventional skid-to-turn control used by most tactical missiles. The advantages and disadvantages of each approach are related to the performance of the airframe, propulsion, guidance and autopilot subsystems.

Several bank-to-turn control laws are presented. The relative merits of each are discussed with respect to the type of airframe, propulsion and guidance required for the missile mission under consideration. Performance penalties are presented along with the advantages of including a skid-to-turn capability.

Coupling between the roll control and the guidance for terminal homing missiles is reviewed. Some methods of decoupling are presented. The impact of signal noise and radome error for missiles with radar seekers is discussed.

Simulation studies have shown that some performance penalties may be incurred using bank-to-turn control for some types of missions, particularly for anti-air engagements, but these penalties are frequently small compared to other performance benefits derived from its utilization. These simulation studies and their results are discussed in appropriately general terms.

INTRODUCTION

In recent years there has been much interest in bank-to-turn (BTT) control for guided missiles. The desire to extend range or to shorten the time to the target has led missile designers to consider incorporating airbreathing engines in place of boost-glide rocket motor propulsion. This is an especially attractive alternative with the development of the integral rocket ramjet, which incorporates the booster rocket into the combustion chamber of the ramjet engine for a relatively small propulsion section suitable for air launched missiles.

Most of the work on which this paper is based was accomplished during the development of a BTT guidance system for a ramjet-powered radar guided medium range air-to-air missile configuration. Though the guidance and control algorithms developed under this effort have been verified with simulations, no flight tests have been conducted to show that these algorithms will actually provide good miss performance.

During the next few years a ramjet missile configuration utilizing BTT control algorithms similar to those presented in this paper will probably be flight tested. However, this will most likely be a Control Test Vehicle to validate engine and airframe performance. In parallel, a terminally guided boost-glide missile with these BTT algorithms is needed to validate the guidance and control system performance against real targets. This should ultimately lead to a guided flight test of a ramjet powered homing missile, validating the performance of the integrated airframe, propulsion, guidance and control.

DESIGN CONSIDERATIONS

The question is often asked "Why do we need a bank-to-turn control?" The answer to that question for a guided missile depends on the nature of the missile. For a missile incorporating a ramjet propulsion system, good engine performance with a simple inlet design requires some form of BTT control to provide the inlet with an efficient angle of attack. A long range glide weapon could be made lighter and more aerodynamically efficient by using BTT control. With recent interest in conformal carriage for weapons to reduce launch aircraft radar cross-section, a flat pancake-like configuration is desirable. All of these configurations would maneuver more efficiently with BTT control.

Why don't we have more missiles with BTT control? The guidance problems for homing missiles are compounded with BTT control. Generally, response time is slower with BTT control. It is more difficult to maintain tracking of the target using a simple

© COPYRIGHT 1990 HUGHES AIRCRAFT COMPANY

two-gimbal seeker with BTT control. Body-rate coupling between the autopilot and guidance is increased with BTT control. For these reasons and others, very few missiles have been designed for use with BTT control. Until recently, the guidance and control disadvantages have outweighed the airframe and propulsion advantages. This tradeoff conclusion is no longer valid. Some solutions to the guidance and control problems are presented in this paper.

Providing control logic to accommodate an airbreathing engine for a homing missile is a guidance and control challenge. In order to satisfy carry constraints, minimize weight, and optimize engine performance, airbreathing airframes are generally designed asymmetrically and have a preferred maneuver plane. This asymmetric vehicle tends to benefit from a BTT autopilot. The conventional skid-to-turn (STT) autopilot, if used with the asymmetric vehicle, would not only require complicated engine and inlet designs in order to accommodate sideslip but the air inlets would induce significant pitch-yaw-roll aerodynamic coupling moments. Thus the asymmetric rolling airframe has new and different control problems that must be solved by the guidance and autopilot design. These include response time penalties and coupling through the guidance sensor. The last is the most serious because the bank angle steering commands, responding to target motion, come from the guidance sensor that has the coupling paths in roll through gimbal dynamics, boresight errors, tracking dynamics, steering laws, filtering and for radar seekers, radome errors and polarization attenuation (for passive or semiactive systems).

BANK-TO-TURN CONTROL

The goal of the pure BTT control law is to roll the the missile so that it always maneuvers in its preferred maneuver plane. A maneuver in this plane will be called a pitch maneuver with a pitch load factor. A BTT control must be such that the load factor in the orthogonal yaw plane, is driven toward zero.

If the load factor commands ($\hat{a}_H$) and ($\hat{a}_V$) are referenced to horizontal and vertical planes, then the achieved horizontal and vertical plane load factors will be defined as a function of pitch and yaw load factors and the inertial roll angle, ϕ.

$$a_V = a_P \cos\phi - a_Y \sin\phi$$
$$a_H = a_P \sin\phi + a_Y \cos\phi \qquad (1)$$

If a_Y is to be equal to zero, then the load factor commands $\hat{a}_V$ and $\hat{a}_H$ must be responded to by an autopilot structure that commands the pitch load factor $\hat{a}_P$ and the appropriate roll angle as a function of $\hat{a}_V$ and $\hat{a}_H$. The pitch and yaw commands can be obtained from the inverse of Equations 1.

$$\hat{a}_P = \hat{a}_V \cos\phi + \hat{a}_H \sin\phi$$
$$\hat{a}_Y = -\hat{a}_V \sin\phi + \hat{a}_H \cos\phi \qquad (2)$$

Since the goal of BTT is to drive a_Y to zero, the command $\hat{a}_Y$ from the guidance system should also be zero. To satisfy this requirement, the roll angle command can be obtained from the second of Equations 2.

$$\hat{\phi} = \tan^{-1} \frac{\hat{a}_H}{\hat{a}_V} \qquad (3)$$

A bank-to-turn control system could then be postulated which would use Equation 3 for the roll channel command and the first of Equations 2 for the pitch channel command. The yaw channel command would be set equal to zero.

Another BTT control law can be formulated based on the roll error, if the yaw load factor is to be driven to zero. The error in the roll angle, ϕ_ε, can be determined directly from the measured load factors in body coordinates.

$$\phi_\varepsilon = \tan^{-1} \frac{a_Y}{a_P} \qquad (4)$$

Using the control law of Equation 4 causes the yaw control channel dynamics to appear within the roll attitude control loop. Earlier studies showed that the phase lag, produced by the yaw dynamics, limits the gain and results in a significant response time penalty. This penalty might be acceptable for some combined BTT and STT systems, but there does not appear to be any advantage to this implementation. A better approach uses the command values of a_P and a_Y in Equation 4 to obtain:

$$\phi_\varepsilon = \tan^{-1} \frac{\hat{a}_Y}{\hat{a}_P} \qquad (5)$$

This control law is especially convenient when the body referenced load factor commands can be generated directly from a two-gimbal seeker and guidance law with pitch and yaw channel outputs. A good approximation to the arctangent function is the argument itself. To avoid dividing by zero in the algorithm, $\hat{a}_P$ can be limited to some small positive value, or a constant (i.e., unity load factor) can be added to $\hat{a}_P$ in the divisor of the argument. The latter approach for developing the roll channel command is particularly useful for certain BTT configurations.

If the guidance commands are roll stabilized, the roll angle command of Equation 3 can be used. Functionally, roll angle control with Equation 5 is equivalent to that using Equation 3 except for the impact of filtering in the guidance loop. This will be discussed later in this paper.

CONTROL LAW ALTERNATIVES

Because a monowing or planar airframe autopilot should be designed to take maximum advantage of aerodynamic maneuverability, it will require BTT control; however, a cruciform airframe may use some form of STT or even a combination of STT and BTT. The fundamental difference between BTT and STT is that with STT control, the roll control channel receives no commands from the guidance system, while with the BTT control some form of command comes from the guidance system to the roll channel. Figure 1 shows a typical STT control with the yaw channel of a two-gimbal seeker providing an acceleration command to a load factor autopilot in response to a yaw (azimuth) line-of-sight rate. Only aerodynamic coupling exists between the yaw and roll channels. A typical BTT control shows the yaw acceleration command going to the roll control channel with an optional input to the yaw autopilot channel.

The several types of BTT control laws include those that 1) require the missile to roll as much as 180 degrees to produce a maneuver in the desired direction, or 2) limit the bank angle to something less than 180 degrees. A cruciform aerodynamic configuration might use a ±45° BTT control. The ±45-degree BTT could minimize induced rolling moments. The improvement in performance over a STT control might not justify the additional complexity. However, a ±90-degree BTT control is worthy of consideration for a missile with one plane of symmetry.

The different BTT control laws differ largely in how they perform a downward maneuver, i.e. to go straight down, the ±180-degree BTT control shown in Figure 2 requires a 180-degree roll. This allows the vehicle to be designed with a preferred maneuver plane and a positive angle of attack for maximum propulsion efficiency. While this BTT control law has the poorest response time for a downward maneuver, it is suitable for midcourse flight where efficient engine operation is important.

In Figure 2 and in the following figures, the roll angle control or BTT gain is labeled K_R. It is assumed that it will drive a roll rate control channel in the autopilot. The control deflection commands for the pitch, yaw and roll channels are labeled δ_{pc}, δ_{yc} and δ_{ac}, respectively. The gravity bias (g bias) is assumed to be a function of the measured roll angle, ϕ.

Some work has been done to show that response time with a 180-degree BTT control can be faster than that of a 90-degree BTT control. This would require an accurate cross feed between the yaw and roll control channels to make the yaw rate equal to the roll rate times the pitch angle of attack. This cross feed is difficult to mechanize, and it appears questionable whether the response time advantage can be realized. The real advantage of this approach is the elimination of transient side slip. This may be desirable if propulsion system operation is very sensitive to sideslip angle. Past work has revealed great difficulty in eliminating transient sideslip with cross feed without some penalty in response time.

The ±90-degree BTT control laws can be made self-righting or not and, because negative as well as positive load factors and angles of attack occur, they provide faster response time for downward maneuvers than the ±180-degree BTT. Negative angle of attack operation is generally unsuitable during midcourse because it compromises engine performance. Figure 3 illustrates a ±90-degree BTT implementation which, because of a sign change with negative pitch load factor commands ($\hat{a}_p$), may be flying upside down with negative angles of attack at impact. Figure 4 shows an approach that will always be selfrighting, but may require a snap-roll as the vertical plane command ($\hat{a}_y$) goes from negative to positive. These ±90-degree BTT control laws have reduced sensitivity to noise and boresight error.

The pitch and yaw channels for the autopilot are assumed to be load factor control (see Figure 5). An integrator is included in the acceleration control loop of both channels to reduce the sensitivity of the closed-loop steady-state gain to flight condition. The integrator may not be needed for the yaw channel with BTT control, but the integrator provides a path for static stability augmentation of the airframe (K_θ in Figure 5). This path may be necessary because of unstable values of $C_{n\beta}$ especially during the boost flight phase. Removing the integrator in the yaw channel is desirable in that it would speed up the response thereby reducing the transient sideslip generated during a rapid bank maneuver.

Some compensation is shown in the rate damping path of Figure 5. This is assumed to be a simple filter to attenuate noise and to control the high frequency gain margins of the control channel. Gain scheduling is assumed to be provided by an inertial reference system as a function of altitude and Mach number. The gain K_{ss} is provided to keep the steady-state gain of the load factor control equal to unity.

To maintain satisfactory engine performance and to provide stable autopilot conditions, some angle of attack control must be exercised. This can be accomplished by programming the load factor control limits on $\hat{a}_p$ and $\hat{a}_y$, and the control deflection command limits (δ_{LIM} in Figure 5) as a function of Mach number, altitude, and time.

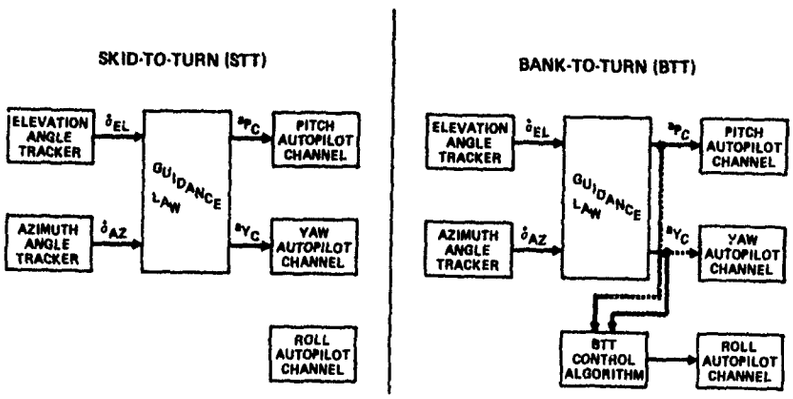

Figure 1 - Guidance and Control Configurations

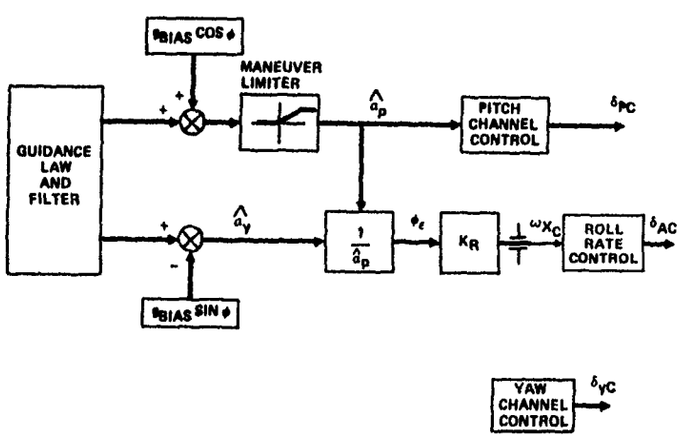

Figure 2 - 180 Degree Bank-to-Turn Control

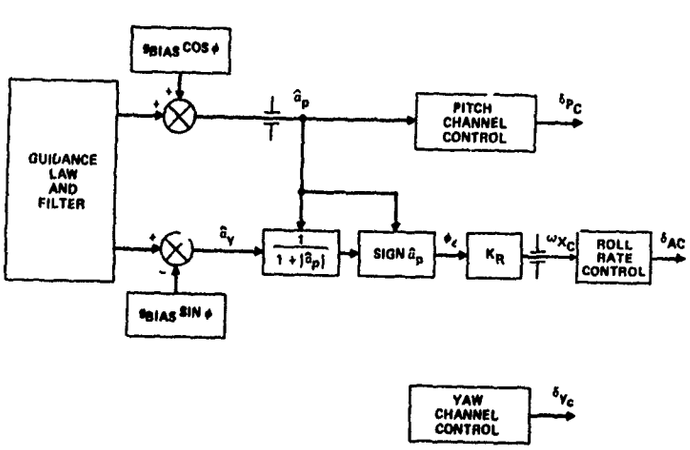

Figure 3 - 90 Degree Bank-to-Turn (Non-Righting)

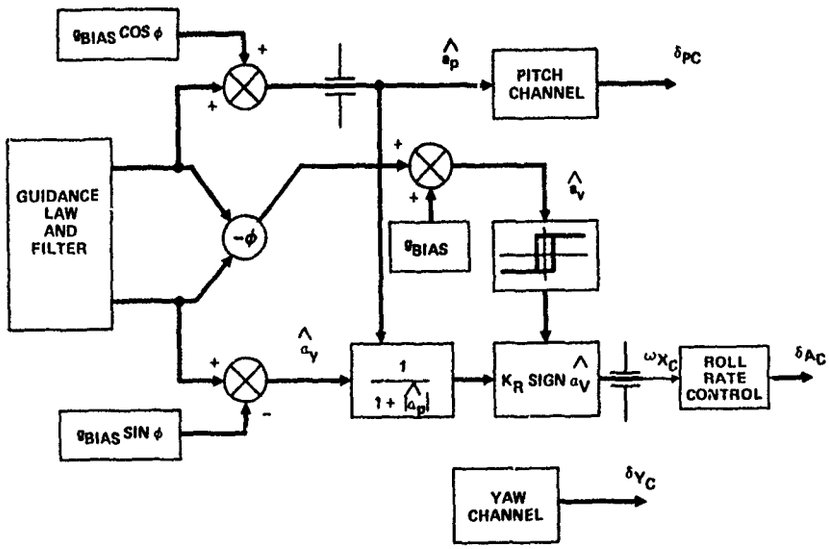

Figure 4 - 90 Degree Bank-to-Turn (Self-Righting)

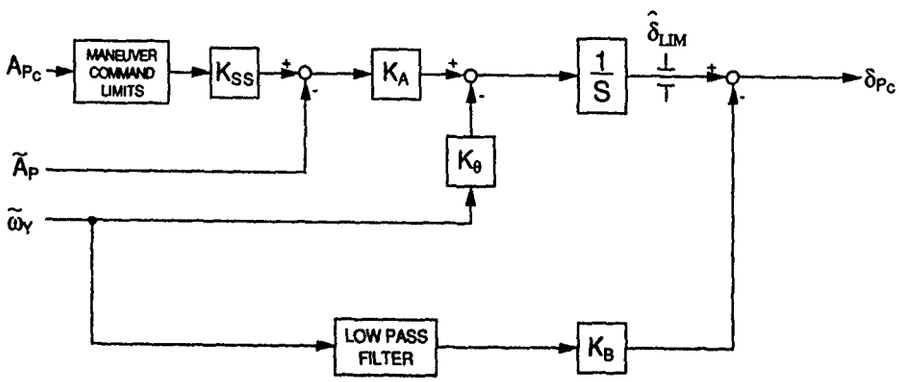

Figure 5 - Pitch (Yaw) Control

RESPONSE TIME CONSIDERATIONS

Much discussion has been devoted to the so-called response time penalty paid for BTT control because missile response time has been a traditional criterion for evaluating autopilot performance. However, establishing the minimum range capability by using six to ten time constants may not be appropriate for BTT control. This is because the BTT time constant is nonlinear or at least time-varying; e.g., to pitch down with ±180-degree BTT, the initial response may be slow, but the response to subsequent commands may be faster if smaller roll maneuvers are required. Although there is some amount of response time penalty, the use of the initial response time as the sole c iterion for performance evaluation unduly penalizes the BTT control law. The traditional response time relationships are still applicable to BTT against targets that maneuver just prior to intercept because it is the initial response that is important for this type of engagement.

Measured response times on a simulation show a BTT penalty that is large if a 180-degree roll is required, especially at low altitudes where the response of the roll channel is significant compared to the pitch response. Figure 6 shows that high maximum roll rates help, but the penalty appears large enough to make a 180 degree BTT configuration an unlikely candidate for terminal control. This response time is defined as the time required to reach 63 percent of the commanded maneuver in the desired plane. The maneuver response is affected by the response time of the roll channel as well as the limit on roll rates.

From Figure 6 it can be noted that the response time penalty for a 90 degree bank maneuver is modest and is not a strong function of roll rate, especially at higher altitude where the response time is largely a function of the pitch channel response.

By combining BTT control with STT control as shown in Figure 7 an improvement in response time can be achieved. This is especially useful against maneuvering targets as shown in Figure 8. Figure 8 illustrates the normalized miss performance of a typical air-to-air missile against a typical target as a function of the ratio of the yaw load factor limit to the pitch load factor limit. Note that pure ±90-degree BTT control appears adequate against a non-maneuvering target, but some small yaw load factor capability provides substantial reduction of miss against a maneuvering target.

AIRFRAME CONSIDERATIONS

Autopilot design for BTT homing missiles is more complex than for STT missiles, largely because of the coupling of the guidance system into the high gain roll control channel. However, it is also important to note that a BTT missile will maneuver in primarily one plane. It is therefore desirable to provide an aerodynamic configuration which is easily controllable in that maneuver plane.

An airframe with stable induced aerodynamic rolling moment is especially desirable if the missile is expected to generate high angle of attack maneuvers. Figure 9 shows a front view of three typical air-breathing missile configurations. Figure 9a shows a configuration with a single underslung air inlet and a "plus" tail (and possibly wing) orientation. This configuration will likely have an unstable C_{l_β} (rolling moment coefficient, C_l, variation with sideslip, β) at supersonic Mach numbers for both positive and negative angles-of-attack. The configuration of figure 9b with the tails rotated to an "X" orientation has better roll stability characteristics, though the inlet may still produce an unstable C_{l_β} for positive angles of attack.

The best aerodynamic roll stability is likely to be produced by a dual "cheek" inlet configuration with an "X" tail arrangement (See Figure 9c). A shoulder or side mounted inlet will also provide good aerodynamic roll stability with an "X" tail orientation and will also support a wing, if needed and if launcher fitment allows. This latter configuration is usually more difficult to fit onto present aircraft launch stations.

The autopilot designer should attempt to influence the missile aerodynamic design early in the configuration study phase to provide favorable aerodynamic induced roll characteristics. This should make design of a BTT control, with its inherent guidance coupling paths, easier than if the autopilot must just be designed to accomodate the unstable C_{l_β}. Other factors, such as missile weight, engine performance and fitment, may be overiding considerations, but aerodynamic roll stability should be weighed into the missile configuration tradeoffs.

GUIDANCE SYSTEM CONSIDERATIONS

Homing missiles, especially anti-air missiles, generally use some form of proportional navigatio guidance law to develop an efficient trajectory to the target with a high probability of kill. This form of guidance law requires measurement of the line-of-sight (LOS) rate to the target. The target is tracked by a sensor which is assumed to be mounted on a stabilized two gimbal platform located in the nose of the missile. This platform will generally roll with the missile. This rolling of the guidance sensor is the major source of coupling between the autopilot and the guidance system.

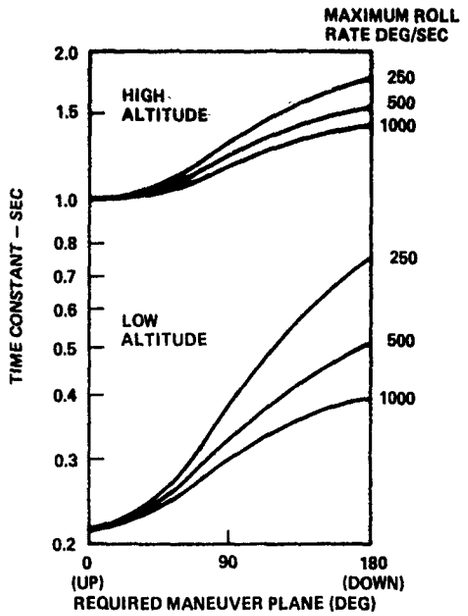

Figure 6 - Response Time Sensitivity to BTT Control

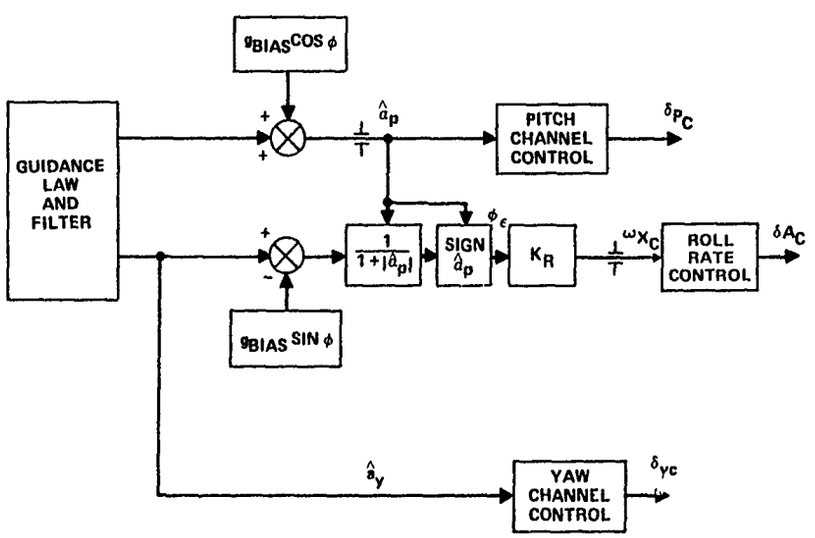

Figure 7 - 90 Degree Bank-to-Turn Combined with Skid-to-Turn

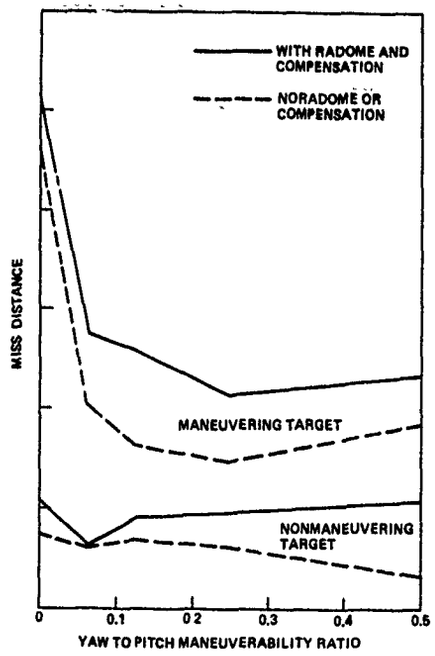

Figure 8 - Effect of Combined BTT and STT

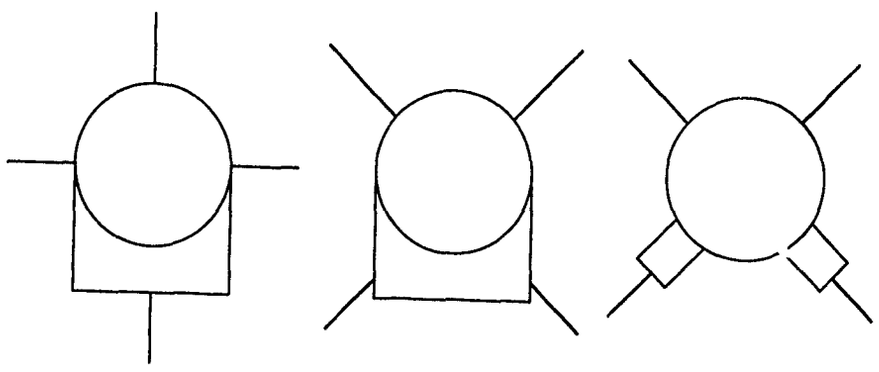

(a) Poor (b) Better (c) Best

Figure 9 - Airbreather Inlet-Tail Configuration/Roll Controllability Considerations

The dynamics of the tracking errors (ε) and LOS rates ($\dot{\sigma}$) in the pitch and yaw coordinates of the sensor platform are given by the following equations.

$$\dot{\varepsilon}_y = \dot{\sigma}_y - \omega_{sz} - \omega_{sx}\,\varepsilon_p$$

$$\ddot{\sigma}_y = \frac{1}{R}(a_{ty} - a_{my}) - \frac{2\dot{R}}{R}\dot{\sigma}_y - \omega_{sx}\,\dot{\sigma}_p \qquad (6)$$

$$\dot{\varepsilon}_p = \dot{\sigma}_p - \omega_{sy} + \omega_{sx}\,\varepsilon_y,$$

$$\ddot{\sigma}_p = \frac{1}{R}(a_{tz} - a_{mz}) - \frac{2\dot{R}}{R}\dot{\sigma}_p + \omega_{sx}\,\dot{\sigma}_y,$$

where ε_y (ε_p) is the tracking error in yaw (pitch),
$\dot{\sigma}_y$ ($\dot{\sigma}_p$) is the LOS rate in yaw (pitch),
ω_{sx} is the sensor roll rate,
ω_{sz} (ω_{sy}) is the sensor yaw (pitch) rate,
a_{ty} (a_{tz}) is the target acceleration in yaw(pitch),
a_{my} (a_{mz}) is the missile acceleration in yaw (pitch),
R is the range to the target, and
$\dot{R}$ is the missile to target range rate.

The pitch channel is the primary steering channel for a BTT missile. Neglecting gimbal angles and tracking dynamics, a simple block diagram of the pitch plane guidance (Figure 10) shows that the rolling of the missile creates a disturbance to the guidance loop, but does not affect stability. The guidance loop is closed primarily through the pitch autopilot as with a STT missile.

For the yaw channel, however, the yaw autopilot command is primarily used to control the roll of the missile and a feedback loop is created through the autopilot roll control. The simple block diagram of Figure 11 shows that the yaw guidance channel is closed through the roll autopilot. The loop gain, as seen in figure 11, is the product of pitch LOS rate $\dot{\sigma}_p$, the guidance gain for proportional navigation $\lambda\dot{R}$ and the gain K_R, divided (approximately) by the pitch channel lead factor command a_{pc}. An integration is included between the roll rate ω_x and the roll rate command ω_{x_c}. Since the pitch command is equal to $\lambda\dot{R}\,\dot{\sigma}_p$ the loop is basically a roll attitude feedback through a gain K_R. The addition of other dynamics and feedback paths creates stabilization problems for this simple roll attitude feedback control. These problems are discussed in the following paragraphs.

If a simple angle tracking loop is added to the guidance loop and the seeker pointing command is used as a LOS rate estimate, the pitch tracking error also becomes a feedback parameter for the roll control channel as shown in figure 12. The pitch tracking error can be reduced by adding an integral control to the angle tracker. However, due to boresight errors, the true pitch pointing error will rarely be driven to zero. Therefore, considerable effort must be directed toward minimizing boresight error for seekers when using BTT guidance.

Before proceeding further, some discussion must be directed toward seeker stabilization. For a responsive roll control, the seeker stabilization must be a high bandwidth configuration to maintain small tracking errors and to avoid loss of lock on the target. For imaging seekers, or low data rate seekers, the roll rate may have to be limited to avoid image smear or loss of target data. Also, to minimize the size of the outer gimbal torquers, the angular acceleration may have to be limited.

Generally, for a BTT guided missile, the preferred gimbal orientation is to have the outer gimbal be the pitch gimbal and the inner gimbal be the yaw gimbal. If the gimbals are oriented so that the outer gimbal is the yaw gimbal, there is a coupling path from roll angular acceleration which can be destabilizing to the BTT control. This is illustrated in figure 13. A comparable coupling path from roll into the inner gimbal does not exist. Note also, that by designing the on-gimbal mass to have a small moment of inertia in roll, the coupling from roll into the outer gimbal stabilization loop can be reduced.

Assuming the outer gimbal is the pitch gimbal, some techniques for compensating for the dynamic lag of the angle tracking loop in the BTT feedback path can now be discussed. Figure 12 shows a simple angle tracking loop. If an integrator is added to the loop in both the pitch and yaw channels, the tracking errors will be maintained small. This will reduce the gain through the pitch tracking error in the BTT control and provide a path for coupling the pitch and yaw channels with the seeker roll rate as shown in figure 14. This coupling will provide some lead compensation for the measure of the yaw LOS rate variation as the missile rolls. Thus if the estimated pitch LOS rate is equal to the actual LOS rate, the dynamic lag of the angle tracking loop is removed from the BTT feedback path through the yaw channel of the guidance system. This is shown in figure 15.

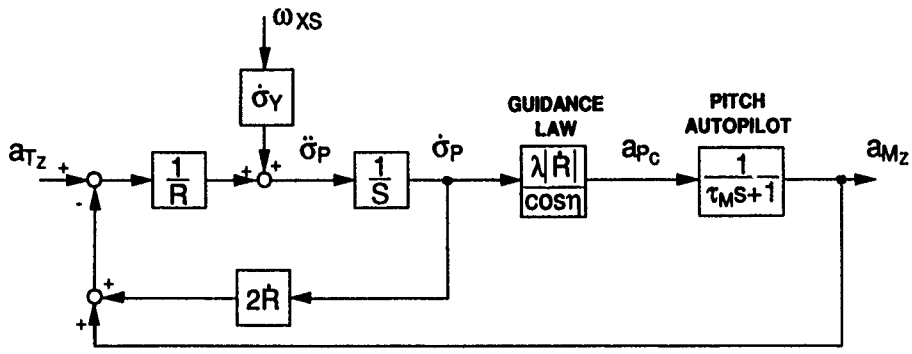

Figure 10 - Pitch Plane guidance with BTT Control

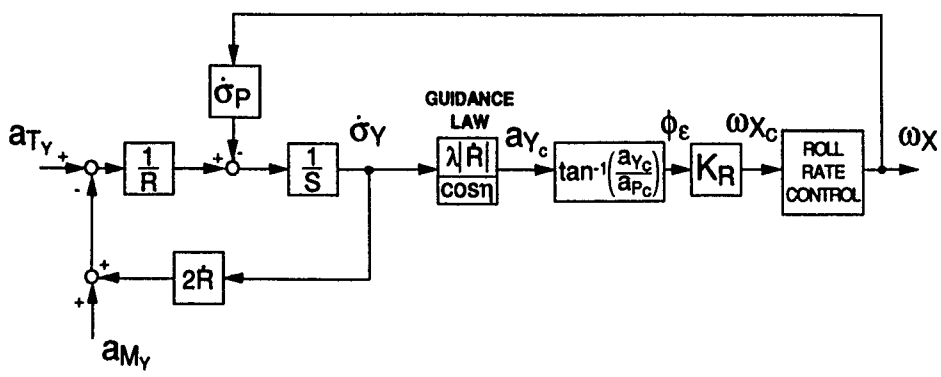

Figure 11 - Yaw Plane Guidance with BTT Control

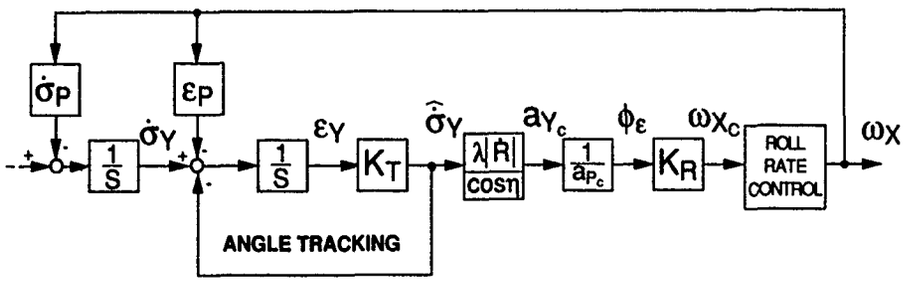

Figure 12 - Yaw Plane Guidance with Angle Tracking

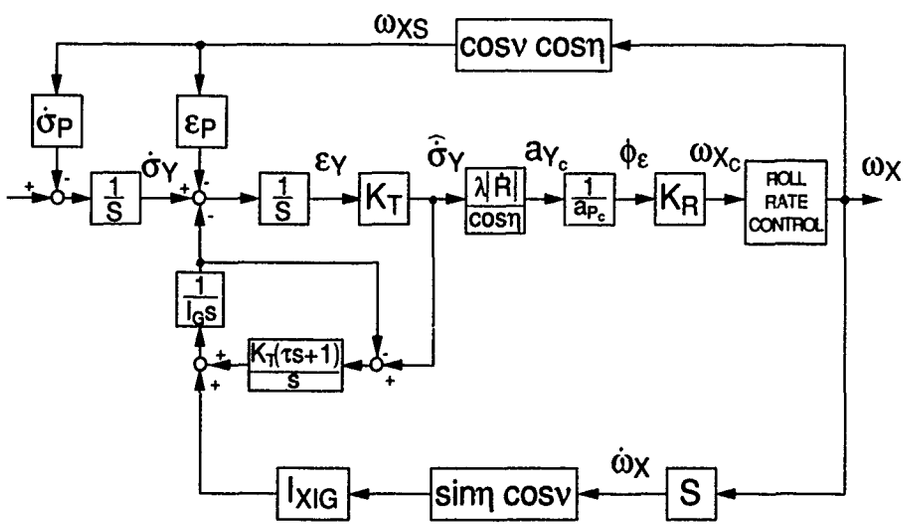

Figure 13 - Roll Coupling into Outer Gimbal Stabilization

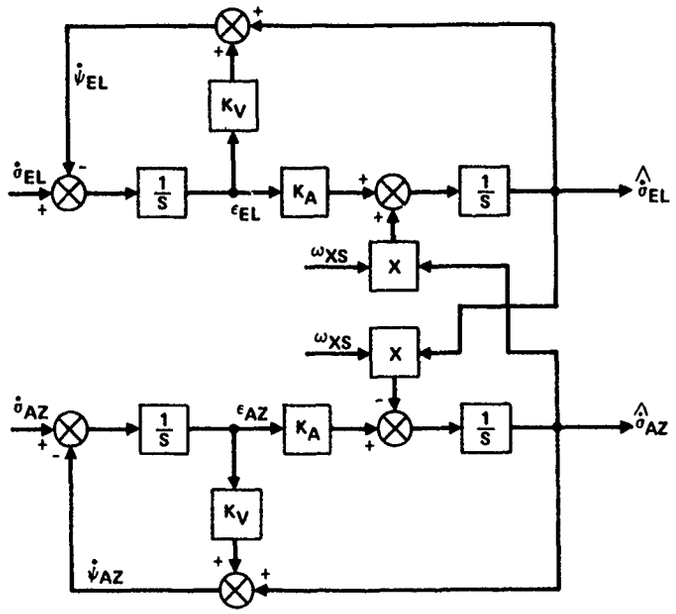

Figure 14 - Angle Tracking with Roll Decoupling

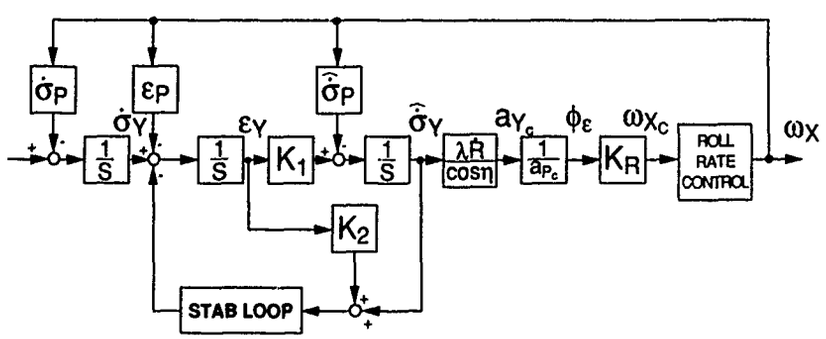

Figure 15 - Yaw Guidance with Roll Decoupling

The above approach does not remove the pitch tracking error as a feedback path. However, the integral control for the pitch angle tracker will keep the tracking error small (except for noise and boresight error). Another approach is to implement a more complicated angle tracker mechanization, i.e. a multi-state coupled Kalman filter.

EFFECT OF BORESIGHT ERROR

The pitch tracking error due to boresight error is difficult to compensate for. This error can be attributed to misalignment between the guidance sensor axes and the reference axes of the inertial instruments used for stabilization, the electromagnetic window through which the guidance sensor must "look" at the target, or the reflections of the sensed electromagnetic radiation within the compartment on the missile which houses the guidance sensor.

The misalignment can be made small by specifying tight alignment accuracies, but this could be costly in manufacturing, and the residual error may still be significant. Accuracies of 0.1 degree or less are desirable. An alternative approach is adjustment after assembly. If compensation for the error due to the electromagnetic window, such as a radome, is made after assembly, all three effects can be compensated for at the same time. This would require each guidance section to have a unique compensation which would vary with gimbal angle and, probably, frequency. A total residual error of about 0.1 degrees or less is required for a high performance BTT control.

A simple block diagram of the boresight error feedback path is shown in figure 16. Note that the gain through this path is very high if the pitch acceleration command a_{pc} is small. The 90° BTT algorithm with the one g bias added to the a_{pc} before dividing into a_{yc} reduces the sensitivity to the boresight error. However, the residual boresight error for radar seekers will generally limit the gain K_R, even after compensation.

Radome boresight error 'slope' compensation is used on some modern radar-guided missiles. This compensation is required to reduce in-channel body rate coupling for these skid-to-turn missiles. For BTT missiles, boresight error compensation can be used for in channel body rate coupling compensation as well as the BTT roll feedback compensation. The ideal approach to compensation is to add it directly to the measured pitch and yaw tracking errors. The compensation values are taken from tables which are functions of the measured gimbal angles and the frequency of the radar transmissions.

EFFECT OF GUIDANCE SENSOR NOISE

Noise on the tracking error signals from the guidance sensors and signal processing can be a problem for BTT control. Even after filtering acceptable for steering commands, the residual noise can cause significant roll rate transients because of the relatively responsive roll rate control. This is especially true for radar seekers. Figure 17 shows the roll rate time history from a simulation of a radar guided BTT missile. The early portion of the flight used command-inertial midcourse guidance with a 180° degree BTT control similar to that of figure 2. The latter portion, where the noise is significant, is an active radar terminal homing mode with a ±90 BTT combined with STT control. Additional filtering was added to the acceleration commands used for the BTT control algorithm as shown in figure 18. This simple lag filter for both the pitch and yaw acceleration commands had to be roll rate-coupled as illustrated in figure 19. The resultant roll rate time history was considerably more active than that for a typical STT missile. The filter time constant was selected empirically to reduce the roll rates due to noise without affecting miss distance performance.

SUMMARY OF SIMULATION STUDIES

Six degree-of-freedom (6 DOF) simulation with relatively detailed models has shown that performance with BTT control for a ramjet-powered, radar guided, medium range air-to-air missile was excellent. Much of the performance advantage over a similar size boost-glide missile was due to the higher terminal velocities of the ramjet-powered configuration. But miss performance achieved with the 90° BTT control combined with STT control (see figure 18.) was comparable to that of the pure STT missile at comparable terminal velocities. The slightly increased response time of the BTT control produced a small increase in the inner launch zone and a modest increase in maneuvering target miss for maneuvers at short time-to-go.

The 6 DOF simulation was used to validate the BTT control algorithms discussed in the previous paragraphs. Included in the simulation were the guidance roll coupling algorithms, radome error compensation and the antenna stabilization control loops. The impact of not including the roll coupling in the angle tracking loop and other guidance filtering was increased miss and frequent loss of roll control. This was also true for operation without radome boresight error compensation.

Further verification of the algorithms was achieved with implementation in a hardware-in-the-loop (HIL) simulation using an actual radar seeker and a guidance and control processor. Though the amount of testing was limited due to budget and time constraints, stability and controllability were demonstrated for several engagement conditions.

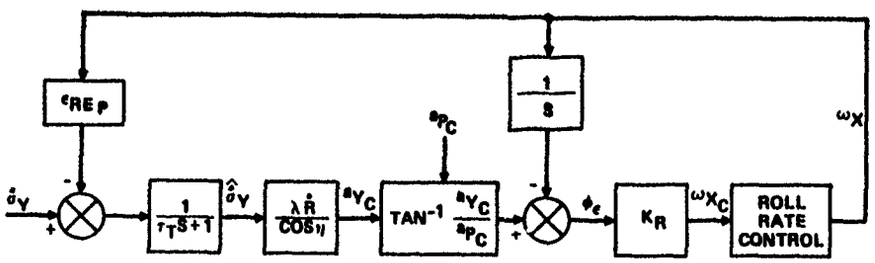

FOR STABILITY: $\frac{\lambda \dot{R}}{\cos\eta} \frac{1}{a_{P_C}} \left(-\epsilon_{RE_P}\right) < \tau_T + \frac{1}{K_R}$

Figure 16 - Yaw Guidance with Pitch Boresight Error

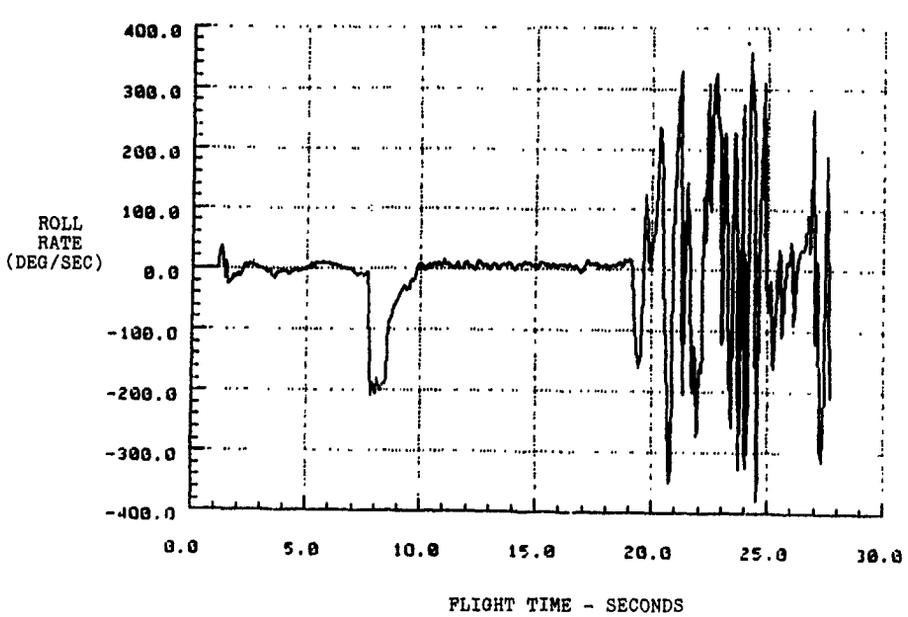

Figure 17 - Effect of Radar Noise on BTT Roll Rate

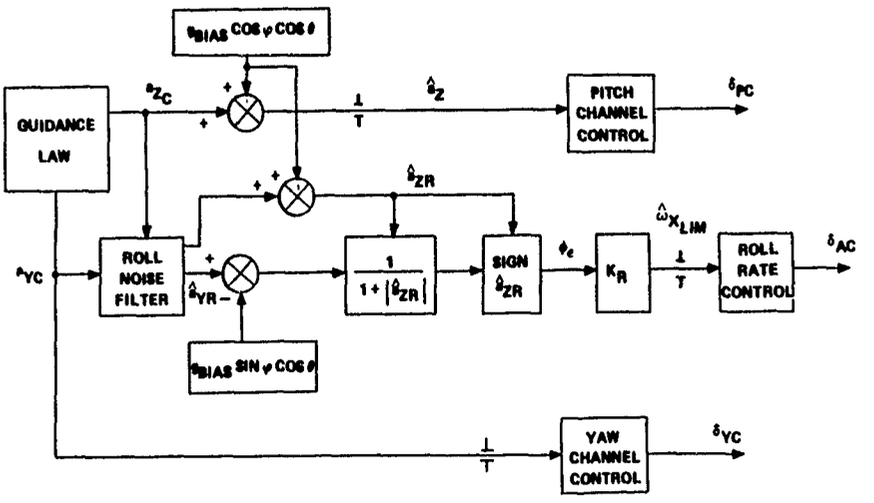

Figure 18 - Noise Filter in BTT Control

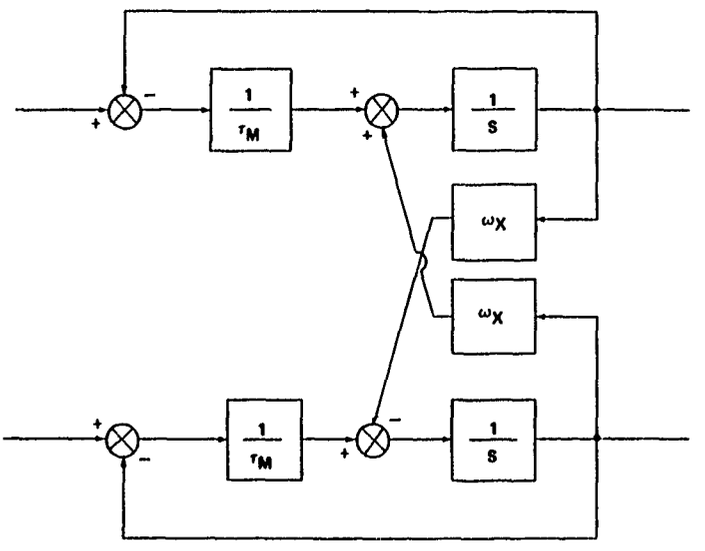

Figure 19 - Roll Noise Filter with Roll Decoupling

The HIL simulation was especially effective in evaluating the radome boresight error compensation. Simulation runs were made with and without the compensation and with and without the radome. Though RMS miss for runs made with the radome and compensation was increased by 50 percent over the miss for runs made without radome or compensation, good controllability was exhibited, and the results from the digital 6 DOF simulation produced a similar increase in miss. When radome error compensation was removed, the controllability was poor and the miss was increased by 100 percent over the miss with compensation, or 300 percent greater that the miss without radome or compensation. This evaluation was only made for one engagement condition, but it appears to validate the feasibility of maintaining a stable BTT control with radome error compensation tables.

The simulatio` studies conducted on this missile configuration demonstrated the feasibility of using BTT guidance and control for terminal homing missiles. The results further illustrate that the autopilot designer must work closely with the guidance designer to assure that body rate coupling through the guidance system can be controlled in an integrated high performance guidance and control system.

Reference: Proceedings of the Workshop on Bank-to-Turn Controlled Terminal Homing Missiles, 19-20 September 1984, GACIAC PR-85-01

GUIDANCE SIMULATION MODEL OF ANTISEA-SKIMMER UTILIZATION FOR WEAPON SYSTEM DEFINITION

by G. VALLAS - "DASSAULT ELECTRONIQUE " -
55, quai Marcel Dassault - 92214 SAINT-CLOUD - FRANCE

and F. BUREL - "AEROSPATIALE DIVISION ENGINS TACTIQUES"
2 à 18, rue Béranger - 92320 CHATILLON - FRANCE

ABSTRACT:

This article summarizes the way of quantifying the main parameters which size an antisea-skimmer missile by using numerical simulations.

The ammunition-sizing can only be correctly defined when a sufficient number of iterations is achieved with the modelization tools, taking into account the specification of the threat and cost constraints.

This text describes a method of evaluation of the main parameters and specifies the primary function of the simulation during the various phases of the project.

1.- INTRODUCTION

The design of the anti-missile system, and in particular, of the antisea-skimmer missile is broadly based on requirements specified by the Defence Ministry Officials.

The description below covers a method for defining an antisea-skimmer based on the following main threat characteristics:

- highly maneuvering target,
- high constraint environment (jamming) requiring all-weather defence capabilities,
- saturating and multidirectional attack scenarios.

Based on these characteristics, a vertically-fired missile is required with:

- a mid-course guidance system operating on information from the IMU* and fire control system periodically refreshing data concerning the target,
- an independent terminal guidance system using an active electromagnetic seeker,
- a "lethality" function ensured through an electromagnetic proximity fuze and a warhead, detonated by the on-board computer of the missile to obtain optimum results.

* IMU = Inertial Measurement Unit

2.- MAIN INTERACTIONS BETWEEN SYSTEM COMPONENTS

An accurate description of the threat is fundamental to system definition, in particular that of the missile.

CHART 1 shows the main characteristics of the threat:

- electromagnetic representations of the target are required in order to design the radar, the seeker and the proximity fuze,
- all of the average trajectory types and penetration maneuvers are incorporated to define guidance/control requirements, to characterize (in part) the radar, the fire control and seeker systems,
- data relative to target vulnerability are taken into account to design the warhead,
- the environment, whether natural or not, is an essential aspect which intervenes in:
  - the design and sizing of the radar, the seeker and its antenna, and the proximity fuze,
  - generation of guidance methods and seeker software.

The multi-target nature of the threat (not shown in chart 1) which can be apprehended through the scenario definition (number of targets, directions and rates of attack, spacing between targets, target objectives, etc.) should not be neglected as these can have multiple repercussions on the definition of the radar, the fire control system, the missile and its seeker, and the launcher. These various aspects are not covered in this document but should however be taken into account from the beginning of the project due to the technical and financial implications.

It is therefore necessary to define the main requirements relative to performance of the missile and its equipment.

CHART 2 provides an overall block diagram of the procedure adopted:

- the characteristics of the threat, shown in chart 1, lead to definition of the guidance/control requirements:
  - requirements related to trajectory shaping following vertical firing for interception at the specified short range. These requirements will bear on the aerodynamic profile and propulsion profile during the boost phase at least. These will have repercussions on the sizing of the structure and can be viewed in terms of performances required of the steering control components,
  - requirements related to autoguidance: load factor, static margin, autoguidance time constant, i.e. time constant of autopilot and time constant for generation of guidance signal. These parameters in turn condition the dynamic performances of the IMU and the steering control components, and limit the angular error measurement extraction time of the seeker.
- in view of the specified domain, and more particularly, the maximum intercept range, and taking account of the radar's detection capacities and the minimum duration of the firing sequence, the average missile speed requirement is defined.
- similarly, carrying constraints relative to the launcher also contribute in defining the the airframe.

The choice of aerodynamic definition, the propulsion project and missile architecture must satisfy the first two requirements mentioned above while observing geometry constraints and characteristics (weights in particular) of the missile equipment.

CHART 3 shows the main interdependent links between the various system parameters. This chart shows certain key aspects in the antisea-skimmer missile design:

- as concerns the equipment:
  the lock-on range of the seeker depends on the seeker itself, the target's radar cross section and the environment (jamming), but also on the trajectory shaping process used to minimize the influence of jamming and target designation errors which will be covered in paragraph 4. These can be due to a certain number of items, including the static accuracy of the IMU for which the static performance requirements must be defined.
- as concerns the missile software:
  the trajectory shaping, seeker logics and processing circuits for signals received by the homing head and autoguidance functSions are highly conditioned by the "countermeasures" component of the threat.

When satisfying the requirements relative to the autoguidance function mentioned above, when obtaining a seeker lock-on range providing a sufficient autoguidance duration with respect to aim-offs to be corrected and ensuring the quality of the guidance signal generated by the logics and seeker signal processing circuits, then the intercept miss-distances will be reduced as far as possible.

As a function of these parameters, the proximity fuze/warhead pair must be optimized to ensure maximum terminal efficiency. Electromagnetic characteristics of the target for the proximity fuze, environmental conditions, geometry and kinematics of interception at the end of the autoguidance phase, as well as the target's vulnerability, form the context in which this optimization process must be carried out.

Chart 3 shows the complexity of the system to be designed: the arithmetic simulations at this level are an indispensable design aid.

3.- ANALYSIS OF CONSTRAINTS RELATIVE TO AUTOGUIDANCE DESIGN

3.1 Threat

3.1.1 Maneuvers

3.1.1.1 Effect of maneuvers on intercept miss-distance: influence of interceptor time constant

The sea-skimmer maneuvers performed to penetrate the ship(s) defences are defined by:

- their type (acceleration by levels, for example),
- load factor, which may be very high (+ or - 15G),
- maneuver period.

These maneuvers, associated to the sea-skimmer's autopilot with a low time constant are sizing factors in the interceptor's autoguidance function: required maneuverability, guidance time constant and therefore time constant relative to the autopilot can be observed, and seeker time constant.

With respect to such maneuvers, the influence of the antisea-skimmer's autopilot time constant on the miss distance can be quickly evaluated through a simplified numerical simulation for which a block diagram is given in CHART 4.

This type of simulation is easy to produce and quickly executed. It is therefore moderate in cost. Another advantage is that it can be used to define guidance/control requirements in autoguidance phase in the presence of certain non-linearities (saturations), and supply, in particular, the miss-distance distribution.

CHARTS 5 and 6 show the results obtained for a target maneuvering in steps with amplitudes of 10 or 15 γ, filtered by a second order with 100 ms time constant and damping ratio of 0.7 representing the target pilot. The maneuver period and time constant of the antisea-skimmer (2nd order; $\xi = 0.7$) vary.

Note: The representation of the autopilot transfer in the form of a second order is considered here as an example. It is clear that the user must ensure that the transfer is sufficiently representative (order, damping) of the "actual" loop.

These charts show that, for example, with respect to a threat operating with load factor steps of 10 G and a period of 1.5 s, the miss distances less than n meters in 70% of the cases require a fast antisea-skimmer autopilot: pilot < 1.5τ(ms).

3.1.1.2 Weight of warhead required according to intercept miss-distance inorder to obtain structural kill of the target

For a short range interception, structural kill, rather than functional kill(system kill), of the target is required (i.e. target broken into two sections) to minimize the risk of the target hitting the ship. Furthermore, it is unlikely that a sufficient system kill probability be obtained with respect to the diversity of the geometrical characteristics and the vulnerability of the targets.

Structural kill can be obtained using a fragmentation charge whose efficiency is assessed according to the number $\frac{E}{\sqrt{S}}$(E = total energy of fragment hitting target and S = area covered by impacts on target), corresponding to a classical criterion.

As with all anti-aircraft warheads, the weight of the metal is approximately equal to the weight of the explosive to maximize the kinetic energy of the fragments per kilo of total weight of warhead and obtain fragments of sufficient weight. The energy E is thus optimized and thus the number $E/\sqrt{S}$.

This criterion also shows the interest in minimizing the impacted area (S). Therefore, the design of the warhead must be oriented to focus the direction of the burst.

Furthermore, the aspect ratio of the warhead must be sufficient to minimize the effect of leaks at the ends thus optimizing the ejection speed of the fragments. This provides two advantages:

- for head-on interceptions, fragment impact incidence on target sharply lower than ricochet incidence,
- highest possible time range between target detection by the proximity fuze and detonation of the warhead, thus maximizing the explosion delay adjustment margin.

The total weight of the warhead required as a function of the intercept miss-distance to obtain structural kill of the target can be determined through a conventional numerical simulation tool structured as follows:

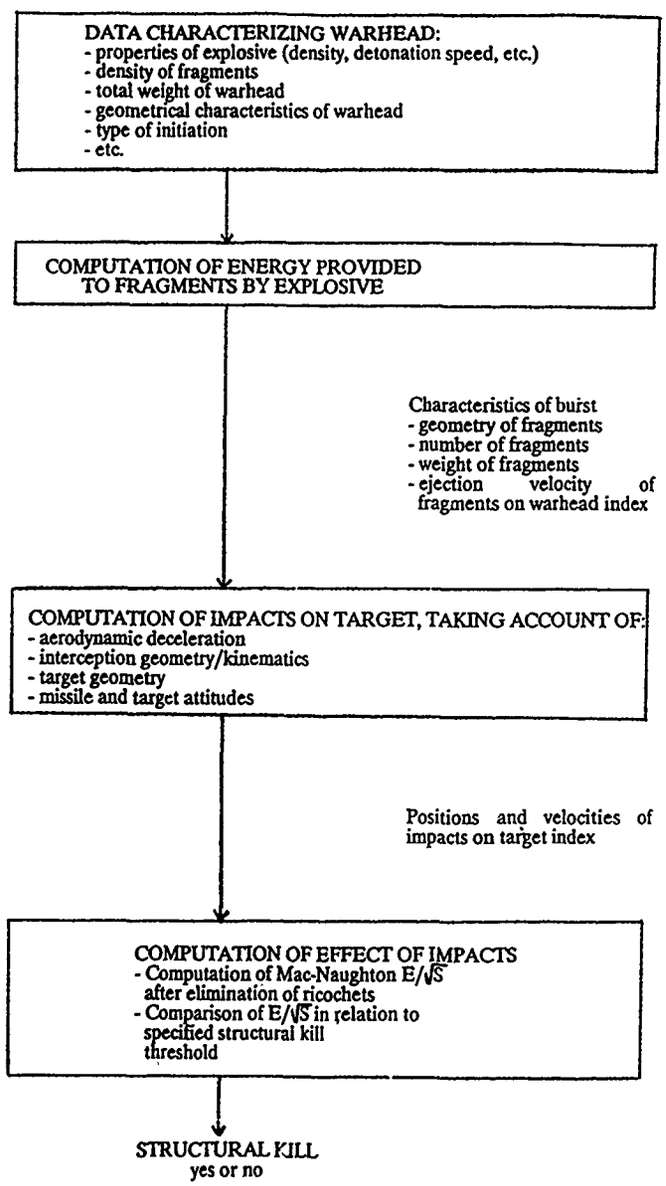

CHART 7 shows the results obtained by using a model of this type for focused-burst warheads with various weights, but all comprising 50% fragments and 50% explosive and all with the same aspect ratio. By maintaining a constant aspect ratio, when the weight increases, the increase in diameter and length of the warhead is limited to the minimum.

This chart shows, as a function of intercept miss-distance, the warhead weight required to obtain structural kill of the target, i.e. so that the number $E/\sqrt{S}$ reaches either the threshold corresponding to a conventional target, or a double threshold corresponding to a hardened target. The considered interception is head-on interception and takes place at 800 m/s (speed of sea-skimmer and interceptor).

It appears that structural kill of the hardened target:

- is obtained, even with a low weight and diameter warhead (≥ 1.5 u kilograms, ≥ 180 mm) when the intercept miss-distance is within a meters,
- is only obtained with larger weight and diameter warheads (≥ 9 u kilograms, ≥ 330 mm) when the intercept miss-distance is high (3.5 a meters).

3.1.1.3 Autopilot constraints

As discussed in paragraph 3.1.1.1, the autopilot time constant must be low, i e. the flight control system bandwidth must be high (a few Hertz). As a result, the equipment bandwidths are high and can be, for some equipment, higher than the natural frequencies of the structural modes.

Let us consider the conventional autopilot structure shown in CHART 8.

At high frequency:

- only the internal loop with gain K3 subsists,
- the rigid missile behaves as a pure inertia, i.e. $\Omega \propto M/Is$.

The loop, opened before the actuator, is therefore:

K3 M/Is x Structure filter x exp (- tc s) x Actuator x IMU

The structural filter, tuned to the natural frequency of the bending modes, is intended to attenuate the peak resonance created by these modes and capable of destabilizing the closed loop.

The presence of this filter, which is necessary with respect to stability, does however introduce a phase lag which requires to increase the response time of the autopilot, and therefore of the guidance loop.

The higher the frequency of these modes, the more the peak resonance will be located in an area where high attenuation is produced by the equipment, and therefore the less this peak will interfere: the need for filtering will therefore decrease. Moreover, the lag at low frequency introduced by the filter, for a given attenuation, decreases when the filter is tuned to higher frequency. So, with higher frequency mode, the autopilot time constant can be made lower with prescribed stability margin. This means that the desired guidance time constant feasibility will be facilitated.

It is therefore preferable to design an antisea-skimmer with low weight and aspect ratio for which the natural frequency of the structural modes will be effectively high.

In sum, the target's maneuver leads to considering the following loop:

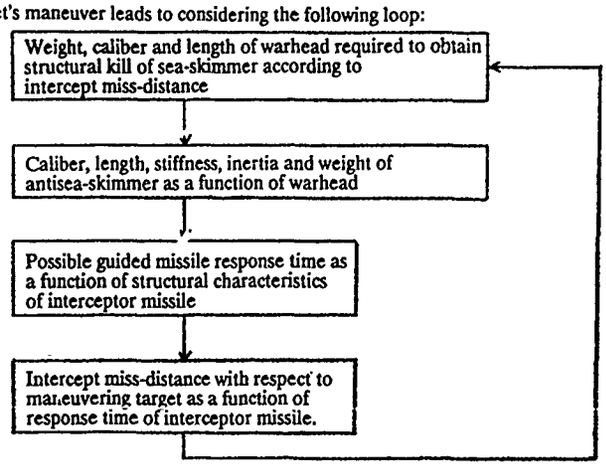

One of the key points in the antisea-skimmer design consists in identifying the solution which will integrate the parameters in this loop through a solution expressed in terms of weight of warhead/weight of missile/guidance time constant/intercept miss-distance.

3.1.2 Definition of seeker antenna satisfying previously established requirements

To obtain command extraction with the lowest possible time constant, the antenna must be a two-axis monopulse type antenna.

Furthermore, to obtain the lowest possible command noise, all things equal, the antenna must have the highest possible efficiency.

This leads to a slotted flat antenna.

The antenna will therefore be formed by four basic arrays providing, by association, the sum (Σ) and difference (ΔE, ΔC) channels.

The model will incorporate the basic pattern of each slot, and mutual couplings.

The quality of the model is shown by comparing the computed model (CHART 9) with measurements performed on the antenna developed (CHART 10) for a 52-slot antenna with a uniform illumination law.

3.1.3 Electromagnetic model of target: glint representation

The seeker and radar use the energy reflected by the target to locate and track it.

This localization function has random interference called glint which must be incorporated in the model when assessing performance with respect to intercept miss-distance.

The angular glint is defined as the difference between the angular location measured and the actual angular position of the target.

The geometrical theory of diffraction shows that the set of different geometrical surfaces forming an aircraft radiates, in the incident direction, a portion of the energy received on a point located on the surface. The position and brightness of each of these points will vary as a function of the target's presentation and small movements of the target around the center of gravity.

The method used to model the glint consists in breaking down the target into elementary facets which are subjected to small relative movements.

An example of glint modelization, confirmed by experience, was performed on an aircraft broken down into 18 facets as shown in CHART 11.

The quality of this model is assessed by comparing the theoretical model (CHART 12) with the measurements performed in carried flight (CHART 13) under the same conditions.

An electromagnetic model of the sea-skimmer can be constructed using the same method.

3.1.4 Electromagnetic modelization of environment

3.1.4.1 Stand-off jammer

The stand-off jammer decreases the range (R) of the seeker according to the following relation:

$$\left(\frac{R_0}{RJ}\right)^4 = \frac{KTF + PJ}{KTF}$$

$$PJ = \frac{(RP)\, G\, \lambda^2\, Lr}{(4\pi)^2\, D^2}$$

Where
- R_0: range in clear mode
- RJ: range in jammed mode
- K: Boltzman constant
- T: absolute temperature
- F: receiver noise factor
- PJ: density of jamming (by Hz) received in line with mixers
- G: gain of antenna in direction of jammer
- λ: length of reception wave
- Lr: reception losses
- D: distance
- (RP): density of jamming output (by Hz)

The stand-off jammer also increases the noise level affecting the angular error measurements. However, these effects can be reduced by appropriate trajectory shaping (see paragraph 5) or through suitable processing.

3.1.4.2 Attenuation due to rain

This is introduced through tables in the modelization process.

3.1.4.3 Image effect

The image effect is due to multiple reflections on the sea of incident and reflected rays.

At low incidence angles, this phenomenon results in a symmetrical image, and is similar to glint at higher incidence angles.

The modelization is achieved by dividing the reflecting surface into elementary facets which re-radiate with a retro-scatter coefficient adapted to the incidence angles.

The quality of this model can be seen by comparing the computed spectrums (skin echo + image) with the measurements taken during carried flight: an example of comparison is given in CHART 14.

The scale of abscissas on this figure is given in Doppler frequency (100 Hz/ms^{-1}) around an arbitrary reference.

The spectrum observed at frequencies higher than that of the skin echo is due to noise produced by the sources, and not incorporated in the model.

The image results in a spectrum increasing the angular error measurement noise at the end of the trajectory and which, subsequently, can increase the intercept miss-distance.

3.1.4.4 Clutter

Clutter is due to the retro-scatter of the sea (CHART 15). This occurs when sea returns have the same Doppler frequency as the target and have a distance related to the missile which is equal to the missile-target distance within a whole number of ambiguity ranking. This type of situation can occur, for example, for a sea-skimmer intercepted from behind in a zone defence configuration.

This phenomenon reduces the range of the seeker and increases angular error measurement noise.

The clutter computation principle is as follows.

The reflecting surface is divided into elementary facets.

P is the center of a facet.
dP is the clutter power received by one facet

$$dP = \frac{Pe\, G^2\, \lambda^2\, \sigma_0\, dS\, (\delta e)^2}{(4\pi)^3\, d^4}$$

d: MP distance
G: gain of antenna in direction of MP (function of Y)
Pe: peak transmission power
δe: transmission shape factor
σ_0: sea retro-scatter coefficient, as a function of sea state, length of wave λ and incidence β

The overall scatter power is written:

$$P = \sum (C)\, dP$$

where C is all of the basic surfaces resulting from the intersection of the iso distances and iso speeds.

This results in a range reduction τ

$$\tau = \left(\frac{KTBF}{KTBF + P}\right)^{1/4}$$

In practice,for each point of ground is performed the computation of both β and Y as well as the clutter doppler frequency using the expression:

$$\frac{2VM \cos \alpha}{\lambda}$$

This provides the scatter spectrum; the value of the target iso frequency clutter is used to compute the τ.

The quality of the model can be seen by comparing the theoretical and experimental results recorded under the same conditions (CHARTS 16 and 17).

3.2 Seeker requirements

3.2.1 Thermal noise

The signal-to-noise ratio is defined by the well-known relation:

$$\frac{S}{N} = \frac{Pe\, G^2\, \lambda^2\, \sigma\, L}{(4\pi)^3\, R^4\, KTBF}$$

where
- Pe: average transmission power
- G: antenna gain
- σ: target's radar cross section
- L: losses
- R: target-missile distance
- K: Boltzman constant
- T: absolute temperature
- B: reception band
- F: noise factor

KTBF represents the thermal noise power

A noise variance is used $(\sigma th)^4$.

The signal value is then standardized by S/N $(\sigma th)^2$.

The thermal noise modelization is achieved by adding a Gaussian random variable of variance $(\sigma th)^2/2\Delta B$ for each of the two channels (real and imaginary) forming the signal,

where Δ is the sampling step
B is the reception band

With P and Q representing the power levels in phase and quadrature of the signal alone, we have:

$$P^2 + Q^2 = \frac{S}{N} (\sigma th)^2$$

The real and imaginary values overall (signal + noise) are then:

$$\text{Real S} = P + \frac{\sigma th}{\sqrt{2\Delta.B}} g$$

$$\text{Imaginary S} = Q + \frac{\sigma th}{\sqrt{2\Delta.B}} g$$

where g is the Gaussian random variable with variance 1.

3.2.2 Radome aberrations

The radome aberrations are numerically compensated by means of a table and only a residue remains. For each simulation case, the model creates a residual aberration table for the antenna rotation angles which vary between - 55° and + 55° in elevation and circular.

The residual aberration is modelled for the seeker through spatial filtering of a Gaussian white noise.

The residues obtained are representative (CHART 18) of those obtained on a seeker (CHART 19).

4.- DESIGN OF THE SYSTEM FOR SEEKER LOCK-ON

4.1 Description of problem

In view of best limiting the seeker lock-on duration to provide a maximum autoguidance duration, in order to avoid possible lock-on on an attacker other than the target tracked by the fire control system in a multi-target environment and to maintain the anti-stand-off jammer capability (see paragraph 5.1.1), the lock-on process uses no scan function. In search phase, the antisea-skimmer computer generates the target designation to the seeker made of the distance, relative speed and missile-target angular direction.

This target designation based on range, Doppler frequency and angle uses the position and velocity of the target supplied by the fire control system through the up-link, as well as the position, velocity and attitude of the missile generated by the interceptor's navigation computer.

The target designation is then tainted by errors induced:

- by navigation errors and their evolution (*) during flight, mainly due:
  - to static errors induced in the IMU,
  - to alignment errors between the IMU trihedron and the reference trihedron,
- by target tracking errors produced by the fire control system which depend, in addition to the target itself (altitude, maneuvers, speed, radar cross section):
  - on the quality of the radar measurements, i.e. the design of the radar itself,
  - the prediction/estimation algorithms of the fire control system,
  - the data refresh rate of the up-link,
  - the alignment errors between the radar trihedron and the reference trihedron.

These errors which affect the target designation must remain compatible with the seeker's "capabilities" to allow it to effectively lock on to the target. Lock-on should take place at a range providing a sufficient autoguidance time to compensate for errors with respect to collision at the start of the autoguidance phase.

Sizing of the system with respect to seeker lock on is therefore essentially aimed at defining requirements in terms of static accuracy of the IMU, alignment precision, data refresh rate and target tracking accuracy.

This also leads to sizing certain parameters of the seeker and its antenna through specification of the lock-on range and the error domain relative to distance, Doppler frequency and angle in which lock-on should take place.

* this evolution will depend on static errors from the IMU and is conditioned during the flight by accelerations and angular rates created by mid-course guidance and autopilot.

4.2 Methodology using numerical simulation

The numerical simulation can be used effectively during the sizing process. In view of its objective, this simulation:

a) should show the target's kinematics (speed, altitude, maneuvers) and its radioelectric representations for the seeker and the radar,

b) should integrate a model representative of radar measurements and tracking algorithms, taking account of, in particular, jamming, rain, and image effect (i.e. all the associated interference),

c) should integrate a six-degrees of freedom model of the missile flight including a representation of the IMU measurements tainted by static errors, navigation computations initialized with alignment errors, mid-course guidance algorithms, a representation of autopilot algorithms, aerodynamics, propulsion, in-flight mechanical data, and target designation computations for the seeker,

d) should include a seeker model for which the lock-on range takes account of jamming, rain and clutter,

e) should include a model of the radar-missile link determining whether the missile receives (or not) the link message on each transmission. Non-reception of the message will have an effect on quality of target designation to the seeker and therefore on the lock-on probability. Such a model will involve models of the receiver, the reception antenna, attenuation of the radioelectric signal through the propulsion unit flame, the transmission antenna, and the transmitter and should also take account of the environment (rain, image effect, jamming). In addition, errors in the direction of up-link transmission should be taken into account, errors depending on tracking (or not) of the missile by the radar and presence (or not) of a down-link.

Using a numerical simulation of this type and for each specified threat, it is possible to analyze the contribution to target designation errors on one hand, by each of the error items taken separately, and on the other hand, by all of the error items together.

In parallel, the extrapolated intercept miss-distances at switch homing time, supplied by the same simulation tool, are examined to ensure that these can be corrected according to available maneuverability and autoguidance duration.

CHARTS 20, 21 and 22 show the evolution, during the interception, of the errors in target designation to the seeker in range, Doppler frequency and angle. The interception concerns a supersonic sea-skimmer (800 m/s) maneuvering with penetration + dog-leg maneuvers ; there is no scatter on the moment the track is initialized by the fire control system and the up-link operates at a rate of 1 s.

These charts show the error assessment as a function of missile-target range incorporating all the error items mentioned above.

Chart 22 shows in particular that for a seeker with range on axis equal to 6500 m for the considered target and a total beamwidth of - 3 dB equal to 2°, the lock-on/autoguidance range will be 5 to 6 km (provided also that the Doppler search takes place on about ± 40 m/s at least: see chart 21). As a result, if the corresponding autoguidance duration is sufficient, taking account of the relative speed, the chart shows the suitability between the seeker characteristics mentioned above and the performance levels considered for the IMU, the alignment and the tracking accuracy.

This type of study therefore pr[illegible] considerable aid in designing the various components in the lock-on chain and those of th[illegible] missile link chain, and in defining the specifications to the seeker designer relative to distance, speed and angle errors at lock-on.

4.3 Design of the seeker with respect to lock-on

The angular acquisition domain (or basket) as a function of range is the result of the type of study carried out in paragraph 4.2.

This domain is approached by a cone trunk defined by the main lobe of the antenna at 3 dB and by the range on a target of 0.1 m^2.

Electromagnetically, this basket depends on:

- the diameter of the antenna (and therefore the diameter of the missile),
- the weight of the seeker (and therefore the transmission power for a given diameter),
- the wavelength.

CHART 23 shows the general aspect of the variations of this basket as a function of the different parameters.

In view of the required capabilities (see paragraph 4.2) and the technological constraints, this leads to the compromise between band/beamwidth ($2\theta_0$)/ range /diameter (ϕ).

5. ANALYSIS OF MAIN REQUIREMENTS FOR MID-COURSE GUIDANCE

The mid-course guidance objectives for the antisea-skimmer can be divided into two categories:

- those relative to trajectory shaping in the vertical plane following vertical firing,
- those relative to trajectory shaping in the horizontal plane following firing in a launch direction to be defined.

Another objective must be added which is common to both planes: placing the missile at the end of the mid-course guidance phase in a collision trajectory with the target to best initialize the auto-guidance phase.

The definition of the mid-course guidance law and associated logics depends on the analysis of these objectives where the contribution of numerical simulations is of major significance.

5.1 Vertical and/or Horizontal shaping:Rejection of stand-off jammers

One of the basic goals of pre-guidance is to contribute to rejecting the stand-off jammers in order to provide a sufficient angle with the seeker antenna axis at the end of the mid-course guidance phase. This is used to:

- minimize the power of the noise received by the seeker and therefore, on a target with a low radar cross section such as a sea-skimmer and despite the presence of a stand-off jammer, to obtain lock-on distances which are sufficient for autoguidance,
- minimize angular error measurement noise due to jammers and their influence on intercept miss-distances.

Aiming at a sea-skimmer protected by stand-off jammers, rejection of these jammers is obtained by providing the right angle of the interceptor's trajectory,as shown in the diagram below:

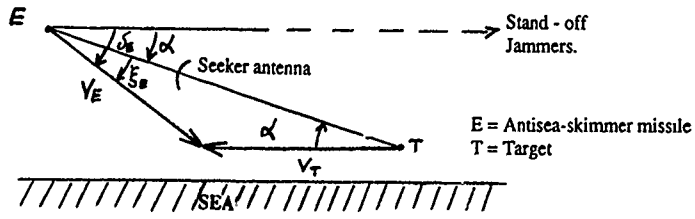

Where α is the desired angle of rejection.

The collision relation is written: $V_E \sin \delta_E = V_B \sin \alpha$

For $V_E = 1000$ m/s, $V_B = 800$ m/s and $\alpha \geq 12°$ for example, $\xi_E \geq 9°5$ is required, therefore $\delta_E = \alpha + \xi_E \geq 21°5$

<u>The guidance law thus enslaves the angle of the line-of-sight with the jammers or, in an equivalent way,the direction of the missile's velocity vector.</u>

5.2. Vertical shaping:

5.2.1. Turn-over:

This brings us to the analysis of the turn-over following vertical launch for a short-range interception. As a component of the pre-guidance law, the turn-over law provides a compromise:

- turn-over from the vertical to the horizontal plane can be achieved rapidly following exit from the launcher since the missile speed is slow. However, this is limited to allow the missile to climb to a sufficient altitude and attain the desired trajectory with respect to the rejection with a reasonable load factor at the end of flight:

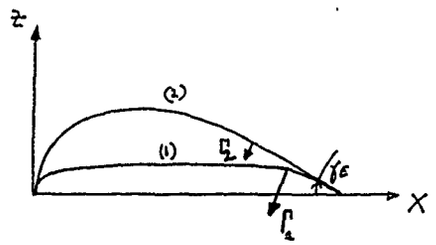

(1) Trajectory with maximum turn-over: $\Gamma_1 >> \Gamma_2$
(2) Trajectory with limited turn-over

- this turn-over is however not limited or delayed too far so that the required load factor not be excessive:

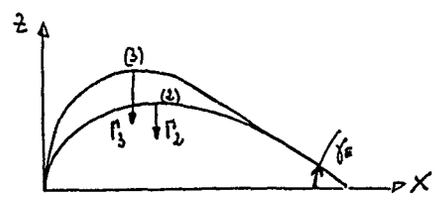

(2) Trajectory with limited turn-over
(3) Trajectory with excessively delayed turn-over: $\Gamma_3 >> \Gamma_2$

CHART 24 shows an example of trajectory shaping in the vertical plane for an interception at 2800 m.

5.2.2. Optimization of antisea-skimmer kinematic performances

The mid-course guidance law is also aimed at defining the best compromise between minimizing the flight duration and maximizing the speed of the missile at interception. This definition is achieved through research on the optimum altitude profile. The greater the altitude, the lower the aerodynamic drag, which is favorable to the final speed and the flight duration. However, this produces a longer trajectory which is unfavorable with respect to the same parameters. This question only arises with respect to "long" ranges for which the altitude profiles can substantially differ according to the slope at start and end of the mid-course guidance phase and which remain compatible with the maneuverability of the interceptor.

5.3 Horizontal shaping

5.3.1 Predicted point of interception

The predicted point of interception is the point in space where interception is expected to take place The interceptor trajectory is directed to this point at least at the end of the mid-course guidance phase so that the autoguidance phase begins with a collision situation.

The prediction of its position is based on an extrapolation of the target trajectory.

It is clear that the closer the predicted point of interception is to the actual future trajectory of the target, the lower will be the errors with respect to collision at the start of the autoguidance phase and the better will be the kinematic performances of the antisea-skimmer on interception (speed and available maneuverability, duration of flight achieved). It is therefore important to optimize the point of interception prediction method in this respect, taking account of the entire diversity of the specified target trajectories (in particular, dog-leg trajectories) and all the possible positions of the ships to be protected (self-defence and zone defence).

5.3.2 Trajectory shaping with respect to presentation of interception and direction of launch in horizontal plane

In a zone defence situation, full broadside interception can occur when firing does not occur sufficiently soon to provide a head-on interception (whether due to a "late" detection or a saturating threat requiring a "late" interception) and when the engagement takes place as shown in the drawing below:

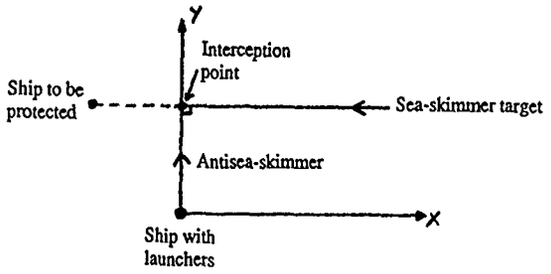

a) For interception of this type with a broadside presentation, the angle ξ between the missile axis and the seeker antenna axis (aimed at target) is wide, and becomes increasingly wider as the speed of the antisea-skimmer decreases and the speed of the sea-skimmer increases

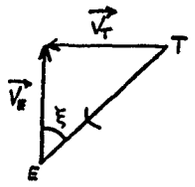

The maximum intercept range is then limited to the range where the speed of the missile leads to an angle ξ exceeding the maximum angular limits of the antenna.

b) With respect to head-on interceptions at the same range against the same sea-skimmer, the Doppler frequency of the target is lower and that of the clutter higher. This is unfavorable to the lock-on range and the angular error measurement noise.

c) With respect to head-on interceptions, the broadside interceptions are less favorable in the terminal phase since:

- it raises the problem of determining the part of the target which the proximity fuze has detected,
- it does not systematically lead to an intercept geometry ensuring structural kill of the target.

In view of points a), b) and c), it is therefore useful to implement a mid-course guidance which limits the interception presentation angle and leads to a head-on interception whenever possible:

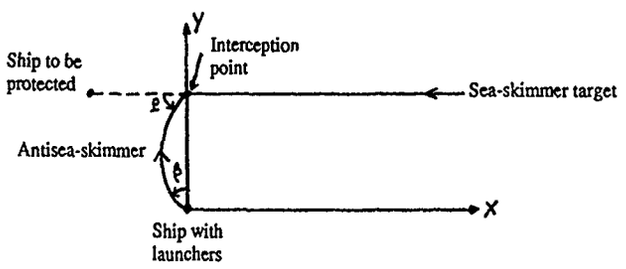

This can be obtained through a horizontal shaping of the trajectory, being understood that this type of shaping is not possible for short-range interception (due to the required load factor).

Once this law is implemented, the horizontal direction of launch of the antisea-skimmer can be optimized, observing that, at a given angle P, the greater the angle β :

- the lower the load factor at the end of flight and the greater at the start of flight,
- the longer the trajectory, and therefore the duration of flight, the slower the final speed.

All of these aspects relative to vertical and horizontal trajectory shaping can be processed through a numerical simulation integrating the models relative to the target, the fire control system, the missile flight and the seeker corresp[illegible]ng to paragraphs a), b), c) and d) in paragraph 4.2:

- optimization of turn-over (paragraph 5.1.2[illegible] [illegible]c performances of the antisea-skimmer (paragraph 5.1.3), horizontal sh[illegible] limiti[illegible] the presentation angle and the associated horizontal direction of launch (para[illegible].2) is related to knowledge of the load factor and speed profiles during the flight in [illegible]on-linear environment forme[illegible] by the atmosphere.

- the study of the influence of the stand-off jammer rejection function (paragraph 5.1.1) and the horizontal trajectory shaping in zone defence with respect to clutter (paragraph 5.2.2) requires the use of a seeker model within the guidance/control loop and with the representation of the geometry and flight kinematics which the considered simulation provides.

6.- TYPES OF NUMERICAL SIMULATIONS AND THEIR USES

Several types of models or numerical simulations can be distinguished:

- specific and detailed models of missile and airframe equipment: this concerns the seeker, IMU, proximity fuze, warhead, steering control components, missile computer, structure modes and those relative to aerodynamics and propulsion.

  At first these are schematic models, then models of developed equipment, obtained when necessary through identification, used for fine behaviour study and logic development (seeker and autoguidance). Detailed comprehension of their operation often proves to be of major importance as part of their specification.

- models of more or less simplified equipment depending on the case, and simplified simulations for which the number of degrees of freedom may be limited and may only represent certain phases of the interception. These simulations are used to analyze certain requirements (such as those relative to autoguidance, for example) and are useful in generating specifications.

- missile flight simulations (6-degrees of freedom models) in all phases, associated to an overall fire control model, the seeker and the environment models. These are "one-on-one" or "one-on-many" models.

  The missile model integrates all of the equipment models which may be more or less simplified depending on use.

  This type of simulation is useful to define certain requirements (relative to propulsion, drag, weight, etc.) to draw up specifications (for example, those subsequent to studies on seeker lock-on) for the purpose of precise studies (for example, study of mid-course guidance).

  These form the references for hardware on-the-loop simulations, for preparation of in-flight trials (nominal trajectory, scattered trajectories), and for interpretation of these trials. The models built into the simulations are therefore updated throughout all these development phases.

  Finally, these simulations are used to assess the performances of the anti-missile system:

  - performances relative to intercept miss-distances and kill probabilities,
  - performances relative to firing and interception envelopes,
  - performances relative to scenarios which are extremely difficult or even impossible to process under in-flight trials, whether for technical or financial reasons.

- the technical-operational simulation (many-on-many) which, fed by the kill probabilities generated by the one-on-one or one-on-many models, contributes to definition of the firing policy algorithms and is used to assess the defence capabilities of the system under saturation attack conditions.

These simulations, developed methodically and thoroughly, are used to precisely predict an in-flight trial. In this way, they achieve a reliability standing which is indispensable when, in view of the complexity of a given scenario, the system is not tested through an in-flight trial, but assessed through simulation only.

The search for this level of reliability motivates the engineer to obtain the most refined models, building a more and more complex simulation throughout the development process.

This is inevitable. However, this should go hand in hand with control of computation durations and costs which, for an anti-missile system as complex as this one, could quickly become incompatible.

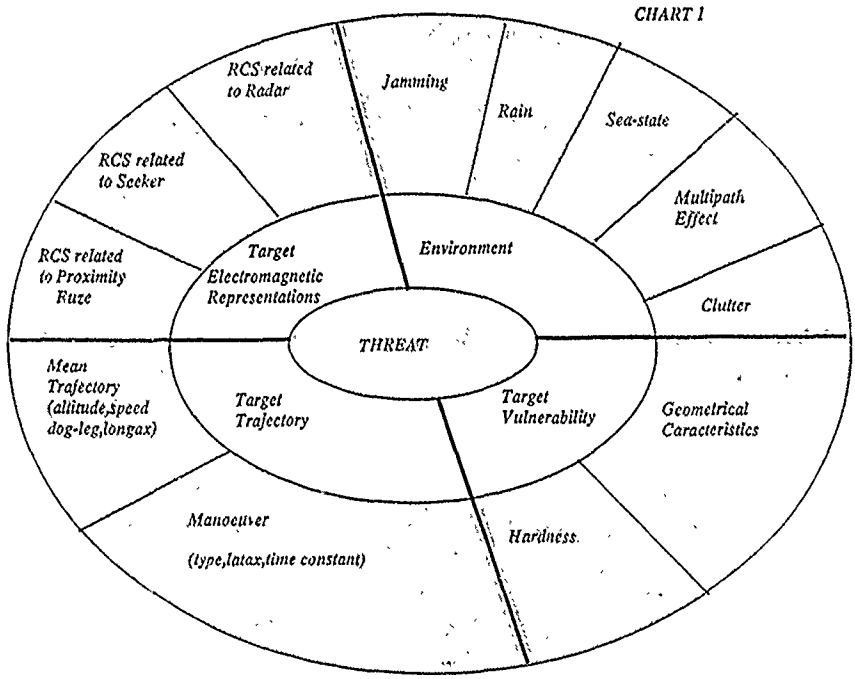
CHART 1
RCS related to Radar
Jamming
Rain
Sea-state
RCS related to Seeker
Multipath Effect
RCS related to Proximity Fuze
Target Electromagnetic Representations
Environment
Clutter
THREAT
Mean Trajectory (altitude,speed dog-leg,longax)
Target Trajectory
Target Vulnerability
Geometrical Caracteristics
Manoeuver (type,latax,time constant)
Hardness

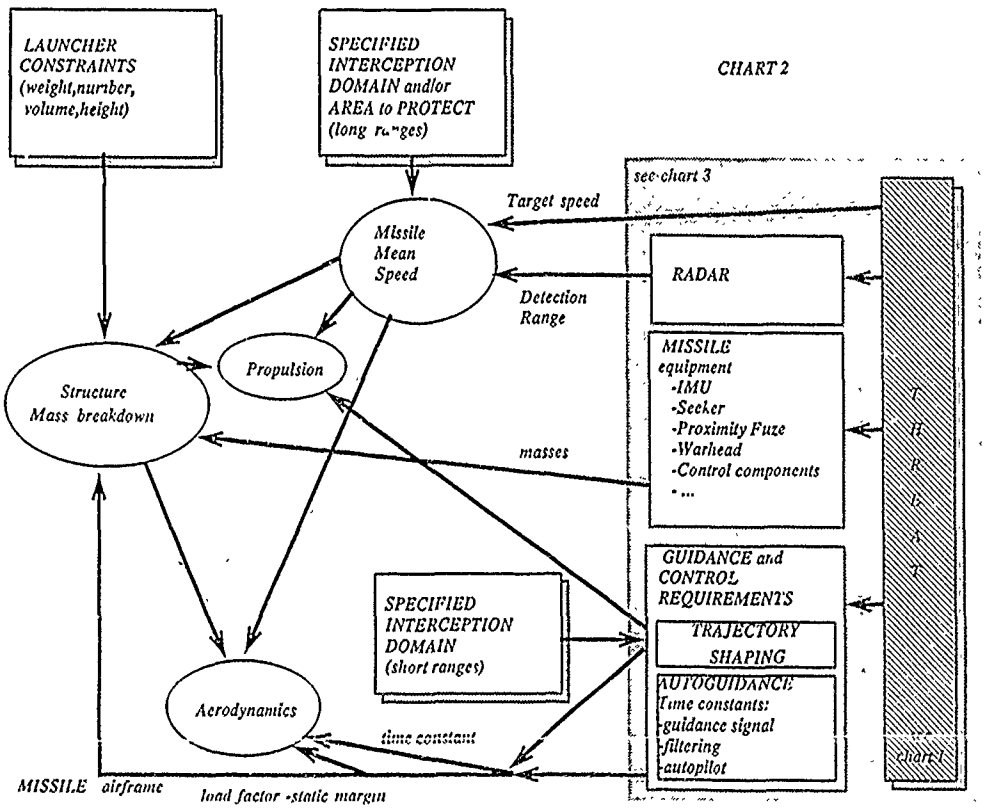
LAUNCHER CONSTRAINTS (weight,number, volume,height)
SPECIFIED INTERCEPTION DOMAIN and/or AREA to PROTECT (long ranges)
CHART 2
see chart 3
Target speed
Missile Mean Speed
RADAR
Detection Range
MISSILE equipment
-IMU
-Seeker
-Proximity Fuze
-Warhead
-Control components
- ...
Propulsion
Structure Mass breakdown
masses
GUIDANCE and CONTROL REQUIREMENTS
TRAJECTORY SHAPING
AUTOGUIDANCE
Time constants:
-guidance signal
-filtering
-autopilot
SPECIFIED INTERCEPTION DOMAIN (short ranges)
Aerodynamics
time constant
MISSILE airframe
load factor -static margin
chart 1

aerospatiale
DIVISION ENGINS TACTIQUES

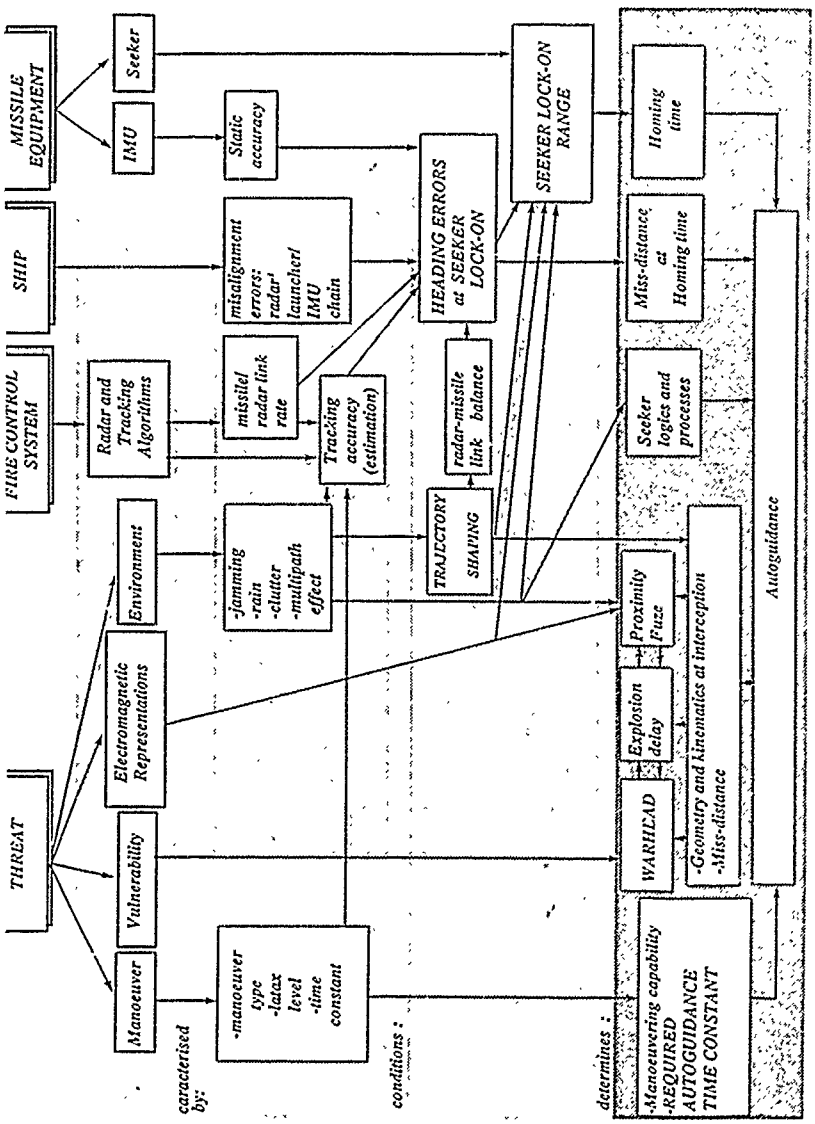

aerospatiale
DIVISION ENGINS TACTIQUES

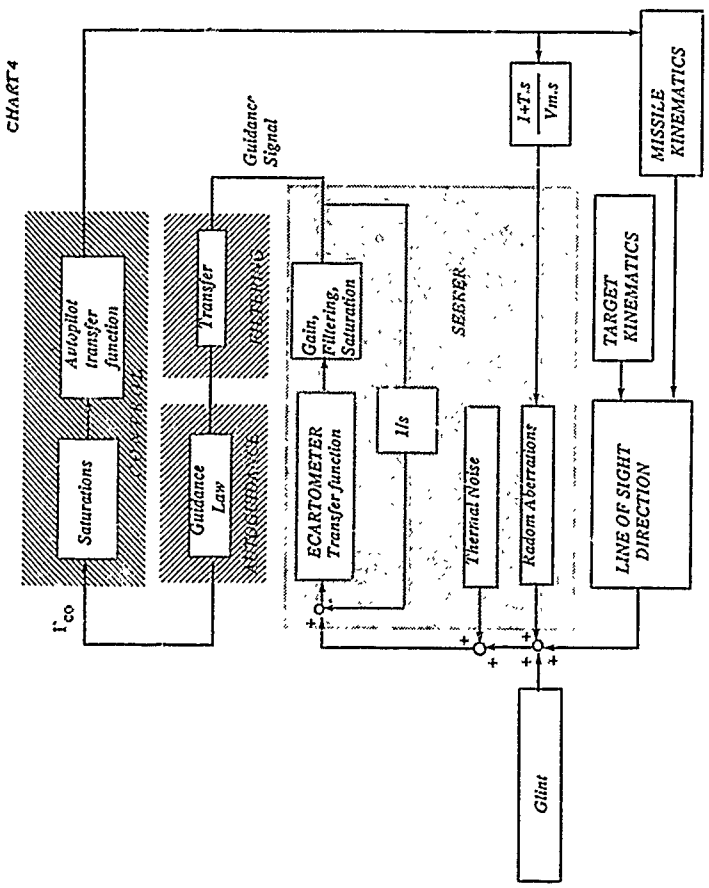

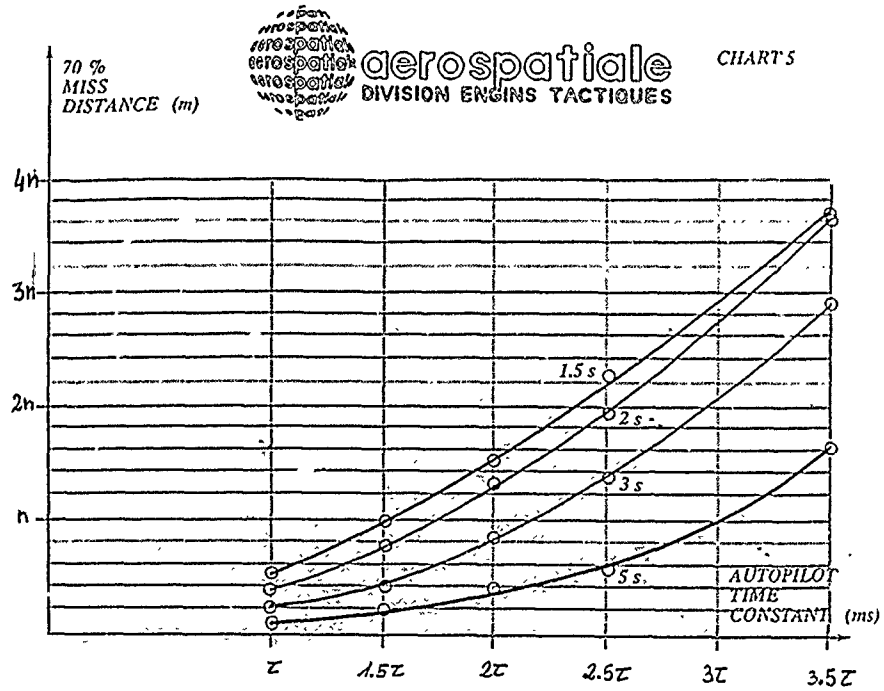

TARGET : latax = steps of 10 g amplitude
autopilot = second order (100 ms, damping 0.7)

MISSILE : autopilot = second order (damping 0.7)
autoguidance = proportionnel navigation (a=3.5)

50 runs : interceptions throughout all target manoeuvering phases

aerospatiale
DIVISION ENGINS TACTIQUES

CHART 6

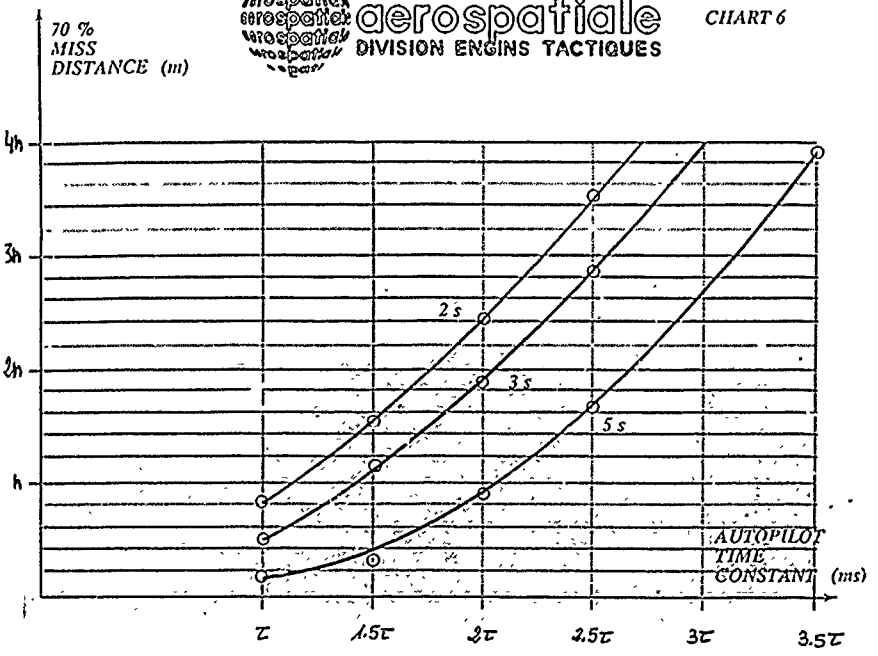

TARGET : latax = steps of 15 g amplitude
autopilot = second order (100 ms, damping 0.7)

MISSILE : autopilot = second order (damping 0.7)
autoguidance = proportionnel navigation (a=3.5)

50 runs : interceptions throughout all target manoeuvering phases

aerospatiale
DIVISION ENGINS TACTIQUES

CHART 7

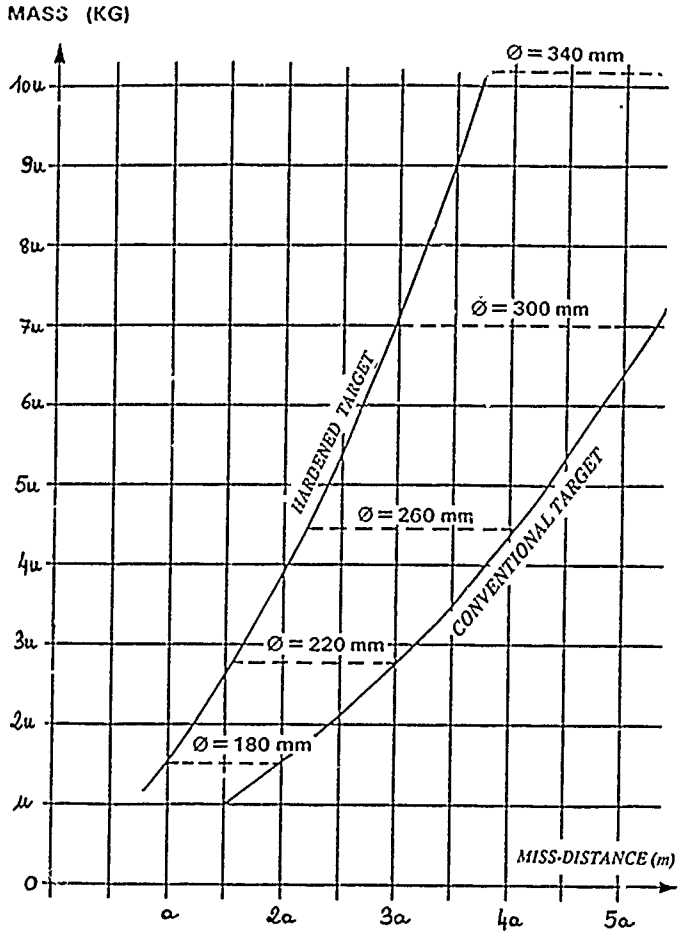

CHART 8

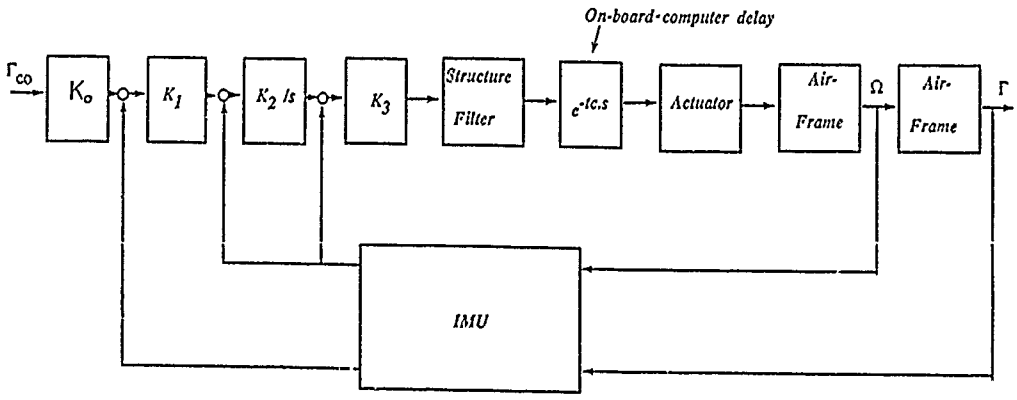

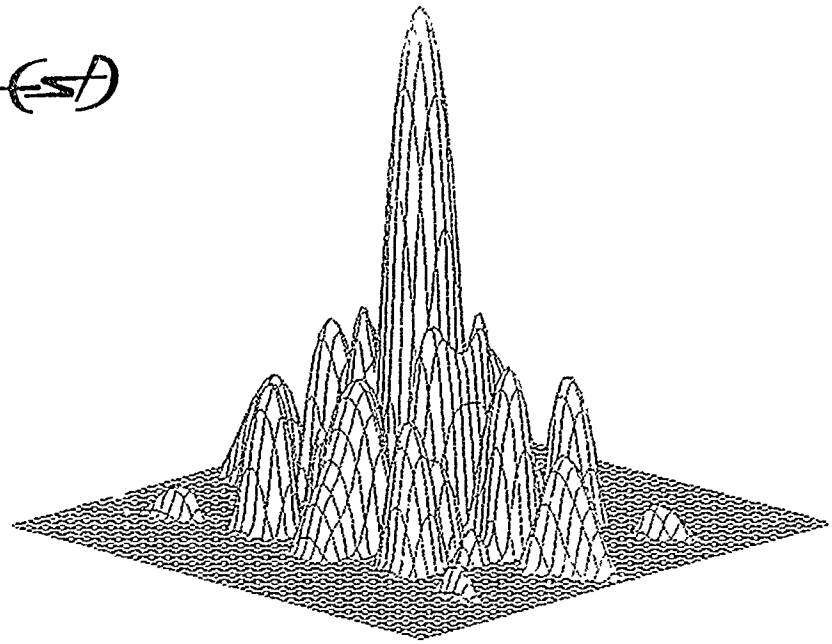

CHART 9

Theoritical antenna pattern

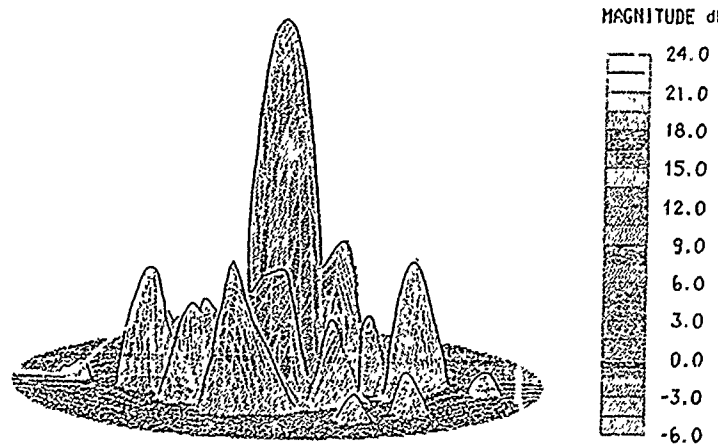

CHART 10

Antenna pattern measurement

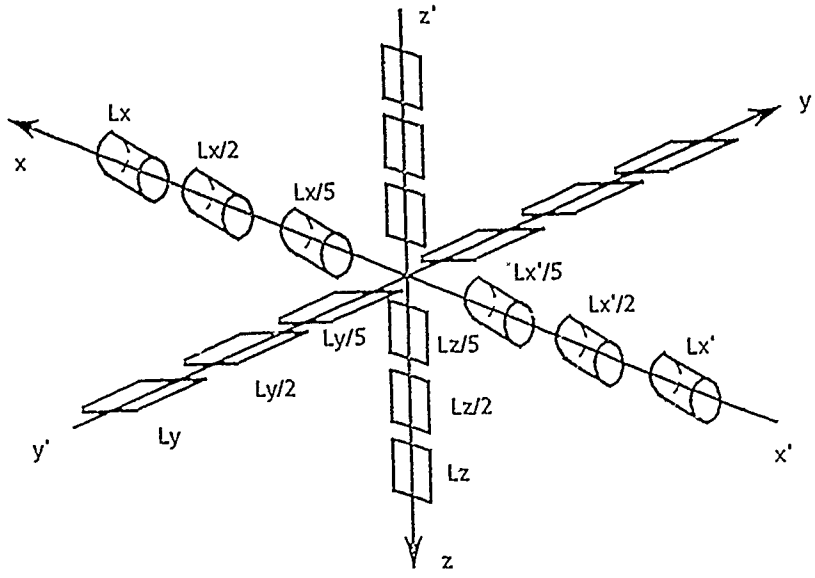

CHART 11

18 facets model

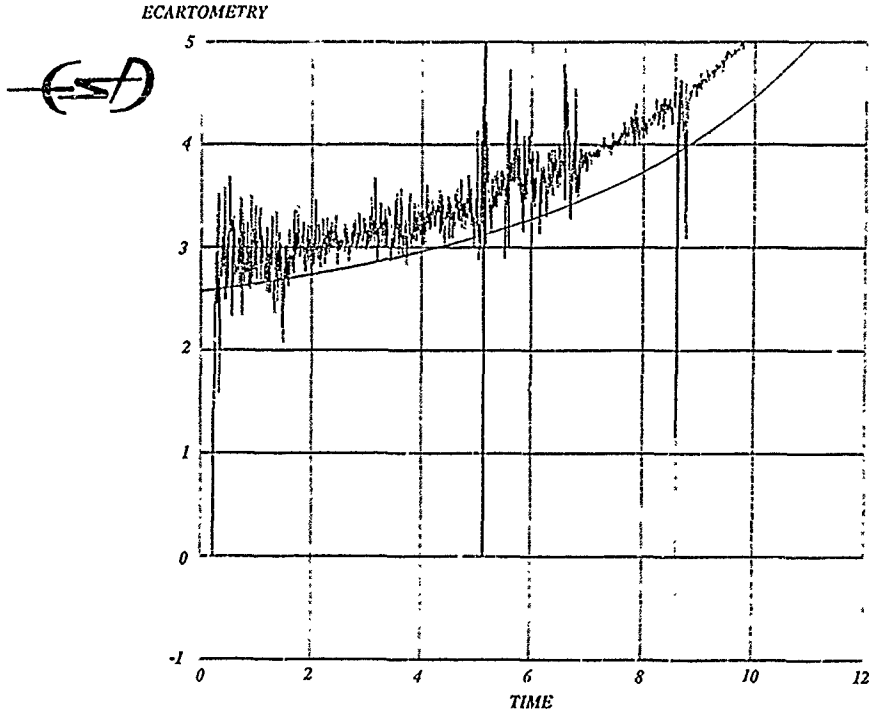

CHART 12

Glint theoritical model

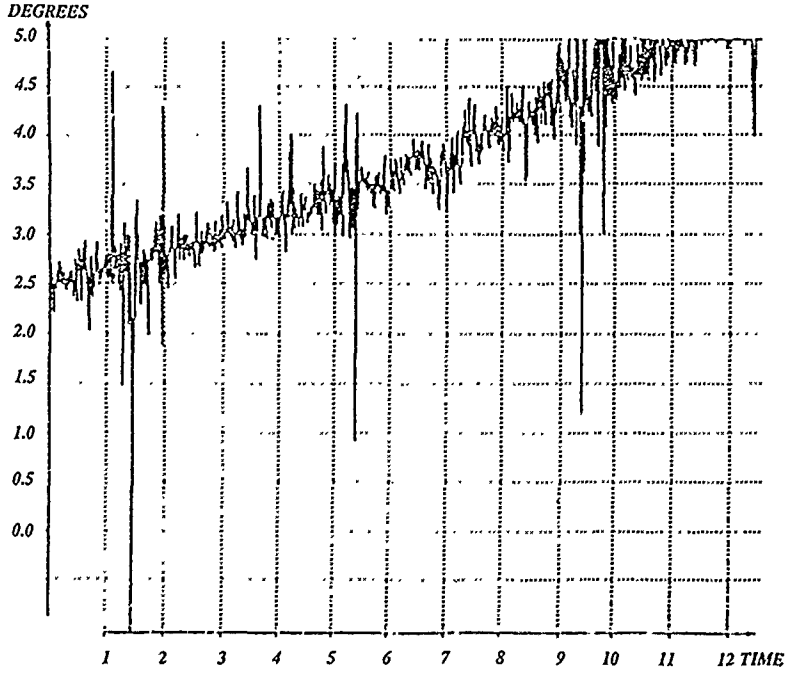

CHART 13

Glint measurement

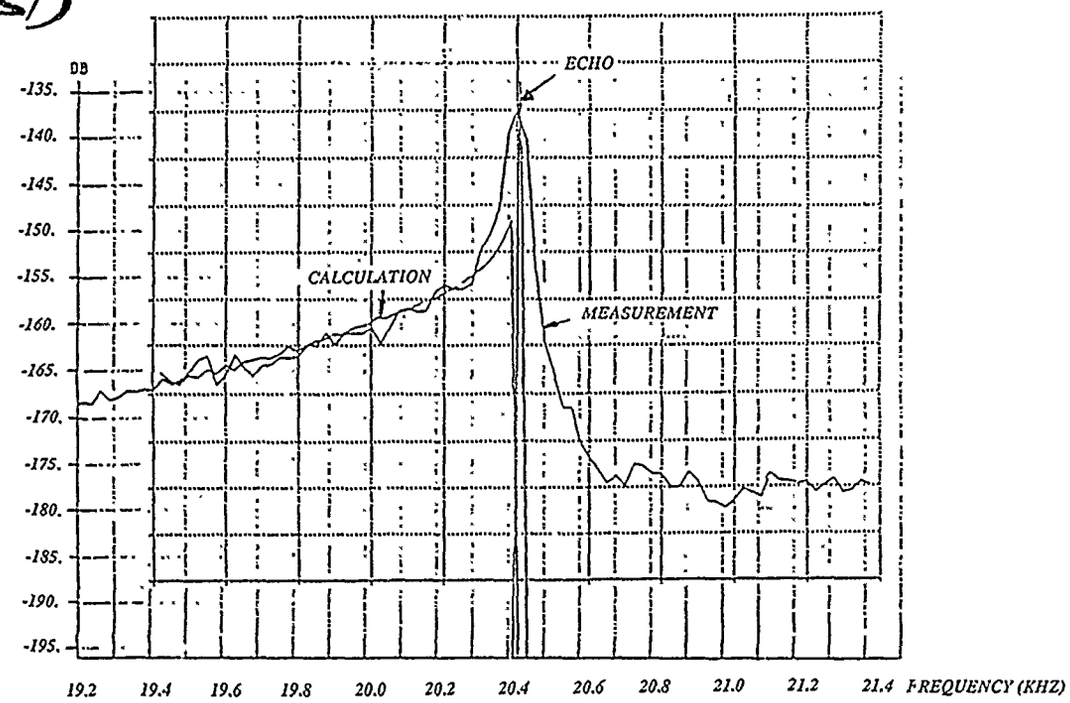

CHART 14

MULTIPATH EFFECT

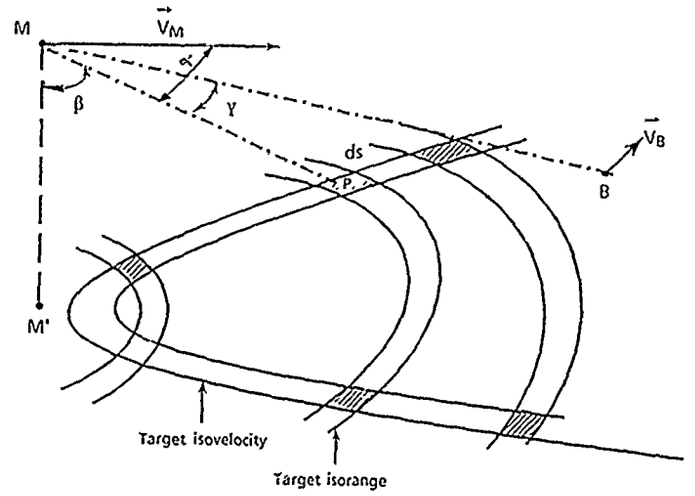

- Target isovelocity results of the intersection with ground of two cones definit by :

$$Vr = V_M \cos\alpha + \frac{B}{2} \times \frac{\lambda}{2}$$

$$Vr = V_M \cos\alpha - \frac{B}{2} \times \frac{\lambda}{2}$$

where : Vr : Target missile radial velocity
VM : Missile velocity
B : réception band width

- Target isorange results of the intersection with ground of two spheres centred on M with a radius of MB ± k λr ± δr

where : $\lambda r = \frac{C}{fr}$

fr : repetition frequency
C : light velocity
δr : duration of the range select window

CHART 15

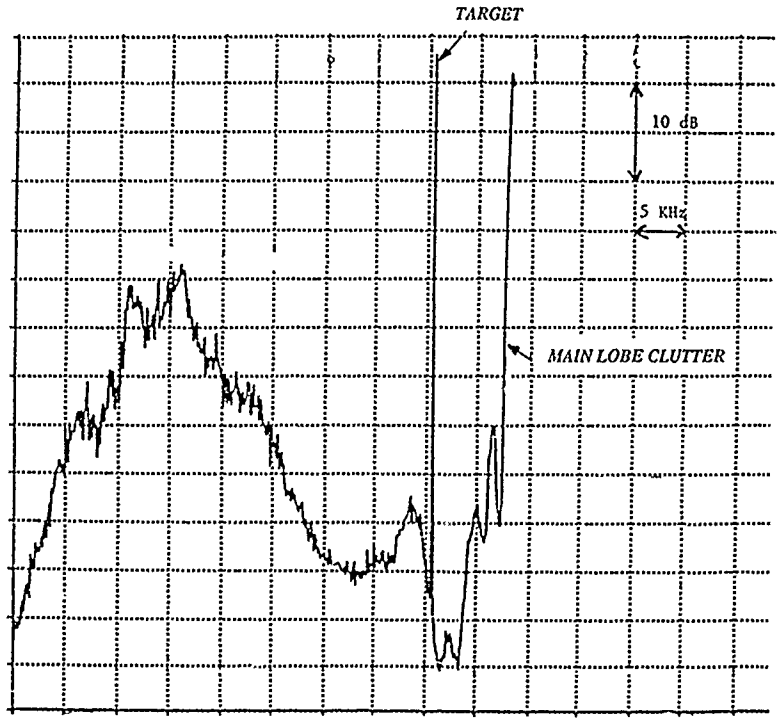

CHART 16

Calculated clutter spectrum

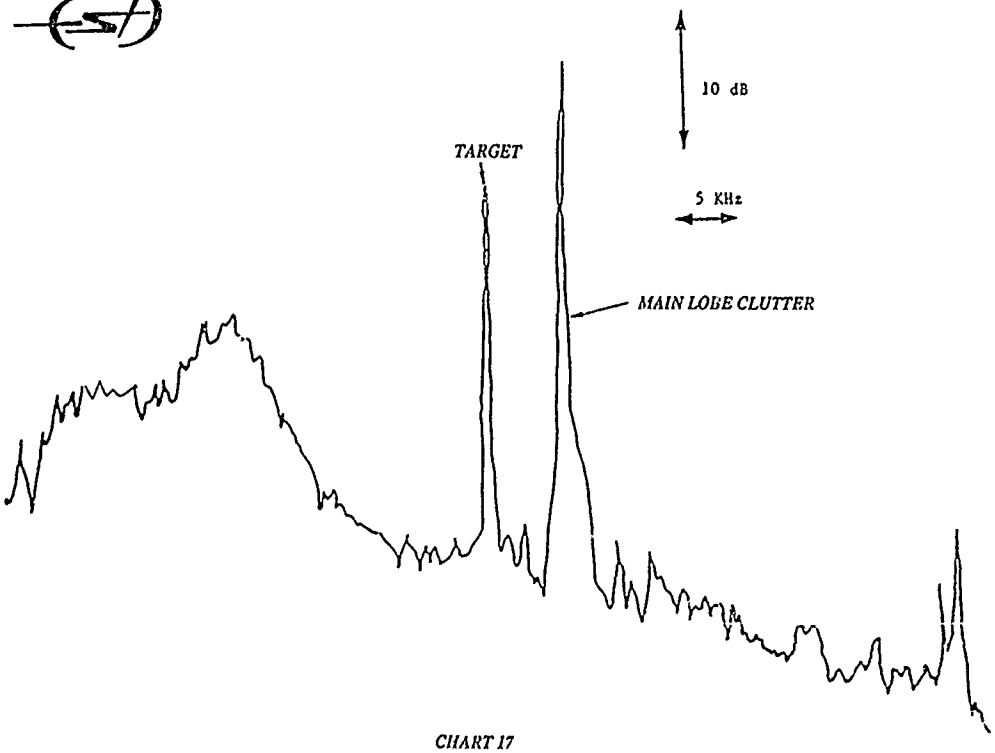

CHART 17

Measurement of clutter spectrum

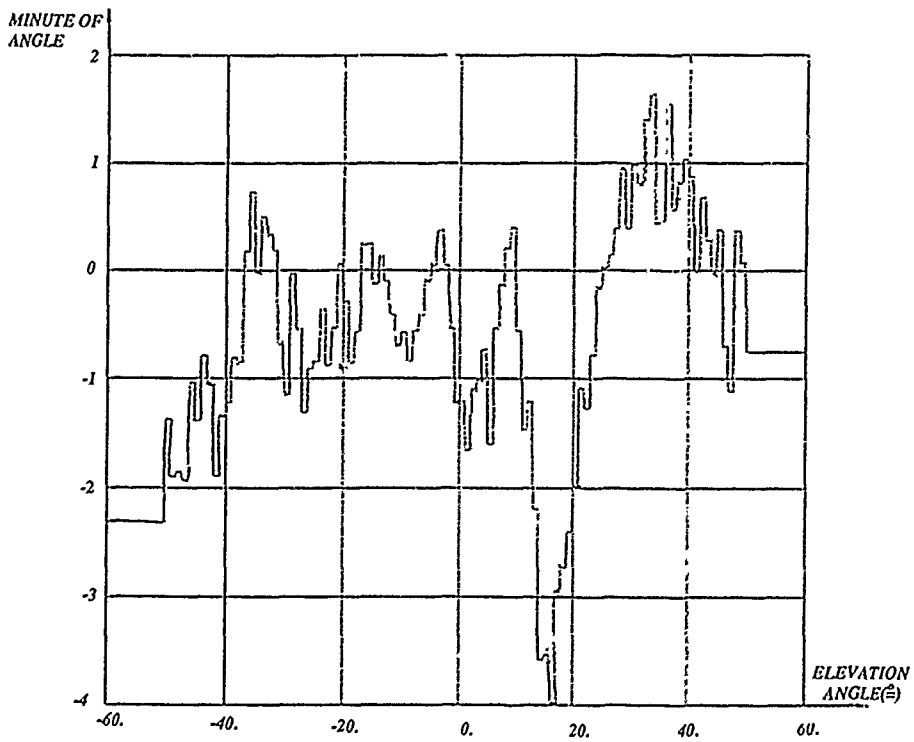

CHART 18

Modelisation of radome aberration residue

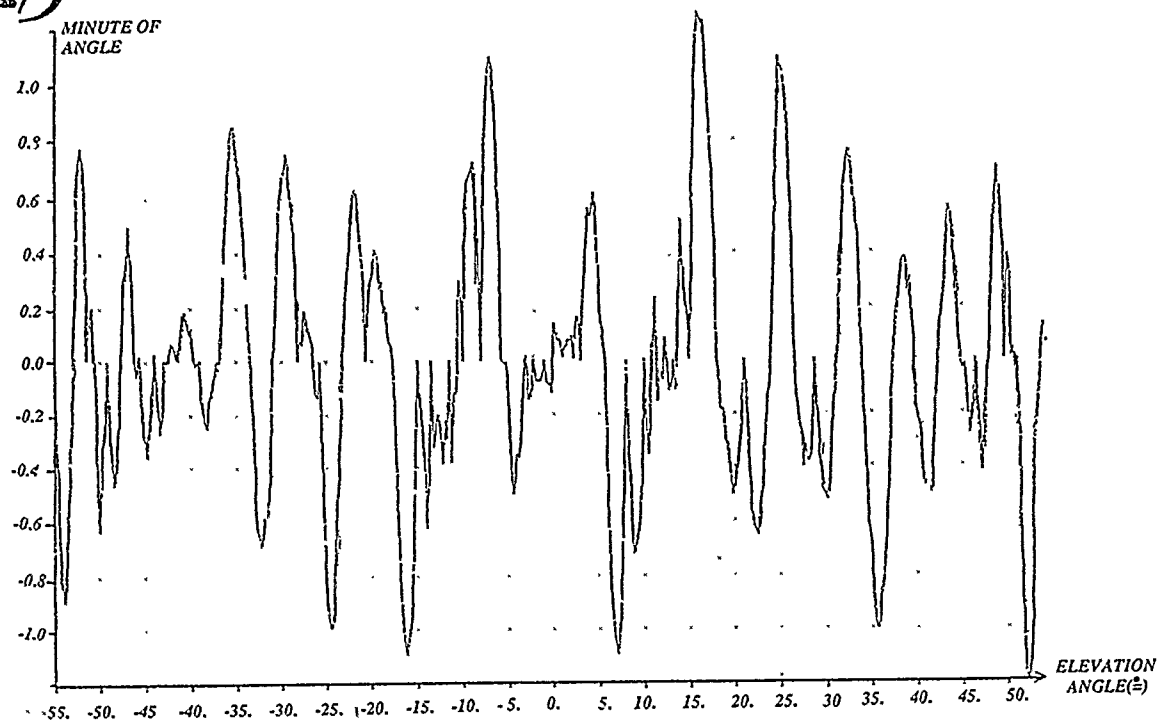

CHART 19

Radome aberration residue (measurement)

aerospatiale
DIVISION ENGINS TACTIQUES

CHART 20

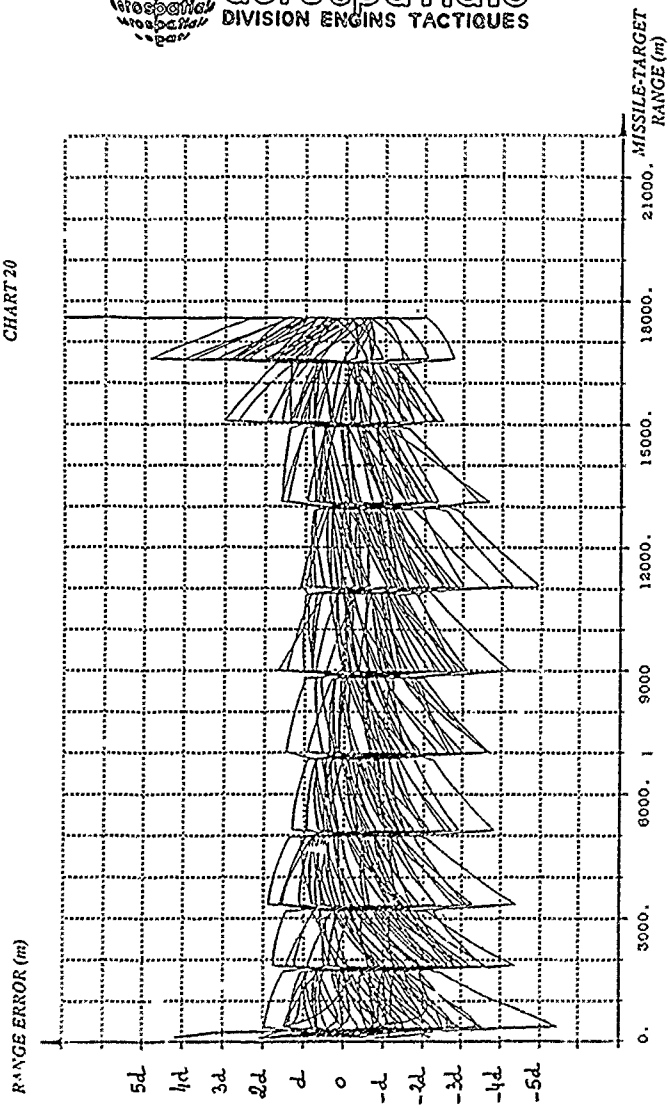

aerospatiale
DIVISION ENGINS TACTIQUES

CHART 21

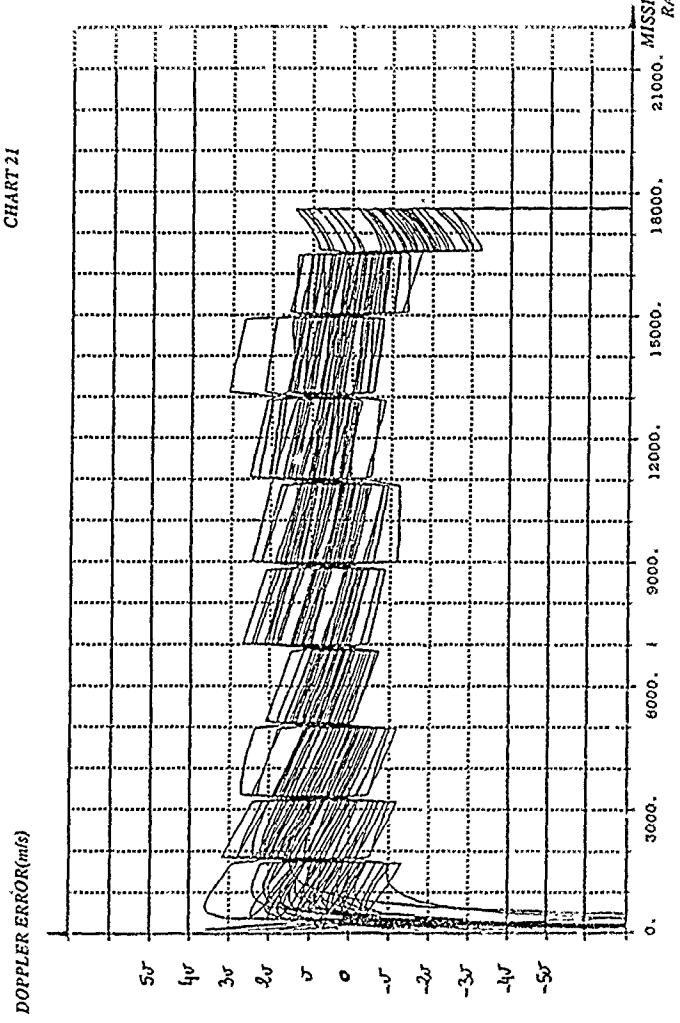

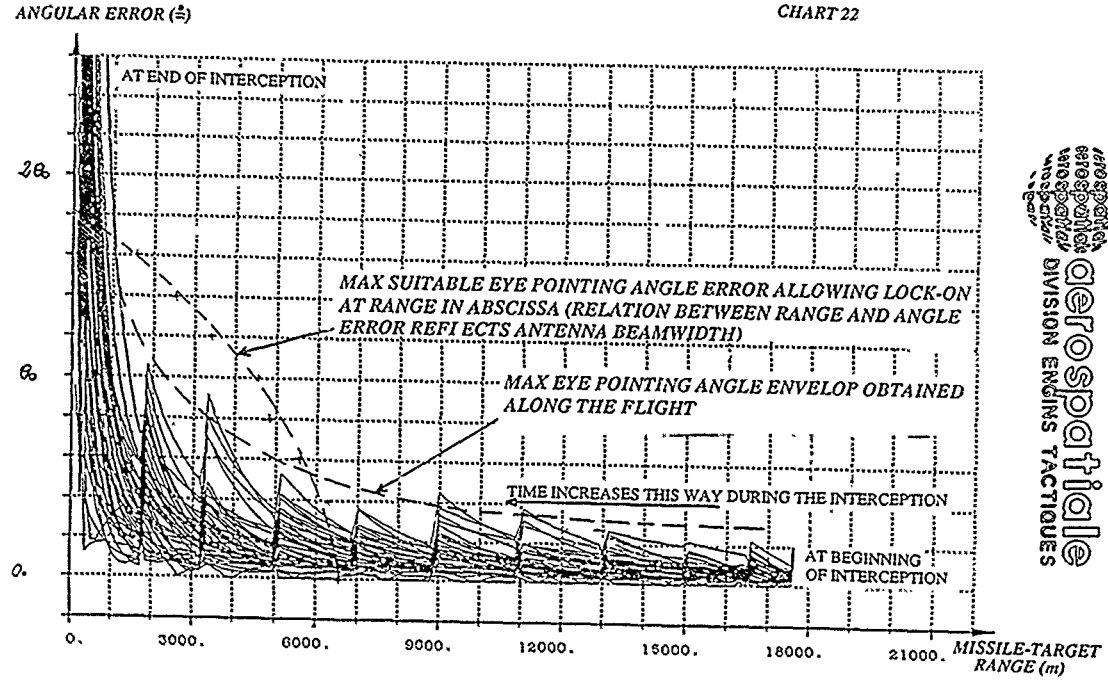

aerospatiale
DIVISION ENGINS TACTIQUES

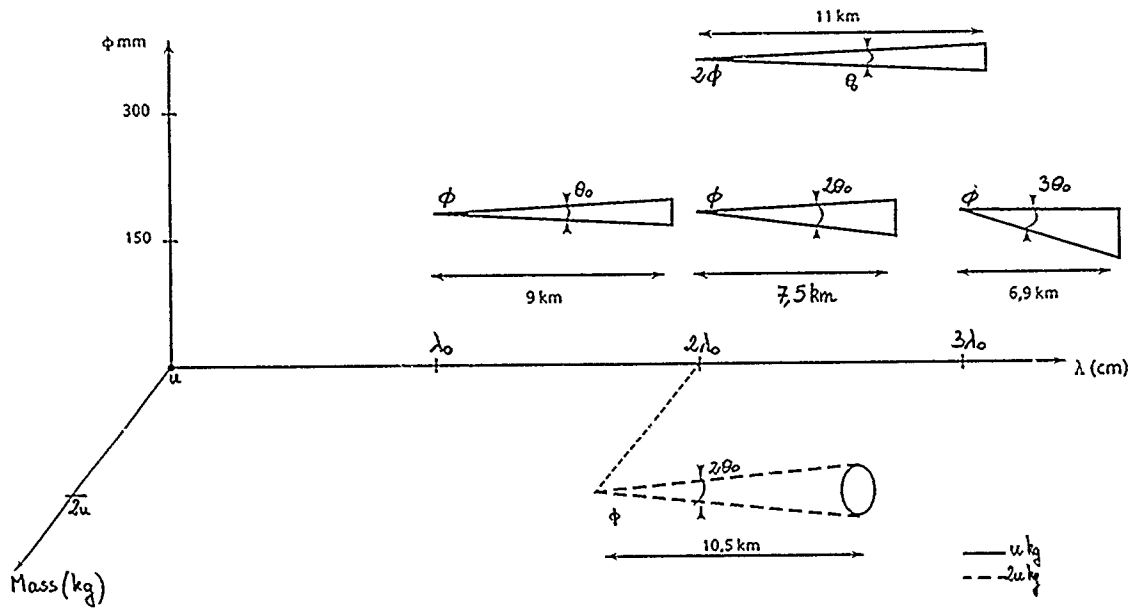

CHART 23

Basket size variations

aerospatiale
DIVISION ENGINS TACTIQUES

CHART 24

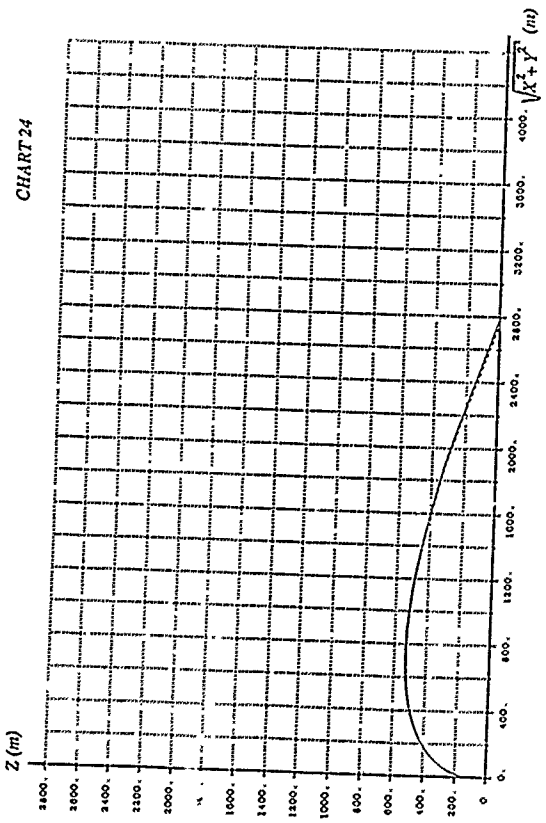

ADVANCED MISSILE GUIDANCE

by
R. V. LAWRENCE
Senior Principal Scientific Officer (PP)
Defensive Systems Department, Royal Aerospace Establishment,
Farnborough, Hampshire GU14 6TD, UK

SUMMARY

The paper discusses the problem of bringing a missile into collision with a moving target.

The zero-control miss (ZCM) guidance concept is introduced. It is shown how errors in the estimates of the current system state and the future zero-control response of the system lead to errors in estimating the ZCM, and consequently how the missile suffers an aiming error. The missile generally suffers a miss, because of its limited ability to follow the changing error, due to restricted bandwidth and control saturation.

Optimal control laws based on the ZCM are derived, and expressions for the idealised terminal miss obtained. The equations suggest how the target might choose an optimal evasion strategy to maximise the miss. This leads to some discussion of game theory, and the basis for multiple hypothesis guidance.

1. INTRODUCTION

The primary function of a missile guidance system is to bring the missile into collision with the target.

A 'common sense' method of achieving this is to configure the guidance so that it brings the missile onto a heading which results in a collision with the target. This is equivalent to bringing the missile into a state which will evolve into a collision state, given no further missile control input.

By implication, the expected *zero-control miss* on the collision trajectory is zero.

One control strategy therefore is to bring the missile into a state for which the expected control-free miss is zero.

This approach involves an element of prediction. It is necessary to estimate the current missile-target relative state, and to predict from it the future missile-target relative trajectory, given zero missile control. From this, the closest pass can be predicted, and used to construct a control for the missile.

The zero-control miss concept was, to the Author's knowledge, first mentioned [illegible] the UK in connection with joint missile guidance research between MOD and BAC [illegible]ter BAe). Nesline and Zarchan[1] developed the 'zero-effort miss' concept in the US [illegible] connection with modern guidance. The full background work upon which this paper [illegible] des[illegible]ribed by Lawrence in Ref 2.

[illegible]LL GAZING

[illegible] [illegible]ll see later, the 'common sense' zero-control miss idea is confirmed by optimal co[illegible] theory. If the system is linear, or can be linearised, the control-free final state at time t_f (the time of closest pass) can be written

$$x_f(t)_{u_c=0} = \Phi(t_f,t)x(t) \quad , \tag{1}$$

where $x(t)$ is the missile-target relative state vector at time t, and $\Phi(t_f,t)$ is the state transition matrix for the interval t to t_f.

Optimal control theory suggests that the best control for the missile is some linear combination of the state variables in $x_f(t)$. The linear combining matrix, which is generally a function of t, emerges from the theory.

We cannot know the system state $x(t)$ precisely. However, measurements on x will be made by some guidance sensor, such as a seeker. Using these measurements, we must construct an estimate of $x(t)$, $\hat{x}(t)$. An estimate of the final system state in the absence of missile control is then

$$\hat{x}_f(t)_{u_c=0} = \Phi(t_f,t)\hat{x}(t) \quad . \tag{2}$$

The control-free state transition matrix Φ contains *a priori* information about the behaviour of the target and missile in the interval t to t_f. Our knowledge about the *target* behaviour will generally be very limited. Unless we know the target *strategy*, we can only guess at the target components of Φ.

Ideally, our knowledge about the future control-free *missile* behaviour should be perfectly complete, because we designed the missile! However, in practice, because of uncertainty about the aerodynamics, we cannot know even the missile components of Φ precisely.

Since both $x(t)$ and $\Phi(t_f,t)$ are uncertain, our estimate of the control-free end state, computed at time t, must be

$$\hat{x}_f(t)_{u_c=0} = \widehat{\Phi(t_f,t)x(t)} \quad . \tag{3}$$

By our assumptions of linearity, Φ is not a function of x, and so Φ and x are uncorrelated, and hence

$$\hat{x}_f(t)_{u_c=0} = \hat{\Phi}(t_f,t)\hat{x}(t) \quad . \tag{4}$$

Writing

$$\hat{x}(t) = x(t) + \tilde{x}(t) \quad , \tag{5}$$

where $\tilde{x}$ is the error in the estimate $\hat{x}$, and similarly for the other variables, we find that

$$\tilde{x}_f(t)_{u_c=0} \triangleq \Phi(t_f,t)\tilde{x}(t) + \tilde{\Phi}(t_f,t)x(t) \quad . \tag{6}$$

Since the estimate $\hat{x}_f(t)_{u_c=0}$ is used to construct the missile control, the error will cause the guidance to 'aim' the missile incorrectly. It will, therefore, be guided towards the wrong point in space. The prediction error $\tilde{x}_f(t)_{u_c=0}$ is the primary cause of miss in all guided weapon systems.

The prediction error tends to get smaller as the missile-target range falls, particularly in a *homing* missile system, because

(i) the guidance sensor is closing with the target,
and (ii) the prediction interval is getting shorter.

Usually $\tilde{x}_f(t)$ tends to be oscillatory, so that the aim point oscillates around the collision point. However, it can also be biassed.

The final miss is determined by two primary factors -

(i) the magnitude of the prediction error throughout the flight, and particularly in the final stage;

(ii) the ability of the missile to follow the changing aim point.

(i) is associated with an estimation problem, and is information limited;

(ii) is associated with a control problem, and is missile agility limited.

The prediction error $\tilde{x}_f(t)$ may fall to zero as t approaches t_f, but this does not necessarily mean that the missile will hit the target. It will only do so if it is agile enough to follow the demanded aim point motion throughout the terminal phase.

If the missile is sluggish the control-free state transition matrix $\Phi(t_f,t)$ will be a complicated function of the missile response parameters. Hence $\tilde{\Phi}(t_f,t)$ will be heavily influenced by any uncertainty in the missile response. The prediction error will in turn be dependent on this uncertainty.

The more agile the missile, the smaller the terms in $\Phi(t_f,t)$, and the smaller are those in $\tilde{\Phi}(t_f,t)$,

Missile control response limiting can have a serious effect on the miss. Many nonlinear elements can be approximated by an equivalent gain, or describing function, G_e. This turns out to be a function of the variance of the missile control input, u_c. As $\mathrm{var}(u_c)$ increases, G_e reduces. The result tends to be a rapid fall in the effective guidance loop gain in the very last stages of interception. A significant increase in miss distance results.

2.1 The optimal state estimate

The predicted terminal state $\hat{x}_f(t)$ is used to generate the missile control. Since we require the variance of the control to be minimal, we desire $\hat{x}_f(t)$ to be a minimum variance prediction. Hence $\hat{x}(t)$ should be a minimum variance estimate.

2.2 Information limited performance

The fundamental cause of the miss is uncertainty, about the current state $x(t)$, and about the future behaviour of the system $\Phi(t_f,t)$. The prediction error due to this uncertainty induces an aiming error, and the actual miss is determined by the ability of the missile to track the reducing aiming error as the uncertainty falls.

For a given missile agility, the missile performance is information limited.

3. THE ZERO-CONTROL MISS

For a linear system, the zero-control miss, a scalar quantity, can be written as

$$z(t) = g^{T}(t_f,t)x(t) \quad , \tag{7}$$

where g is called an adjoint, or co-state vector. If only the miss distance is of primary concern, $z(t)$ is used to construct the missile control.

3.1 Lag-free missile, non-manoeuvring target

We find the zero-control miss, as a function of missile-target range r, to be given by

$$z(r) = \omega_s(r)r^2/V \quad , \tag{8}$$

where ω_s is the inertial sightline spin and V is the missile-target closing speed.

3.2 Simple lag missile, non-manoeuvring target

We find

$$z(r) = \omega_s(r)r^2/V - a_{msy}(r)d\left(r - d - e^{(r_1-r)/d}(r_1 - d)\right)\Big/V^2 \quad , \tag{9}$$

where a_{msy} is the missile acceleration normal to the sightline, and

$$d = VT$$

is a 'characteristic distance' for the system, T being the missile lag time-constant. The distance r_1 is some small range below which the miss distance is effectively unalterable by system inputs.

3.3 Quadratic-lag missile, non-manoeuvring target

We find

$$z(r) = \omega_s(r)r^2/V + g_2 a_{msy}(r) + g_3\dot{a}_{msy}(r) \quad , \tag{10}$$

where g_2 and g_3 are complicated functions of the missile quadratic response parameters, in particular the characteristic distance

$$d = \frac{V}{\omega_0} \quad ,$$

where ω_0 is the missile natural frequency.

3.4 Lag-free missile, weaving target

$$z(r) = \omega_s(r)r^2/V + \left(\frac{d}{V}\right)^2 \left[\left\{1 - \cos\left(\frac{r - r_1}{d}\right) + \frac{r_1}{d}\sin\left(\frac{r - r_1}{d}\right)\right\}a_{tsx} - \left\{\frac{r}{d} - \sin\left(\frac{r - r_1}{d}\right) - \frac{r_1}{d}\cos\left(\frac{r - r_1}{d}\right)\right\}a_{tsy}\right] \quad , \tag{11}$$

where $d = V/\omega_W$,

ω_W being the target weave frequency, and a_{tsx}, a_{tsy} are the components of the weave acceleration in sightline axes.

4 OPTIMAL CONTROL

Consider a system whose linearised dynamics is

$$\dot{x}(t) = A(t)x(t) + B(t)u(t) \quad , \tag{12}$$

where $u(t)$ is the total control input due to missile control, target control, and system disturbances, ie

$$u = u_c + u_t + u_d \quad . \tag{13}$$

At some end time t_1, the system state is

$$x(t_1) = \Phi(t_1,t)x(t) + \int_t^{t_1} \Phi(t,\tau)B(\tau)u_c(\tau)d\tau + W_n \quad , \tag{14}$$

where W_n is a perturbation due to the target and disturbance parts of the control. Generally we want to choose u_c so that $x(t_1)$ is close to some desired end state.

A frequently used, mathematically convenient performance index (PI), which measures the missile effectiveness for a given control energy, is

$$J(t_0,t_1) = \mathcal{E}\left\{x^T(t_1)P(t_1)x(t_1) + \int_{t_0}^{t_1} u_c^T(\tau)R_2(\tau)u_c(\tau)d\tau\right\} . \tag{15}$$

$J(t_0,t_1)$ measures the weighted sum of the mean-square end-state and the weighted control energy used in the interval t_0 to t_1 .

We seek the sequence of control vectors, or control functional, which minimises J . This is the so-called optimal control.

The solution of this problem yields the optimal control

$$u_0(t) = -R_2^{-1}(t)B^T(t)P(t)x(t) , \tag{16}$$

where the weighting matrix P obeys the Ricatti equation

$$\frac{dP(t)}{dt} = -P(t)A(t) - A^T(t)P(t) + P(t)B(t)R_2^{-1}(t)B^T(t)P(t) . \tag{17}$$

The end-condition $P(t_1)$ defines the weighting on the terminal state $x(t_1)$.

4.1 Optimal control in terms of the ZCM

It is possible to transform the optimal control equations for the full state x into equivalent ones for the expected zero-control miss (EZCM), z .

For a linear system the EZCM is given by

$$z(t) = g^T(t_1,t)x(t) . \tag{18}$$

The dynamical equation for the EZCM is

$$\dot{z}(t) = g^T(t_1,t)B(t)u(t) . \tag{19}$$

The optimal control turns out to be

$$u_0(t) = -R_2^{-1}(g^TB)^TP_z z . \tag{20}$$

P_z is related to the full state weighting P by

$$P = gP_zg^T . \tag{21}$$

If the EZCM is scalar, then so is P_z .

To compute the optimal control for the z system, we must know the vector $g(t_1,t)$ which links z to the system state x .

Examples of g have been inferred earlier for various missile and target hypotheses.

The weighting P_z , which is scalar, obeys the equation

$$\dot{P}_z(t) = R_2^{-1}(t)\left[g^T(t_1,t)B(t)P_z(t)\right]^2 . \tag{22}$$

The end condition for P_z can be chosen as

$$P_z(t_1) = 1 . \tag{23}$$

Using

$$\frac{dx}{dt} = \frac{dx}{dr}\cdot\frac{dr}{dt} , \tag{24}$$

the time-dependent dynamics can be transformed into a range-dependent dynamics, to obtain

$$\frac{dz}{dr} = (g^TB)^2P_z z/VR_2 \tag{25}$$

and

$$\frac{dP_z}{dr} = -(g^TB)^2P_z^2/VR_2 , \tag{26}$$

where V is the missile-target closing speed.

The optimal (scalar) control is

$$u_0(r) = -g^T B P_z R_2^{-1} z(r) \quad . \tag{27}$$

The solution of the scalar Ricatti equation for P_z is

$$P_z(r_0) = \left\{1 + \int_{r_1}^{r_0} \frac{\left(g^T(r_1,r)B(r)\right)^2 dr}{VR_2}\right\}^{-1} \tag{28}$$

which can be solved analytically if we make some approximation for V .

These various equations can be used to design an optimal control law for any specified system, simply by making the relevant substitutions for the particular g and B vectors.

Of course, it may not be a trivial matter to obtain an algebraic expression for g!

It is worth remarking that the miss due to initial heading error under optimal control can be obtained by noting that

$$\frac{dz}{dP_z} = -\frac{z}{P_z} \quad . \tag{29}$$

The solution of this DE at $r = r_1$ is the expected miss

$$m \triangleq z(r_1) = z(r_0)P_z(r_0) \quad . \tag{30}$$

5 EXAMPLE CONTROL LAWS GENERATED BY THE THEORY

Applying the theory to the missile-target system, for which the sightline spin evolves according to the DE

$$\dot{\omega}_s = -2\frac{\dot{r}}{r}\omega_s + \frac{a_{tsy} - a_{msy}}{r} \quad , \tag{31}$$

we obtain the following results for three simple cases.

5.1 Lag-free missile, constant velocity target

We find that the optimal control is

$$u_0(r) = \frac{3Vr^3\omega_s}{3R_2V^3 + r^3 - r_1^3} \triangleq 3V\omega_s \quad . \tag{32}$$

This is proportional navigation (PN) with a navigation constant of 3.

5.2 Simple-lag missile, constant velocity target

The optimal control is

$$u_0(r) = \frac{3f_1(r,d)\left\{V\omega_s - a_{msy}\frac{d}{r}f_1(r,d)\right\}}{3R_2\left(\frac{V}{r}\right)^3 + f_2(r,d)} \quad , \tag{33}$$

where $f_1(r,d) = 1 - \frac{d}{r} + \frac{b}{r}e^{-a/d}$,

$$f_2(r,d) = \left(\frac{r-d}{r}\right)^3 + \left(\frac{b}{r}\right)^3 - \frac{3}{r^3}\left\{e^{-a/d}\left(2bdr + \frac{b^2d}{2}e^{-a/d}\right) + 2bdr_1 + \frac{b^2d}{2}\right\} \quad ,$$

$$a = r - r_1 \quad , \qquad b = d - r_1$$

and

$$d = VT \quad .$$

The parameter d is a 'distance constant' associated with the missile lag T .

At long range, the terms involving d are insignificant, and the optimal control converges on PN . The effect of these terms becomes important as the range r becomes comparable with d .

5.3 Lag-free missile, target weaving at frequency ω_W

The optimal control is

$$u_0(r) = u_{01} + u_{02} + u_{03} \quad , \tag{34}$$

where

$$u_{01} = \frac{3r^3 V\omega_s}{3R_2V^3 + r^3 - r_1^3} ,$$

$$u_{02} = \frac{3rd^2}{3R_2V^3 + r^3 - r_1^3}\left\{1 - \cos\left(\frac{r - r_1}{d}\right) + \frac{r_1}{d}\sin\left(\frac{r - r_1}{d}\right)\right\} a_{tsx} ,$$

$$u_{03} = \frac{-3rd^2}{3R_2V^3 + r^3 - r_1^3}\left\{\frac{r}{d} - \sin\left(\frac{r - r_1}{d}\right) - \frac{r_1}{d}\cos\left(\frac{r - r_1}{d}\right)\right\} a_{tsy}$$

or, approximately

$$u_0(r) \simeq 3V\omega_s + 3\left(\frac{d}{r}\right)^2 \left\{\left(1 - \cos\left(\frac{r}{d}\right)\right) a_{tsx} - \left(\frac{r}{d} - \sin\left(\frac{r}{d}\right)\right) a_{tsy}\right\}$$

and

$$d = \frac{V}{\omega_W} . \tag{35}$$

This is PN with additional terms due to the target weave. The extra terms are significant only when r becomes comparable with d .

6 COMMENT ON PN GUIDANCE

As we have seen in section 5, proportional navigation guidance emerges as a solution to the optimal control problem when it is hypothesised that the missile is lag-free and the target non-manoeuvring. It is based on a hypothesis of the zero-control miss (from section 3.1)

$$\hat{z}(r) = \omega_s(r) r^2/V , \tag{36}$$

and yields a demand for missile acceleration, normal to the sightline, of

$$a_{msy} = K_n V\omega_s , \tag{37}$$

where K_n is the navigation factor, recommended by optimal control theory to be 3.

As we have seen, if the hypothesis is incorrect, ie the missile is not lag-free and the target manoeuvring, PN guidance is non-optimal. There are extra terms in $z(r)$ which are ignored by PN . This is why PN fails to achieve a small miss distance in the general case.

6.1 Higher order guidance laws

Generally speaking, PN guidance yields a stable trajectory, with a steadily decreasing zero-control miss, until the range r becomes comparable with the characteristic distance d . After this, the additional terms in the EZCM, due to missile lag and target manoeuvre, become significant. PN ignores these terms, and the terminal relative trajectory becomes oscillatory, with a resultant miss.

As we have seen, the use of linear optimal control theory suggests higher order laws which are effectively linear modifications of PN. Over the years, many workers have suggested specific modifications of PN which are often referred to as 'augmented PN' (APN) control laws. They correspond to specific hypotheses of target manoeuvre and missile response in the optimal theory.

7 THE TERMINAL MISS

The dynamics of the missile-target state, and that of the state estimator employed to generate an estimate of the state, can be summarised (in the linearised case) by

$$\frac{dx}{dr} = Fx + Gu , \tag{38}$$

where x is the joint state vector (obtained by adjoining the true and estimated state vectors), r is the missile-target range, F is the closed-loop dynamics, u is an input due to target manoeuvre, seeker noise etc, and G is an input distribution matrix.

When u is zero, the joint state at some small range r_1 is

$$x(r_1) = \Phi(r_1, r_0) x(r_0) , \tag{39}$$

where Φ is the closed-loop state transition matrix and r_0 is the initial range.

When the input u is non-zero, $x(r_1)$ is given by

$$x(r_1) = \Phi(r_1,r_0)x(r_0) + \int_{r_0}^{r_1} \Phi(r_1,r)G(r)u(r)dr \quad . \tag{40}$$

The miss distance can be shown to be given approximately by

$$m \simeq \frac{\omega_s(r_1)r_1^2}{V} \quad . \tag{41}$$

Consequently, if ω_s is the first element of x, we need only the first row of Φ to compute the miss. Call this row Z^T. Then

$$m \simeq \frac{r_1^2}{V}\left[Z^T(r_1,r_0)x(r_0) + \int_{r_0}^{r_1} Z^T(r_1,r)G(r)u(r)dr\right] \quad . \tag{42}$$

The miss due to target manoeuvre and noise is thus

$$m \simeq \frac{r_1^2}{V}\int_{r_0}^{r_1} Z^T(r_1,r)G(r)u(r)dr \quad . \tag{43}$$

Z obeys the adjoint differential equation

$$\frac{dz}{dr} = -F^T Z \tag{44}$$

and has the initial condition

$$Z(r_1,r_1) = [1 \quad 0 \quad 0 \quad \ldots]^T \quad . \tag{45}$$

Z can thus be computed for all r.

7.1 Miss due to target manoeuvre against PN guidance

If we suppose that our missile is effectively lag-free, and employs PN guidance as its interception strategy, using a quadratic lag state estimator to form an estimate of the sightline spin ω_s, then we find that the miss due to target acceleration a_{tsy}, normal to the sightline, is given by

$$m_a \simeq \frac{r_1^2}{V^2}\int_{r_1}^{r_0} \frac{Z_1(r_1,r)}{r} a_{tsy}(r)dr \quad . \tag{46}$$

7.2 Optimal target evasion strategy

From equation (46), it is clear that there is an optimal counter-strategy to the missiles' PN strategy (which is based on a hypothesis of zero target manoeuvre). To maximise the miss, the target should choose its acceleration $a_{tsy}(r)$ so that the term under the integral is always of one sign. It should reverse the sign of a_{tsy} whenever the adjoint variable Z_1 changes sign.

To achieve this, the target needs information. It must know the range r, and have a model for the dynamics of Z.

8 GAME THEORY

For a given deterministic target strategy, T1, there is an optimal guidance law, G1, which will minimise the miss distance.

Against this guidance law G1, there is an optimal target counter-strategy, T2, which will *maximise* the miss.

And so-on, ad infinitum.

Each guidance law requires estimates of the target manoeuvre states. An optimal estimator, embodying a model of the target manoeuvre strategy, can in principle supply these estimates. Its estimation accuracy depends on the noise level from the homing seeker, and the accuracy of the target model.

To implement any particular optimal control, we require information, or intelligence, about the particular target strategy.

9 MULTIPLE HYPOTHESIS GUIDANCE

Fig 1 shows the structure of a guidance system. Observations on the true missile-target relative state $x(t)$ are made by the missile seeker. These measurements are used in an optimal estimator to construct an estimate of the relative state, $\hat{x}(t)$. The outputs of inertial instruments are used within the missile model parts of the estimator. Both the seeker and the inertial instruments may be strapdown devices.

Using the estimated state $\hat{x}(t)$, an optimal controller constructs control inputs for the missile.

The 'missing block' in Fig 1 is the target model. In the absence of *a priori* data, we can only hypothesise about the target manoeuvre motion.

Fig 2 shows the structure of a multiple hypothesis guidance system. Multiple hypotheses of the possible target behaviour are run in the guidance state estimator. The estimator consists of a bank of extended Kalman filters. The residuals of each filter are monitored, and compared with the residual variances predicted by the optimal theory. The hypotheses are thus weighted according to their likelihood.

Each estimator hypothesis is paired with a corresponding optimal controller. The most likely hypothesised state estimate is used to construct the missile control, via its associated optimal controller.

This approach is currently being examined. It shows promise in those cases where *a priori* intelligence about target behaviour is available. It is unlikely to work well in situations where the homing seeker is very noisy, because of the resultant poor discrimination between alternative hypotheses, or where the diversity of the target behaviour is so wide that the hypothesis space cannot be adequately sampled. In this latter case, the target behaviour may be effectively unpredictable, ie noise-like, in which case the domain of the hypotheses might best be regarded as noise power spectral density. In Ref 3, Maybeck discusses such an approach.

10 CONCLUSION

We have discussed the problem of bringing a missile into collision with a moving target. The expected zero-control miss (EZCM) guidance concept has been introduced. It has been shown how errors in the estimates of the current system state and the future zero-control response of the system lead to errors in estimating the EZCM, and consequently how the missile suffers an aiming error. The missile generally suffers a miss, because of its limited ability to follow the changing error, due to restricted bandwidth and control saturation.

Expressions for the EZCM have been indicated for the case of a hypothesised non-manoeuvring target, where the missile has a lag-free, simple lag, and quadratic lag response, and also for the case of a weaving target with a lag-free missile.

Example optimal control laws based on minimising the mean-square EZCM subject to a constraint on the control energy have been derived. Because of the linearity assumptions, the laws are linear modifications of the proportional navigation (PN) law, which turns out to be optimal to a non-manoeuvring target, lag-free missile hypothesis. The additional terms in the high order laws are significant only when the missile approaches within some characteristic distance of the target, determined by the closing velocity and the characteristic time constants of the system.

Expressions have been derived for the idealised miss due to initial heading error, target manoeuvre, and noise. Given that the missile employs some particular guidance law which is optimal to some particular hypothesised target behaviour, and which *minimises* the miss given that the target actually exhibits that behaviour, the equations suggest how the target might choose an *alternative* behaviour which *maximises* the miss, and therefore corresponds to an optimal evasion strategy.

The concept of multiple hypothesis guidance has been briefly introduced.

REFERENCES

1. Nesline, F.W., and Zarchan, P., A new look at Classical versus Modern Homing Missile Guidance; Journal of Guidance and Control, Vol 4, No.1, January-February, 1981.

2. Lawrence, R.V., Unpublished MOD(PE) Report.

3. Maybeck, P.S., Adaptive Tracking of Manoeuvring Targets based on IR Image Data; AGARD Lecture Series No.166, 1989.

Copyright
©
Controller HMSO London
1989

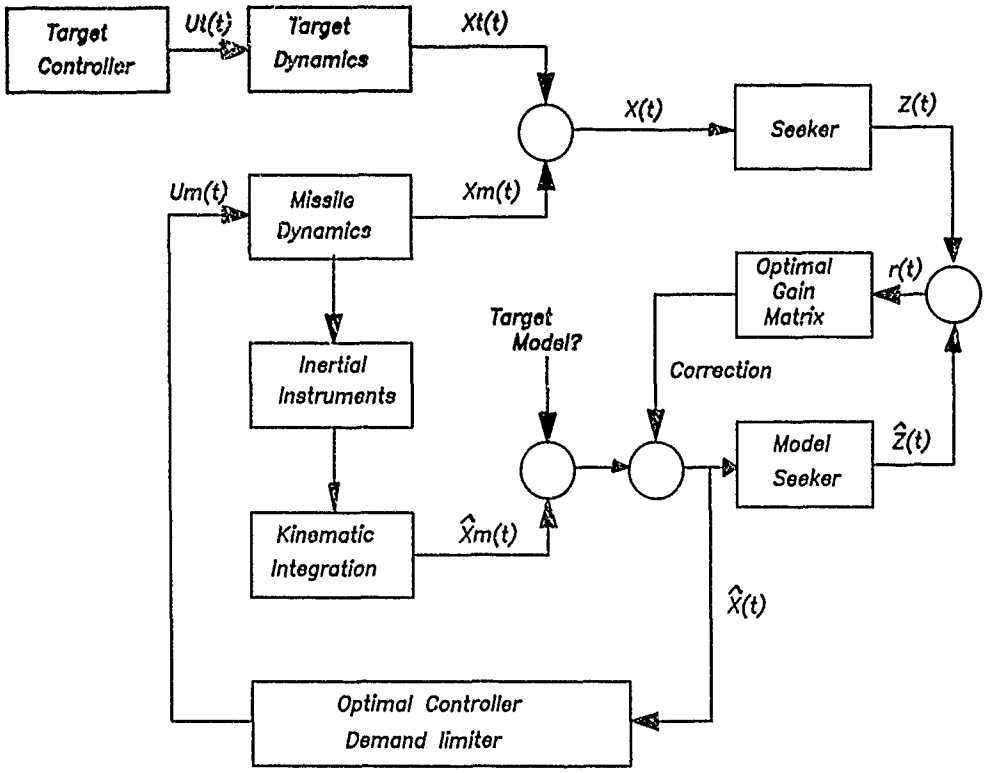
Target Controller
Ut(t)
Target Dynamics
Xt(t)
X(t)
Seeker
Z(t)
Um(t)
Missile Dynamics
Xm(t)
Optimal Gain Matrix
r(t)
Target Model?
Correction
Inertial Instruments
Model Seeker
Ẑ(t)
Kinematic Integration
X̂m(t)
X̂(t)
Optimal Controller Demand limiter

Fig 1

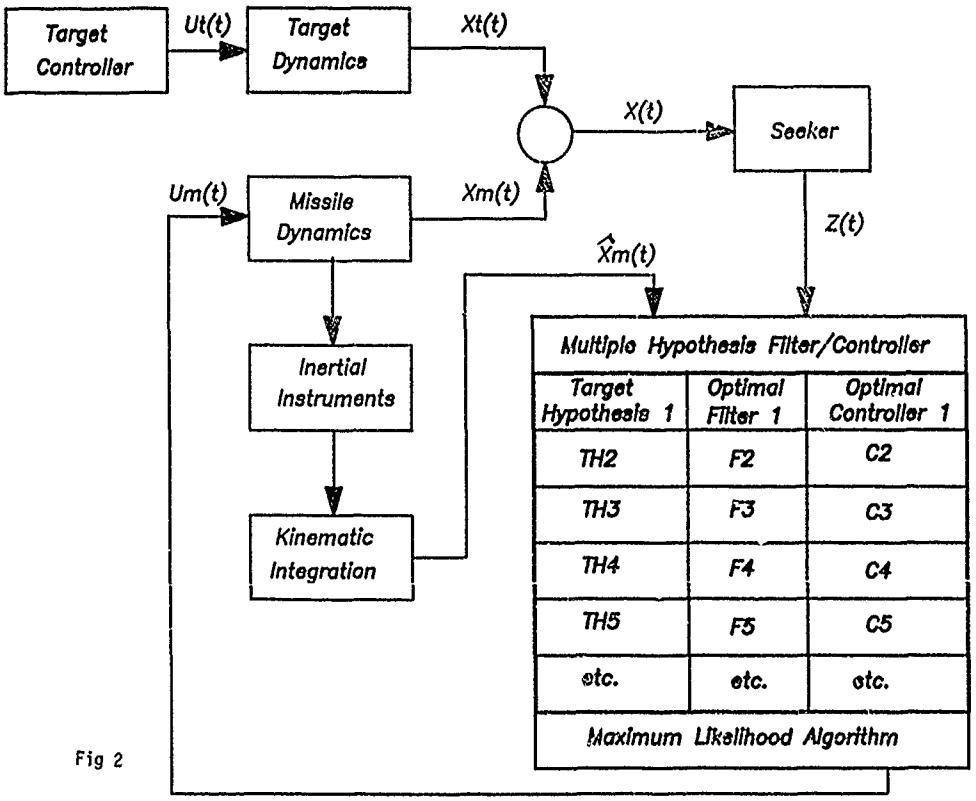
Target Controller
Ut(t)
Target Dynamics
Xt(t)
X(t)
Seeker
Um(t)
Missile Dynamics
Xm(t)
Z(t)
X̂m(t)
Inertial Instruments
Kinematic Integration
Multiple Hypothesis Filter/Controller
Target Hypothesis 1
Optimal Filter 1
Optimal Controller 1
TH2
F2
C2
TH3
F3
C3
TH4
F4
C4
TH5
F5
C5
etc.
etc.
etc.
Maximum Likelihood Algorithm

Fig 2

Micro Based Technology - A New Tool For Missile Guidance System Design and Visualization

by
Paul Zarchan
The Charles Stark Draper Laboratory, Inc.

Abstract

This paper shows how simulation output can be generated and enhanced, in real time, with the computational horsepower and graphics visualization technology which is currently available with microcomputers. Examples are presented which demonstrate how microcomputer based technology offer the designer a visualization which not only gives a deeper insight into the problem being solved, but in addition allows and encourages rapid iteration in order to get an acceptable design.

Introduction and Overview

In the last five years we have witnessed a proliferation of desktop personal computers unimagined only a decade ago. The 32-bit 80386 and 68030 microcomputers are computationally as powerful as a mainframe was only 10 years ago. Currently $5000 of microcomputer provides about as much computational horsepower as a $500,000 super minicomputer[1]. The intent of this paper is to show how the power of the microcomputer can be harnessed by the missile guidance system engineer, not only to computationally solve useful guidance system related problems, but also to provide a visualization which can be used to speed up the design process.

The paper presents several interceptor guidance system related examples which, until recently, were normally solved on mainframes. It is first demonstrated that these examples can be made to work on microcomputers with CPU running times which are very attractive and turn around times (i.e. time for engineer to get the answer in a useful form) that are far superior to that offered by a time-shared mainframes. It is then shown how these answers can be enhanced, in real time, with the graphics visualization technology which is currently available with microcomputers. The enhanced answers will offer the designer a visualization which not only gives a deeper insight into the problem being solved, but in addition allows the user to rapidly iterate cases to get an acceptable design.

The first example presented is that of a rate gyro flight control system for a tactical radar guided homing missile. The purpose of the example is twofold. First it is used as a reference to compare answers and CPU timings from a variety of hardware platforms in the microcomputer, minicomputer and mainframe worlds. Next it will be shown how instantaneous graphical output from both a time and frequency point of view enables the designer to rapidly understand the influence of the autopilot gain on the relative stability and performance characteristics of the flight control system.

A second example considers a satellite in circular orbit. The paper first shows how the satellite can be simulated on a microcomputer. Next it is shown how commercially available mapping data bases can be incorporated in the satellite microcomputer simulation to provide geographical context to the resultant satellite ground tracks. Finally it is shown how linear and orthographic transformations of the mapping data and satellite trajectory provide complementary three-dimensional visualizations on a two-dimensional microcomputer screen.

A final example extends the satellite simulation to include a strategic surface-based interceptor pursuing the satellite. It is shown how the use of dialog boxes with edit fields and buttons can be used to input simulation data and provide the user with complex options in a "user-friendly" way. It is also demonstrated how the simultaneous presentation of information in different windows provides insight which is invaluable in understanding interceptor performance related issues and in visualizing the engagement.

Rate Gyro Flight Control System Example

In order to illustrate the use of graphics in an interactive microcomputer environment, a representative example, is taken from missile guidance and control. A rate gyro flight control system for a radar guided missile[2] is shown in Fig 1. The purpose of this flight control system is to ensure that the achieved body rate follows the body rate command. The gain, K, provides unity transmission between input and output while the autopilot gain, K_R, influences the system dynamic response. In this flight control system the autopilot generated fin deflection command, δ_c, is sent to the actuation system. The electrical command is converted by the

actuator to a mechanical deflection, through an angle δ, of the missile's control surface. The control surface deflection causes the missile body to pitch. A rate gyro is used to measure the achieved body pitch rate thus completing the feedback path. In this simplified model the body pitching can be described by rigid body dynamics expressed as differential equations or in transfer function form as shown in Fig. 1.

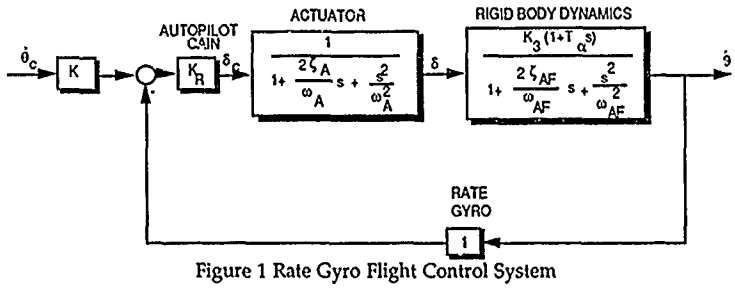

Figure 1 Rate Gyro Flight Control System

From Fig. 1 we can see that the differential equations that govern the system behavior are given by

$$\frac{d\theta}{dt} = -K_3\theta - K_3 T_\alpha \frac{d\theta}{dt}$$

$$\delta_c = K_R\left(K - \frac{d\theta}{dt}\right)$$

$$\frac{d^2\delta}{dt^2} = \omega_A^2\left(\delta_c - \delta - \frac{2\zeta_A}{\omega_A}\frac{d\delta}{dt}\right)$$

$$\frac{d^2\theta}{dt^2} = \omega_{AF}^2\left(\delta - \theta - \frac{2\zeta_{AF}}{\omega_{AF}}\frac{d\theta}{dt}\right)$$

where the autopilot gain, K, provides unity transmission and can easily be shown to be

$$K = \frac{1 - K_R K_3}{-K_R K_3}$$

Nominal parameter values for the rate gyro flight control system appear in Table 1.

Symbol	Name	Definition	Value
ζ_A	za	Actuator damping	.7
ω_A	ωa	Actuator natural frequency	300 rad/sec
K_3	k3	Airframe gain	-.2 sec^{-1}
T_α	ta	Airframe turning rate time constant	2 sec
ζ_{AF}	zaf	Airframe damping	.1
ω_{AF}	ωaf	Airframe natural frequency	10 rad/sec
K_R	kr	Autopilot gain	1.5 sec

Table 1 Nominal Rate Gyro Flight Control System Parameter Values

This flight control system can be simulated using FORTRAN and the second-order Runge-Kutta integration technique[3] for solving the preceding differential equations. The program listing of the rate gyro flight control system appears in Listing 1. We can see, that because of the high frequency actuator dynamics, a very small integration step size is required (H=.001 sec) to accurately numericaily integrate the differential equations. The system differential equations appear after statement label 200. Special logic is included in the listing so that the answers are displayed every .005 sec.

```
      INTEGER STEP
      REAL K,KR,K3
      DATA ZA,WA,K3,TA,ZAF,WAF/.7,300.,-.2,2.,.1,10./
      DATA KR,THDC/1.5,1./
      K=(1-KR*K3)/(-KR*K3)
      DEL=0.
      DELD=0.
      E=0.
      ED=0.
      T=0.
      H=.0001
      S=0.
5     IF(T.GE.1.)GOTO 999
      S=S+H
      DELOLD=DEL
      DELDOLD=DELD
      EOLD=E
      EDOLD=ED
      STEP=1
      GOTO 200
66    STEP=2
      DEL=DEL+H*DELD
      DELD=DELD+H*DELDD
      E=E+H*ED
      ED=ED+H*EDD
      T=T+H
      GOTO 200
55    CONTINUE
      DEL=.5*(DELOLD+DEL+H*DELD)
      DELD=.5*(DELDOLD+DELD+H*DELDD)
      E=.5*(EOLD+E+H*ED)
      ED=.5*(EDOLD+ED+H*EDD)
      IF(S.GE..004999)THEN
        S=0.
        WRITE(9,*)T,THD
      END IF
      GOTO 5
200   CONTINUE
      DELC=KR*(K-THD)
      DELDD=WA*WA*(DELC-DEL-2.*ZA*DELD/WA)
      EDD=WAF*WAF*(DEL-E-2.*ZAF*ED/WAF)
      THD=-K3*E-K3*TA*ED
      IF(STEP-1)66,66,55
999   CONTINUE
      PAUSE
      END
```

Listing 1 FORTRAN Simulation of Rate Gyro Flight Control System

The transient response of the rate gyro flight control system with a 1 deg/sec step input is shown in Fig. 2. From this figure we can see that initially the system output overshoots the input (i.e., output body rate reaches a peak of 4 deg/sec) but eventually follows the input. The response is stable and appears to be well behaved for the autopilot gain setting of K_R=1.5.

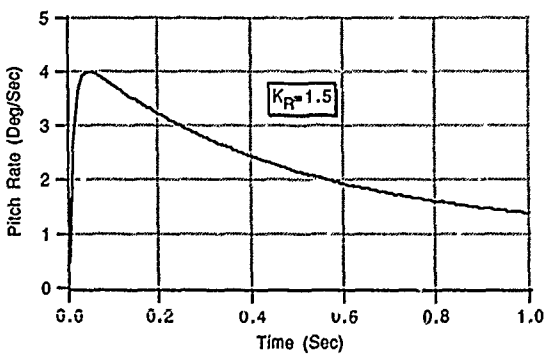

Figure 2 Nominal Response of Rate Gyro Flight Control System

FORTRAN Comparison

The simulation of the rate gyro flight control system, using the FORTRAN source code of Listing 1 was solved on microcomputers representative of the 8-bit, 16-bit, and 32-bit world and their running times were compared in the 1987 time frame.[2] The machines used in this comparison were the original IBM PC, an improved PC, an IBM AT, a Macintosh Plus, and Macintosh II microcomputers. The performance of the machines are compared with and without math coprocessors. Table 2 presents the running time comparisons.

Coprocessor	IBM PC	Improved PC	IBM AT	Macintosh Plus	Macintosh II
Out	520 s	75 s	39 s	61 s	15.4 s
In	———	40 s	35 s	———	7.4 s

Table 2 FORTRAN Running Time Comparison For Rate Gyro Flight Control System Example

Table 2 indicates that the original IBM PC is very slow, compared to the other machines on the rate gyro flight control system example. However, newer versions of the 4.77-Mhz, 8-bit IBM PC and clones are significantly faster (and less expensive too). For example, the IBM AT is about twice as fast as the improved IBM PC, and the Macintosh II is four times faster than the Macintosh Plus. Addressing the math coprocessor significantly improves the speed of both the Macintosh II and the improved IBM PC. However, addressing the math coprocessor on an IBM AT results in negligible speed improvement. The performance improvement for the IBM AT is not as significant because the math coprocessor operates at 4 Mhz whereas the machine is running at 6 Mhz. From Table 2 we can see that the 32-bit Macintosh II is nearly 35 times faster than the original 8-bit IBM PC. When the math coprocessor is addressed, it is nearly 70 times faster. The current generation of 25 Mhz 80386 clones and 68030 based microcomputers are even faster than the Macintosh II. Clearly there have been many improvements since the introduction of the first IBM PC.

The sample problem was also run in FORTRAN on two super minicomputers and one mainframe computer. The running times are summarized in Table 3.[2]

IBM PC	IBM AT	Macintosh II	VAX/785	VAX/8600	IBM/3084Q
520 s	35 s	7.4 s	3.1 s	0.74 s	0.61 s

Table 3 Microcomputer, Minicomputer, Mainframe Running Time Comparison

In this table the running time for the larger machines corresponds to CPU time with a single-user load on a time-sharing system. Usually large machines are shared among many users, and the CPU time is indicative only of what the user is charged for a session. In addition, on large machines the turnaround time (the elapsed time it takes the user to get the output) may be hours, even though the CPU time may be in seconds. On a microcomputer the CPU time is the turnaround time. Nonetheless, Table 3 indicates that the Macintosh II is only 2.4 times slower than the VAX/785 and 12 times slower than the mainframe. Considering that the Macintosh II costs about $5,000, whereas the VAX/785 is about $250,000 and the IBM/3084Q is several million dollars, the comparison is more impressive. Most importantly, the sample rate gyro flight control system problem could be solved on a microcomputer in a very reasonable amount of time.

Open-Loop Transfer Function

Valuable information is available from the time-domain simulation of the system differential equations. However, additional information is also available from the system open-loop transfer function. The concept of the open-loop transfer function is the basis of feedback control systems analysis. While the whole open-loop transfer function is interesting, its frequency response characteristics are most useful to the designer when examined in the frequency domain. Both relative stability and robustness can be determined from an analysis of the magnitude and phase of the open-loop frequency response, and even more importantly, the designer can determine from it what changes to make in the system dynamics in order to achieve design goals.[4,5]

The open-loop transfer function is the transfer function around the loop when the loop is broken at a point. Although the loop can be broken anywhere, it is usually broken in series with some parameter whose value the designer can control to achieve a desired characteristic. For example, we can break the loop of a single-loop feedback control system at the error signal as shown in Fig. 3.

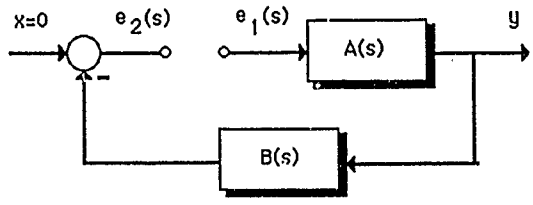

Figure 3 Sample Open-Loop System

In this case the open-loop transfer is defined as

$$HG(s) = -\frac{e_1(s)}{e_2(s)} = A(s)B(s)$$

In order to fully understand open-loop concepts, it is first required to understand the mechanics of finding the magnitude and phase of an open-loop transfer function. This can be done by replacing the complex frequency s in the transfer function with

$$s = j\omega$$

where

$$j=(-1)^{1/2}$$

Usually the magnitude of the open-loop transfer function is expressed in db where

$$db=20\log_{10}(\text{Magnitude})$$

and the phase is expressed in degrees.

With the open-loop transfer function other quantities are also important. For example, the gain margin gm is the value of additional gain required at the loop break (assuming the phase remains constant) to cause instability while the phase margin ϕ_{pm} is the amount of phase lag required at the loop break (assuming that the gain remains constant) to cause instability. In addition to these margins, crossover frequencies are also of interest. The gain crossover frequency ω_{cr} is the frequency at which the open-loop magnitude is unity, while the phase crossover frequency ω_{180} is the frequency at which the open-loop phase is -180 deg. Both these crossover frequencies indicate the frequency of the ensuing oscillation in the time domain, should the system go unstable due to an increase in gain or decrease in phase.

In order to demonstrate the utility of the open loop transfer function, let us revisit the rate gyro flight control system of Fig. 1. Figure 4 shows the same system, except this time the loop is broken at the error signal. The loop is broken here because the designer can control the autopilot gain K_R.

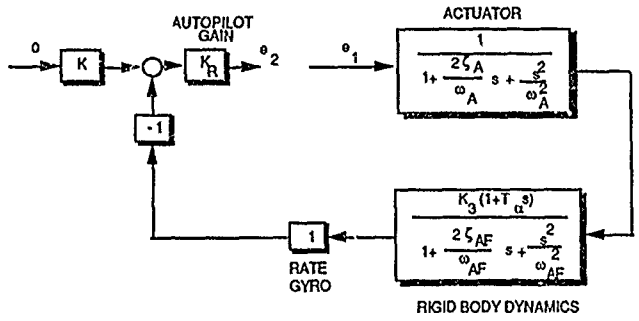

Figure 4 Open-Loop Model Of Rate Gyro Flight Control System

From the definition of open-loop transfer function, we can express HG(s) as

$$HG(s) = \frac{-K_3 K_R (1 + T_\alpha s)}{\left[1 + \frac{2\zeta_A s}{\omega_A} + \frac{s^2}{\omega_A^2}\right]\left[1 + \frac{2\zeta_{AF} s}{\omega_{AF}} + \frac{s^2}{\omega_{AF}^2}\right]}$$

By going to the complex frequency domain we can rewrite the open-loop transfer function as

$$HG(j\omega) = \frac{-K_3 K_R (1 + j\omega T_\alpha)}{\left[1 - \frac{\omega^2}{\omega_A^2} + \frac{j2\zeta_A \omega}{\omega_A}\right]\left[1 - \frac{\omega^2}{\omega_{AF}^2} + \frac{j2\zeta_{AF}\omega_{AF}}{\omega_{AF}}\right]}$$

where care has been taken in the preceding equation to separate the real and imaginary parts. The magnitude and phase of the open-loop transfer function can now be expressed as

$$|HG(j\omega)| = -K_R K_3 \sqrt{\frac{1 + \omega^2 T_\alpha^2}{\left[\left[1 - \frac{\omega^2}{\omega_A^2}\right]^2 + \left[\frac{2\zeta_A \omega}{\omega_A}\right]^2\right]\left[\left[1 - \frac{\omega^2}{\omega_{AF}^2}\right]^2 + \left[\frac{2\zeta_{AF}\omega_{AF}}{\omega_{AF}}\right]^2\right]}}$$

$$\angle HG(j\omega) = \tan^{-1}\omega T_\alpha - \tan^{-1}\left[\frac{\frac{2\zeta_A \omega}{\omega_A}}{1 - \frac{\omega^2}{\omega_A^2}}\right] - \tan^{-1}\left[\frac{\frac{2\zeta_{AF}\omega_{AF}}{\omega_{AF}}}{1 - \frac{\omega^2}{\omega_{AF}^2}}\right]$$

Therefore the open-loop gain (magnitude) and phase can be expressed in conventional units as

$$\text{Gain} = 20\log_{10} |HG(jw)| \quad \text{(db)}$$

$$\text{Phase} = 57.3 \angle HG(j\omega) \quad \text{(deg)}$$

Designers have found several useful ways of displaying open-loop data. One of these ways is a Bode plot in which the magnitude, expressed in db, and phase, expressed in degrees, are displayed versus frequency on a logorithmic scale. The preceding equations were programmed in FORTRAN in order to generate a Bode plot for the rate gyro flight control system and the resultant program appears in Listing 2. Note that in this program we are

incrementally updating the frequency logorithmically and then solving for the magnitude and phase. This program runs quickly because integration is not involved.

```
      REAL K3,KR
      DATA ZA,WA,K3,TA,ZAF,WAF,KR/.7,300.,-.2,2.,.1,10.,1.5/
      DO 10 I=2,16)
      W=10**(.025*I-1)
      XMAG1=SQRT(1+(W*TA)**2)
      XMAG2=SQRT((1-(W/WAF)**2)**2+(2*ZAF*W/WAF)**2)
      XMAG3=SQRT((1-(W/WA)**2)**2+(2*ZA*W/WA)**2)
      GAIN=20*LOG10(-K3*KR*XMAG1/(XMAG2*XMAG3))
      PHASE1=57.3*ATAN2(W*TA,1.)
      PHASE2=57.3*ATAN2(2*ZAF*W/WAF,1-(W/WAF)**2)
      PHASE3=57.3*ATAN2(2*ZA*W/WA,1-(W/WA)**2)
      PHASE=PHASE1-PHASE2-PHASE3
      WRITE(9,*)W,GAIN,PHASE
10    CONTINUE
      PAUSE
      END
```

Listing 2 FORTRAN Program to Generate Open-Loop Bode Plot

Figure 5 presents the resultant Bode plot, using the data generated by the FORTRAN program. Here we can see that the gain (or magnitude) peaks due to the low airframe damping (ζ_{AF}=.1) and then is quickly attenuated due to the dynamics of the actuator. The phase and gain margins are 75 deg and 17 db respectively. This means that if the system phase is decreased by 75 deg or if the system gain is increased by 17 db the system will go unstable. We can also see from Fig. 5 that the gain and phase crossover frequencies are 60 rad/sec and 302 rad/sec respectively. If the system goes unstable because of a decrease in phase, its frequency of unstable oscillation will be the gain crossover frequency. If the system goes unstable because of a gain increase, the frequency of the unstable oscillation will be the phase crossover frequency.

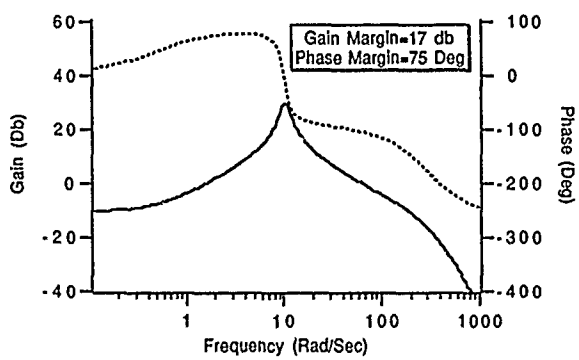

Figure 5 Bode Plot for Rate Gyro Flight Control System

Analysis and Verification of Open-Loop Results

The open-loop analysis of the previous section indicated that the system gain margin was 17 db. This means that if the gain K_R was increased by 17 db the system would go unstable. A gain increase of 17 db means that K_R must increase from 1.5 to 11 to destabilize the system. In other words,

$$20\log_{10}(K_{UNSTABLE}/1.5) = 17 \text{ db}$$

or

$$K_{UNSTABLE} \approx 11$$

In addition, the frequency response analysis indicated that the phase crossover frequency (i.e. frequency when phase is -180 deg) was 302 rad/sec. This means that if the rate gyro flight control system were destabilized by a gain increase, the system would oscillate at 302 rad/sec. Figure 6 shows that when the gain in the FORTRAN time-domain simulation of the rate gyro flight control system of Listing 1 is increased from 1.5 to 11 that the system breaks into growing oscillations at a frequency very close to the phase crossover frequency predicted by the frequency-domain analysis.

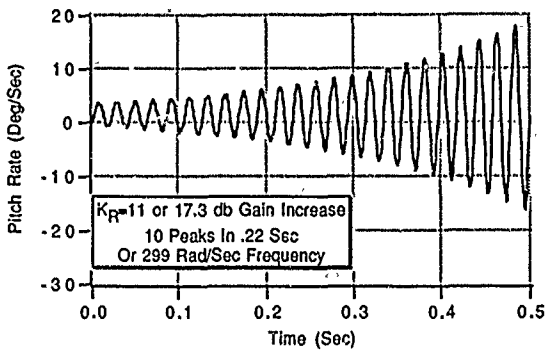

Figure 6 Flight Control System Goes Unstable If Gain Increased Too Much

Therefore this example demonstrates the relationship between the time or simulation domain and frequency or open-loop domain. Both time and frequency domain output information can easily be graphically incorporated into a microcomputer simulation.

We can also illustrate the concept of phase margin by first observing that an ideal delay can be represented by the transfer function

$$\text{DELAY} = e^{-sT}$$

Converting this representation to the complex frequency domain yields

$$\text{DELAY}(j\omega) = e^{-j\omega T} = \cos\omega T - j\sin\omega T$$

The magnitude and phase of the ideal delay is therefore

$$|\text{DELAY}(j\omega)| = (\cos^2\omega T + \sin^2\omega T)^{1/2} = 1$$

$$\angle\text{DELAY}(j\omega) = \tan^{-1}\left[\frac{\sin\omega T}{\cos\omega T}\right] = -\omega T$$

In summary, an ideal delay can be represented in the frequency domain as a function with unity magnitude and pure phase loss. The phase loss at 60 rad/sec (open-loop gain crossover frequency ω_{CR}) can be obtained from the preceding equation as

$$\text{DELAY PHASE LOSS} = -60T$$

Table 4 summarizes the phase loss of an ideal delay for various delay times.

T (sec)	Phase Loss (deg)
0.0	0.0
0.01	-34.3
0.022	-75.0

Table 4 Phase Loss From an Ideal Delay

We can see from Table 4 that a pure delay of .022 sec in the time domain results in a 75 deg phase loss in the frequency domain. Since the phase margin of the open-loop system (with the loop broken at K_R) is 75 deg, this means that if a pure delay of .022 sec were inserted in series with K_R, the system would go unstable and oscillate at a frequency of 60 rad/sec (open-loop gain crossover frequency). The rate gyro flight control time domain simulation of Listing 1 was modified to include a pure time delay of .022 sec and the system step response is shown in Fig 7. Here we can see that the system does go unstable at the predicted value of time delay and also oscillates at the predicted frequency.

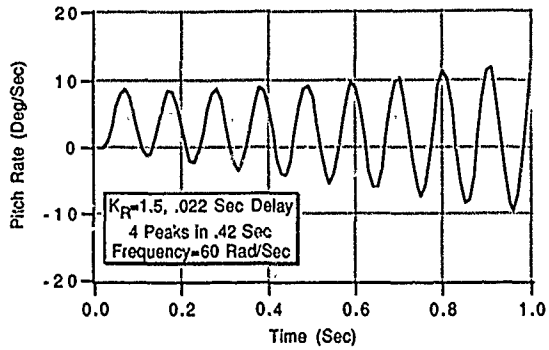

Figure 7 Decreasing the Phase Too Much Can Cause an Instability

The purpose of this section was to show the relationship, via an example, between the open loop frequency response and time domain simulation. The analyst uses both of these computerized methods of analysis for design because of the unique perspective that can be obtained from both the frequency and time domain. Both the time and frequency domain visualizations of the rate gyro flight control system can be presented simultaneously in different windows on a microcomputer screen so that the designer can rapidly iterate on acceptable values of autopilot gain.

Satellite Simulation

The purpose of this section is to provide a more dramatic example of how microcomputer based computation and graphics can be used to enhance the understanding of satellite dynamics. Let us begin by stating the satellite nonlinear differential equations. A convenient coordinate system for the simulation of a satellite is an Earth-centered Cartesian coordinate system as shown in Fig. 8. Since this coordinate system is fixed in inertial space (even though the earth rotates), all satellite acceleration differential equations can be integrated directly to yield velocity and position, without having to worry about Coriolis effects.

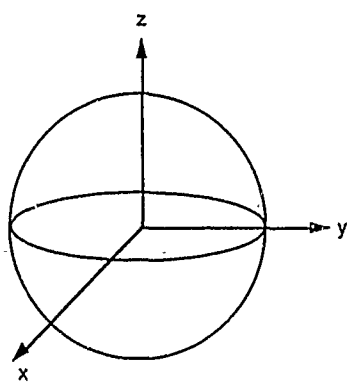

Figure 8 Earth-Centered Coordinate System

The differential equations describing the acceleration of a satellite in a gravity field can be derived from Newton's law of universal gravitation in the Earth-centered Cartesian coordinate system as[1,6]

$$\ddot{x} = \frac{-gmx}{(x^2+y^2+z^2)^{1.5}}$$

$$\ddot{y} = \frac{-gmy}{(x^2+y^2+z^2)^{1.5}}$$

$$\ddot{z} = \frac{-gmz}{(x^2+y^2+z^2)^{1.5}}$$

where x, y, and z are component distances of the satellite from the center of the Earth and gm is the gravitational parameter with value

$$gm = 1.4077 * 10^{16}\ ft^3 / sec^2$$

The velocity of a satellite in circular orbit is related to it's altitude according to[6]

$$V = \sqrt{\frac{gm}{a + alt}}$$

where alt is the altitude of the satellite, measured from the surface of the Earth, and a is the radius of the earth with value

$$a = 2.0926 * 10^7\ ft$$

Given the initial altitude, latitude and longitude of the satellite, we can express the initial location of the satellite in Earth-centered coordinates as

$$x(0) = (a + alt) \cos(lat) \cos(long)$$
$$y(0) = (a + alt) \cos(lat) \sin(long)$$
$$z(0) = (a + alt) \sin(lat)$$

where lat is latitude and long is longitude. The initial velocity components of the satellite in Earth-centered coordinates can be expressed in terms of the satellite velocity, location and inclination. For a satellite at a 90 deg travelling in a prograde, ascending trajectory, the appropriate velocity initial conditions are

$$\dot{x}(0) = -V \sin(lat) \cos(long)$$
$$\dot{y}(0) = V \sin(lat) \sin(long)$$
$$\dot{z}(0) = V \cos(lat)$$

After integrating the satellite acceleration differential equations twice to get position, we must take Earth rotation into account. A coordinate frame moving with the Earth (x_e, y_e, z_e) is related to the inertial coordinate frame (x, y, z) according to

$$x_e = x \cos \omega t + y \sin \omega t$$
$$y_e = x \sin \omega t - y \sin \omega t$$
$$z_e = z$$

where ω is the rotation of the Earth with value

$$\omega = 360\ deg / 24\ hrs = 6.283185\ rad / 86400\ sec$$

The expressions for latitude and longitude can then be expressed in terms of the moving frame as

$$lat = \sin^{-1}\left[\frac{z_e}{\sqrt{x_e^2 + y_e^2 + z_e^2}}\right]$$

$$long = \tan^{-1}\frac{y_e}{x_e}$$

The FORTRAN code for a satellite in circular orbit,using the preceding differential equations and initial conditions, appears in Listing 3. From the source code we can see that the nominal case considered is that of the first 20,000 sec of a satellite travelling in a circular orbit at 1000 km altitude and 90 deg inclination. The acceleration differential equations, which are integrated using the second-order Runge-Kutta numerical technique, appear after statement label 200.

```
      REAL LATMDEG,LONGMDEG,LATM,LONGM,LATITUDEM,LONGITUDEM
      INTEGER STEP
      ALTMKMIC=500.
      LATMDEG=50.
      LONGMDEG=20.
      TF=20000.
      H=10.
      A=2.0926E+07
      GM=1.4077E+16
      W=6.283185/86400.
      T=0.
      LATM=LATMDEG/57.3
      LONGM=LONGMDEG/57.3
      ALTM=ALTMKMIC*3280.
      VS=SQRT(GM/(A+ALTM))
      XM=(A+ALTM)*COS(LATM)*COS(LONGM)
      YM=(A+ALTM)*COS(LATM)*SIN(LONGM)
      ZM=(A+ALTM)*SIN(LATM)
      XMD=-VS*SIN(LATM)*COS(LONGM)
      YMD=-VS*SIN(LATM)*SIN(LONGM)
      ZMD=VS*COS(LATM)
101   CONTINUE
      IF(T>=(TF-.00001))GOTO 999
      XMOLD=XM
      YMOLD=YM
      ZMOLD=ZM
      XMDOLD=XMD
      YMDOLD=YMD
      ZMDOLD=ZMD
      STEP=1
      GOTO 200
66    STEP=2
      XM=XM+H*XMD
      YM=YM+H*YMD
      ZM=ZM+H*ZMD
      YMD=YMD+H*YMDD
      ZMD=ZMD+H*ZMDD
      T=T+H
      GOTO 200
55    CONTINUE
      XM=.5*(XMOLD+XM+H*XMD)
      YM=.5*(YMOLD+YM+H*YMD)
      ZM=.5*(ZMOLD+ZM+H*ZMD)
      XMD=.5*(XMDOLD+XMD+H*XMDD)
      YMD=.5*(YMDOLD+YMD+H*YMDD)
      ZMD=.5*(ZMDOLD+ZMD+H*ZMDD)
      XME=XM*COS(W*T)+YM*SIN(W*T)
      YME=-XM*SIN(W*T)-YM*COS(W*T)
      ZME=ZM
      LATITUDEM=57.3*ASIN(ZME/SQRT(XME**2+YME**2+ZME**2))
      LONGITUDEM=57.3*ATAN2(YME,XME)
      IF(LONGITUDEM>180)THEN
            LONGITUDEM=LONGITUDEM-360
      ENDIF
      ALTKM=(SQRT(XM**2+YM**2+ZM**2)-A)/3280.
      WRITE(9,*)T,ALTKM,LONGITUDEM,LATITUDEM
      GOTO 101
200   CONTINUE
      TEMPBOTM=(XM**2+YM**2+ZM**2)**1.5
      XMDD=-GM*XM/TEMPBOTM
      YMDD=-GM*YM/TEMPBOTM
      ZMDD=-GM*ZM/TEMPBOTM
      IF(STEP-1)66,66,55
999   CONTINUE
      PAUSE
      END
```

Listing 3 FORTRAN Satellite Simulation

By running the simulation of Listing 3 and projecting the results into longitude-latitude space in conjunction with a linear projection of a publically available world map data base[7] as a background, we can get a better graphical visualization. We can see from Fig. 9 that orbits do not overlap because of the rotation of the Earth. We can also see that in 20,000 sec the satellite went through three revolutions. The map provides important geographical context to the satellite simulation. Information missing from the linear mapping display of Fig. 9 is three-dimensional perspective. In addition, there appears to be confusion concerning the motion of the satellite at 90 deg latitude.

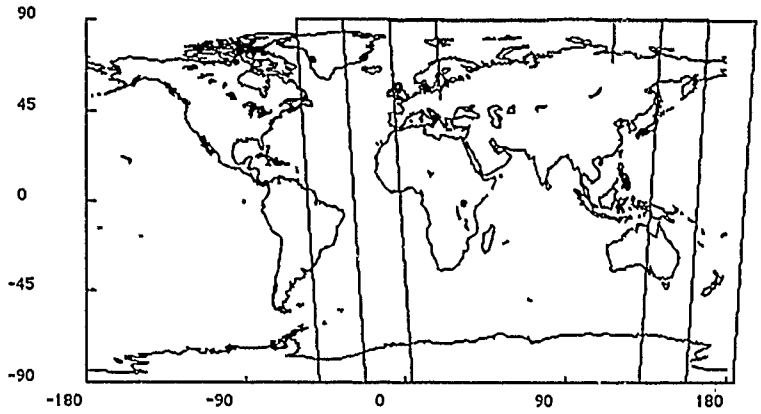

Figure 9 Ground Track of Satellite Motion Provides Geographical Context

Although orthographic mapping projections of the world are the least useful as maps because of the extreme distortion near the edges, they are useful in providing three-dimensional perspective on a two-dimensional microcomputer screen. For example, Fig. 10 with its mapping origin at 0 deg latitude and -45 deg longitude, provides an orthographic view of the same satellite trajectory of Fig. 9. The orthographic projection provides an excellent visualization for both the altitude and inclination of the circular satellite orbit. In addition, confusion concerning motion at 90 deg latitude in the linear display of Fig. 9 has been eliminated in the orthographic display. However, part of the trajectory is missing since an orthographic view can only show one hemisphere at a time.

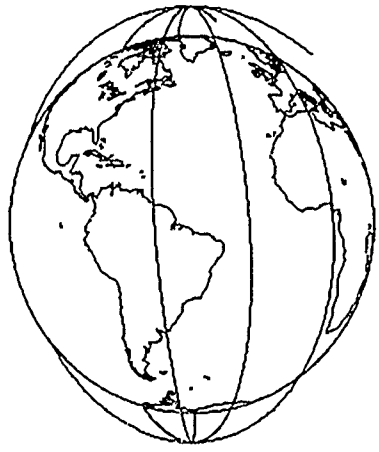

Figure 10 Orthographic View of Satellite Trajectory (Origin=-45 Deg Longitude and 0 Deg Latitude) Adds Perspective

By rotating the orthographic viewing angle we can obtain even more information about the trajectory. For example, if we want a view of the trajectory from infinity looking at the North Pole, we simply change the latitude origin of the map from 0 deg to 90 deg. The resulting North Pole orthographic view is shown in Fig. 11.

Figure 11 North Pole View of Satellite Trajectory (Origin=-45 Deg Longitude and 90 Deg Latitude)

We can see from Figs. 10 11 that microcomputer based graphics technology can add a new dimension to the visualization of trajectories.

Interceptor-Satellite Engagement Simulation

As a final example, let us consider extending the satellite simulation to include a strategic surface-based interceptor pursuing the satellite. Since this engagement simulation is more complex, easier ways of specifying large data sets and user options are required. In this scenario it is appropriate to borrow many of the user-interface concepts popularized by the Macintosh technology. For example, dialog boxes can be implemented as a "user-friendly" way of inputting data into a detailed engagement simulation. Figure 12 shows how the satellite orbital parameters can easily be specified with edit fields and buttons. The satellite location and inclination can be entered in the edit fields by use of an input pointing device known as a mouse. The type of orbit (i.e., prograde or retrograde) is specified by clicking on the appropriate button in the dialog box. When the user is satisfied with all the inputs, a simple mouse click on OK enters the data into the program. Recalling the dialog box from a menu, also controlled by the mouse, allows the user to discover how the satellite orbital parameters influence interceptor performance

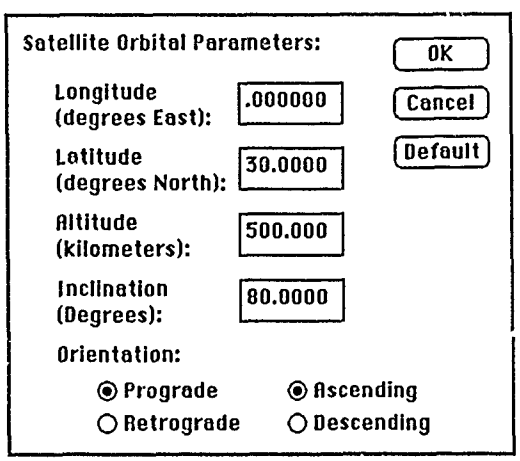

Figure 12 A Dialog Box Is A User-Friendly Way of Entering Data

The dialog box can also be used as a convenient way for providing the user with many complex options. For example, the use of buttons in the dialog box of Fig. 13 allows the user to choose between many sophisticated interceptor guidance laws. Edit fields are used to specify, in even greater detail, many guidance related parameters. Studies can be rapidly conducted in which the effectiveness of each guidance law is quantified.

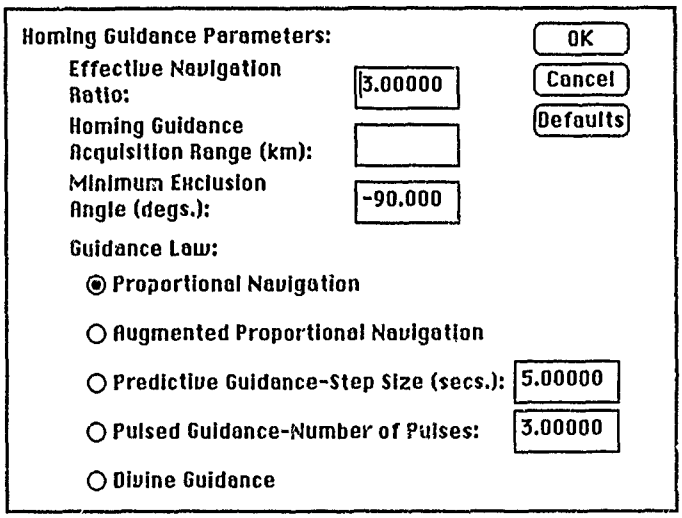

Figure 13 A Dialog Box Is A User-Friendly Way of Making Sophisticated Choices

Finally, after entering the data, the user needs a easy way to both visualize and understand the results of the simulation. Figure 14 presents a possible way of presenting some of the resultant data in different windows simultaneously. The "Ground Tracks" window presents a linear projection of a satellite (solid line) being pursued by a surface-based interceptor (partially dashed curve). A box at the top of the window presents simulation time, interceptor-satellite separation, the lateral divert required for this engagement, and interceptor altitude as the simulation is running. In order to convey perspective, an "Orthographic Projection" window simultaneously presents the same trajectory data. However, this time we get a better visualization of the three-dimensional aspect of the engagement. A "Global View" window provides a macroscopic view of the engagement using orthographic projection techniques. More precise altitude information concerning the interceptor and target can be found in the "Trajectories" window. We can see that the satellite is at constant altitude whereas the interceptor must climb to an altitude higher than the satellite and dive. The "Missile Acceleration" window presents the required missile acceleration, which in this case was miniscule, to effect an intercept.

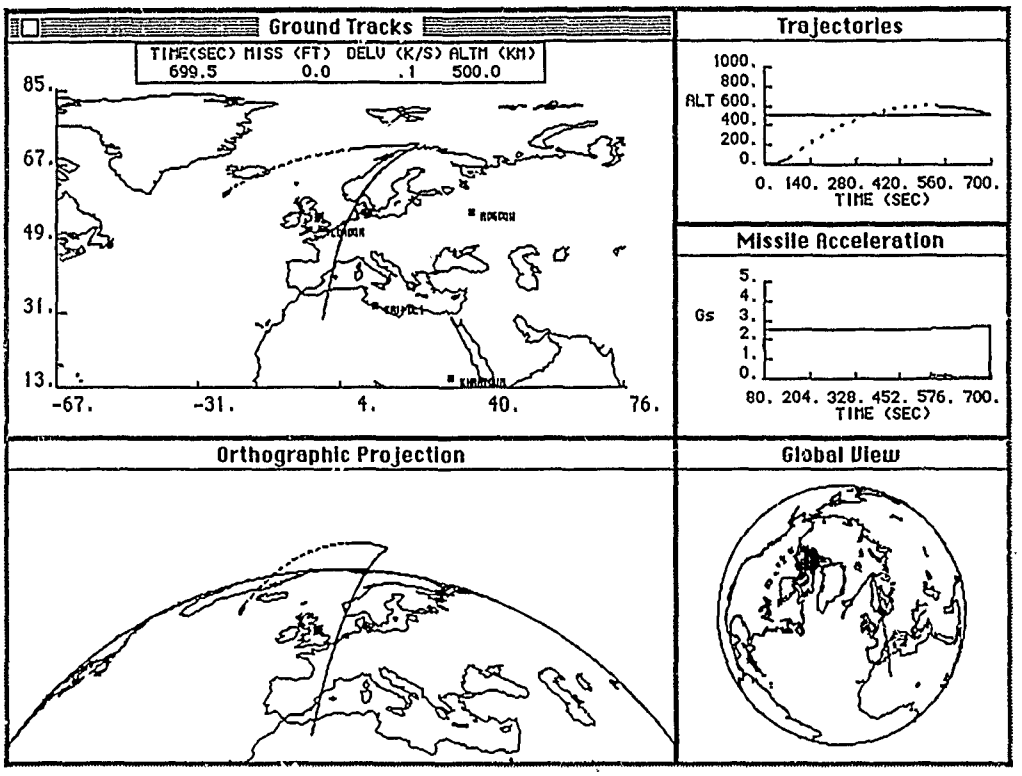

Figure 14 Simulation Data Can Be Presented Simultaneously In Different Windows

Summary

Several interceptor guidance system related examples have been presented. The paper first demonstrates that these examples can be made to work on microcomputers with CPU running times which are very attractive and turn around times (i.e. time for engineer to get the answer in a useful form) that are far superior to that offered by a time-shared mainframes. It is then shown how numerical output can be enhanced, in real time, with the graphics visualization technology which is currently available with microcomputers. Each of the examples demonstrates how the enhanced answers offer the designer a visualization which not only gives a deeper insight into the problem being solved, but in addition allows an engineer to rapidly iterate cases to get an acceptable design.

References

1. Zarchan, P., Tactical and Strategic Missile Guidance, Vol. 124, Progress in Astronautics and Aeronautics, AIAA, Washington, DC, 1990.

2. Zarchan, P. "Micros For Guidance and Control," Proceedings of AIAA Guidance and Control Conference, AIAA, Washington, D.C., Aug. 1987.

3 Press, W. H., Flannery, B. P., Teukolsky, S. A., and Vetterling, W. T., Numerical Recipes: The Art of Scientific Computation, Cambridge, University Press, London, 1986.

4. Bode, H. W., Network Analysis and Feedback Amplifier Design, D. Van Nostrand Company, Inc., Toronto, 1945.

5. Newton, G. C., Gould, L. A., and Kaiser, J. F., Analytical Design of Linear Feedback Controls, John Wiley & Sons, N.Y., 1957.

6 Bate, R. R., Mueller, D. D., and White, J. E., Fundamentals of Astrodynamics, Dover, New York, 1971.

7. Miller, R., and Reddy, F.,"Mapping the World in Pascal," BYTE, Vol. 12, Dec. 1987, pp 329-334.

Interactions Between Battle Management And Guidance Law Design For A Strategic Interceptor

Dr. Owen L. Deutsch
The Charles Stark Draper Laboratory

Abstract

The design of strategic interceptor systems presents many unique challenges. Considering a space-based system with orbiting interceptors, performance requirements may include near-zero miss distances, nearly complete coverage of many simultaneous threat launches and successful interception against maneuvering targets. Cost constraints, on the other hand, will limit the interceptor weight and the numbers deployed. Also, the interceptor may operate at an acceleration disadvantage with respect to target, the range and time-to-go may not be precisely known, and there may be substantial prediction errors for the initial flyout. All of these factors conspire to place great importance on an integrated system design process that provides visibility into the interactions between battle management functions (eg., sensor management, weapon-target assignment and fire-control) and the interceptor guidance law and component technologies. In particular, guidance-related issues must be taken into account in the weapon-target assignment and fire-control functions of the battle manager.

As an example, the minimum time for lateral guidance (with limited acceleration capability) to null out heading errors resulting from prediction error must be accounted for in the timeline decisions of the assignment and fire-control processes. The battle manager may select assignments that avoid unfavorable engagement geometries, where possible. Finally, the fire control manager may select between different guidance laws based on engagement conditions. Once there is visibility into the existence and phenomenology of potential guidance problems, there may be easy opportunities for correction by system-level solutions.

Introduction

Strategic Interceptor Concept

For exposition in this paper, a space-based strategic defense system contains orbiting elements with sensors, interceptors and indigenous communications and processing capabilities. During a conflict, the space-based interceptors are dispatched against targets or threats consisting of strategic ballistic missiles that are boosting or executing post-boost maneuvers. The threats are observed by angle-only optical sensors prior to the launch of the interceptors and by sensors onboard the interceptors that support autonomous homing guidance without external communication. The interceptors attempt to achieve a miss distance that results in a direct collision with the ascending targets. The overall objective for the operation of the defense system is to destroy as many of the threats as is possible for a given defense deployment. The objective for the defense design is the lowest cost system that satisfies a stated requirement for "negation" of an hypothesized threat. For any reasonable constraint on system cost, the performance that will be achievable will fall short of total negation of numerous threat launches. Nonetheless, significant negation may be a useful alternative to total reliance on offensive deterrence and may play synergistically with reduced offensive force levels.

The basic elements of the strategic interceptor system are depicted in Figure 1. The defense may consist of hundreds to thousands of interceptors that may be arrayed individually or clustered on "carrier vehicle" satellite platforms that provide prelaunch support functions including communications, navigation, power, cooling, etc. The interceptors will be stationed in relatively low earth orbits to facilitate kinematic reachability within prescribed timelines [1]. The interceptor flyout distance may range up to 2500 kilometers but will typically be about 1200 kilometers. Typical timelines include a delay time relative to threat launch time of 40 to 80 seconds during which time the target rises above an unknown cloud cover and is tracked for 20 to 40 seconds before the interceptor is dispatched. The larger delay times may result from delay in release authorization and system activation during the initial wave of an assault. Also, later firing times may result from the earliest kinematic opportunity for intercept occurring during or well into the post-boost phase of the threat launch. Depending on the engagement geometry, the interceptor closing velocity may range from 4 to 15 kilometers per second. Typical flyout times are in the range of 80 to 200 seconds, with longer flyouts corresponding to late post-boost intercepts with beyond the horizon targeting.

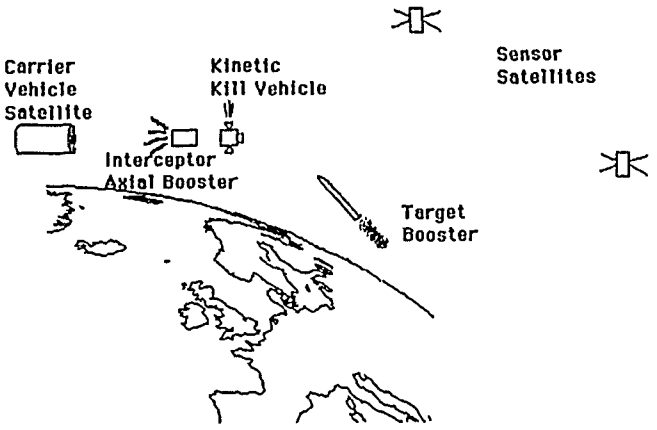

Figure 1. Elements of a space-based kinetic energy strategic defense system.

System Elements and Functions

The sensor elements of the system detect and track threat launches and support the battle management functions of target track correlation, intercept point prediction, weapon-to-target assignment and fire-control for each individual intercept engagement. The interceptors carry homing sensors that allow onboard guidance to execute autonomously after the flyout has commenced. A large number of architectural possibilities can be postulated for the design of the sensor systems. The design space includes issues of spectral bands, mono versus stereo-track coordination, scanning versus staring coverage, multiple levels of resolution, degree of onboard processing, communication network modalities and connectivities, deployment of a small number of highly capable sensors versus proliferation of lower cost sensors or collocation of all sensing on interceptor platforms, and others.

The interceptors operate exoatmospherically and hence must maneuver using thrusters and expending solid or liquid fuels that are carried on board. A typical interceptor design is staged so that the empty weight of tankage or motor casing for thrust used initially during the flyout does not penalize the agility that is required for the endgame maneuvers. The flyout may be arbitrarily divided into an initial phase during which "axial" thrusting is used to deorbit and place the interceptor along a trajectory that is believed to facilitate endgame success followed by a terminal maneuver phase of "lateral" thrusting of the staged "hit-to-kill vehicle." The terminal maneuver phase is required because the axial flyout can never be accurate enough to achieve hit-to-kill without terminal homing and more importantly because the future trajectory of the boosting target is substantially unknown to the defense during the flyout. Even if the threat is known to be a well-characterized type of booster, the aimpoint, reentry angle and threat maneuver uncertainties can easily result in intercept point prediction errors of several hundred kilometers over the interval of the initial flyout.

The battle management functions admit of a number of architectural possibilities ranging from completely centralized to distributed or fully autonomous on the part of the interceptor elements. If, for example, the target locations and constellation status are broadcast to all interceptor elements, then each element can execute the same battle management algorithms and coordinate fire-control decisions implicitly. Alternatively, a number of "stochastic" and "informed stochastic" algorithms permit highly effective fire-control without communication to or between interceptor elements. With suitable algorithm design, the processing capability to perform battle management can most likely be provided by near-term RISC processor designs and does not require great technological advances.

In closing the discussion of the system elements, it is probably fair to state that a number of design alternatives can be postulated that will achieve reasonable performance goals with near-term technology and at constrained cost. For the purposes of this paper, a point design will be constructed to provide illustration of the interaction of battle management with interceptor design issues. The parameters of the design will be chosen to be "round numbers" that are representative of the design space. The point design includes a constellation of carrier vehicles arrayed in 15 rings of 25 satellites per ring in prograde 70 degree inclination orbits at 500 kilometers altitude. Each carrier vehicle contains 10 interceptors. The interceptors are

made up of two solid-fueled booster stages and a pulse-throttleable kill stage. The kill stage contains an infrared focal plane sensor, maneuver engines, attitude control, battery, computer, navigator, and other components packaged into an empty mass assumed to be 10 kilograms. For an allocation of 2.0 kilometers per second ΔV for the kill stage at a specific impulse of 250 seconds, the rocket equation yields a fueled mass of 22.6 kilograms:

$$m_i = m_f e^{\Delta V/(I_{sp} g)} \qquad [1]$$

m_i = initial mass $\quad I_{sp}$ = specific impulse
m_f = final mass $\quad g$ = gravitational acceleration

If we assume that each of the 4 kill vehicle main thrusters comprises 10% of the empty mass and that 100:1 thrust to weight ratio is achievable, then the kill vehicle acceleration capability varies between 4.5 and 10.2 g's between full and empty conditions. The solid fueled booster stages are sized to yield a ΔV of 3 kilometers per second per stage. Assuming a specific impulse of 280 seconds and that the motor casing/nozzle comprises 10% of the booster weight, the total interceptor mass is 330 kilograms. If we constrain the peak axial acceleration to 50 g's, then the burn time for both solid stages to deliver 6 kilometers per second ΔV is 28.5 seconds.

The sensor elements are assumed to be located in a higher altitude constellation. The sensors are mid-infrared focal planes with stereo-coordinated target tracking. Each platform is assumed to carry a sensor suite including a hierarchy of wide-angle coverage at low resolution and several independently steerable medium resolution sensors to support high traffic targeting of individual threat boosters. The target track association problem will not be modeled and only the time delays in servicing the threat traffic and the sensor random errors and navigation error will be modeled. The sensor aboard each interceptor is constrained in optics size and again only the random angle errors of the line of sight observation to the target will be modeled.

The remaining sections of this paper will discuss battle management functions and decisions, interceptor guidance law options, and the interaction of battle management and guidance law design in the context of overall system performance.

Battle Management Functions

Intercept Point Prediction

In order to determine which targets are kinematically accessible from which interceptors, the battle manager must first perform intercept point prediction for each of the targets as they first enter the target queue. Because the flyouts are quite long compared to tactical missile experience and because the targets are accelerating and pitching and may operate at an acceleration advantage with respect to the kill stage, some form of predictive guidance is necessary for the initial axial part of the flyout. Proportional navigation type tactical guidance laws may be suitable for the endgame, but a guidance policy that uses only the currently observed target location or simple constant acceleration extrapolations for future location will consume too much ΔV to be practical. Hence, the accessibility calculation is done with the predicted future location of the target over a range of possible intercept times.

Considering the operational uncertainties in threat booster aimpoint, reentry angle and evasive maneuvers, the intercept point prediction may have 100 to 300 kilometers error with respect to the true location of the threat booster at the selected intercept times 150 to 300 seconds in the future. If the current threat booster acceleration and velocity vectors could be estimated, simple extrapolation would yield prediction errors that were in the range of 500 to several thousand kilometers. Knowledge of the booster acceleration profile and allowance for gravitational acceleration would improve the extrapolation but still would not yield acceptable prediction errors.

Two techniques that yield acceptable intercept point prediction will be described. One technique flies a crude model of the booster from the estimated launch location to an estimated aimpoint at a minimum energy reentry angle. The aimpoint can be estimated to be the centroid of the geographic area that is a priori believed to be the intended target of the threat booster (i.e., Continental United States, CONUS). Alternatively, the aimpoint within this area can be estimated by hypothesizing that the threat booster trajectory lies in a plane in inertial

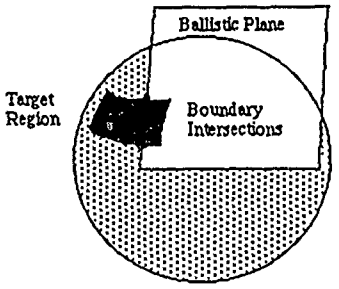

Figure 2. Geometric construct for aimpoint prediction.

space and by projecting the plane to find the intersections with the defined target area on a rotating Earth surface for a nominal impact time. The geometric construct is illustrated in Figure 2. If the target area is represented as a rectangle in latitude-longitude space, there will in general be zero or two intersections with this nonreentrant region. The estimated aimpoint can be taken to be the midpoint of the two intersections. This technique has been found to yield acceptable prediction errors if the threat booster trajectory plane can be estimated from sensor observations. For a range of threat booster launch point-true aim point variations, the projection technique for estimating the threat booster aimpoint has been found to result in intercept point prediction errors that are an average factor of two to three lower than the errors resulting from the use of the target region centroid for the threat booster aimpoint. An additional benefit to the use of this technique is that it does not require an accurate target state estimate but only the target positional location at two time-separated observations early in the target trajectory.

The second technique for intercept point prediction utilizes a template to represent the nominal trajectory of a threat booster instead of the crude simulation of the thrust-time history in a gravitational field. The template can be represented by the altitude and downrange coordinates as a function of time, for example. Sensor line of sight observations over time are filtered to estimate the current point, launch azimuth, launch time and reentry angle. The predicted intercept point is obtained by extrapolation along the template from the current estimated location. The launch point can also be predicted for threat tagging by extrapolation backward along the template. Although the extrapolation along the template is relatively inexpensive computationally, the effort to estimate the template parameters is equivalent to the computational effort in using the first technique described. The template technique also shows somewhat greater brittleness to discrepancies between the flight profile of the booster model used in constructing the template and that of the actually observed threat booster. If monotracking (i.e., observations from a single sensor) is used, however, the template technique and careful selection of sensor geometry to insure observability may be necessary in order to estimate target location from the line of sight angle-only measurements over a short period of time.

Weapon-Target Association

The calculation of the list of kinematically feasible targets for each interceptor is referred to as weapon-target association. The data structure that is used also contains a coarse solution of the interceptor firing time corresponding to each of a number of discrete intercept times relative to the time of the threat booster launch. Hence, the feasibility list also encodes the feasible firing times and the intended intercept time. The decision as to which interceptor engages which target and the intended intercept time is referred to as the weapon-target assignment function. A number of algorithmic approaches for weapon-target assignment will be described in the next section. The association data structure is essential to support most of these approaches.

The calculation of kinematic feasibility for large numbers of satellites against large numbers of targets can be computationally intensive. A standard approach to the reduction of this effort is the use of the "cookie cutter" heuristic to thin out the total number of kinematic calculations. If interceptor satellites are represented in list A and targets (actually predicted intercept locations) in list B, then for each element of either list, a geometric calculation is performed to determine the subset of elements from the other list that are located within a cookie-cutter template positioned at the location of the element of the first list. In other words, satellites on the far side of the Earth from a target are ruled out as kinematically infeasible for that target. The cookie-cutter template is not a true representation of the kinematic footprint, but a quickly evaluated approximation that rules out apparent infeasibilities without yielding

any false negative results. Because some engagements may be at very long range with beyond-the-horizon targetting, the cookie-cutter heuristic tends to be quite coarse but may nonetheless cut down the total number of kinematic calculations by a factor of twenty.

A second layer of heuristic thinning can also be employed to speed up the overall weapon-target association process. Whereas the cookie-cutter heuristic was based on some approximation of reachability in terms of ground-track distance, the second heuristic is based on timeline considerations. For elements of A associated with subsets of B, or vice versa, as determined from the first heuristic, a calculation is made of the transit time feasibility assuming that the interceptor is fired immediately, assuming impulsive acceleration and ignoring gravity. If

ΔR = vector distance to be covered between interceptor satellite location and predicted intercept point

V_o = orbital velocity

$\cos A$ = cosine of angle between V_o and ΔR

ΔV_{ax} = interceptor axial ΔV

V_{net} = resultant interceptor velocity = $V_o + \Delta V_{ax} = V_{net}\,\Delta R / \| \Delta R \|$

then we solve the quadratic equation for V_{net} :

$$V_{net}^2 - 2\,V_o \cos A - \left(V_o^2 - \Delta V_{ax}^2 \right) = 0 \qquad [2]$$

If the discriminant is negative then there is no way that ΔV_{ax} can be added vectorially to the orbital velocity to send the interceptor along ΔR. If there is a solution, then this optimistic impulsive transit time is compared with the actual time to go to the intended intercept time. If this time underbounds the actual time to go then the impulsive velocity required is calculated:

$$\| Vreq \| = \| \Delta R / T_{go} - V_o \| \qquad [3]$$

If the impulsive velocity required exceeds the actual interceptor ΔV_{ax} and is increasing with time, then the heuristic declares that the particular interceptor-predicted intercept point pair is infeasible. The effectiveness of this heuristic depends on the thinning achieved relative to the time spent evaluating the heuristic. The association process was observed to speed up by a factor of about 40 with the use of this heuristic.

Finally, for those pairs between sets A and B that survive the heuristic thinning, the kinematic feasibility calculation is performed by computing a coarse-grained fire control solution as follows. The gravitational acceleration along the flyout trajectory is assumed to be constant and is taken as the value at the midpoint between the interceptor location at firing time and the predicted intercept point:

$$\langle \vec{A}_g \rangle = .5 \left(\vec{A}_g^{\,i} + \vec{A}_g^{\,pp} \right) \qquad [4]$$

Also, the flyout program assumes that the interceptor acceleration due to axial thrusting occurs along a fixed direction in inertial space. These approximations permit a great deal of analytic simplification and enable fire control solutions to be efficiently calculated. The distance that the interceptor travels during the acceleration along the constant direction is denoted by ΔR_{boost} and can be analytically calculated. As before, the vector distance to be covered between initial interceptor location and the predicted intercept point is denoted by ΔR. The simplified kinematics corresponding to these assumptions is given by:

$$\overrightarrow{\Delta R} = \vec{\Delta R}_{boost} + \overrightarrow{\Delta V}_{axial} \cdot \left(T_{fly} - T_{boost} \right) + \vec{V}_i \cdot T_{fly} + .5 \langle \vec{A}_g \rangle \cdot T_{fly}^{\,2} \qquad [5]$$

where

$\vec{V}_I$ = initial orbital velocity

T_{fly} = intended flyout time = Tintercept - Tfire

T_{boost} = total axial boost burn time

ΔR_{boost} = analytically calculated distance traveled during constant direction boost

All quantities in this equation are known except T_{fire}. A solution for T_{fire} can be obtained using a bounded one-dimensional search algorithm and the solution simultaneously yields the thrusting direction for the axial boost. Although several approximations have been made, the firing times and directions are sufficiently accurate that flyout accuracies are several kilometers over a flyout distance of a thousand kilometers. Since the predicted intercept point to which the interceptor is initially directed may be in error by several hundred kilometers, the flyout accuracy stated above is quite acceptable.

Weapon-Target Assignment

Weapon-target assignment is the crux of battle management, although sensor and communications management are no less important. The weapon-target assignment decisions can be made according to a number of policies and much depends on the architecture of the space-defense system. Perfect firing decisions require foreknowledge of all targets and will not be further discussed. Given an evolving knowledge of targets as they are launched and detected by the system sensors, the best achievable performance is defined by "fully coordinated" firing decisions between platforms. However the effectiveness of firing policy is defined, fully coordinated fire is the standard against which firing decisions that are constrained by communications are measured.

Fully coordinated fire can be achieved by an architecture that supports centralized battle management. Because of the vulnerability of this approach, alternatives have been devised to achieve the same effectiveness but with distributed fire management. The main requirement for full coordination is the knowledge of the location and status (i.e., carrier vehicle functionality and number of interceptors remaining) of all carrier vehicles and a knowledge of the complete current target set. If this data is broadcast to every carrier vehicle, for instance, and if every carrier vehicle runs the same algorithm for weapon-target assignment that would be run by the centralized battle manager, then implicit coordination is achieved. This concept is sometimes referred to as the "virtual battle group" concept. The difficulty in implementation is not overwhelming as the number of bytes to be communicated is quite manageable (i.e., ~20 bytes per new target or changed status) and the processing load for the weapon-target assignment algorithm is readily accommodated on current technology commercially available microprocessors. If some of the carrier vehicles receive corrupted information, then the firing decisions degrade gracefully from the optimal depending on the extent of the data loss. If lost connectivity can be detected, then particular platforms can switch to autonomous firing policy modes that will be described shortly.

The quantitative objectives for weapon-target assignment can be defined in a number of ways. There is, of course, the essential objective of destroying as many of the threat boosters as possible. There may be some a priori knowledge, however, that some threat boosters are worth more than others in that they carry more reentry vehicle warheads and so the objective may be posed in terms of number of boosters or numbers of warheads. Considering warheads as the primary objective, there is then a premium toward achieving earlier intercept times for post-boost intercepts or for achieving a boost-phase intercept. Another issue is the casting of the objective as a maximization of the number of warhead kills or the minimization of damage from leakage. This leads to consideration of adaptive defense in the allocation of interceptors against targets. Considering the uncertainties in inferring the threat booster aimpoints, however, this is less of a concern for boost and post-boost strategic defense than for midcourse or terminal defense where the ballistic track is well established. Other issues include the distribution of interceptor offload so as to delay depletion of interceptor resources and the creation of opportunities for subsequent threat salvos to fly through with impunity. Finally, there may be some advantages to consideration of engagement geometry in the weapon-target assignment. For instance, precedence may be given to engagements within the horizon so that the sensor onboard each interceptor can acquire before launch or to engagements that emphasize small crossing angles that achieve a higher likelihood of successful interception. All of these considerations can be factored into the objective function and the weapon-target assignment problem formulated as a constrained optimization problem with primary and secondary optimization criteria.

Among the fully coordinated firing policies, an important distinction can be made amongst those policies that strive for the earliest feasible time of interception (leading to immediate firing orders) and those that utilize the time of intercept as an additional degree of freedom. Although intercepts earlier in the post-boost phase or no later than the end of the boost phase are generally desirable, the earliest firing time policy results in "hair trigger"

allocations of interceptor resources. In other words, selection of an intercept time that is up to 10 or 20 seconds later than the earliest feasible time allows for additional information to be developed in the target queue and for the more optimal reassignment of interceptors not already fired. If all of the threat boosters are detected simultaneously, then this is to no avail. However, most postulated scenarios contain a time structure as well as a spatial structure to the launch activities and significantly improved performance accrues to the policy with some latency to the firing orders.

The mathematical statement of the assignment problem is given in Figure 3.

Targets: $j = 1,2,\ldots J$ CV's: $i = 1,2,\ldots I$ # Interceptors/CV: n_i
Feasibility of fire control solutions for CV_i at target j at any time: $g_{ij} = 1$ or 0
Assignment variables: $x_{ij} = 1$ for assignment of CV_i at target j, 0 otherwise
Constraints: $\sum_{j}^{J} x_{ij} \le n_i$ (Magazine Load) $\sum_{i}^{I} x_{ij} \le 1$ (Interceptors assigned per target)
Define Utility: U_{ij} such that: $\max\left[\sum_{i \text{ or } j} x_{ij} U_{ij}\right]$ results in assigned x_{ij} with $\sum_{i}^{I} x_{ij} g_{ij}$ maximized
$\max\left[\min\left(n_i - \sum_{j}^{J} x_{ij}\right)\right]$ as a secondary consideration (Levelized Offload)

Figure 3. Formulation of Weapon-Target Assignment Problem

Given the data structure describing the feasible associations between weapons and targets, a number of algorithmic approaches are possible [2]. A purely heuristic approach may be constructed as follows:

- For each target, count the number of carrier vehicles that can fire upon it and that have unassigned interceptors remaining
- Sort the targets by this count and assign targets in inverse order (i.e., assign targets that can be fired upon by only one carrier vehicle first). In the case of ties, assign the target with the most warheads first and break ties again with the assignment of the earliest intercept amongst the discrete intercept times.
- For a given target, assign the interceptor from the carrier vehicle with the largest magazine load of unassigned interceptors remaining. Decrement the unassigned magazine load for that carrier vehicle.

This method works reasonably well and yields assignments quickly. An alternative approach that utilizes the auction algorithm also executes rapidly and yields even better results [3]. The auction algorithm functions analogously to the commercial auction process with the exception that all items to be sold are auctioned concurrently instead of consecutively and that some buyers are limited to subsets of all items to be sold (i.e., feasibility constraints). The auction algorithm can be configured with targets bidding for interceptors or vice versa. The utility of each item to be sold to each potential buyer is initialized and the price for each item is set to zero at the beginning of the auction. For each buyer not currently assigned an item, that buyer bids on the item that presents the maximum difference between utility and price (marginal utility) for the buyer. The item is assigned to the buyer and any previous assignment of that item is nullified. Also, the price is incremented. As the auction proceeds the prices escalate and the marginal utilities decrease. The auction stops when there are no bids that represent a nonnegative marginal utility. The final auction prices and assignments reflect the maximization of the aggregate marginal utility for all bidders.

The auction algorithm can be shown to be optimal when the utilities are appropriately normalized [3]. The process can also be speeded up by scheduling a number of bidding rounds with initially large price increments and successively smaller price increments in successive bidding rounds. Each round is initialized to the prices resulting from the previous round but the items start out unassigned.

If fully coordinated weapon-target assignment is not possible, there are a number of alternatives that may yield 60 - 90% of the fully coordinated effectiveness depending on the structure of the threat scenario. The assumption is that the carrier vehicle receives target information only for the subset of targets that are accessible to it. One of the simplest assignment techniques that statistically avoids the assignment of large numbers of interceptors to the same target is the random fire assignment. If a carrier vehicle has any accessible targets, it fires with probability one and the assignment is randomly chosen from a uniform distribution from amongst all of its accessible targets. For a target-rich environment, the inefficiency from dispatch of multiple interceptors to the same target is statistically quite small and a distributional "feeding frenzy" of many interceptors attacking the same target is avoided. There is the unfortunate property, however, that if the coverage regions of adjacent carrier vehicles overlap, then a single isolated threat launch will draw an interceptor from each of the accessible carrier vehicles. For proliferated architectures, an isolated target may draw quite a few interceptors and there are easy opportunities for the threat to structure an attack that draws down the defensive resources.

An alternative weapon-target assignment approach that avoids this problem is the "informed stochastic" approach. Again the carrier vehicle knows only about the targets that are accessible to it. The assumption is made that the carrier vehicle also knows the locations of the surrounding carrier vehicles that also are accessible to its target set. The carrier vehicle in question then counts all of the interceptors that can be brought to bear on its target set and decides to fire a number of interceptors equal to the ratio of its targets to the number of accessible interceptors. In general, the number is not integer and the remainder is treated as the probability of firing its n+1st interceptor. Assuming that each carrier vehicle executes the same policy, the mean number of interceptors fired can be controlled to be equal to the number of targets. If defensive resources permit, then the average number of interceptors per target can be set to a number greater than unity. The informed stochastic approach avoids the distributional feeding frenzy on multiple targets and also avoids the succeptibility to draw down from isolated launches.

Interceptor Guidance Laws

Information Sources

The interceptor guidance must function with information that is loaded prelaunch from the battle manager fire controller, with modelled information on the threat, and with line of sight information that is obtained from an infrared optical sensor that is observing the threat booster plume on a midwave infrared focal plane. The latter information source may be available before launch, acquired after launch, or possibly acquired and then "winked out" but available during the endgame. If there is the possibility of communication with the interceptor after launch, then information from other sensors can be combined with onboard sensor information to drive the guidance function. Apart from the difficulty in tracking and communicating with interceptors, there is the additional issue of target track association between sensors wherein large numbers of targets as seen on the focal plane of one sensor need to be correlated with the multiplicity of targets on a different focal plane. [4] For the present purposes, it is assumed that the interceptor is autonomous after launch and that acquisition of the intended target after launch is successful. If there are ambiguities in the target designation, then the fully coordinated weapon-target assignment may devolve to the stochastic target assignment levels of performance.

Axial Guidance

As mentioned earlier, the use of predictive guidance for the axial thrusting part of the interceptor trajectory seems to be a prerequisite for arriving within a suitable "handover basket" for the endgame. That is, there is little opportunity for pursuit or proportional type guidance laws to succeed over such long flyouts where the target has such a large ΔV reserve and is accelerating in unknown directions and where the pursuer is severely constrained in ΔV. To provide a significantly large coverage "footprint" or area on the ground within which the orbiting interceptor may achieve a fire-control solution against the ascending threats, the intercept trajectory must be energy efficient.

A simple approach to the axial guidance is to fly the interceptor to the predicted intercept point to arrive at the predicted intercept time. The predicted intercept point and time is specified to the interceptor guidance at launch time. If the axial ΔV is delivered impulsively, then this is a simple problem in Keplerian physics and the direction to apply the ΔV is obtained from the solution of the classical Lambert problem [5]. That is, a $V_{Lambert}$ is calculated for the orbital transfer and the impulse is oriented along the vector difference between $V_{Lambert}$ and the orbital velocity V_o. Of course, the ΔV is delivered with finite thrust over a period of time and the predicted intercept point may be updated if the sensor onboard the interceptor has the target acquired during axial boosting. The steering of the thrust vector under these conditions can be done in a variety of ways. The Lambert solution can be used in a feedback approach wherein the velocity to be gained for the orbital transfer is updated and the thrust oriented along the most recently calculated velocity to be gained vector. For trajectories where the thrusting time is long compared to the total flyout time this approach is not particularly energy efficient. An alternative approach is to orient the thrust vector along the fixed direction in inertial space that was calculated by the fire control solution. The solution of equation 5 for the time of firing the interceptor implicitly yields the firing direction. If we define

$$T_{eff} = \frac{\Delta R_{boost}}{\Delta V_{boost}} + T_{fly} - T_{boost} \qquad [6]$$

then the solution for the time of firing also minimizes:

$$\varepsilon = \left\{ \Delta V_{boost} - \frac{1}{T_{eff}} \left| \left[\overrightarrow{\Delta R} - \vec{V}_I \cdot T_{fly} - \langle \vec{A}_g \rangle \cdot \frac{T_{fly}^2}{2} \right] \right| \right\} \qquad [7]$$

and implicitly yields the firing direction. If ΔR_{boost}, ΔV_{boost}, T_{fly} and T_{eff} are updated to reflect the remaining distance to be travelled and ΔV to be gained and the times are updated during the axial boost, the solution that minimizes equation 7 can be used in a closed loop feedback form that leads to more accurate steering and accommodates any update of the predicted intercept point.

Other steering law approaches for axial thrusting may attempt to factor in the changing uncertainty in the predicted intercept point in order to expend more axial ΔV where the uncertainties are lower. For example, the standard deviation of the predicted intercept point may be estimated and the axial thrusting steered to effect an intersection with the closest point on the surface described by the points at distance one or two sigma from the predicted intercept point. This policy recognizes that noisy information sources leading to noisy predicted intercept point locations may waste axial fuel in responding to the noisy predictions. As the time interval over which the prediction is made is decreased and as the uncertainty in the predicted intercept point decreases, the axial thrust is steered closer to the center of the prediction. The actual implementation can be with continuous thrusting with steering commands updated at a high rate or with discrete axial "midcourse" corrections, depending on the propulsion mode.

Lateral Guidance

As discussed earlier, lateral guidance using high data rate line of sight angle information from the sensor onboard the interceptor is essential to reduce the miss distance in the endgame. The situation is common to a number of tactical antiaircraft missiles except that control authority is achieved by thrusting instead of aerodynamic maneuvering. A variety of guidance laws can be designed to achieve the desired small miss distance with the limited acceleration capability of the interceptor and with the limited ΔV capability. The problem is not trivial, however, in that the target may be operating at an acceleration advantage with respect to the interceptor, the target acceleration is not constant and is changing direction, the line of sight measurement of the onboard seeker may be noisy, the differential gravity between the interceptor and target locations may be substantial and the initial heading error may lead to an open loop miss of hundreds of kilometers.

In a conventional tactical guidance type approach, the commanded interceptor acceleration is given by "proportional navigation [6]":

$$\overrightarrow{A_{cmd}} = k\left[\tilde{V}_c\,\dot{\lambda} + \frac{1}{2}\vec{A}_T\cdot\hat{\Omega}\right]\hat{\Omega} \qquad [8]$$

where

$\overrightarrow{A_{cmd}}$ = commanded acceleration

k = "navigation constant"

$\tilde{V}_c$ = estimated closing velocity

$\dot{\lambda}$ = line of sight rate

$\vec{A}_T$ = estimate of target inertial acceleration

$\hat{\Omega}$ = unit vector perpendicular to line of sight

The A_T term is the "augmented proportional navigation" term and is set to zero for pure proportional navigation. Pure proportional navigation is highly efficient when the true target acceleration is zero. This guidance law has the salutary property of straightforward implementation and robustness. Accurate inertial navigation is not required as only the line of sight rate, a relative coordinate measurement must be accurately measured. Errors in the estimated closing velocity simply change the effective navigation constant to which results are not particularly sensitive to variation in the range of 10 to 20%. During operation, the interceptor acceleration commands null out the line of sight rate at a rate that depends on the navigation constant. For long flyouts in a gravity field, however, the variation in the gravitational direction across the flyout will result in the generation of line of sight rates even though the interceptor and target are on a Lambertian collision course. Hence, lateral ΔV will be wasted because the simple proportional guidance law does not know about gravity. Compensation for gravitational effects can be introduced in the augmented term by adding a target acceleration equal to the gravitational acceleration halfway between the interceptor and the target. This simple compensation does not completely eliminate ΔV wastage in the gravity field, but does reduce the magnitude to manageable levels for flyouts up to 200 to 300 seconds duration.

The augmentation term is an approximation that provides some anticipation of line of sight rates to be generated by a constantly accelerating target. Because that is not the case for the strategic defense application, the A_T vector must be updated by the onboard sensor measurements. The use of higher derivatives such as a jerk term would improve performance if these terms could be accurately estimated. Usually, the errors resulting from estimation of these terms from noisy sensor data preclude their usefulness. The estimation of the acceleration correction term from angle only sensor measurements requires some additional modeling. In the current approach, a simple closing distance model is initialized from the fire controller:

$$D(t) \approx D_0\left[1 - \frac{t}{T_{fly}}\right]$$

where $D_{(t)}$ = distance between interceptor and target at time t

D_0 = distance at firing time
T_{fly} = total flyout time interval

Assuming that the interceptor can determine its own navigated location in inertial space, R_I, the inferred location of the target in inertial space R_T, is constructed from R_I, the line of sight measurement, and the distance model:

$$\vec{R}_T \approx \vec{R}_I + \hat{\Theta}\,D(t)$$

where

$\hat{\Theta}$ = line of sight vector

The reconstructed target vector is then processed through a polynomial Kalman filter to extract the estimate of the target inertial acceleration A_T to be used in the augmented proportional navigation term. The resulting acceleration estimate is not particularly accurate, but does improve performance with respect to pure proportional navigation in most engagement geometries.

Other issues in the use of proportional navigation concern the selection of the navigation constant. To respond effectively to accelerating targets, the navigation constant must have a value at least equal to 3. Larger values are closer approximations to an impulse guidance law and are more ΔV efficient in the absence of noise, but they can be considerably less efficient when sensor noise is present. Another significant issue is the saturation of achievable acceleration. Proportional navigation with perfect line of sight information and continuous control will always achieve a zero miss distance if infinite acceleration can be achieved. With finite acceleration capability on the part of the interceptor, the acceleration command is said to be saturated when it exceeds the achievable acceleration. In practice, the two symptoms associated with excessive miss distance (i.e., failure to intercept) are guidance saturation and exhausting the ΔV capability (i.e., running out of maneuver fuel). Saturation may result from excessive heading error (i.e., discrepancy between predicted intercept point used for the flyout and the true target trajectory), from high apparent target accelerations that generate large line of sight rates and are not included in the augmented proportional term, from target acceleration transients that accompany threat booster staging, and from excessively high navigation constants. Many intercept trajectories will exhibit guidance saturation during part of the flyout and especially at the very last instant before intercept. Saturation during any significantly long portion of the flyout will quickly exhaust the ΔV capability and may be indicative of other underlying problems.

A simple strategy for achieving the simultaneous objectives of efficient ΔV usage and small miss distances in the presence of significant prediction errors and sensor noise is the use of a navigation constant that varies according to a predetermined schedule. During the initial part of the endgame, large values of k result in quicker unwinding of the line of sight rates resulting from initial heading errors. The earlier that heading error corrections are applied, the smaller the ΔV required to complete the correction. Unfortunately, large values of k also exaggerate the wastage of ΔV from sensor noise. Finally, large values of k are necessary to enable the control authority necessary for the achievement of small miss distances at the back end of the endgame. Hence, a useable strategy is to begin the engagement with a navigation constant of 5 and to schedule an increase to perhaps a value of 10 as the distance model ramps down to some threshold distance.

Another strategy for dealing with excessive ΔV usage on long flights (because of imperfect gravity compensation or sensor noise) is to constrain the operational times for lateral guidance between a minimum and a maximum guidance on-time. In other words, the lateral guidance is turned on only when there are a specified number of seconds remaining before the intended intercept time. The minimum lateral guidance time is enforced by the battle manager and is an important constraint for dealing with anticipated errors in the predicted intercept point. For a given interceptor lateral acceleration capability, it can be determined that a minimum time interval is necessary to null out a two sigma prediction error. For example, if the prediction error is 200 kilometers and the average lateral acceleration capability is 8 g's, then about 20 seconds is the minimum time necessary for saturated guidance commands to null out the prediction error. The battle manager selects the intercept time and with allowance for the axial thrusting time, a firing time can be determined that enforces the minimum guidance time. The maximum guidance time is used to switch guidance on after a dormant period during a long flyout. The maximum guidance time is empirically determined by the performance tradeoff between failed interceptions resulting from guidance saturation and those resulting from running out of maneuver fuel.

Other guidance laws may be constructed that attempt to achieve better operational performance by increased modeling or greater extraction of sensor information. Both of these generic approaches result in greater computational and implementational complexity. For example, reference model-based guidance laws may require a "mini-simulation" within the guidance loop of the anticipated future trajectory of both interceptor and target. When the reference model assumptions and parameters are in consonance with reality, significant reductions in ΔV usage can be obtained. On the other hand, the reference model-based techniques are significantly more "brittle" and prone to failure when there is not agreement between reality and modelling assumptions. Guidance laws that rely on higher order corrections than augmented proportional navigation require higher order filters that are slower to respond to new data trends and frequently require accurate estimates of the time to go before interception. There may be some advantage to the employment of these advanced guidance

laws, but the performance needs to be quantified in the presence of plausible estimates of operational uncertainties.

System Performance

Measures of Effectiveness

To guide the search through the trade space for the many parameters, architectures, algorithms and guidance laws of a strategic defense system, Measures Of Effectiveness (MOEs) must be formulated against which competing selections can be evaluated. Several obvious candidates for the MOE include the probability of coverage for an arbitrary single threat booster launched from an arbitrary location at an arbitrary time and at the opposite end of the spectrum, the maximum number of simultaneous threat launches from a single site that can be covered before the defense is exhausted of resources in the vicinity of that threat. The latter can be further generalized as will be seen shortly.

Because the previous two MOEs focus on the limits of the threat spectrum, it can be argued than an additional MOE is necessary to characterize the nonlinear performance for a "representative" type of threat scenario. Hence, a "baseline" threat may be defined with a sequence of threat launches that are heterogeneous, structured in space and time, and credible in number.

Finally, in recognition that the cost of a potential space defense system is of strategic importance, a final MOE consists of the total mass that must be placed in orbit to achieve a fixed performance criterion such as universal coverage of an arbitrary launch or a certain percentage negation of warheads launched in the baseline threat. In this MOE, mass in orbit is used as a proxy for system cost.

Figure 4 illustrates the coverage MOE and is derived from system simulation of the battle management functions of a constellation of carrier vehicles. A threat booster is launched

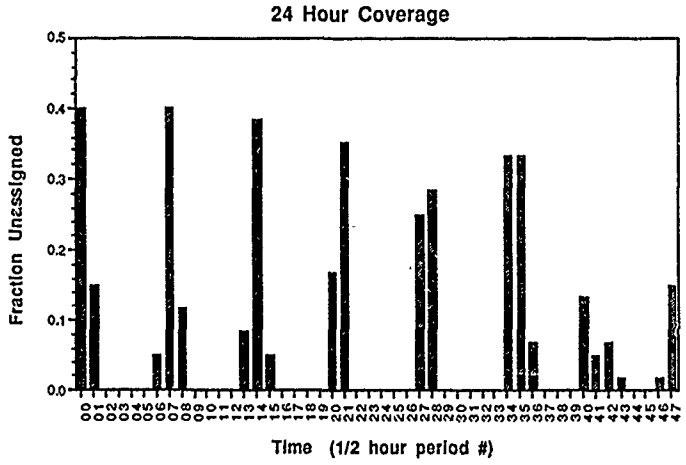

Figure 4. Temporal Coverage Gaps For Boost-Phase Interception

every 30 seconds from a single launch site to evaluate the continuity of coverage from the space defense system with a constraint of boost phase interception. The launch rate of the threat boosters is low enough so that the defense is never depleted of interceptors from any location and so any gaps in coverage reflect the limitation in kinematic coverage (i.e., the axial ΔV and the deployment configuration and numbers). The results of this simulation exercise were scored in one half hour bins and presented in Figure 4 as the fraction of threat launches that could not be assigned during each time period. It is seen that there are half hour periods when 40% of the launches could not be covered by an interceptor from any carrier vehicle. There is also a macrostructure of approximately 3.5 hour periodicity to the distribution of coverage gaps. The totality of the gaps amounted to some 2 hours of launch opportunities over the 24 hour period during which the offense could fly through the defense without suffering loss with respect to boost phase interception. These results need to be generalized for a variety of launch locations to fully address the isolated launch coverage MOE. The lack of coverage could be addressed by distributing interceptors on more stations, by increasing the interceptor reach with

larger axial ΔV allocation, by extending the reach into the post-boost phase, or by some combination of the above. The increase in numbers of interceptors obviously increases the mass in orbit as does increasing the ΔV for each interceptor while retaining the same number of interceptors. If the strategy is to to reallocate the total interceptor ΔV between axial and lateral, the larger footprint accorded to the higher axial ΔV will come at the expense of a lower probability of kill because interceptors with inadequate lateral ΔV will run out of fuel against highly uncertain and maneuvering target trajectories. Meaningful trades can be accomplished only with an analysis that ties together the battle management functions with the guidance functions. If this is done, there are probably a variety of point designs that achieve full coverage by deployment of small numbers of highly capable interceptors with large footprints as well as designs with massive proliferation of limited capability interceptors. The MOE on total mass in orbit can then be used to discriminate between these designs.

The MOE concerned with the maximum number of simultaneous launches from a single site that can be covered addresses the resiliency of a design to highly intense threat scenarios. With a constrained number of interceptor on station, the offense can always "punch through" the defense if a sufficiently large number of threat boosters are launched

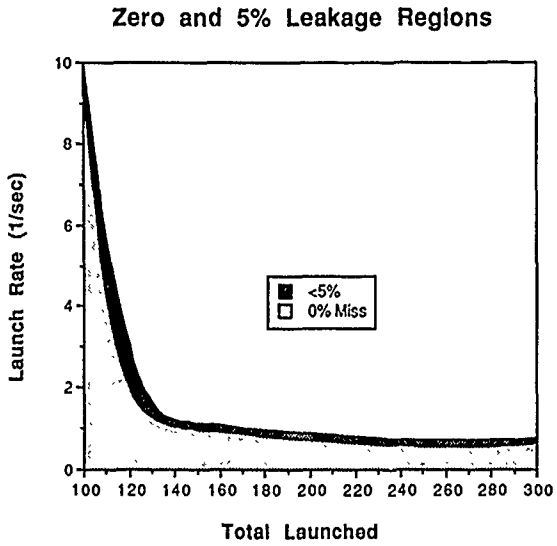

Figure 5. Universal performance curve for single site launch.

from a common location within a short period of time. Of course, the defense deployment can be sized to a given upper limit on the estimated offensive capability for "spike launches." Figure 5 illustrates the performance of a defense system for single launch site scenarios as a function of the intensity of the launch. Simulation results indicate that the details of the launch time distribution are unimportant to the gross performance over a wide range of launch rates. In other words, the defense system exhibits the same performance against a launch rate of one per second as against 10 launches that occur every 10 seconds or 60 launches occurring in an instant every 60 seconds. Only the average launch rate is significant. In Figure 5, large values of the vertical axis represent an infinite launch rate. The asymptotic part of the "0% Miss" curve along the ordinate axis represent the maximum number of simultaneous launches that can be covered. The asymptotic part of the curve along the horizontal axis represents the maximum launch rate that can be covered on a sustained basis and represents the situation where interceptors on station in the vicinity of the launch site are replenished by orbital motion of carrier vehicles entering the battle space. In Figure 5, for example, the defensive system can handle up to 100 simultaneous launches from a single site before depletion of interceptors causes coverage gaps. Alternatively, a launch rate of about one per second can be covered on a sustained basis. In between these extremes, any particular value for launch rate will yield a maximum total number of launches that can be covered before coverage gaps appear. In recognition of the fact that complete coverage may not be economically or technically feasible, a family of curves representing different coverage criteria can be generated as is represented by the second curve labeled "<5% " That is, the area between the 0% and 5% curves represents all cases with <5% missed coverage. It can also be noted that the single launch site performance can be characterized by the two asymptotic values of maximum simultaneous launches and maximum sustained launch rate.

When the threat launch scenario is generalized to include distribution of launches over a number of sites, it is seen that launch sites within a small fraction of the footprint characteristic distance, say within 200 kilometers, can be treated as a single site for prediction of defense performance using a universal curve such as shown in Figure 5. Launch scenarios with widely separated sites usually can be treated independently. Launch scenarios involving sites that are separated by 300 to 400 kilometers show interesting space-time correlation interactions. In other words, the system performance for a simultaneous launch at one site followed by a simultaneous launch at a second site can be worse than for the case of both sites launching at the same time if the interval between spikes is appropriately timed. The first site creates a region in the defensive constellation that is depleted in interceptors and this hole drifts over to the second site creating opportunities for threat launches to ascend without attack by the defense.

The baseline scenario MOE exercises the defense for what is estimated to be a credible launch policy on the part of the offense in terms of numbers, spatial and temporal distribution of threat launches. If the scenario is standardized than comparison can be made across a number of different analysis tools. Also, the effects of individual error sources and architecture or parameter variations can be investigated against the backdrop of a common problem with plausible distributions of threat launches.

Finally, the orbital mass alias cost MOE serves as a sanity check on the overall architectural construct. Assuming a launch cost per kilogram placed in low Earth orbit and using a gross estimate that the hardware costs are about the same as the launch costs, an overall system cost can be inferred that is likely within a small factor of a more elaborate cost analysis. This can be used for comparisons between architectures and for finding the parameters of the lowest cost point design that satisfies a given performance requirement or the best performing design that satisfies a cost constraint.

Guidance Versus Battle Management Trades

As illustrated in Figure 6, the failure to intercept a particular threat booster can be categorized in three ways. The threat may escape interception if it is not fired upon, if it is fired upon but the interceptor guidance command saturates for any length of time immediately prior to the point of closest approach, or if the interceptor lateral DV is exhausted.

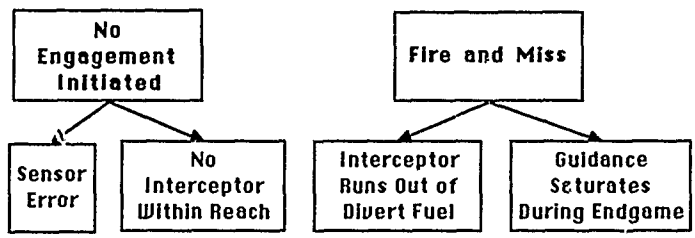

Figure 6. Reasons for failure to intercept.

The first category of failure indicates the lack of an interceptor within kinematically accessible reach of a particular target. If this symptom is addressed at the level of battle management, the conclusion might be that the spacing between interceptors in orbit is too large. If addressed from a guidance point of view, the conclusion may be that the interceptor needs a larger coverage footprint from more axial ΔV. The best system solution may be some combination of the two strategies. In either case the mass required in orbit is increasing nonlinearly, approximately as the inverse square of the interceptor spacing and exponentially with increased axial ΔV if everything else is held constant. If the axial ΔV is added at the expense of lateral ΔV so as to hold the interceptor mass constant, then the trade may be increasing the failure to intercept from the second and third category of symptoms.

The failure to intercept from saturation during the endgame can be addressed at the interceptor guidance level by requiring a greater acceleration capability for the kill stage or by increasing the navigation constant earlier and decreasing the navigation constant later in the flyout. For a given technology assumption on achievable thrust to weight ratios for the maneuver engines, increased acceleration capability will be accompanied by substantial mass increase for the interceptor. Recalling that in the current point design an individual engine mass of 10% of the empty kill stage mass and a thrust to weight ratio of 100 result in a 10g capability at the end of fuel. To achieve a 15g capability, for example, with the same engine technology requires that the individual engine mass be increased to 15% of the empty mass. Assuming that the tankage, batteries, seeker, flight computer, etc. are essentially unchanged, the

assumed 10 kilogram empty mass then increases to 15 kilograms. This 50% increases is reflected in the total interceptor mass and essentially in the overall on-orbit mass if all of the ΔV parameters are unchanged.

The strategy of adjusting the navigation constant to reduce saturation effects has the defect that increasing the navigation ratio early in the flyout increases the 10 - 15% of the lateral ΔV that is wasted in responding to false line of sight rates induced by sensor noise. Also, high navigation ratios at the end of the flyout are necessary to enable sufficient control authority to achieve small miss distances. Hence, the mitigation of interceptor failures occasioned by guidance saturation may be more effectively addressed as a battle management issue. The obvious response is to improve the accuracy of the predicted intercept point so that less heading error remains to be nullified by the lateral guidance or to alter the flyout timelines so that more guidance time remains for the operation of the limited acceleration capability of lateral guidance. Improved predictions are always welcome but not easily achievable in view of operational uncertainties. A minimum guidance time constraint, on the other hand, is easy to enforce in the battle manager.

The last category of intercept failure, the misses due to exhaustion of lateral ΔV capability can be addressed at the guidance level by increasing the lateral ΔV, by decreasing the guidance filter bandwidth and sensitivity to noise, or by improving the guidance law. Increasing the lateral ΔV carries exponential mass increase penalties if the other parameters are held constant. If lateral ΔV is added at the expense of axial ΔV, then the first category of intercept failures may be exacerbated. Decreasing the filter bandwidth will reduce the ΔV expended in responding to sensor noise, but will also slow down the guidance response to target maneuvers and may occasion the expansion of the miss distance distribution so that the kill probability may fall below acceptable levels. Improved guidance laws are always a good strategy as long as the improved performance is consistent with the angle information available from the sensor (i.e., accuracute time to go may not be available) and as long as the guidance law is robust with respect to unmodelled dynamics.

The battle management strategy for dealing with intercept failures from lateral ΔV exhaustion includes the selection between guidance laws depending on the engagement geometry, enforcing constraints on the engagement geometry, and assignment of a maximum guidance on-time. Because of difficulties in estimating the target acceleration for the augmented term in the proportional navigation equation for some engagement geometries, it may be determined empirically that pure proportional guidance performs better than augmented proportional guidance for some easily quantifiable engagement conditions. The battle manager may then initialize the flyout to use one or the other guidance law, as appropriate for the particular geometry. Because a greater fraction of the target acceleration "winds up" the line of sight rate for near perpendicular crossing angle geometries, the battle manager may also be programmed to totally avoid those geometries. Finally, a simple response to excessive lateral ΔV usage on very long flyouts is to limit the guidance on-time by turning on guidance at a specified time to go or by delayed firing of the interceptor by the fire control manager.

Conclusions

It can be seen from the brief, mostly qualitative discussions in this paper that the trade space for space-based strategic interceptors is highly dimensional and tightly coupled along many of the dimensions. Individual interceptor performance is important, but is not the sole determinant of system performance. This is especially true when cost is a primary constraint and achievable performance falls short of complete negation of numerous threats in a massive launch scenario. The resolution of identifiable performance deficiencies will sometimes lie in the realm of battle management, sometimes within the interceptor design, and frequently will involve both.

Measures of effectiveness were introduced to quantify the performance of system designs. Specific problems in achieving desired performance were identified, the interaction of battle management with interceptor design and guidance law design were illustrated, and solutions were suggested. It cannot be overemphasized that it is always necessary to consider important system interactions. Not previously mentioned, an integrated end-to-end simulation including sensor operation, battle management, and interceptor flyout simulation was essential to the uncovering of the performance and sensitivies given the many system nonlinearities.

Identifiable problems in battle management and guidance law implementation sometimes admit of very simple and straightforward corrections. The availability of an integrated simulation testbed to comparatively evaluate strategies and algorithms and to permit experimentation with new ideas has lead to significant progress. Such a testbed has been constructed in an interactive microcomputer environment. The simulation has a user-friendly interface, animated graphical output and is scoped to a level of modeling fidelity that permits rapid execution yet captures the essential error sources including operational uncertainties. The ability to quickly run very large problems in terms of threat scenarios and cardinality of the space-based constellation has permited much useful analysis to be accomplished.

References

[1] Fletcher, J.C., "The Technologies for Ballistic Missile Defense," Issues is Science and Technology, Fall 1984.

[2] Chang, S.C., James, R.M., and Shaw, J.J., "Assignment Algorithms For Kinetic Energy Weapons In Boost Phase Defense," Proc. of 26th Conf. on Decision and Control, Los Angeles, pp 1678 -1683, December 1987.

[3] Ahuja, R.K., Magnanti, T.L., and Orlin, J.B., "Network Flows," Sloan Working Paper No. 2059-88, Massachusetts Institute of Technology, August 1988.

[4] Brogan, W.L., "Algorithm For Ranked Assignments With Application To Multi-Object Tracking,", J. Guidance, Control and Dynamics, May-June 1989, pp. 357-364.

[5] Bate, R.R., Mueller, D.D., and White, J.E., Fundamentals of Astrodynamics, Dover Publication, Inc., 1971.

[6] Zarchan, P., Tactical and Strategic Missile Guidance, AIAA Progress Series in Astronautics and Aeronautics, Vol. 124, New York, 1990.

GUIDANCE METHODS FOR TACTICAL AND STRATEGIC MISSILES

by
PAUL ZARCHAN
The Charles Stark Draper Laboratory, Inc.

Abstract

The paper reviews methods of guidance which are applicable to both tactical and strategic missiles. It is shown how the various guidance law technologies are related. "Rules of thumb," which were originally developed for the tactical world, are extended for application to the strategic world not only to gain insight but also to predict strategic interceptor fuel consumption and performance. Numerous examples are presented to clarify and illustrate concepts.

Introduction

Methods of tactical missile guidance have been in existence for more than 3 decades.[1] These methods work well not only against stationary or predictable targets but also are effective against responsive threats whose future position is highly uncertain. In the tactical arena, current guidance law technology is effective if the flight time is long compared to the effective time constant of the guidance system, and if the missile enjoys a considerable acceleration advantage over the target. It is not uncommon for a tactical missile to have an acceleration advantage of more than five against an aircraft target, which is more than adequate for a successful intercept with current guidance law technology.

Strategic ballistic missiles generally intercept stationary targets whose location is known precisely.[2] In this type of scenario all of the guidance is in the boost phase of the interceptor. Since the boost phase represents a small fraction of the flight of a strategic ballistic missile, the interceptor glides without guidance most of the way towards the target. In this type of strategic application, precise instrumentation is necessary so that the interceptor can reach the correct position and velocity states at the end of the boost phase so that it will be able to glide ballistically towards the target.

In newer systems interceptors will have to fly strategic distances against moving targets whose future position is unknown. In these applications it is not sufficient to apply ballistic missile technology all the way to intercept. Some type of guidance system is required after the boost phase to take out inevitable errors due to lack of knowledge of the intercept point and due to angular measurement errors of the missile-target line-of-sight. Since the newer interceptors are exoatmospheric, fuel is required for the missile to maneuver in response to guidance commands. If all the fuel is depleted the interceptor can not maneuver. In addition, fuel is also at a premium since interceptor weight grows exponentially with fuel weight. Therefore exoatmospheric interceptors require guidance laws which minimize fuel consumption. In addition, because of practical limits on achievable engine thrust to weight ratios, the newer interceptors may no longer enjoy an acceleration advantage over the target. In fact they may be working at an acceleration disadvantage!

Heading error and target maneuver are two major contributors to miss distance and acceleration requirements in the tactical missile world. Formulas have been developed showing how missile acceleration requirements are related to these error sources. Heading error and target maneuver are also important error sources in the strategic world. Heading error is an angular representation of the intercept point prediction error. An upper bound on this number is critical for interceptor sizing. Although a strategic target, such as a booster, may not maneuver intentionally, its longitudinal acceleration perpendicular to the line-of-sight appears as an evasive maneuver to the interceptor. Therefore, the apparent maneuver capability of the target is not only important in setting interceptor weight requirements but also in sizing the required thrust to weight ratio of the lateral divert engines.

Heading Error and Prediction Error

A one-dimensional linearized homing loop, typically used in the analysis of tactical guided missiles,[3] appears in Fig. 1. In this diagram missile acceleration n_c is subtracted from target acceleration n_T to form a relative acceleration. After two integrations relative position y is obtained which at the end of the flight t_F is the miss distance. A division by range (or the closing velocity multiplied by the time to go until intercept) yields the geometric line of sight angle, λ. In proportional navigation guidance[4] the acceleration command is directly proportional to the line of sight rate according to

$$n_c = N' V_c \dot{\lambda}$$

where N' is a designer chosen constant known as the effective navigation ratio and V_c is the missile-target closing velocity.

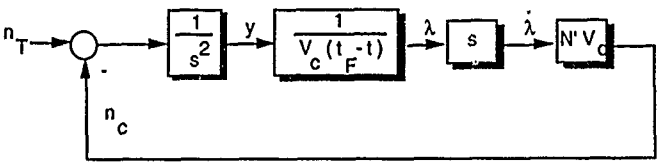

$$\dot{\lambda} = \frac{d\lambda}{dt}$$

Figure 1 - Proportional Navigation Homing Loop

In the absence of target maneuver (n_T=0) we can see from Fig. 1 that the relative acceleration (target acceleration minus missile acceleration) can be expressed as

$$\ddot{y} = -N' V_c \dot{\lambda}$$

Integrating the above differential equation once yields

$$\dot{y} = -N' V_c \lambda + C_1$$

where C_1 is the constant of integration. Substitution of the formula for the line-of-sight angle (which can be derived from Fig. 1 as $\lambda = y/R_{TM}$) in the preceding expression yields the time-varying first-order differential equation

$$\frac{dy}{dt} + \frac{N' y}{t_F - t} = C_1$$

The preceding trajectory equation can be solved analytically because a first-order differential equation of the form

$$\frac{dy}{dt} + a(t) y = h(t)$$

has solution

$$y = e^{-\int_0^t a(T)\,dT} \int_0^t h(n)\, e^{\int_0^n a(T)\,dT}\, dn + C_1 e^{-\int_0^t a(T)\,dT}$$

In the case of a heading error disturbance, only the initial conditions on the differential equation have to be modified.[5,6] The initial condition on the first state is zero or

$$y(0) = 0$$

whereas the initial condition on the second state is related to the heading error by

$$\dot{y}(0) = -V_M HE$$

where V_M is the missile velocity and HE is the heading error in radians. Under these circumstances, after much algebra, we find that the closed form solution for the missile acceleration due to heading error is given by

$$n_c = \frac{-V_M HE\, N'}{t_F} \left(1 - \frac{t}{t_F}\right)^{N'-2}$$

where t_F is the flight time. We can see that the magnitude of the initial missile acceleration is proportional to both the heading error and missile velocity and inversely proportional to the flight time. Doubling the missile velocity or heading error will double the initial missile acceleration while doubling the flight time or time available for guidance will halve the initial missile acceleration.

The closed-form solution for the missile acceleration response due to heading error is displayed in normalized form in Fig. 2. We can see that in a proportional navigation guidance system, higher effective navigation ratios require more missile acceleration at the beginning of flight than at the end of the flight. From a system sizing point of view, the designer usually wants to ensure that the acceleration capability of the missile is adequate at the beginning of flight so that acceleration saturation can be avoided. For a given missile acceleration capability, Fig. 2 shows how requirements are placed on minimum guidance or flight time and maximum allowable heading error and missile velocity.

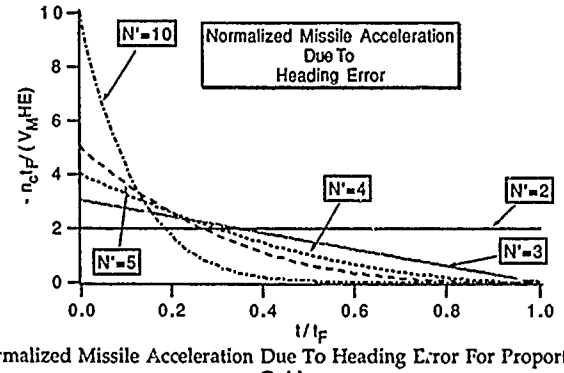

Figure 2 Normalized Missile Acceleration Due To Heading Error For Proportional Navigation Guidance

With strategic missiles it is often more convenient to talk in terms of prediction error rather than heading error. A prelaunch calculation or prediction must be made of where the target will be at intercept. The estimated location of the target at intercept is known as the predicted intercept point. If the calculation is imperfect, a prediction error results, and the missile will not be fired on a perfect collision triangle. The prediction error and heading error are related by

$$\text{Pred Err} = -V_M\, HE\, t_F$$

where Pred Err is the prediction error in units of ft. Therefore substitution of the preceding relationship into the closed form acceleration solution indicates that the missile acceleration required by the proportional navigation guidance law to take out an initial prediction error is given by

$$n_c = \frac{\text{Pred Err}\, N'}{t_F^2} \left[1 - \frac{t}{t_F}\right]^{N'-2}$$

Lateral divert is directly related to the amount of fuel required by the interceptor to implement the guidance law and effect an exoatmospheric intercept. The missile lateral divert is defined as the integral of the absolute value of the missile acceleration or

$$\Delta V = \int_0^{t_F} |n_c|\, dt$$

The strategic interceptor ΔV requirements are related to the total interceptor weight by the rocket equation. Increasing a missile's divert requirements can increase the total weight requirements dramatically. We can find a closed-form solution for the required lateral divert to take out a prediction error by substituting the closed-form solution for the missile acceleration due to prediction error into the preceding integral. After some algebra we obtain

$$\Delta V = \frac{\text{Pred Err } N'}{(N'-1)\,t_F}$$

Thus increasing the effective navigation ratio or increasing the flight time (or guidance time) will tend to reduce the lateral divert requirements of the interceptor due to prediction error.

Proportional Navigation and Target Maneuver

If the only guidance system disturbance is a target maneuver (HE=0), the appropriate second-order trajectory differential equation, derived from Fig. 1, becomes

$$\ddot{y} = -N' V_c \dot{\lambda} + n_T$$

with initial conditions

$$y(0) = 0$$

$$\dot{y}(0) = 0$$

After conversion to a first order differential equation and much algebra the solution for the required missile acceleration can be found to be[4]

$$n_c = \frac{N'}{N'-2}\left[1 - \left(1 - \frac{t}{t_F}\right)^{N'-2}\right] n_T$$

Unlike the heading error case, the maximum missile acceleration due to maneuver is independent of flight time and missile velocity and only depends on the magnitude of the maneuver and the effective navigation ratio. Doubling the maneuver level of the target doubles the missile acceleration requirements.

The closed-form solution for the missile acceleration response due to target maneuver is displayed in normalized form in Fig. 3. We can see that higher effective navigation ratios relax the acceleration requirements at the end of the flight. Unlike the heading error response, the missile acceleration required to hit a maneuvering target increases as the flight progresses.

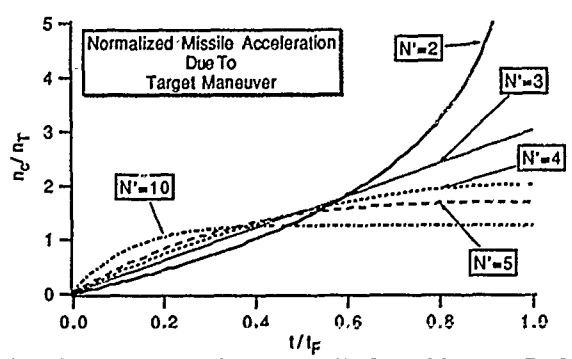

Figure 3 Normalized Missile Acceleration Due To Target Maneuver For Proportional Navigation Guidance

From a system sizing point of view, the designer must to ensure that the acceleration capability of the missile is adequate at the end of flight so that saturation can be avoided in order for the missile to hit the target. The maximum missile acceleration induced by target maneuver in a proportional navigation guidance system occurs at the end of the flight and is given by

$$n_{cMAX}\Big|_{PN} = \frac{N' n_T}{N' - 2}$$

Therefore, for an effective navigation ratio of 3, the missile must have a 3 to 1 acceleration advantage over the target in order to avoid target maneuver induced saturation.

The divert requirements for a proportional navigation guidance system due to a maneuvering target can be found by integrating missile acceleration or

$$\Delta V_{PN} = \int_0^{t_F} \left| n_{c_{PN}} \right| dt = \int_0^{t_F} \frac{N'}{N' - 2} \left[1 - \left(1 - \frac{t}{t_F}\right)^{N'-2} \right] n_T dt$$

After some algebra we obtain

$$\Delta V_{PN} = \frac{N' n_T t_F}{N' - 1}$$

Thus we can see that increasing the effective navigation ratio reduces the lateral divert requirements .

Augmented Proportional Navigation

Extra information can increase guidance law effectiveness by reducing the missile acceleration and lateral divert requirements due to target maneuver. Augmented proportional navigation can make use of target acceleration information, if it is available. A zero-lag augmented proportional navigation homing loop is shown in block diagram form in Fig. 4.[7] The additional target maneuver term, required by the guidance law, appears as a feed forward term in the homing loop block diagram.

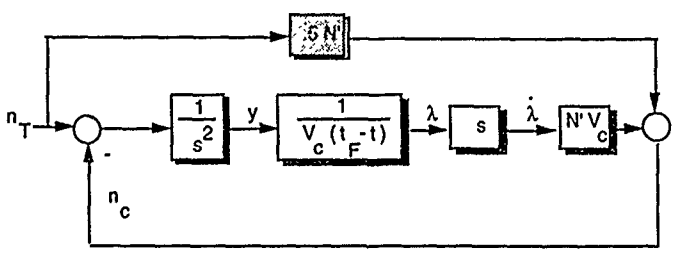

$$\dot{\lambda} = \frac{d\lambda}{dt}$$

Figure 4 Augmented Proportional Navigation Homing Loop

From Fig. 4 we can see that the augmented proportional navigation guidance law can be expressed as

$$n_c\Big|_{APN} = N' V_c \dot{\lambda} + .5 N' n_T$$

As with the proportional navigation guidance law, we can also obtain closed-form solutions for the required missile acceleration due to a constant target maneuver for the zero-lag homing loop depicted in Fig. 4. After much algebra the resultant solution for the required missile acceleration turns out to be

$$n_c\Big|_{APN} = .5\, n_T N' \left[1 - \frac{t}{t_F}\right]^{N'-2}$$

The closed-form solution for the missile acceleration required to hit a maneuvering target with augmented proportional navigation is displayed in normalized form in Fig. 5. Here we can see that the required missile acceleration decreases monotonically with time, regardless of effective navigation ratio, rather than increasing monotonically with time as was the case with proportional navigation. Increasing the effective navigation ratio increases the maximum acceleration at the beginning of the flight but also reduces the time at which the acceleration decays to negligible levels.

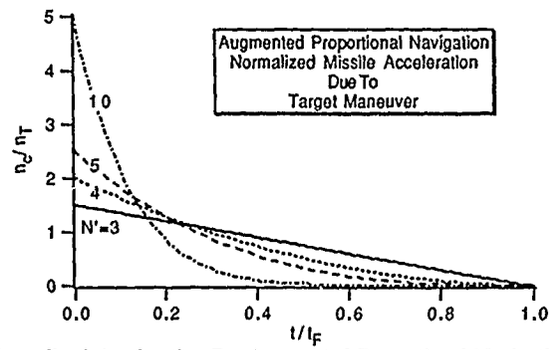

Figure 5 Normalized Acceleration For Augmented Proportional Navigation Acceleration Required to Hit a Maneuvering Target

The maximum required acceleration required by augmented proportional navigation to hit a maneuvering target is

$$n_{cMAX}\Big|_{APN} = .5\, N' n_T$$

This means that for a navigation ratio of three, augmented proportional navigation requires half the acceleration requirements of a missile utilizing proportional navigation guidance. However, for an effective navigation ratio of 5, augmented proportional navigation requires a larger maximum acceleration when compared with proportional navigation guidance.

We can express the lateral divert required for augmented proportional navigation by first setting up the lateral integral as

$$\Delta V_{APN} = \int_0^{t_F} \left| n_{c_{APN}} \right| dt = \int_0^{t_F} .5\, n_T N' \left[1 - \frac{t}{t_F}\right]^{N'-2} dt$$

Integration and simplification yields

$$\Delta V_{APN} = \frac{.5\, N' n_T t_F}{N' - 1}$$

Figure 6 presents a comparative plot of the normalized lateral divert required by the interceptor as a function of the effective navigation ratio for both proportional and augmented proportional navigation due to a maneuvering target. The figure shows that the lateral divert requirements decrease with increasing effective navigation ratio for both guidance laws. We can also see, from the formulas and figure, that augmented proportional navigation always has one half the lateral divert requirements of proportional navigation for the case of a target maneuver disturbance, regardless of effective navigation ratio. Therefore, for strategic applications, in which the threat is an accelerating target such as a booster, augmented proportional navigation is a more fuel efficient guidance law than proportional navigation.

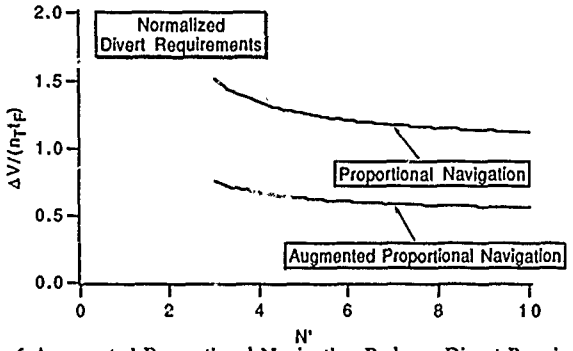

Figure 6 Augmented Proportional Navigation Reduces Divert Requirements

Engagement Simulation Examples

So far we have developed closed-form solutions for the missile acceleration and lateral divert requirements due to an intercept point prediction error and target maneuver. These analytical solutions are based on a one-dimensional linearized model of a missile-target engagement. In order to see if the insights generated by the closed-form solutions are valid, it is necessary to run simulation tests based on a more realistic engagement model. A strategic nonlinear two-dimensional missile-target engagement model can be developed by using an Cartesian Earth-centered coordinate system as shown in Fig. 7. In this figure both the missile and target are in a gravity field as described by Newton's law of universal gravitation.

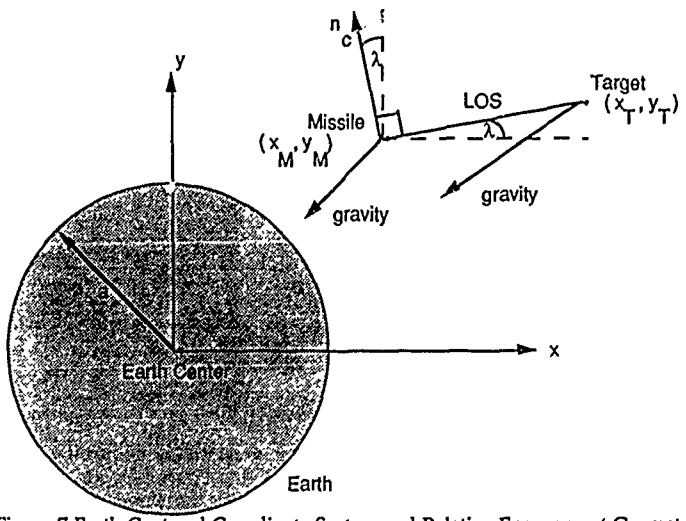

Figure 7 Earth Centered Coordinate System and Relative Engagement Geometry

The acceleration differential equations acting on a ballistic target in a Cartesian Earth-centered coordinate system can be shown to be[8,9]

$$\ddot{x}_T = \frac{-gm\,x_T}{(x_T^2 + y_T^2)^{1.5}}$$

$$\ddot{y}_T = \frac{-gm\,y_T}{(x_T^2 + y_T^2)^{1.5}}$$

where gm is the gravitational parameter with value $1.4077*10^{16}$ ft^3/sec^2 and x_T and y_T are the coordinates of the target with respect to the center of the Earth. Since these differential equations are in an inertial coordinate system they can be numerically integrated directly to yield the velocity and position of the target with respect to the center of the Earth. The components of the relative position between the missile and target can be expressed as

$$R_{TM1} = x_T - x_M$$

$$R_{TM2} = y_T - y_M$$

while the components of the relative velocity are given by

$$V_{TM1} = \dot{x}_T - \dot{x}_M$$

$$V_{TM2} = \dot{y}_T - \dot{y}_M$$

Application of the distance formula shows that the relative separation between the missile and target can be found from

$$R_{TM} = (R_{TM1}^2 + R_{TM2}^2)^{.5}$$

The closing velocity, which is defined as the negative rate of change of separation between missile and target, can be obtained by taking the negative derivative of the preceding expression yielding

$$V_c = \frac{-(R_{TM1}V_{TM1} + R_{TM2}V_{TM2})}{R_{TM}}$$

The line-of-sight angle can be found by trigonometry from Fig. 7 as

$$\lambda = \tan^{-1}\frac{R_{TM2}}{R_{TM1}}$$

Therefore the instantaneous value of the line-of-sight rate can be found by taking the derivative of the line-of-sight angle yielding

$$\dot{\lambda} = \frac{R_{TM1}V_{TM2} - R_{TM2}V_{TM1}}{R_{TM}^2}$$

We now have sufficient information to form a nonlinear proportional navigation homing loop for a strategic interceptor. As was previously mentioned, the proportional navigation acceleration command n_c is proportional to the line-of-sight rate and has magnitude

$$n_c = N' V_c \dot{\lambda}$$

and is in is a direction which is perpendicular to the instantaneous line-of-sight. From Fig. 7 we can see that the components of the guidance command in the Earth-centered coordinate system can be found by trigonometry and are given by

$$a_{XM} = -n_c \sin\lambda$$

$$a_{YM} = n_c \cos\lambda$$

Therefore the acceleration differential equations describing a non boosting missile consists of two parts: the gravitational term, and the guidance command term. The components of the missile acceleration in earth centered coordinates are given by

$$\ddot{x}_M = \frac{-gm\,x_M}{(x_M^2 + y_M^2)^{1.5}} + a_{XM}$$

$$\ddot{y}_M = \frac{-gm\,y_M}{(x_M^2 + y_M^2)^{1.5}} + a_{YM}$$

where a_{XM} and a_{YM} are the guidance components and have already been defined.

A nominal case was considered in which the guidance system was turned off. The resultant trajectories for the 500 sec flight of a non boosting missile placed on a ballistic collision triangle and impulsive target is shown in Fig. 8. In this case the missile hit the target. The fact that the missile was initially placed on a collision triangle implies that our knowledge of the intercept point was perfect. The slight curvature in both missile and target trajectories is due to the fact that both objects have been in a gravity field for 500 sec.

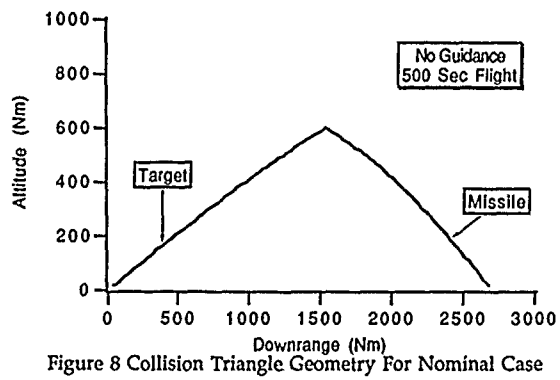

Figure 8 Collision Triangle Geometry For Nominal Case

A guidance system is required since it is not always possible for the missile to be on a collision triangle. There will always be errors in predicting the location of the intercept point. Consider a case for a proportional navigation guidance system with an effective navigation ratio of 3 in which there is a 100 kft prediction error. This means that if we turned off the guidance system we would miss the target by 100 kft. Theory predicts, based upon the formula derived in this paper, that the required missile lateral divert should be

$$\Delta V = \frac{\text{Pred Err } N'}{(N'-1)\,t_F} = \frac{100000 * 3}{2 * 500} = 300 \text{ ft/sec}$$

Figure 9 shows the result nt commanded acceleration and lateral divert profiles for a nonlinear strategic engagement due to the 100 kft prediction error for a proportional navigation guidance system with an effective navigation ratio of 3. We can see that for this case the missile acceleration requirements are small (less than 2 ft/sec^2) for the entire flight. However, even at small acceleration levels, Fig. 9 shows that approximately 420 ft/sec of lateral divert is required for a successful intercept. This number is somewhat larger than the theoretically predicted value of 300 ft/sec because the gravity differential between missile and target also contributes to the missile lateral divert requirements.

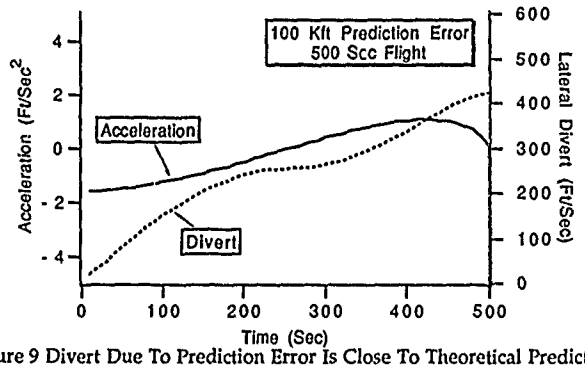

Figure 9 Divert Due To Prediction Error Is Close To Theoretical Prediction

Our lateral divert formula also indicates that for a fixed prediction error, the divert requirements will increase if the flight time is decreased. Figure 10 presents the nonlinear strategic engagement geometry for a 100 sec flight. In this case both the missile and target are initially on a collision triangle.

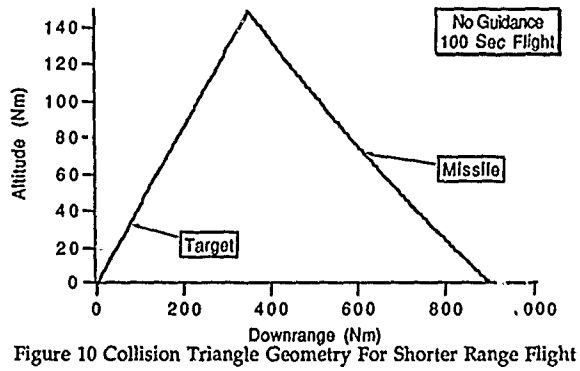

Figure 10 Collision Triangle Geometry For Shorter Range Flight

If we introduce the same 100 kft prediction error into the short flight time example, our formula indicates that the lateral divert requirements should increase substantially. According to the lateral divert formula, reducing the flight time by a factor of 5 should increase the missile lateral divert requirement by a factor of 5 or

$$\Delta V = \frac{\text{Pred Err } N'}{(N'-1)\,t_F} = \frac{100000 * 3}{2 * 100} = 1500 \text{ ft/sec}$$

Figure 11 displays the commanded acceleration and actual divert requirements obtained by actually simulating the engagement. We can see from the figure that the required lateral divert required is indeed nearly 1500 ft/sec. Thus we have demonstrated that the two-dimensional nonlinear engagement model yields performance projections which are in close agreement with the theoretical formula.

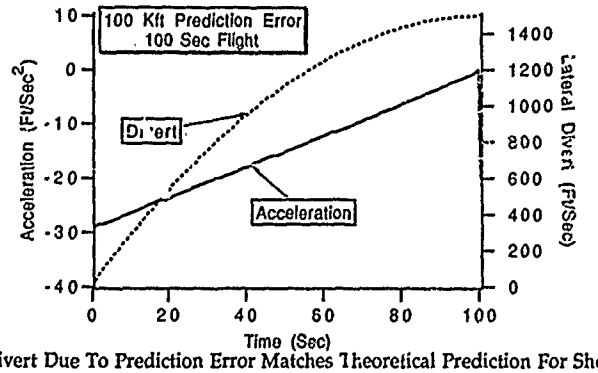

Figure 11 Divert Due To Prediction Error Matches Theoretical Prediction For Shorter Flight

Boosting Target Considerations

Although a booster does not normally execute evasive maneuvers as does an aircraft target, any longitudinal booster acceleration which is perpendicular to the line-of-sight will appear as a target maneuver to the missile. We have already shown that the closed-form solution for the acceleration required by a missile utilizing proportional navigation guidance is given by

$$n_c\Big|_{PN} = \frac{N'}{N'-2}\left[1-\left[1-\frac{t}{t_F}\right]^{N'-2}\right]n_T$$

and that the lateral divert required to hit a maneuvering target is

$$\Delta V\Big|_{PN} = \frac{N'}{N'-1}\, n_T t_F$$

We can develop a model in which the target is a booster performing a gravity turn. The longitudinal acceleration of the booster a_T can be expressed as

$$a_T = \frac{32.2\,T}{W}$$

where T is the booster thrust and W is the booster weight. In a gravity turn, the thrust and velocity vectors are aligned. Therefore the acceleration differential equations for a booster in a gravity field are

$$\ddot{x}_T = \frac{-gm\,x_T}{(x_T^2+y_T^2)^{1.5}} + \frac{a_T\dot{x}_T}{V_T}$$

$$\ddot{y}_T = \frac{-gm\,y_T}{(x_T^2+y_T^2)^{1.5}} + \frac{a_T\dot{y}_T}{V_T}$$

where the target velocity, V_T, is given by

$$V_T = (\dot{x}_T^2 + \dot{y}_T^2)^{.5}$$

The component of the booster acceleration perpendicular to the line-of-sight a_{TPLOS} can be found from Fig. 7 as

$$a_{TPLOS} = \ddot{y}_T \cos\lambda - \ddot{x}_T \sin\lambda$$

A nominal case was run with the guidance system turned off to ensure that the missile and booster were on a collision triangle. Figure 12 shows the missile hitting the target in the nominal 100 sec flight in which the booster target is accelerating the entire time.

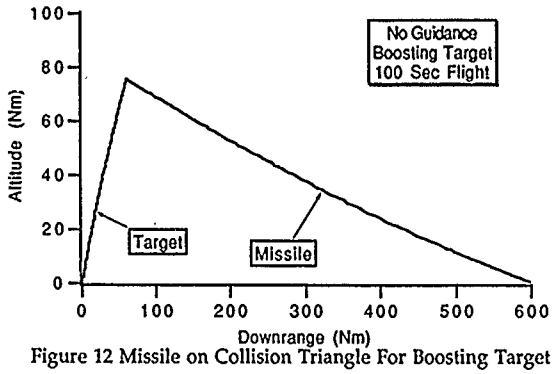

Figure 12 Missile on Collision Triangle For Boosting Target

The same nominal case was rerun with the proportional navigation guidance system turned on. Figure 13 displays the booster acceleration perpendicular to the line of sight for this engagement along with the resultant lateral divert requirements. We can see from the figure that the magnitude of the booster acceleration perpendicular to the line-of-sight is approximately 100 ft/sec^2 on the average. This means that the booster appears to the missile to be a target executing a 3 g maneuver. The missile lateral divert requirements for this case can be seen from the figure to be approximately 12000 ft/sec.

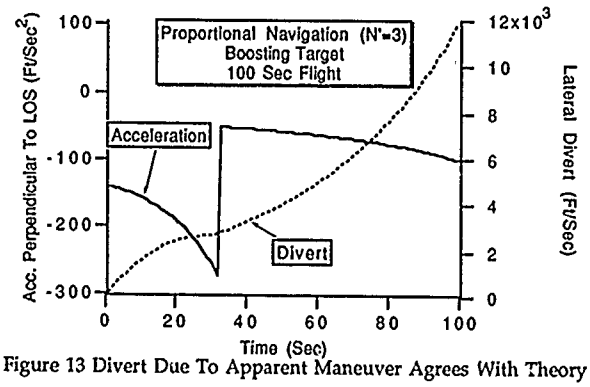

Figure 13 Divert Due To Apparent Maneuver Agrees With Theory

For this case our closed form solution based upon the one-dimensional homing loop indicates that the divert requirements should be

$$\Delta V\Big|_{PN} = \frac{N'}{N'-1}\, n_T t_F = \frac{3 * 100 * 100}{2} = 15000 \text{ ft/sec}$$

In other words theory and simulation are in close agreement.

Our closed-form solutions also indicates that the augmented proportional navigation guidance law reduces the missile acceleration requirements due to a maneuvering target. The closed-form solution for the acceleration required to hit a maneuvering target with the augmented proportional navigation guidance law was shown to be

$$n_c\Big|_{APN} = .5\, n_T N' \left[1 - \frac{t}{t_F}\right]^{N'-2}$$

and the lateral divert is given by

$$\Delta V\Big|_{APN} = .5\, \frac{N'}{N'-1}\, n_T t_F = .5\, \Delta V\Big|_{PN}$$

In other words, theory says that the divert requirements for an augmented proportional navigation guidance system are half the divert requirements of a proportional navigation guidance system.

In order to implement augmented proportional navigation guidance in the nonlinear two-dimensional strategic engagement model it is necessary to modify the missile guidance command to

$$n_c\Big|_{APN} = N' V_c \dot{\lambda} + \frac{N'}{2} a_{TPLOS}$$

where a_{TPLOS} is the booster acceleration perpendicular to the line of sight. The nominal simulation case was rerun, except this the time the augmented proportional navigation guidance law was used. Figure 14 shows that the missile lateral divert requirements were dramatically reduced to about 7500 ft/sec (down from about 12000 ft/sec in the proportional navigation case.

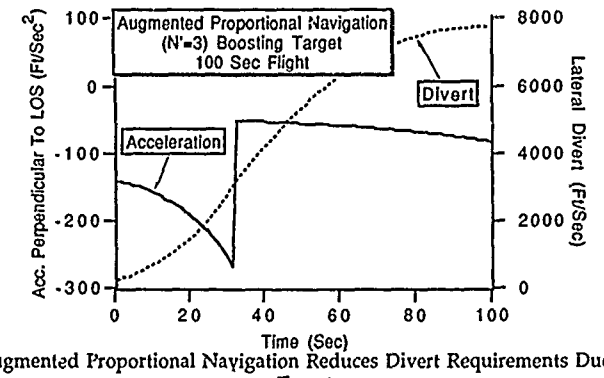

Figure 14 Augmented Proportional Navigation Reduces Divert Requirements Due To Boosting Target

Theory says the divert requirements for the augmented proportional navigation guidance law should be

$$\Delta V\Big|_{APN} = .5 \frac{N'}{N'-1} n_T t_F = \frac{.5 * 3 * 100 * 100}{2} = 7500 \text{ ft/sec}$$

which is in total agreement with the simulation results.

Predictive Guidance[10]

We have seen how interceptor lateral divert requirements can be reduced when extra information, if it exists, is incorporated in the guidance law. If an exact model of the target and missile dynamics is available, one could achieve the best performance with the ultimate guidance law - predictive guidance. The principle behind predictive guidance is quite simple. We take our dynamic models of the target and missile and, at each guidance system update, numerically integrate them forward until the desired intercept time. In other words, we are predicting the future location of the missile and target by brute force. The difference between the predicted missile and target position at the intercept time is known as the zero effort miss. If the predicted coordinates of the missile at intercept, in the earth centered system, is given by (x_{MF}, y_{MF}) and the coordinates of the target are given by coordinates of the target (x_{TF}, y_{TF}) then the Earth-centered components of the zero effort miss are given by

$$ZEM_x = x_{TF} - x_{MF}$$

$$ZEM_y = y_{TF} - y_{MF}$$

We can find the component of the zero effort miss perpendicular to the line-of-sight by trigonometry in Fig. 7. The zero effort miss perpendicular to the line-of-sight is given by

$$ZEM_{PLOS} = - ZEM_x \sin\lambda + ZEM_y \cos\lambda$$

In theory[7] the instantaneous acceleration guidance command should be proportional to the zero effort miss perpendicular to the instantaneous line-of-sight (which in this case is obtained by numerical integration) and inversely proportional to the square of time to go until intercept or

$$n_c = \frac{N' ZEM_{PLOS}}{t_{go}^2}$$

Proportional navigation and augmented proportional navigation can all be expressed in the above form. In these guidance laws we have closed-form expressions for the zero effort miss. In other words, an integration of simple dynamics (assumed to be a polynomial in time) was conducted to get a closed form expression. In predictive guidance, we ignore closed-form solutions of approximate processes and obtain the exact solution for the zero effort miss, at each guidance update by numerical integration. The resultant accuracy of the computed zero effort miss depends on the size of the integration interval. Small integration intervals yield accurate answers but may impose unrealistic computer throughput requirements on the interceptor guidance system. Of course the accuracy also depends on the validity of the differential equations used. Having inaccurate models of the target will lead to erroneous predictions of the zero effort miss and in this case the performance of predictive guidance may be substantially worse than that of proportional navigation.

The nominal 100 sec boosting target case of the previous section (i.e. see Fig. 12) was repeated to see the effectiveness of the new guidance law. Figure 15 compares the commanded missile acceleration requirements for proportional navigation, augmented proportional navigation and predictive guidance. We can see, as expected, augmented proportional navigation requires significantly less acceleration than proportional navigation. The required acceleration is large for augmented proportional navigation, because as we saw in the previous section, much of the longitudinal booster acceleration was perpendicular to the line-of-sight (on the average about 100 ft/sec^2) and thus appeared as a target maneuver to the missile. However, we can also see that predictive guidance virtually requires zero acceleration to intercept the boosting target. The reason for this is that the missile is initially on a collision triangle with the target. Therefore no commands are really necessary for a successful intercept.

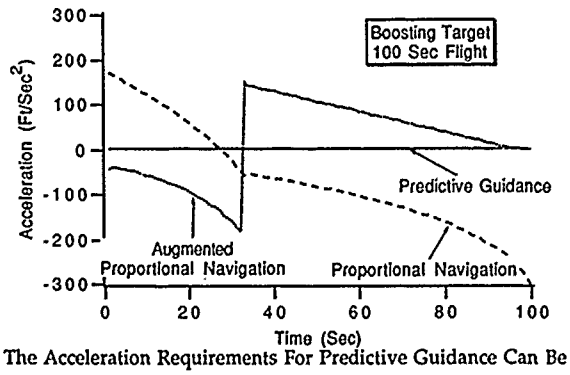

Figure 15 The Acceleration Requirements For Predictive Guidance Can Be Very Small

Figure 16 presents the missile lateral divert requirement profiles for the same case. Here we can see that proportional navigation required about 12000 ft/sec of lateral divert, augmented proportional navigation required about 7500 ft/sec of lateral divert and predictive guidance only required 39 ft/sec of lateral divert!

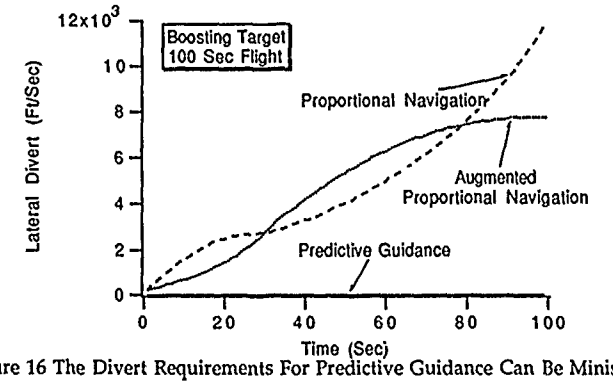

Figure 16 The Divert Requirements For Predictive Guidance Can Be Miniscule

Predictive guidance can dramatically reduce the interceptor lateral divert requirements due to a boosting target because it is making use of a priori information on the booster. If there is an initial prediction error, predictive guidance should yield about the same divert requirements due to prediction error as proportional navigation because predictive guidance has no a priori information about the prediction error. Figure 17 shows that nonlinear two-dimensional engagement simulation results indicate that predictive guidance yields approximately 1600 ft/sec of lateral divert in the case where there is a 100 kft prediction error in the nominal boosting target case.

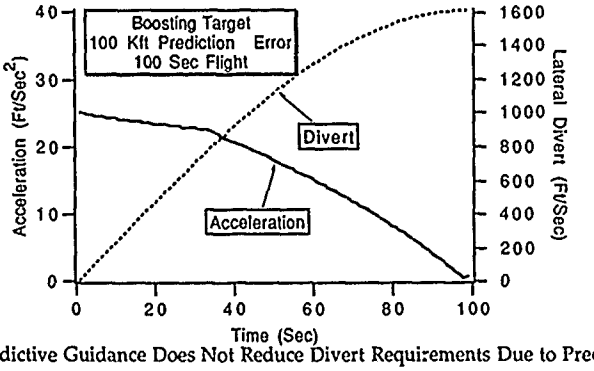

Figure 17 - Predictive Guidance Does Not Reduce Divert Requirements Due to Prediction Error

Theory predicted that the lateral divert due to prediction error alone would be

$$\Delta V = \frac{\text{Pred Err } N'}{(N'-1)\,t_F} = \frac{100000 * 3}{2 * 100} = 1500 \text{ ft / sec}$$

which is in total agreement with the simulation results.

Summary

In this paper it has been demonstrated that the guidance concepts originally developed for the tactical world are applicable to the strategic world. In fact, closed-form solutions for the required missile acceleration to hit targets can be converted to lateral divert formulas. Nonlinear engagement simulation results indicate that the divert requirement formulas for prediction error, apparent target acceleration and guidance law are not only useful but are in fact accurate indicators of strategic interceptor requirements.

References

1. Fossier, M. W., "The Development of Radar Homing Missiles", Journal of Guidance, Control and Dynamics, Vol. 7, Nov.-Dec. 1984, pp 641-651.

2. Haeussermann, W., "Developments in the Field of Automatic Guidance and Control Of Rockets", Journal of Guidance, Control and Dynamics, Vol. 4, May-June 1981, pp 225-239.

3. Zarchan, P. "Complete Statistical Analysis of Nonlinear Missile Guidance Systems - SLAM," Journal of Guidance and Control, Vol. 2, Jan. - Feb., 1979, pp. 71-78.

4. Garnell, P. and East, D. J., Guided Weapon Control System, Pergamon Press, 1977.

5. Locke, A. S., Guidance, D. Van Nostrand, Inc., Toronto, 1955.

6. Jerger, J. J., System Preliminary Design, D. Van Nostrand, Inc., Princeton, New Jersey, 1960.

7. Nesline, F. W. and Zarchan, P., "A New Look at Classical Versus Modern Homing Guidance," Journal of Guidance and Control, Vol. 4, No. 1, Jan.-Feb., 1981, pp. 78-85.

8. Bate, R. R., Mueller, D. D. and White, J. E. Fundamentals of Astrodynamics, Dover Publication, Inc., 1971.

9. Regan, F., Re-Entry Vehicle Dynamics, AIAA Education Series, New York, 1984.

10. Zarchan, P., Tactical and Strategic Missile Guidance, AIAA Progress Series in Astronautics and Aeronautics, Vol. 124, New York, 1990.

REPORT DOCUMENTATION PAGE

1. Recipient's Reference	2. Originator's Reference	3. Further Reference	4. Security Classification of Document
	AGARD-LS-173	ISBN 92-835-0587-5	UNCLASSIFIED

5. Originator Advisory Group for Aerospace Research and Development
North Atlantic Treaty Organization
7 rue Ancelle, 92200 Neuilly sur Seine, France

6. Title MISSILE INTERCEPTOR GUIDANCE SYSTEM TECHNOLOGY

7. Presented at

8. Author(s)/Editor(s)	9. Date
Various	September 1990

10. Author's/Editor's Address	11. Pages
Various	160

12. Distribution Statement This document is distributed in accordance with AGARD policies and regulations, which are outlined on the Outside Back Covers of all AGARD publications.

13. Keywords/Descriptors

Antiaircraft missiles
Missile guidance
Guidance computers
Missile control
Command guidance

14. Abstract

Most operational interceptor tactical guidance systems are employing technologies which were developed more than two decades ago. Newer technologies have been slow to replace these mature technologies that meet the requirements; however, future interceptor guidance systems will have more demanding requirements and technological advances have great payoff potential. The Lecture Series will bring together a group of speakers with both outstanding practical and theoretical experience in interceptor guidance system technology. These speakers will provide the audience with the guidance system technology fundamentals which will serve as background so that theoretical advances in future and proposed systems can be both understood and appreciated.

This Lecture Series, sponsored by the Guidance and Control Panel of AGARD, has been implemented by the Consultant and Exchange Programme.

AGARD Lecture Series No.173
Advisory Group for Aerospace Research and Development, NATO
MISSILE INTERCEPTOR GUIDANCE SYSTEM TECHNOLOGY
Published September 1990
160 pages

Most operational interceptor tactical guidance systems are employing technologies which were developed more than two decades ago Newer technologies have been slow to replace these mature technologies that meet the requirements; however, future interceptor guidance systems will have more demanding requirements and technological advances have great payoff potential. The Lecture Series will bring together a group of speakers with

P.T.O.

AGARD-LS-173

Antiaircraft missiles
Missile guidance
Guidance computers
Missile control
Command guidance

AGARD Lecture Series No.173
Advisory Group for Aerospace Research and Development, NATO
MISSILE INTERCEPTOR GUIDANCE SYSTEM TECHNOLOGY
Published September 1990
160 pages

Most operational interceptor tactical guidance systems are employing technologies which were developed more than two decades ago. Newer technologies have been slow to replace these mature technologies that meet the requirements; however, future interceptor guidance systems will have more demanding requirements and technological advances have great payoff potential. The Lecture Series will bring together a group of speakers with

P.T.O.

AGARD-LS-173

Antiaircraft missiles
Missile guidance
Guidance computers
Missile control
Command guidance

AGARD Lecture Series No.173
Advisory Group for Aerospace Research and Development, NATO
MISSILE INTERCEPTOR GUIDANCE SYSTEM TECHNOLOGY
Published September 1990
160 pages

Most operational interceptor tactical guidance systems are employing technologies which were developed more than two decades ago. Newer technologies have been slow to replace these mature technologies that meet the requirements; however, future interceptor guidance systems will have more demanding requirements and technological advances have great payoff potential. The Lecture Series will bring together a group of speakers with

P.T.O.

AGARD-LS-173

Antiaircraft missiles
Missile guidance
Guidance computers
Missile control
Command guidance

AGARD Lecture Series No.173
Advisory Group for Aerospace Research and Development, NATO
MISSILE INTERCEPTOR GUIDANCE SYSTEM TECHNOLOGY
Published September 1990
160 pages

Most operational interceptor tactical guidance systems are employing technologies which were developed more than two decades ago. Newer technologies have been slow to replace these mature technologies that meet the requirements; however, future interceptor guidance systems will have more demanding requirements and technological advances have great payoff potential. The Lecture Series will bring together a group of speakers with

P.T.O.

AGARD-LS-173

Antiaircraft missiles
Missile guidance
Guidance computers
Missile control
Command guidance

both outstanding practical and theoretical experience in interceptor guidance system technology. These speakers will provide the audience with the guidance system technology fundamentals which will serve as background so that theoretical advances in future and proposed systems can be both understood and appreciated.

This Lecture Series, sponsored by the Guidance and Control Panel of AGARD, has been implemented by the Consultant and Exchange Programme.

ISBN 92-835-0587-5

both outstanding practical and theoretical experience in interceptor guidance system technology. These speakers will provide the audience with the guidance system technology fundamentals which will serve as background so that theoretical advances in future and proposed systems can be both understood and appreciated.

This Lecture Series, sponsored by the Guidance and Control Panel of AGARD, has been implemented by the Consultant and Exchange Programme.

ISBN 92-835-0587-5

both outstanding practical and theoretical experience in interceptor guidance system technology. These speakers will provide the audience with the guidance system technology fundamentals which will serve as background so that theoretical advances in future and proposed systems can be both understood and appreciated.

This Lecture Series, sponsored by the Guidance and Control Panel of AGARD, has been implemented by the Consultant and Exchange Programme.

ISBN 92-835-0587-5

both outstanding practical and theoretical experience in interceptor guidance system technology. These speakers will provide the audience with the guidance system technology fundamentals which will serve as background so that theoretical advances in future and proposed systems can be both understood and appreciated.

This Lecture Series, sponsored by the Guidance and Control Panel of AGARD, has been implemented by the Consultant and Exchange Programme.

ISBN 92-835-0587-5